THE ANALYSIS AND DESIGN OF MULTIRATE SAMPLED-DATA FEEDBACK SYSTEMS VIA A POLYNOMIAL APPROACH

A THESIS

SUBMITTED TO THE DEPARTMENT OF MECHANICAL ENGINEERING,

THE FACULTY OF ENGINEERING, UNIVERSITY OF GLASGOW

IN FULFILMENT OF THE REQUIREMENTS

FOR THE DEGREE OF

DOCTOR OF PHILOSOPHY

By

Michelle Govan

September 2002

Abstract

This thesis describes the modelling, analysis and design of multirate sampled-data feedback via the polynomial equations approach. The key theoretical contribution constitutes the embedding of the principles underpinning and algebra related to the switch and frequency decomposition procedures within a modern control framework, thereby warranting the use of available computer-aided control systems design software. A salient feature of the proposed approach consequently entails the designation of system models that possess dual time- and frequency-domain interpretations. Expositionally, the thesis initially addresses scalar systems excited by deterministic inputs, prior to introducing stochastic signals and culminates in an analysis of multivariable configurations. In all instances, overall system representations are formulated by amalgamating models of individual subsystems. The polynomial system descriptions are shown subsequently to be compatible with the Linear Quadratic Gaussian and Generalised Predictive Control feedback system synthesis methods provided causality issues are dealt with appropriately. From a practical perspective, the polynomial equations approach proffers an alternative methodology to the state-variable techniques customarily utilised in this context and affords the insights and intuitive appeal associated with the use of transfer function models. Numerical examples are provided throughout the thesis to illustrate theoretical developments.

ACKNOWLEDGEMENTS

I would like to take this opportunity to acknowledge my appreciation to my supervisor, Dr. Alan W. Truman, for sharing his knowledge, invaluable insights and challenging perspectives in the field of multirate sampled-data control systems, together with support given throughout my time at university.

I would also like to express my thanks to the Engineering and Physical Sciences Research Council for providing financial support during the first three years of my study at the University of Glasgow.

In addition, I would like to take this opportunity to express my special thanks and sincere gratitude to my teachers – but especially to those who have helped shape my academic life, providing me with enlightening ideas which fired my imagination and the valuable skills required to achieve my ambitions in life.

Last, but most, on a personal side, I would like to thank my parents for their unfailing kindness, patience, guidance and their kind words of encouragement and support, but more importantly for making it possible for me to have the best possible start in life I could have hoped for.

PUBLICATIONS

The following papers have emanated from the research undertaken for this thesis:

(i) Truman, Alan W. & Govan, Michelle, (1999), Polynomial models for multirate-sampled digital feedback system design, *Proceedings 1st Europoly Workshop on Polynomial Systems Theory & Applications*, Strathclyde, UK, 19–34.

(ii) Truman. Alan W. & Govan, Michelle, (2000), Multirate-sampled digital feedback system design via a predictive control approach, *IEE Proceedings – Control Theory & Applications*, **147**(3): 293–302.

(iii) Truman, Alan W. & Govan, Michelle, (2000), Polynomial LQG design of subrate digital feedback Systems via frequency decomposition, *Optimal Control Applications & Methods*, **21**: 211–232.

(iv) Truman, Alan W. & Govan, Michelle, (2000), Polynomial LQG synthesis of subrate digital feedback systems, *IEE Proceedings – Control Theory & Applications*, **147**(3): 247–256.

(v) Truman, Alan W. & Govan, Michelle, (2000), Polynomial design of fast output-sampled digital feedback systems, *Proceedings UKACC International Conference on Control*, Cambridge.

(vi) Truman, Alan W. & Govan, Michelle, (2001), Predictive control of fast output-sampled digital feedback systems via a polynomial approach, *Proceedings of the Institution of Mechanical Engineers, part I*, **215**: 211–233.

The following papers have been submitted for publication:

(i) Truman, Alan W. & Govan, Michelle, LQG synthesis of SISO multirate sampled-data feedback systems via a polynomial approach.

(ii) Truman, Alan W. & Govan, Michelle, Optimal control of multirate sampled-data feedback systems via a polynomial approach.

NOTATION AND DEFINITIONS

Matrix- (vector-) valued quantities are indicated by upper- (lower-) case letters in bold type. The determinant, adjugate, trace and transpose of a matrix $\mathbf{X}$ are denoted by $\det(\mathbf{X})$, $\mathrm{adj}(\mathbf{X})$, $\mathrm{tr}(\mathbf{X})$ and $\mathbf{X}'$, respectively. The adjoint of a matrix $\mathbf{X}(p)$, namely, $\mathbf{X}'(p^{-1})$ is denoted by $\mathbf{X}^{\star}(p)$. Diagonal and block diagonal matrices are indicated by $\mathrm{diag}(\cdot)$ and block $\mathrm{diag}(\cdot)$, respectively. $E\{\cdot\}$ signifies the expectation operator. The symbols $\mathbb{Z}$, $\mathbb{R}$ and $\mathbb{C}$ represent, respectively, the sets of integers, real numbers and complex numbers.

The backward-shift operator, generically written as q_K^{-1}, is used in difference equations and related expressions, whereas its counterpart, z_K^{-1}, constitutes a complex variable arising in frequency-domain analysis. The zeros of a polynomial

$$X_K(z_K^{-1}) = x_0 + x_1 z_K^{-1} + \ldots + x_{n_x} z_K^{-n_x}$$

are defined with respect to the z_K-plane; thus, the zeros of the $X_K(z_K^{-1})$, namely, z_{K_i}, $i = 1, 2, \ldots, n_x$, are specified as the roots of $z_K^{n_x} X_K(z_K^{-1}) = 0$. The polynomial $X_K(z_K^{-1})$ is *monic* if $x_0 = 1$. The polynomial $X_K(z_K^{-1})$ (matrix $\mathbf{X}(z_K^{-1})$) is said to be *stable* – i.e., strictly Schur – if and only if the zeros of $X_K(z_K^{-1})$ (its invariant polynomials) lie strictly within $|z_K| = 1$.

A $l|m$ rational matrix $\mathbf{F}(z_K^{-1})$ may be defined as either a left- or right-matrix fraction, namely,

$$\mathbf{F}(z_K^{-1}) = \mathbf{A}_l^{-1}(z_K^{-1})\mathbf{B}_l(z_K^{-1}) = \mathbf{B}_r(z_K^{-1})\mathbf{A}_r^{-1}(z_K^{-1}).$$

The above matrix fractions are said to be *coprime* if there exist pairs $\left(\tilde{\mathbf{A}}_l(z_K^{-1}), \tilde{\mathbf{B}}_l(z_K^{-1})\right)$ and $\left(\tilde{\mathbf{A}}_r(z_K^{-1}),\ \tilde{\mathbf{B}}_r(z_K^{-1})\right)$ such that

$$\mathbf{A}_l(z_K^{-1}) = \mathbf{U}(z_K^{-1})\tilde{\mathbf{A}}_l(z_K^{-1}) \quad \text{and} \quad \mathbf{B}_l(z_K^{-1}) = \mathbf{U}(z_K^{-1})\tilde{\mathbf{B}}_l(z_K^{-1});$$

and

$$\mathbf{A}_r(z_K^{-1}) = \tilde{\mathbf{A}}_r(z_K^{-1})\mathbf{V}(z_K^{-1}) \quad \text{and} \quad \mathbf{B}_r(z_K^{-1}) = \tilde{\mathbf{B}}_r(z_K^{-1})\mathbf{V}(z_K^{-1})$$

only for unimodular matrices $\mathbf{U}(z_K^{-1})$ and $\mathbf{V}(z_K^{-1})$, i.e., $\det\left(\mathbf{U}(z_K^{-1})\right) = \det\left(\mathbf{V}(z_K^{-1})\right) = 1$.

Where there is no possibility of ambiguity, the arguments of certain terms may be omitted for concision.

Definitions of Vector- and Matrix-Valued Quantities

The following tables specify the dimension of vectors and matrices used throughout the thesis.

Table A. Vector-valued quantities.

vector	elements	dimension	equation
$\mathbf{x}_K$	$\mathbb{R}$	K	(3.20)
$\mathbf{x}_{K_f}$	$\mathbb{C}$	K	(3.39b)
$\hat{\mathbf{y}}, \hat{\boldsymbol{\epsilon}}$	$\mathbb{R}$	mN	(4.7)
$\hat{\mathbf{u}}$	$\mathbb{R}$	lN	(4.7)
$\tilde{\mathbf{u}}$	$\mathbb{R}$	$\sum_{j=1}^{l} L_j$	(4.9)
$\tilde{\mathbf{y}}, \tilde{\boldsymbol{\epsilon}}$	$\mathbb{R}$	$\sum_{i=1}^{m} M_i$	(4.11)
$\mathbf{y}_r$	$\mathbb{R}$	$\sum_{i=1}^{m} M_i$	(4.11)
$\mathbf{y}_e$	$\mathbb{R}$	$mN - \sum_{i=1}^{m} M_i$	(4.11)
$\hat{\mathbf{y}}_f$	$\mathbb{C}$	mN	(4.15)
$\hat{\mathbf{u}}_f$	$\mathbb{C}$	lN	(4.15)
$\tilde{\mathbf{u}}_f$	$\mathbb{C}$	$\sum_{j=1}^{l} L_j$	(4.16)
$\tilde{\mathbf{y}}_f$	$\mathbb{C}$	$\sum_{i=1}^{m} M_i$	(4.17)
$\bar{\mathbf{y}}, \bar{\boldsymbol{\epsilon}}$	$\mathbb{R}$	$\sum_{i=1}^{m} M_i$	(4.32)
$\bar{\mathbf{u}}$	$\mathbb{R}$	$\sum_{j=1}^{l} L_j$	(4.33)
$\check{\mathbf{y}}, \check{\boldsymbol{\epsilon}}$	$\mathbb{R}$	$p\sum_{i=1}^{m} M_i$	(5.44a)
$\check{\mathbf{u}}$	$\mathbb{R}$	$p\sum_{j=1}^{l} L_j$	(5.44b)

Table B. Matrix-valued quantities.

matrix	dimension	equation
$\mathbf{P}_K^{(i)}$	$K\|K$	(3.21)
$\mathbf{V}_J$	$J\|N$	(3.32)
$\mathbf{W}_K$	$N\|K$	(3.34)
$\mathbf{P}_{K_f}^{(i)}$	$K\|K$	(3.41)
$\mathbf{W}_{L_f}$	$N\|L$	(3.45)
$\mathbf{V}_{M_f}$	$M\|N$	(3.47)
$\mathbf{T}_K$	$K\|K$	(3.51)
$\mathbf{Q}_{ML}^{(i)}$	$M\|L$	(3.70)
$\hat{\mathbf{P}}_k^{(\lambda)}$	$kN\|kN$	(4.7)
$\mathbf{\Pi}_1$	$mN\|mN$	(4.11)
$\hat{\mathbf{P}}_{k_f}^{(i)}$	$kN\|kN$	(4.15)
$\mathbf{T}_{\tilde{y}}$	$\sum_{\substack{i=1\\l}}^{m} M_i \Big\| \sum_{\substack{i=1\\l}}^{m} M_i$	(4.18a)
$\mathbf{T}_{\tilde{u}}$	$\sum_{j=1}^{m} L_j \Big\| \sum_{j=1}^{m} L_j$	(4.18b)
$\mathbf{\Pi}_2$	$\sum_{\substack{i=1\\l}}^{m} M_i \Big\| \sum_{\substack{i=1\\l}}^{m} M_i$	(4.32)
$\mathbf{\Pi}_3$	$\sum_{j=1}^{m} L_j \Big\| \sum_{j=1}^{m} L_j$	(4.33)
$\mathbf{P}_y^{(i)}$	$\sum_{\substack{i=1\\l}}^{m} M_i \Big\| \sum_{\substack{i=1\\l}}^{m} M_i$	(5.41a)
$\mathbf{P}_u^{(i)}$	$\sum_{j=1} L_j \Big\| \sum_{j=1} L_j$	(5.41b)

Contents

List of Figures

List of Tables

Chapter One

Introduction

Driven mainly by rapid advances in microelectronics and computer technology, automatic control systems nowadays are invariably implemented digitally. Accordingly modelled as sampled-data systems, the initial theoretical contributions in this area assumed that all conversions of signals from analogue to digital format and vice-versa were carried out synchronously at a uniform sampling rate. Subsequently, it became apparent that there was a requirement to extend sampled-data theory to encompass alternative scenarios, such as cyclic-rate and multirate sampling schedules (Jury, 1961).

In practice, unorthodox sampling régimes may either be imposed by hardware constraints or arise from engineering judgement (Horowitz, 1963). A feedback system used for the control of limb movement in paraplegics is one example of a situation in which an unorthodox sampling scheme is prescribed (Schauer and Hunt, 2000). In this instance, joint movement is achieved by the electrical stimulation of muscles at a rate governed by that at which muscle contraction can occur naturally. However, to obtain realistic measurements, the related sampling frequency must be significantly higher, thereby resulting in a multirate-sampled configuration. On the other hand, multirate sampling schemes represent a convenient means of reducing the computational load in large-scale digital control systems, where, rather than adopting a single sampling frequency dictated by the bandwidth of the fastest feedback loop, the selection of individual sampling rates in accordance with the dynamics of each control task will save processor time. Although this practice, which is widespread in aerospace applications such as the Space Shuttle and F18 flight control systems (Glasson, 1983), enables more processor time to be devoted to data-logging and monitoring functions, its economic justification is ever-diminishing, owing to the relatively low cost of the hardware involved.

Reviews of theoretical developments in digital control theory (Araki, 1993, Moore *et al.*, 1993) reveal that much current research views the use of multirate sampling schemes as constituting a prospective design aid. This concept may be alien to many control engineers

who, unfamiliar with the modelling procedures involved, would regard any sampling régime other than a single-rate policy as an unwarranted complication. Nonetheless, the notion that a "problem" in fact may represent a "solution" is intriguing.

1.1 Historical Background

Research into the analysis and design of multirate-sampled feedback systems has evolved from two analytical procedures which were conceived to evaluate the inter-sample "ripple" performance of single-rate sampled-data systems. However, researchers soon began to appreciate the potential value of the so-called "decomposition" methods in analysing bona fide multirate systems.

Introduced by Sklansky and Ragazzini (1955), frequency decomposition is founded upon the principle that by defining a "fast-rate" pulse-transform, the relationship between the frequency spectra produced by a "fast-rate" sampler to that generated by a "slow-rate" sampler could be defined in a simple expression. Subsequently, Coffey and Williams (1966) enhanced this technique and developed an efficient method of numerically evaluating stability by means of classical frequency response methods.

An alternative philosophy attributed to Kranc (1957), switch decomposition, is based upon frequency-domain operations, although it is referred to occasionally as a "time-domain" decomposition. The fundamental principle involves the substitution of a "fast-rate" sampler by a group of parallel forward paths, each comprising a time advance, a "slow-rate" sampling switch and a time delay connected in cascade, thereby relying upon the extensive use of modified z-transforms to handle the effects of the time delay/advance elements introduced. Switch decomposition therefore provided a means of analysing multirate-sampled configurations via existing single-rate methods. Nonetheless, while conceptually straightforward, the topological operations required are computationally problematic. Boykin and Frazier (1975b) subsequently simplified the manipulations involving modified z-transforms by adopting a matrix-vector modelling methodology.

An excellent review of both decomposition techniques is presented by Ragazzini and Franklin (1958), while Jury (1967) demonstrates their equivalence.

In contrast to the above (pulse-) transfer function-orientated approaches, Kalman and

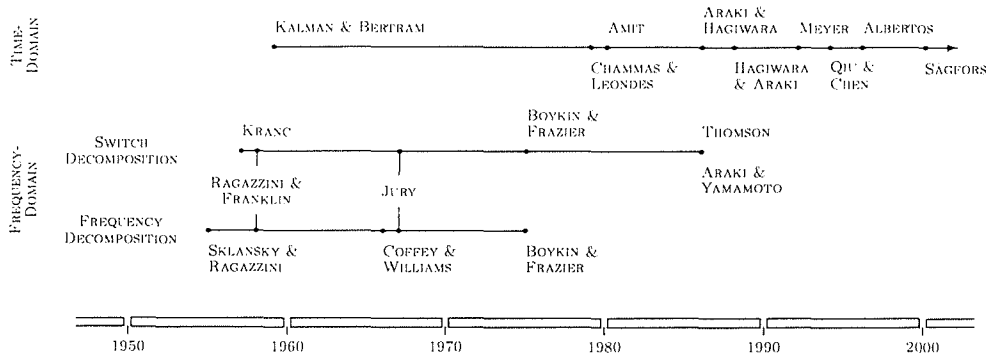

Figure 1.1. Development of multirate sampled-data theory.

Bertram (1959) provided a means of analysing general sampled-data systems via the emergent state-variable methodology. These authors explained how, by defining states for each continuous-time, discrete-time and sample-and-hold element, a valid system representation could be produced by evaluating the propagation of states through one cycle of the sequence of sampling operations.

The decomposition methods will be examined in more detail in the next chapter.

1.2 Literature Survey

The analysis and design of multirate sampled-data feedback systems continues to generate research interest long after the original modelling techniques were formulated. A notable feature of publications within the last two decades concerns the almost exclusive reliance of the state-variable modelling approach in comparison with the decomposition techniques.

A comprehensive assessment of the significant achievements and results within multirate sampled-data feedback system theory can be found in Glasson (1983), Araki and Yamamoto (1986), and Berg *et al.* (1988). Additionally, in an evaluation of the capabilities and limitations of multirate sampling by Moore *et al.* (1993), the potential of unorthodox sampling schemes in conferring additional design freedom was examined. A historical overview of research in multirate control is presented in Figure 1.1.

Although somewhat subjective and by no means clear-cut, it is useful to characterise papers and theses addressing issues related to multirate-sampled digital control theory in this literature review under the following headings: dynamics-assignment, optimal control,

robust control, adaptive and predictive control, frequency-domain analysis and miscellaneous research.

Dynamics-Assignment

A considerable number of contributions within the last two decades may be classified as pertaining to the pole-placement of multirate-sampled feedback systems. The most general situation, in which it is assumed implicitly that the sampling periods of each control and plant output signal are imposed and distinct, has been investigated by Araki *et al.* (1992) and Godbout *et al.* (1994). Nonetheless, the majority of papers on this topic construe the adoption of a multirate sampling schedule as a means of providing sufficient latitude in the pole-placement problem to obviate the need for the deployment of an observer.

Chammas and Leondes (1979) originated an approach in which, with all plant outputs sampled at $1/T$ Hz, the closed-loop poles could be assigned arbitrarily by applying controls at a rate of N/T Hz, where the parameter N was greater than or equal to the controllability index. Araki and Hagiwara (1986) subsequently defined the conditions such that certain controls could be activated at a rate slower than N/T Hz and termed the resultant controller a "Multirate Input Compensator" (MRIC). Additional important contributions related to MRIC design were presented by Kaczorek (1985), Kabamba (1987), and Araki *et al.* (1999), although Liu and Patton (1998) identified that the advantage of non-dynamic compensation was compromised by the likelihood of excessive, oscillatory control activity in the case of plants of large order. These authors demonstrated how this problem could be alleviated by invoking an eigenstructure-assignment technique.

Hagiwara and Araki (1988) examined dynamics-assignment via the complementary sampling strategy, whereby each control was applied at $1/T$ Hz and the outputs sampled at certain integer multiples of this frequency dictated by the relevant observability index. Exploiting the "fast output-sampling" mechanism to emulate full state-feedback, these so-called "Multirate Output Compensators" (MROCs) were always first-order, irrespective of the plant involved. Further theoretical developments in this area have been described by Hagiwara *et al.* (1990), Yen and Wu (1993), and Er *et al.* (1994).

Er and Anderson (1991) evaluated the practical issues associated with this design approach and concluded that MROCs were more suitable for use in industrial applications than MRICs. Nevertheless, a key disadvantage of MROCs concerns the possibility that in certain circumstances the feedback gains could be very large, leading to poor sensitivity to measurement noise.

More recently, Werner (1998) and Viassolo and Rotea (1998) have used Linear Matrix Inequality (LMI) techniques in an attempt to achieve a satisfactory compromise between noise sensitivity and robustness. Furthermore, Werner (1999) investigated the tracking and disturbance rejection properties of MROCs and their ability to cope with nonlinear plants.

Optimal Control

Arguably representing the "core" of modern control theory, researchers have naturally focused a considerable degree of attention on applying optimal control techniques to multirate-sampled configurations. The initial contribution in this area, Amit (1980), recognised that, in common with periodically time-varying single-rate systems, the steady-state solution to the multirate LQG problem was specified by periodic regulator and Kalman filter discrete Riccati equations, thus implying that the optimal controller was periodic with the same period as the sampling schedule. Berg *et al.* (1988) subsequently attempted to produce an acceptable time-invariant counterpart of the optimal multirate control law using constrained optimisation methods. Al-Rahmani and Franklin (1990) proposed a technique in which the optimal multirate control was calculated by solving the continuous-time LQR problem with the control constrained to be a piecewise constant signal. The same authors (Al-Rahmani and Franklin, 1992) then proposed a new approach to multirate LQ regulator synthesis which involved transforming the overall control design by a set of appropriate gains into that of a relatively small-dimensional time-invariant system, for which conventional single-rate techniques could then be applied.

Several papers dealing with multirate LQG control, including Lennartson (1988), Bamieh *et al.* (1991), Meyer (1992) and Colaneri *et al.* (1992), use "lifted" system models, namely, augmented, time-invariant state-variable representations acquired by specifying the control and output signals at the relevant instants during the cyclical sequence of sampling

operations. While conceptually straightforward, this approach may yield system descriptions with large dimensions. Moreover, a further problem concerns the constraints imposed by the requirement that the optimal control law must be causal. However, in spite of this factor, a clear advantage of "lifted" representations is that conventional, single-rate control design methodologies may otherwise be applied directly. Further contributions in this field of a rather detailed technical nature have been provided by Voulgaris *et al.* (1994) and Shu and Chen (1995).

In contrast, exploiting results by Bittanti *et al.* (1988, 1990) pertaining to periodic Riccati equations, Colaneri and De Nicolao (1995) have proposed a method in which the derivation of the optimal control solution uses a time-varying state equation. In an evaluation of the two methodologies, Lee and Oh (2000) conclude that the computational burden associated with the latter approach is lower for sampling mechanisms that are relatively unsynchronised.

Interestingly, a comparative study by Er and Anderson (1992) of the performances of MROCs and corresponding LQG control laws as regulators in the presence of stochastic disturbances revealed that the latter compensator type produced superior results.

Robust Control

Following the development in the 1980s of robust control design methods for continuous-time systems as a response to the perceived deficiencies of LQG control laws, several authors within the last decade have attempted to apply H_∞-optimisation techniques to multirate-sampled discrete-time configurations. In common with several papers dealing with H_2-optimal control, the contributions by Voulgaris and Bamieh (1993), Qiu and Chen (1994), Chen and Qiu (1994) and Voulgaris *et al.* (1994) are based upon lifted system representations, while the H_∞ control solution is derived through constrained model-matching. Recently, again using the lifting approach but representing causality constraints by a set of positive definiteness conditions and coupling criteria, Sågfors *et al.* (2000) derive a two-Riccati equation solution to the multirate H_∞ control problem. A notable feature of this result is that the algebraic Riccati equations are exactly those associated with the H_∞ problem in the absence of any causality constraints.

Adaptive and Predictive Control

Numerous researchers in the last two decades have investigated multirate-sampled feedback systems from an adaptive and/or model-based predictive control standpoint. In the first theoretical contribution in this area, Söderström (1980) proposed minimum-variance control laws for SISO self-tuning feedback systems in which, due to hardware constraints commonly encountered in the process and chemical industries, the plant output measurements were only available at relatively infrequent intervals. Noticing that this sampling mechanism conforms to that of the MRICs discussed previously, Lu *et al.* (1990) established the convergence properties of the controller parameters and incorporated constraints on the control signal in the problem formulation. Independently and employing different approaches, self-tuning controllers with fast-sampling control action were also described by Scattolini (1988), Zhang and Tomizuka (1988) and Carini *et al.* (1990). More recently, Albertos *et al.* (1996) discussed a model-reference adaptive control scheme for slow output-sampled systems which, in contrast to the state space descriptions used elsewhere in this field, employed transfer function models. Subsequently, Arvanitis *et al.* (1999) and Arvanitis *et al.* (2000) have detailed the incorporation of, respectively, the MRIC and MROC algorithms in a modern reference adaptive control setting.

Whereas the above papers attempt to embed a particular control law within an adaptive context, Ling and Lim (1996) describe how, by invoking a state space interpretation of the Generalised Predictive Control strategy (Clarke *et al.*, 1987a,b), it is possible to synthesise fixed controllers for both fast and slow output-sampled multivariable plants. Arguably the contribution which examines controller design from the least restrictive perspective, including multivariable plants with dissimilar sampling intervals at each input and output and the inclusion of pre-filter and actuator nonlinearities, is by Lee *et al.* (1992). These authors explain how the Dynamic Matrix Control approach (see, for example, Garcia *et al.*, 1991), previously applied only to single-rate digital systems, could encompass multirate sampling strategies and described the design of a feedback system for a high-purity distillation column. Beforehand, the related strategy of "inferential control" was employed by Guilandoust *et al.* (1987) to address the slow output-sampling problem. Reflecting the maturity that model-based predictive control has reached within the last decade, Scattolini and Schiavoni (1995) detail controller synthesis via the receding horizon strategy for

multivariable plants with any sampling mechanism.

Frequency-Domain Analysis

In the first paper to investigate the design of multirate-sampled SISO feedback systems, Coffey and Williams (1966) exploited frequency decomposition to propose two methods for acquiring the closed-loop characteristic polynomial of multiloop configurations. While additionally offering an insight into the possible use of classical frequency response techniques, these authors concluded that their approach was computationally cumbersome. Boykin and Frazier (1975a) subsequently explained how the algebraic manipulations entailed in both switch and frequency decomposition could be encapsulated by a lifted system representation in which vector-valued variables were inter-related by matrix-valued operators, whose elements comprised pulse-transfer functions engendered by either decomposition. This paper, which also established the transformation between vectors defined via either decomposition, can be considered to be the first non-state-space contribution to model multirate-sampled systems in a manner compatible with available computational techniques.

The issue of the relative stability of SISO feedback systems containing samplers functioning at non-integer-related rates was examined by Thompson (1986), who used the concept of characteristic gain loci (MacFarlane and Postlethwaite, 1977), customarily employed in continuous-time multivariable control theory, to define gain and phase margins. Moreover, an outline was provided of the possible extension of this approach to specify measures of stability robustness in the multivariable case. Unfortunately, since the frequency responses produced by these loci have no useful interpretation in this context, Thompson's method does not appear to constitute the basis of a simple control design technique. The final significant contribution in this area, by Araki and Yamamoto (1986), extended the Nyquist stability criterion to the multirate-sampled multivariable case.

Miscellaneous Research

Many papers examining particular aspects of multirate digital control theory cannot be strictly classified under the above headings. While the following summary of these is by no means exhaustive, several of the more relevant and interesting contributions within the

last three decades will be assessed.

Motivated by the increasing use of multirate-sampling in digital signal processing (DSP) applications, Meyer and Burrus (1975) detailed the modelling of non-uniform-rate digital filters via a variety of representations which nowadays would be termed "lifted" system descriptions. A further branch of research was opened by Kando and Iwazumi (1986) who, recognising that certain multirate configurations were imposed by plants which could be decomposed into "slow" and "fast" subsystems, described a control design technique based upon singular perturbation theory.

A significant boost to multirate control, exploited in numerous subsequent papers covering optimal and H_∞ feedback system synthesis, came a decade ago with two major contributions. First, Meyer (1990b) and Ravi *et al.* (1990) independently extended the "Youla-Kučera" parameterisation of all stabilising controllers to the multirate/multivariable case using input-output models generated from state-variable descriptions. Secondly, Meyer (1990a) described a new class of shift-varying operator which greatly simplified the modelling of complex multirate-sampled configurations. In fact, this operator was exploited by the same author in his treatment of the multirate LQG problem described above. Nonetheless, as demonstrated by Longhi (1994) in an analysis of the reachability, controllability and stabilisability of multirate sampled-data systems, several problems remained unresolved until fairly recently.

Despite the major theoretical developments taking place, several papers addressing more practical issues continued to be published in the 1990s. Moore *et al.* (1993) investigated both fast input- and fast output-sampled SISO digital feedback schemes from a perspective of pole-placement and inter-sample response and concluded that the former configuration was likely to prove impracticable. In contrast, Berger and Peduto (1997) exploited the design freedom afforded by fast input-sampling to improve stability margins, while Er *et al.* (1994) did likewise with the fast output-sampling scheme. However, none of these papers considered the system response to exogenous disturbance signals.

As stated previously, this literature survey is intended to focus only upon key contributions to multirate sampled-data theory and, in particular, papers of significant relevance to this thesis. Further details of recent developments in multirate digital control can be

found in the survey paper by Araki (1993), while Bittanti and Colaneri (1998) summarise the techniques available to analyse both multirate-sampled and periodically time-varying systems.

1.3 Polynomial Equations Approach

Linear control theory has often been characterised as being either "classical" (i.e., pre–1960) or "modern" (post–1960). Although these dates and terms are somewhat arbitrary, classical control is usually understood to involve design techniques predicated upon scalar transfer function models, while modern control concerns the plethora of contributions addressing issues related to both the analysis and synthesis of feedback systems in which state-space descriptions are used. Despite the attraction that control design via frequency responses held for engineers, it became apparent that models involving the arrangement of differential/difference equations in matrix-vector format were computationally advantageous, while the related controller synthesis procedures addressed multivariable problems reasonably satisfactorily. However, Rosenbrock (1970) renewed interest in the transfer function-based approach by extending the original theory to the multivariable case, developing a simple design technique known as the Inverse Nyquist Array method and, significantly, drawing parallels with, and providing deeper insight into, the burgeoning state-space approach.

By the mid-1970s, a technique which, following the acquisition of the solution to two Riccati equations, entailed deriving an LQG compensator transfer function via a procedure known as Loop Transfer Recovery (LTR), had become the norm in multivariable control design within certain quarters. Nonetheless, in the light of Rosenbrock's work, some researchers began to investigate the derivation of optimal control laws from an input-output perspective. While a scalar result had been published some time previously (see Newton *et al.*, 1957), the theory applied only to open-loop stable plants. Working independently, Youla *et al.* (1976a,b) and Kučera (1979) defined both the input-output LQG result and the "Youla-Kučera" parameterisation of all stabilising controllers in terms of polynomial matrix fractions and diophantine equations. Consequently, methods arising from this work are referred to as using the "polynomial equations" approach.

In fact, since difference equation representations are familiar to the system identification fraternity, several key contributions in the area of self-tuning control (see, for example Peterka, 1972, Åström and Wittenmark, 1973, Clarke and Gawthrop, 1975) had already used scalar polynomial models. Nevertheless, many of the developments in the theory relating to the polynomial equations approach are credited to Kučera and fellow Czech researchers, including Ježek and Šebek (see, for example Ježek, 1982, Ježek and Kučera, 1985, Šebek, 1981, Šebek and Kučera, 1981, 1982, Kučera and Šebek, 1984).

A valid criticism of the polynomial equations approach was that, while proffering intuitive appeal, the computational requirements were much more demanding than those associated with state space methods. However, many of these drawbacks have been solved with the advent of POLYNOMIAL TOOLBOX, a computer-aided control analysis and design package operating in a MATLAB environment. This software implements fast and reliable algorithms to compute, for example, deadbeat or pole-placement control laws, the parameterisation of all stabilising controllers and LQG and H_∞ compensators. Further details on POLYNOMIAL TOOLBOX can be found in Šebek *et al.* (1998) and Kwakernaak and Šebek (1999).

1.4 Aims & Outline of Thesis

This thesis describes the modelling and design of multirate sampled-data feedback systems via the polynomial equations approach. The primary theoretical objective is to embed the principles underpinning and algebra related to the frequency and switch decomposition techniques within a modern control framework, thus encompassing multivariable configurations driven by stochastic inputs and facilitating analysis by available software packages. A further goal concerns the utilisation of polynomial system representations to synthesise multirate-sampled control systems by minimising quadratic performance criteria.

The thesis is arranged in the following manner.

Chapter Two

This chapter reviews the prerequisite background theory related to multirate-sampled system analysis and clarifies concepts that are central to the thesis. Following definitions of

the time-scales concerned, the pulse-transform and pulse-transfer functions and modelling techniques using the frequency and switch decompositions are outlined. A simple example demonstrates the practical application of the two techniques.

Chapter Three

Chapter 3 describes how the decomposition procedures can be subsumed within the framework of the polynomial equations approach. Specifically, by decomposing a multirate-sampled configuration into input, "discretised plant" and output subsystems, it is established that an initial difference equation description can be systematically organised in matrix-vector format. Subsequent manipulations and the designation of a time-to frequency-domain transformation reveal that dual models possessing physically-distinct interpretations can be defined for any scalar multirate digital system. The designation of a compatible stochastic disturbance subsystem model warrants the formulation of an overall "lifted" representation, while a numerically simple case study illustrates the methods involved.

Chapter Four

The scalar modelling techniques detailed in Chapter 3 are generalised to encompass multivariable configurations in this chapter. While the basic modelling approach remains unchanged, the use of matrix fraction representations in place of scalar pulse-transfer functions implies that the resultant system models cannot be specified in such detail. Following the derivation of an overall plant description, attention focuses upon establishing a corresponding representation of the digital controller. In both instances, the arrangement of signals within vectors in accordance with their related sampling instants prescribes particular matrix structures, which conveniently illuminate causality issues. This chapter concludes with an examination of stability robustness measures and an associated illustrative example.

Chapter Five

This chapter is concerned with explaining how the foregoing polynomial system models can be used in conjunction with established control synthesis methodologies. In the adopted

approach, initial considerations of the multirate LQG and predictive regulator problems are modified progressively to include controller integral action and the incorporation of dynamic weighting matrices within the cost function. Several examples are employed to illustrate the procedures utilised.

Chapter Six

The thesis concludes in this chapter with a summary of the principal results and contributions, in addition to a brief outline of possible areas for further research.

Chapter Two
Background Theory

When all sampling operations within a linear sampled-data system are performed at a uniform interval, difference equation or transfer function models can be acquired by using the z-transform. However, if at least one sampling switch is functioning at a dissimilar rate, the familiar single-rate pulse-transform theory cannot be applied directly. It is therefore the aim of this chapter to describe the modifications to the z-transform approach required to address multirate-sampled configurations. The principles established here will be exploited subsequently in the formulation of a polynomial-orientated methodology for multirate digital system modelling in Chapter 3.

This chapter begins with an appropriate definition of the term "multirate", following which two key time-scales are designated. Prior to introducing the two traditional analytical techniques of frequency and switch decomposition, the definition of the z-transform, from both a time- and frequency-domain perspective, is considered, leading subsequently to the designation of pulse-transfer functions. To conclude the chapter, an illustrative example will demonstrate the use of the decomposition methods.

2.1 Problem Definition

It is important to provide a suitable definition of the term "multirate" at the outset. In a review of sampled-data systems, Jury (1961) highlighted a variety of possible sampling strategies, including cyclic-rate and random sampling, in addition to multirate sampling which was specified simply as a sequence of sampling operations which occurred at different rates. In this thesis, "multirate sampling" will define a scenario in which, while individual sampling operations take place at dissimilar intervals, the overall sampling sequence is periodic. The latter statement can be interpreted as implying that the ratios between each pair of sampling rates is a rational, rather than an irrational, number.

2.2 Time-Scales

The periodic nature of a multirate sampling schedule dictates that analysis is based upon two time frames (Kalman and Bertram, 1959), which are referred to in this thesis as the "short time interval" (STI) and the "repetitive time interval" (RTI). The short time interval may be construed as the shortest interval which may elapse between consecutive sampling operations, while the repetitive time interval is specified as the period of the overall sampling sequence.

Consequently, if the sampling operations in a multirate-sampled system take place at intervals of $T/K_1, T/K_2, \ldots, T/K_v$ seconds (abbreviated hereafter to "s"), $K_i \in \mathbb{Z}$, where the K_i's are assumed to be relatively prime, the short time interval and the repetitive time interval can be designated as follows:

$$STI = T/\text{lcm}(K_1, K_2, \ldots, K_v) \triangleq T/N \tag{2.1a}$$

and

$$RTI = T/\text{gcd}(K_1, K_2, \ldots, K_v) \triangleq T, \tag{2.1b}$$

where $\text{lcm}(\cdot)$ and $\text{gcd}(\cdot)$ represent "the least common multiple of" and "the greatest common divisor of", respectively. Thus, for example, in the case of a system in which sampling operations occur at intervals of 0.6 s and 0.4 s, the short time interval and the repetitive time interval are defined as $T/6$ and T respectively, where, observing that $K_1 = 2$, $K_2 = 3$ and $N = 6$, $T = 1.2$ s.

2.3 Pulse-Transform Identities

It is useful to provide two definitions of the pulse-transform at this juncture. With regard to the system depicted in Figure 2.1, in which $x(t)$ is assumed to be one-sided (namely, $x(t) = 0$, $t < 0$), the output of the sampler is $\{x(0), x(T/K), x(2T/K), \ldots\}$. The z_K-transform of $\{x(iT/K)\}$, $X_K(z_K)$, is then designated as:

$$X_K(z_K) = Z_K\{x(iT/K)\} = \sum_{i=0}^{\infty} x(iT/K) z_K^{-i}, \quad z_K = e^{sT/K}. \tag{2.2}$$

An alternative, "frequency-domain" definition of the pulse-transform results from consideration of Figure 2.2, in which the sampled representation $x^{\star K}(t)$ is assumed to be

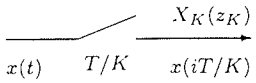

Figure 2.1. Sampling – time-domain interpretation.

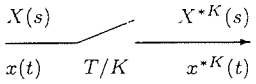

Figure 2.2. Sampling – frequency-domain interpretation.

engendered by modulating the continuous-time signal $x(t)$ by a sequence of impulses, namely,

$$\sum_{l=-\infty}^{\infty} \delta(t - lT/K),$$

where $\delta(\cdot)$ denotes the Dirac impulse function. As shown by, for example Åström and Wittenmark (1997), it can be established that

$$X^{\star K}(s) = \frac{K}{T} \sum_{m=-\infty}^{\infty} X(s + jm\omega_K), \quad \omega_K = 2\pi K/T, \tag{2.3}$$

in which $X(s)$ and $X^{\star K}(s)$ denote the Laplace transforms of, respectively, $x(t)$ and $x^{\star K}(t)$ and where $X^{\star K}(s)$ and $X_K(z_K)$ ((2.2)) are related thus:

$$X_K(z_K) = X^{\star K}(s) \Big|_{s=\frac{K}{T}\ln z_k}.$$

2.4 The Pulse-Transfer Function

Equation (2.2) may be used to obtain the pulse-transfer function of a system enclosed by input and output samplers operating at T/K s. Thus, if the impulse response of the system $\tilde{G}(s)$ is denoted by $\tilde{g}(t)$, the pulse-transfer function related to $\tilde{G}(s)$ is given by

$$\tilde{G}_K(z_K) \triangleq Z_K\left\{\tilde{g}(iT/K)\right\}. \tag{2.4}$$

However, henceforth it will be assumed that plant input data is extrapolated by means of a zero-order hold (ZOH). Accordingly, the transfer function $\tilde{G}(s)$ will incorporate a zero-order hold and therefore may be specified as:

$$\tilde{G}(s) = G(s)H^{(K)}(s), \quad H^{(K)}(s) = \left(1 - e^{-sT/K}\right)/s, \tag{2.5}$$

in which $G(s)$ denotes the plant transfer function.

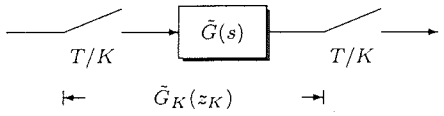

Figure 2.3. Open-loop sampled system.

2.5 Frequency Decomposition

The key problem in pulse-transform/pulse-transfer function analysis lies in relating the pulse-transforms of signals that are sampled at different rates. In this respect, consider the combinations of sampling switches illustrated in Figure 2.4, in which it is assumed (see (2.1a)):

$$J = LK, \quad L > 1.$$

Since the "fast-sampling" of a "slow-sampled" sequence will replicate the original waveform, the situation shown in Figure 2.4(a) may be summarised thus:

$$X_J(z_J) = X_K(z_K). \tag{2.6}$$

Although mathematically trivial, this scenario nonetheless has a practical application whereby the insertion of "fictitious" fast-rate samplers within a multirate sampled-data system can provide a useful analytical tool.

The complementary configuration is dealt with by exploiting the frequency-shift property of the pulse-transform as follows. With a slight abuse of notation, noticing from equation (2.3) that:

$$X_J\left(z_J e^{j2\pi p/L}\right) = \frac{J}{T}\sum_{l=-\infty}^{\infty} X\left(s + jl\omega_J + jp\omega_K\right), \quad \omega_J = \omega_K/L, \quad p \in [0, L-1],$$

then

$$\begin{aligned}\sum_{p=0}^{L-1} X_J\left(z_J e^{j2\pi p/L}\right) &= \frac{J}{T}\sum_{p=0}^{L-1}\sum_{l=-\infty}^{\infty} X\left(s + jl\omega_J + jp\omega_K\right) \\ &= \frac{J}{T}\sum_{m=-\infty}^{\infty} X\left(s + jm\omega_K\right),\end{aligned}$$

whence, again from equation (2.3),

$$X_K(z_K) \triangleq Z_K\left\{X_J(z_J)\right\} = \frac{1}{L}\sum_{p=0}^{L-1} X_J\left(z_J e^{j2\pi p/L}\right). \tag{2.7}$$

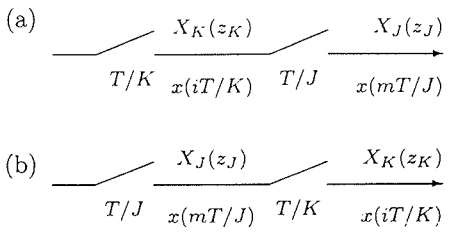

Figure 2.4. Combinations of sampling switches.

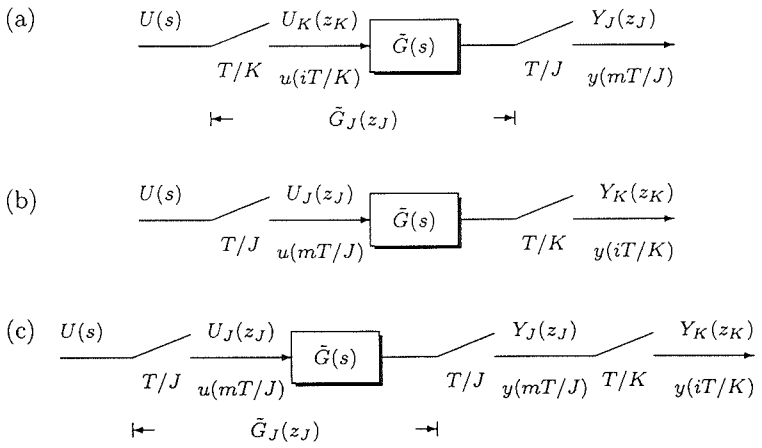

Figure 2.5. Multirate-sampled systems.

The above result, presented originally by Sklansky and Ragazzini (1955) and which equally may be derived from the "time-domain definition" of the pulse-transform ((2.2)), is known as "frequency decomposition".

The foregoing theory can be used to establish pulse-transform/pulse-transfer function models of the multirate-sampled systems depicted in Figures 2.5(a) and (b). In the slow input/fast output-sampled plant of Figure 2.5(a), for example, the relationship between the pulse-transforms $Y_J(z_J)$ and $U_K(z_K)$ is:

$$Y_J(z_J) = \tilde{G}_J(z_J)U_K(z_K). \tag{2.8}$$

It is convenient to analyse the complementary situation (see Figure 2.5(b)), namely, a fast input/slow output-sampled system, by introducing a "fictitious" sampler, operating at the relatively fast rate of T/J s, at the plant output. Thus, as shown in Figure 2.5(c), it is possible to define the pulse-transfer function $\tilde{G}_J(z_J)$ and, consequently, model the system

utilising equation (2.7) as follows:

$$Y_J(z_J) = \tilde{G}_J(z_J)U_J(z_J), \tag{2.9}$$

whence $$Y_K(z_K) \triangleq Z_K\{Y_J(z_J)\} = \frac{1}{L}\sum_{p=0}^{L-1} \tilde{G}_J\left(z_J e^{j2\pi p/L}\right) U_J\left(z_J e^{j2\pi p/L}\right). \tag{2.10}$$

Equations (2.8) and (2.10) demonstrate a salient feature of multirate sampled-data systems in comparison with conventionally-sampled configurations, where, although it is possible to define the pulse-transfer function $\tilde{G}_J(z_J)$ in the former instance, no "explicit" pulse-transfer function relating $Y_K(z_K)$ to $U_J(z_J)$ can be acquired from equation (2.10). Consequently, equation (2.10) is referred to as representing an "implicit" pulse-transfer function.

2.6 Switch Decomposition

The second analytical tool facilitating the input-output analysis of multirate sampled-data systems is known as "switch decomposition" (Kranc, 1957). As illustrated in Figure 2.6, this technique warrants the substitution of a sampling switch functioning at intervals of T/K s with a set of K parallel forward paths, each comprising a cascade connection of a time advance of iT/K s, a sampler operating at T s (namely, the repetitive time interval (see (2.1a))) and a time delay of iT/K s, $i = 0, 1, \ldots, K-1$. The chief advantage of the switch decomposition method thus concerns its reliance upon a single pulse-transform, albeit at the expense of the requirement to evaluate numerous pulse-transfer functions by the modified z-transform.

Thus the slow input/fast output-sampled configuration of Figure 2.7(a) can be modelled by Figure 2.7(b), in which, for notational concision, $A^{(j)}$ and $D^{(j)}$ represent, the transfer functions $e^{jsT/K}$ and $e^{-jsT/K}$, respectively, and $X^{(j)}(z)$ denotes the z-transform of the sequence $\{x(kT + jT/N)\}$. Accordingly, it can be established that

$$Y^{(j)}(z) = Z\left\{\tilde{G}(s)e^{jsT/K}\right\}U(z), \quad j = 0.1, \ldots, K-1. \tag{2.11}$$

The complementary scenario, shown in Figure 2.8, is modelled thus:

$$Y(z) = Z\left\{\tilde{G}(s)e^{-jsT/K}\right\}U^{(j)}(z), \quad j = 0.1, \ldots, K-1. \tag{2.12}$$

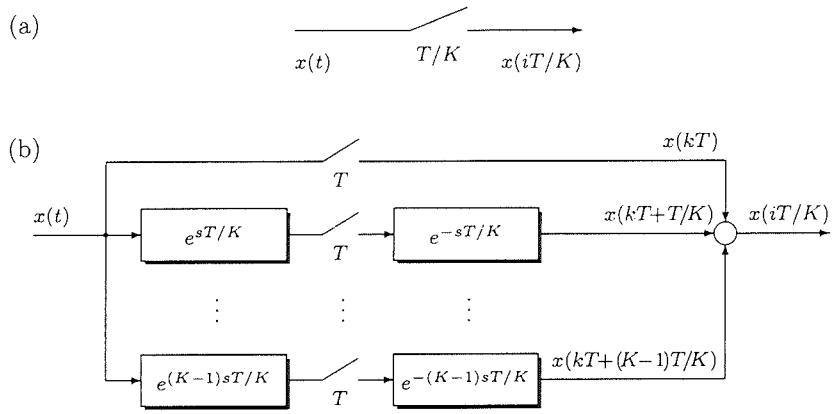

Figure 2.6. The switch decomposition technique.

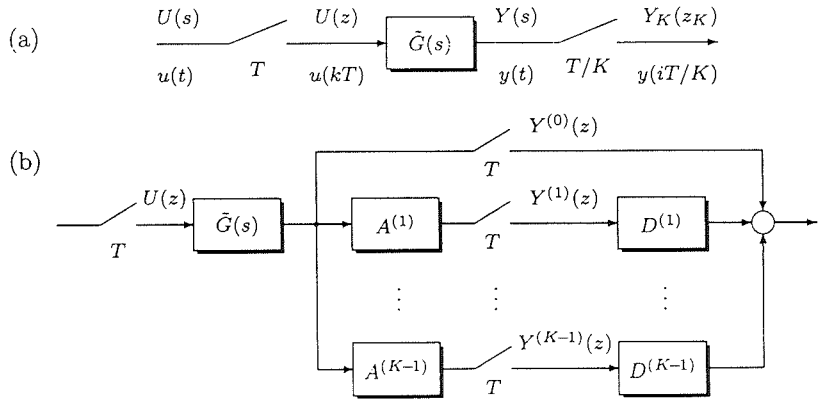

Figure 2.7. Slow input/fast output sampled system.

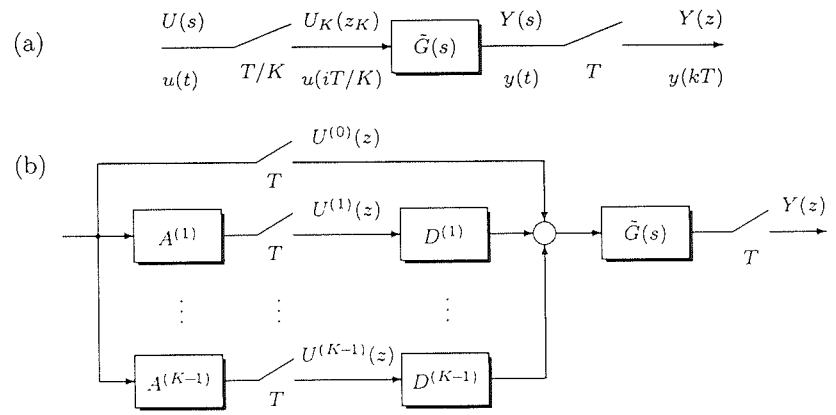

Figure 2.8. Fast input/slow output sampled system.

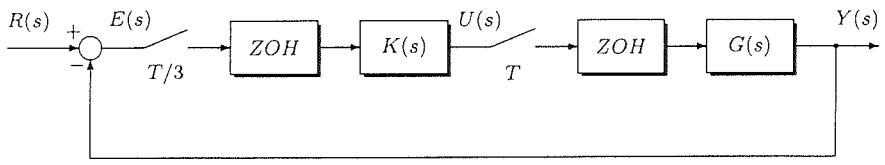

Figure 2.9. Multirate sampled-data feedback system.

2.7 Illustrative Example

The use of each of the analytical techniques in this chapter will be demonstrated by acquiring alternative models of the multirate sampled-data feedback system illustrated in Figure 2.9. In this example it is supposed that the plant and controller transfer functions are,

$$G(s) = \frac{1}{s-1} \quad \text{and} \quad K(s) = \frac{2.6(s+0.8071)}{s},$$

while the sampling period T and ratio N are given by

$$T = 0.2859 \ (= 3\ln 1.1) \quad \text{and} \quad N = 3.$$

Pulse-Transform/Pulse-Transfer Function Analysis

As illustrated in Figure 2.10, the first stage in establishing a pulse-transform/pulse-transfer function description of the feedback system concerns the insertion of fictitious fast-rate samplers at the plant and controller outputs. The discretised pulse-transfer functions $\tilde{G}_N(z_N)$ and $\tilde{K}_N(z_N)$ can then be defined as:

$$\begin{aligned}\tilde{G}_N(z_N) &= Z_N\left\{G(s)H^{(1)}(s)\right\} \\ &= \frac{z_3-1}{z_3} Z_3\left\{\frac{1}{s(s-1)}\right\} = \frac{0.1\left(z_3^2+z_3+1\right)}{(z_3-1.1)\,z_3^2}\end{aligned} \tag{2.13}$$

and

$$\begin{aligned}\tilde{K}_N(z_N) &= Z_N\left\{K(s)H^{(3)}(s)\right\} \\ &= \frac{(z_3-1)}{z_3} Z_3\left\{\frac{2.6\,(s+0.8071)}{s^2}\right\} = \frac{2.6z_3-2.4}{z_3-1}.\end{aligned} \tag{2.14}$$

The pulse-transforms of the output ($Y_N(z_N)$), control ($U(z)$), fast-sampled control ($U_N(z_N)$), error ($E_N(z_N)$) and reference ($R_N(z_N)$) signals are related thus:

$$Y_N(z_N) = \tilde{G}_N(z_N)U(z), \tag{2.15}$$

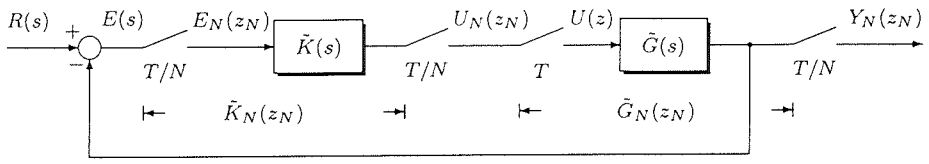

Figure 2.10. Insertion of fast-rate samplers.

$$U(z) = Z\left\{U_N(z_N)\right\}, \tag{2.16}$$

$$U_N(z_N) = \tilde{K}_N(z_N)E_N(z_N) \tag{2.17}$$

and
$$E_N(z_N) = Z_N\left\{R(s) - Y(s)\right\} = R_N(z_N) - Y_N(z_N). \tag{2.18}$$

Combining equations (2.15), (2.16), (2.17) and (2.18), and using equation (2.7) to evaluate

$$Q(z) = Z\left\{\tilde{K}_N(z_N)\tilde{G}_N(z_N)\right\} = \frac{0.9226z - 0.7238}{(z-1)(z-1.331)},$$

the following input-output model is obtained:

$$\begin{aligned} Y_N(z_N) &= \frac{\tilde{G}_N(z_N)Z\left\{\tilde{K}_N(z_N)R_N(z_N)\right\}}{1+Q(z)} \\ &= \frac{0.1\left(z_3^2+z_3+1\right)\left(z_3^2+1.1z_3+1.21\right)Z\left\{(2.6z_3-2.4)\left(z_3^2+z_3+1\right)R_N(z_N)\right\}}{z_3^2\left(z^2-1.4084z+0.6072\right)}. \end{aligned}$$

Switch Decomposition

Replacing the fast-rate sampling switch at the controller input and a fictitious sampler at the plant output with a set of forward paths consisting of a time advance of $iT/3$ s, a switch operating at T s and a time delay of $iT/3$ s, $i = 0, 1, 2$, the feedback system may be viewed as represented by Figure 2.11.

The configuration is described thus:

$$Y^{(i)}(z) = Z\left\{\tilde{G}(s)e^{isT/3}\right\}U(z), \quad i = 0, 1, 2, \tag{2.19}$$

$$U(z) = Z\left\{\tilde{K}(s)e^{-isT/3}\right\}E^{(i)}(z), \quad i = 0, 1, 2, \tag{2.20}$$

and
$$E^{(i)}(z) = R^{(i)}(z) - Y^{(i)}(z), \quad i = 0, 1, 2, \tag{2.21}$$

where

$$Z\left\{\tilde{G}(s)\right\} = \frac{0.331}{z-1.331}, \quad Z\left\{\tilde{G}(s)e^{sT/3}\right\} = \frac{0.1z+0.231}{z-1.331},$$

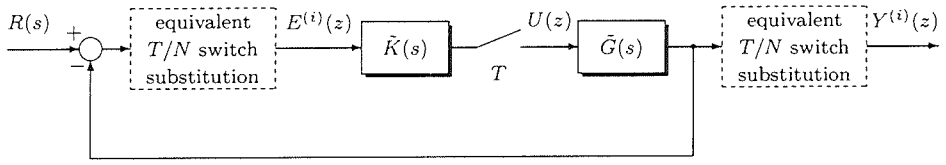

Figure 2.11. Switch decomposition model of feedback system.

$$Z\left\{\tilde{G}(s)e^{2sT/3}\right\} = \frac{0.21z + 0.121}{z - 1.331}, \quad Z\left\{\tilde{K}(s)\right\} = \frac{2.6z - 2.4}{z - 1}$$

and $$Z\left\{\tilde{K}(s)e^{-sT/3}\right\} = Z\left\{\tilde{K}(s)e^{-2sT/3}\right\} = \frac{0.2}{z - 1}.$$

Uniting equations (2.19), (2.20) and (2.21), the following input-output model is obtained:

$$Y^{(i)}(z) = \frac{Z\left\{\tilde{G}(s)e^{isT/3}\right\}\left(\sum_{i=0}^{2} Z\left\{\tilde{K}(s)e^{-isT/3}\right\}R^{(i)}(z)\right)}{1 + Q(z)}, \quad i = 0, 1, 2, \tag{2.22}$$

where $$Q(z) = \sum_{i=0}^{2} Z\left\{\tilde{K}(s)e^{-isT/3}\right\} Z\left\{\tilde{G}(s)e^{isT/3}\right\}.$$

Thus, for example, the pulse-transform $Y^{(1)}(z)$ is

$$Y^{(1)}(z) = \frac{(0.1z + 0.231)\left((2.6z - 2.4)\,R^{(0)}(z) + 0.2R^{(1)}(z) + 0.2R^{(2)}(z)\right)}{z^2 - 1.4084z + 0.6072}.$$

2.8 Conclusion

This chapter has established the basic concepts involved in the modelling of multirate-sampled systems, including the definitions of the pulse-transform and pulse-transfer function. The frequency and switch decomposition procedures outlined here are central to subsequent developments. The demonstrations of the alternative methodologies in the illustrative example confirms that, in comparison with analogous conventionally-sampled digital configurations, multirate-sampled systems analysis is likely to be problematic in all but the simplest cases and impractical without the assistance of dedicated software.

Chapter Three

A Polynomial Modelling Approach

The modelling of scalar multirate-sampled systems by polynomial methods is addressed in this chapter. Specifically, by defining sampled signals as vector-valued variables, the manipulations entailed in analysing multirate digital configurations may then be set within the framework of matrix algebra. In contrast to single-rate sampled-data system analysis, where pulse-transform/pulse-transfer function representations can be derived readily from difference equation models and vice-versa, a notable feature of the polynomial modelling approach concerns the existence of dual, but distinct, time- and frequency-domain system descriptions.

The chapter commences with the examination of a system in which the ratio between the faster and slower of the input and output sampling rates is a rational number, as opposed to an integer. The incorporation of "fictitious" fast-rate sampling switches and definition of certain backward-shift operators then facilitates the formulation of a difference equation model. In the next section, attention focuses upon the structure and properties of the polynomial matrices engendered by arranging sets of cyclically time-varying difference equations in matrix-vector format. The corresponding matrices in an alternative "frequency-domain" representation emanating from the principle of frequency decomposition discussed in Chapter 2 are subsequently specified, in addition to the transformation that relates variables in the time- and frequency-domains. The treatment of stochastic disturbance models in a multirate-sampling context and, in particular, the related problem of sampling rate compatibility, is then described. An illustrative example concludes the chapter.

3.1 Difference Equation Models

This section establishes the salient principles supporting the development of all subsequent polynomial models and concludes in a time-domain interpretation of a pulse-transform/pulse-transfer function description. Of particular significance in this respect

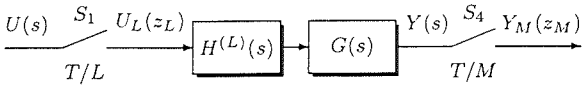

Figure 3.1. Multirate-sampled configuration.

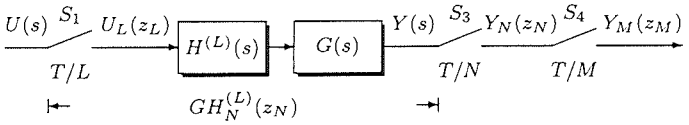

Figure 3.2. Introduction of "fictitious" fast-rate sampler at plant output.

are the designation of particular subsystems created by introducing "fictitious" fast-rate samplers, the definition of the repetitive time interval and the specification of the relevant backward-shift operators.

The multirate-sampled configuration to be considered is illustrated in Figure 3.1, with switches labelled as S_1 and S_4 functioning at intervals of T/L s and T/M s respectively, where it is assumed that L and M are prime. Thus, from the definitions (2.1a,b), the short time interval (STI) and the repetitive time interval (RTI) are defined as:

$$STI = T/\text{lcm}(L, M) = T/LM = T/N \tag{3.1a}$$

and

$$RTI = T/\text{gcd}(L, M) = T. \tag{3.1b}$$

Figure 3.2 illustrates the initial modification to the block diagram model of Figure 3.1, which involves the introduction of the "fictitious" fast-rate switch S_3 at the plant output. As examined in Chapter 2 (see (2.9) and (2.10)), this artifice justifies the modelling of the plant by combining an "explicit" pulse-transform/pulse-transfer function expression with frequency decomposition ((2.7)) as follows:

(S_1 to S_3)
$$Y_N(z_N) = GH_N^{(L)}(z_N)U_L(z_L), \tag{3.2}$$

where
$$GH_N^{(L)}(z_N) = Z_N\left\{G(s)H^{(L)}(s)\right\} = Z_N\left\{\frac{G(s)}{s}\right\}\frac{(z_N^M - 1)}{z_N^M}$$ and

(S_3 to S_4)
$$Y_M(z_M) = \frac{1}{L}\sum_{p=0}^{L-1} Y_N\left(z_N e^{j2\pi p/L}\right), \tag{3.3}$$

in which (see (2.2)), $z_N = z^{1/N}$, $z_L = z_N^M = z^{1/L}$ and $z_M = z_N^L = z^{1/M}$.

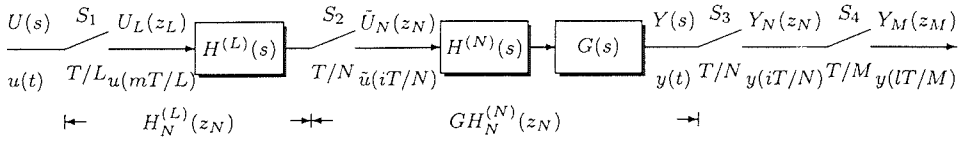

Figure 3.3. Introduction of "fictitious" sampler & zero-order hold at plant input.

In the second alteration to the original block diagram configuration revealed in Figure 3.3, a "fictitious" fast-rate sampler labelled S_2 and associated zero-order hold (ZOH) $H^{(N)}(s)$ are installed at the plant input. The relationship between the pulse-transforms $Y_N(z_N)$ and $U_L(z_L)$, defined originally in equation (3.2), is now given by:

$$(S_2 \text{ to } S_3) \qquad Y_N(z_N) = GH_N^{(N)}(z_N)\bar{U}_N(z_N), \tag{3.4}$$

where $$GH_N^{(N)}(z_N) = Z_N\left\{G(s)H^{(N)}(s)\right\} = Z_N\left\{\frac{G(s)}{s}\right\}\frac{(z_N-1)}{z_N} \quad \text{and}$$

$$(S_1 \text{ to } S_2) \qquad \bar{U}_N(z_N) = H_N^{(L)}(z_N)U_L(z_L), \tag{3.5}$$

where $$H_N^{(L)}(z_N) = Z_N\left\{H^{(L)}(s)\right\} = \frac{z_N}{(z_N-1)}\frac{\left(z_N^M-1\right)}{z_N^M}.$$

Since it is apparent from comparison of equations (3.4) and (3.5) with equation (3.2) that

$$GH_N^{(N)}(z_N)H_N^{(L)}(z_N) = GH_N^{(L)}(z_N),$$

the above modification has no effect upon the dynamics of the system. However, the overall configuration may now be construed as comprising three subsystems: a discretised plant/fast-rate zero-order hold (with pulse-transfer function $GH_N^{(N)}(z_N)$), a discretised slow input-sampled zero-order hold (with pulse-transfer function $H_N^{(L)}(z_N)$) and a sampling rate converter at the output (with pulse-transforms related via frequency decomposition).

The first stage involved in developing an equivalent time-domain model concerns the definition of the repetitive time interval. Denoting the instants at which the samplers functioning at T/L s and T/M s close in synchronisation as

$$t = \ldots, (k-1)T, kT, (k+1)T, \ldots,$$

the repetitive time interval is defined as

$$t \in ((k-1)T, kT]. \tag{3.6}$$

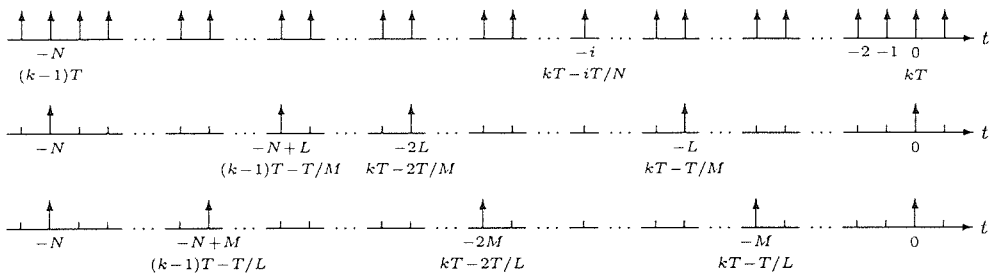

Figure 3.4. Sampling schedule.

Consequently, as revealed by the sampling schedule illustrated in Figure 3.4, the repetitive time interval encompasses the N fast-rate sample instants $t = (k-1)T + T/N$ $(= kT - (N-1)T/N)$ to $t = kT$.

In view of subsequent developments, it is useful to list the sampling instants retrogressively from $t = kT$ and to simplify the notation thus:

$$x(kT - iT/N) \triangleq x(-i), \quad i \in [0, N-1], \tag{3.7}$$

where $x(\cdot)$ represents any of the signals $y(\cdot)$, $u(\cdot)$ and $\bar{u}(\cdot)$. The backward-shift operators related to z_M, z_L, z_N and z may now be specified as:

$$q_M^{-1}x(-i) = x(-i-L) = q_N^{-L}x(-i), \tag{3.8a}$$

$$q_L^{-1}x(-i) = x(-i-M) = q_N^{-M}x(-i), \tag{3.8b}$$

$$q_N^{-1}x(-i) = x(-i-1) \tag{3.8c}$$

and

$$q^{-1}x(-i) = x(-i-N) = q_N^{-N}x(-i), \tag{3.8d}$$

whose significance is distinct from that of the respective complex variables z_M^{-1}, z_L^{-1}, z_N^{-1} and z^{-1}.

It is assumed that the n^{th}-order plant $G(s)$ is strictly proper, but may contain an inherent time delay of τ s. Thus, if $G(s)$ is written as

$$G(s) = G_p(s)e^{-\tau s},$$

then the pulse-transfer function $GH_N^{(N)}(z_N)$ is given by

$$GH_N^{(N)}(z_N) = \frac{b_0 z_N^{n_b} + b_1 z_N^{n_b-1} + \ldots + b_{n_b}}{z_N^d \left(z_N^n + a_1 z_N^{n-1} + \ldots + a_n\right)}, \tag{3.9a}$$

where, with $\upsilon \in \mathbb{Z}$, $\begin{cases} \tilde{d} = \upsilon, & \text{and} \quad n - n_b = 1, \quad \tau = \upsilon T/N \\ \tilde{d} = \upsilon + 1, & \text{and} \quad n - n_b = 0, \quad \upsilon T/N < \tau < (\upsilon + 1)T/N. \end{cases}$

However, in view of ensuing developments in the control design methodologies described in later chapters which favour the use of reciprocal pulse-transform operators, it is convenient to redefine $GH_N^{(N)}(z_N)$ as:

$$GH_N^{(N)}(z_N) = z_N^{-d} \frac{B_N(z_N^{-1})}{A_N(z_N^{-1})}, \tag{3.9b}$$

with $A_N(z_N^{-1}) = 1 + a_1 z_N^{-1} + \ldots + a_n z_N^{-n}$, $B_N(z_N^{-1}) = b_0 + b_1 z_N^{-1} + \ldots + b_{n_b} z_N^{-n_b}$ and $d = \tilde{d} + n - n_b \, (\geq 1)$, and where it is supposed that $A_N(z_N^{-1})$ and $B_N(z_N^{-1})$ do not contain a common factor.

It is now possible to specify a difference equation representation of the multirate-sampled system, which was modelled originally by the pulse-transform/pulse-transfer function relationships in equations (3.5), (3.4) and (3.3) that define each of the three subsystems. The control signal is held constant for a sample interval of T/L s due to the presence of the zero-order hold; therefore, the fast-sampled controls $\bar{u}(\cdot)$ are related to the slow-sampled controls $u(\cdot)$ during the repetitive time interval as follows:

$$\begin{aligned} (S_1 \text{ to } S_2) \qquad & \bar{u}(-i) = u(0), && i = 0, \\ & \bar{u}(-i) = u(-lM), && i = (l-1)M+1, (l-1)M+2, \ldots, lM, \\ & && l = 1, 2, \ldots, L-1; \\ & \bar{u}(-i) = u(-N) = q^{-1}u(0), && i = N-M+1, N-M+2, \ldots, N-1. \end{aligned} \tag{3.10}$$

The discretised plant/zero-order hold combination yields the set of N difference equations:

$$\begin{aligned} (S_2 \text{ to } S_3) \qquad A_N(q_N^{-1})y(-i) &= q_N^{-d} B_N(q_N^{-1})\bar{u}(-i) \\ &= B_N(q_N^{-1})\bar{u}(-i-d), \quad i = 0, 1, \ldots, N-1. \end{aligned} \tag{3.11}$$

Finally, the sampling rate conversion at the system output may be summarised thus:

$$(S_3 \text{ to } S_4) \qquad y^{(M)}(-i) = \begin{cases} y(-mL), & i = mL, \quad m = 0, 1, \ldots, M-1 \\ 0, & \text{otherwise.} \end{cases} \tag{3.12}$$

3.2 A Time-Domain Polynomial System Model

While the difference equation model specified by equations (3.10), (3.11) and (3.12) is perfectly satisfactory from a theoretical perspective, it is neither readily compatible with available computational techniques nor particularly beneficial from an analytical perspective. Consequently, the purpose of this section is to develop a systematic means of arranging sets of difference equations in matrix-vector format and, thereafter, to identify the structures of, and properties related to, the polynomial matrices involved.

Utilising for the moment a framework in which the sampling periods concerned are T/J s and T/K s, where

$$JK = N, \quad J \in \{1, L, M\}, \tag{3.13}$$

the following notational abbreviation, based on the fast Fourier transform, is introduced:

$$e^{j2\pi/K}\left(= e^{j2\pi J/N}\right) = w_K = w_N^J. \tag{3.14}$$

The modelling approach originates by observing that the term $1 - \xi^K q_J^{-1}$, $\xi \in \mathbb{C}$, can be factorised thus:

$$\begin{aligned} 1 - \xi^K q_J^{-1}\left(= 1 - \xi^K q_N^{-K}\right) &= \prod_{p=0}^{K-1}\left(1 - \xi q_N^{-1} w_N^{-Jp}\right) \\ &= \left(1 - \xi q_N^{-1}\right)\left(1 + \sum_{i=1}^{K-1} \xi^i q_N^{-i}\right). \end{aligned} \tag{3.15}$$

Defining the polynomial $F_N(q_N^{-1})$ as

$$F_N(q_N^{-1}) = 1 + \sum_{i=1}^{n_f} f_i q_N^{-i} = \prod_{j=1}^{n_f}\left(1 - \xi_j q_N^{-j}\right), \tag{3.16}$$

the factorisation specified in equation (3.15) indicates that a related polynomial $\bar{F}_N^{(J)}(q_N^{-1})$ can be designated as

$$\bar{F}_N^{(J)}(q_N^{-1}) = \prod_{p=1}^{K-1} F_N(q_N^{-1} w_N^{-Jp}) = \prod_{j=1}^{n_f}\prod_{p=1}^{K-1}\left(1 - \xi_j q_N^{-1} w_N^{-Jp}\right) = 1 + \sum_{i=1}^{(K-1)n_f} \bar{f}_i q_N^{-i}. \tag{3.17}$$

The significance of equations (3.15), (3.16) and (3.17) lies in the possibility of specifying the polynomial $F_J(q_J^{-1})$ as the product of $F_N(q_N^{-1})$ and $\bar{F}_N^{(J)}(q_N^{-1})$, namely:

$$F_N(q_N^{-1})\bar{F}_N^{(J)}(q_N^{-1}) = \prod_{p=0}^{K-1} F_N\left(q_N^{-1}w_N^{-Jp}\right)$$
$$= \prod_{j=1}^{n_f}\prod_{p=0}^{K-1}\left(1-\xi_i q_N^{-1}w_N^{-Jp}\right)$$
$$= \prod_{j=1}^{n_f}\left(1-\xi_{J_j}q_J^{-1}\right) = 1+\sum_{i=1}^{n_f} f_{J_i}q_J^{-i} \triangleq F_J(q_J^{-1}), \qquad (3.18)$$

in which $\xi_{J_j} = \xi_j^K$.

Henceforth, the notational convention adopted involves omitting the subscript N from $F_N(\cdot)$ and $\bar{F}_N^{(\cdot)}(\cdot)$ and, when $J = 1$, designating the following polynomial:

$$\phi(q^{-1}) \triangleq F_1(q^{-1}) = \prod_{j=1}^{n_f}\left(1-\xi_{K_j}^K q^{-1}\right) = \prod_{j=1}^{n_f}\prod_{p=0}^{K-1}\left(1-\xi_{K_j}q_K^{-1}w_K^{-p}\right)$$
$$= \prod_{p=0}^{K-1} F_K\left(q_K^{-1}w_K^{-p}\right). \qquad (3.19)$$

The formulation of matrix-vector representations of cyclically time-varying difference equations is facilitated by specifying the following entities:

$$\mathbf{x}_K(-\lambda J) = \left[\begin{array}{cccc} x(-\lambda J) & x(-(\lambda+1)J) & \ldots & x(-(\lambda+K-1)J)\end{array}\right]' \quad (\in \mathbb{R}^K), \qquad (3.20)$$

where λ, although denoting any non-negative integer, will in general be 0, and

$$\mathbf{P}_K^{(i)}(q^{-1}) = \left[\begin{array}{cc} \mathbf{0} & \mathbf{I}_{K-i} \\ q^{-1}\mathbf{I}_i & \mathbf{0}\end{array}\right], \quad i \in [1, K-1], \text{ with } \mathbf{P}_K^{(0)}(q^{-1}) \triangleq \mathbf{I}_K. \qquad (3.21)$$

The "$\mathbf{P}$" matrices, which may be construed as matrix-valued backward-shift operators, have the following properties:

$$\mathbf{P}_K^{(l)}(q^{-1})\mathbf{x}_K(-\lambda J) = \mathbf{x}_K(-(\lambda+l)J), \qquad (3.22)$$

and, if $l + m = \mu K + k$, $k \in [0, K-1]$,

$$\mathbf{P}_K^{(l)}(q^{-1})\mathbf{P}_K^{(m)}(q^{-1}) = \mathbf{P}_K^{(m)}(q^{-1})\mathbf{P}_K^{(l)}(q^{-1}) = q^{-\mu}\mathbf{P}_K^{(k)}(q^{-1}). \qquad (3.23)$$

Consequently, a Toeplitz matrix $\mathbf{F}_K(q^{-1})$ can be associated with the polynomial

$$F_K(q_K^{-1}) = 1+\sum_{i=1}^{n_f} f_{K_i}q_K^{-i},$$

namely:

(i)

$$\mathbf{F}_K(q^{-1}) = \mathbf{I}_K + \sum_{i=1}^{n_f} f_{K_i}\mathbf{P}_K^{(i)}(q^{-1})$$

$$= \begin{bmatrix} F_{1(1)}(q^{-1}) & F_{1(2)}(q^{-1}) & \cdots & F_{1(K)}(q^{-1}) \\ q^{-1}F_{1(K)}(q^{-1}) & F_{1(1)}(q^{-1}) & \cdots & F_{1(K-1)}(q^{-1}) \\ \vdots & \vdots & \ddots & \vdots \\ q^{-1}F_{1(2)}(q^{-1}) & q^{-1}F_{1(3)}(q^{-1}) & \cdots & F_{1(1)}(q^{-1}) \end{bmatrix}, \quad (3.24)$$

in which, defining,

$$n_f = \upsilon K + k, \quad k \in [0, K-1],$$

$$F_{1(j+1)}(q^{-1}) = \sum_{i=0}^{\tilde{\upsilon}} f_{K_{j+Ki}} q^{-i}, \quad \text{where:} \begin{cases} \tilde{\upsilon} = \upsilon, & j \in [0, k] \\ \tilde{\upsilon} = \upsilon - 1, & j \in [k+1, K-1]. \end{cases}$$

Alternatively, expressing the polynomial $F_K(q_K^{-1})$ as the product of n_f factors, namely

$$F_K(q_K^{-1}) = \prod_{j=1}^{n_f} (1 - \xi_{K_j} q_K^{-1}),$$

then, as a consequence of the commutativity of the $\mathbf{P}$ matrices (see (3.23)), $\mathbf{F}_K(q^{-1})$ can be expressed as:

(ii)

$$\mathbf{F}_K(q^{-1}) = \prod_{j=1}^{n_f} \left(\mathbf{I}_K - \xi_{K_j}\mathbf{P}_K^{(1)}(q^{-1})\right). \quad (3.25)$$

The determinant of the Toeplitz matrix $\mathbf{F}_K(q^{-1})$ is acquired by noticing that it can be established readily that

$$\det\left(\mathbf{I}_K - \xi_{K_j}\mathbf{P}_K^{(1)}(q^{-1})\right) = 1 - \xi_{K_j}^K q^{-1}. \quad (3.26)$$

Therefore, using the multiplicativity property of the determinant function, namely,

$$\det(\mathbf{XY}) = \det(\mathbf{X}) \det(\mathbf{Y}),$$

then, from equations (3.26) and (3.19),

$$\det\left(\mathbf{F}_K(q^{-1})\right) = \prod_{j=1}^{n_f} \left(1 - \xi_{K_j}^K q^{-1}\right) \triangleq \phi(q^{-1}). \quad (3.27)$$

Accordingly, observing that

$$\text{adj}\left(\mathbf{I}_K - \xi_{K_j}\mathbf{P}_K^{(1)}(q^{-1})\right) = \mathbf{I}_K + \sum_{i=1}^{K-1} \xi_{K_j}^i \mathbf{P}_K^{(i)}(q^{-1}), \tag{3.28}$$

then, associated with the polynomial

$$\bar{F}_K(q_K^{-1}) = \prod_{p=1}^{K-1} F_K\left(q_K^{-1}w_K^{-p}\right) = \prod_{j=1}^{n_f}\left(1 + \sum_{i=1}^{K-1} \xi_{K_j}^i q_K^{-i}\right)$$
$$= 1 + \sum_{i=1}^{(K-1)n_f} \bar{f}_{K_i} q_K^{-i},$$

the adjugate of $\mathbf{F}_K(q^{-1})$ is defined as

$$\text{adj}\left(\mathbf{F}_K(q^{-1})\right) = \prod_{j=1}^{n_f}\left(\mathbf{I}_K + \sum_{i=1}^{K-1} \xi_{K_j}^i \mathbf{P}_K^{(i)}(q^{-1})\right)$$
$$= \mathbf{I}_K + \sum_{i=1}^{(K-1)n_f} \bar{f}_{K_i}\mathbf{P}_K^{(i)}(q^{-1}) \triangleq \bar{\mathbf{F}}_K(q^{-1}). \tag{3.29}$$

Therefore, the inverse of the Toeplitz matrix $\mathbf{F}_K(q^{-1})$ is given by

$$\mathbf{F}_K^{-1}(q^{-1}) = \phi^{-1}(q^{-1})\text{adj}\left(\mathbf{F}_K(q^{-1})\right). \tag{3.30}$$

It is appropriate at this juncture to introduce matrices denoted as "$\mathbf{V}$" and "$\mathbf{W}$", which facilitate the modelling of fast- to slow-sampling rate conversion and the switching operations imposed by the slow input-sampled zero-order hold, respectively. The $\mathbf{V}$ matrices are designated as

$$\mathbf{V}_J = \text{block diag}\left(\mathbf{v}_K', \mathbf{v}_K', \ldots, \mathbf{v}_K'\right), \quad \mathbf{v}_K = [\ 1 \quad 0 \quad \ldots \quad 0\ ]', \quad (\in \mathbb{R}^K), \tag{3.31}$$

and are related to the $\mathbf{P}$ matrices thus:

$$\mathbf{P}_J^{(i)}(q^{-1})\mathbf{V}_J = \mathbf{V}_J\mathbf{P}_N^{(Ki)}(q^{-1}). \tag{3.32}$$

The $\mathbf{W}$ matrices, which are specified as

$$\mathbf{W}_K = \text{block diag}\left(\mathbf{w}_J, \mathbf{w}_J, \ldots, \mathbf{w}_J\right), \quad \mathbf{w}_J = [\ 1 \quad 1 \quad \ldots \quad 1\ ]', \quad (\in \mathbb{R}^J), \tag{3.33}$$

are related correspondingly to the $\mathbf{P}$'s as follows:

$$\mathbf{W}_K\mathbf{P}_K^{(k)}(q^{-1}) = \mathbf{P}_N^{(Jk)}(q^{-1})\mathbf{W}_K. \tag{3.34}$$

It is now possible to construct a system model using the $\mathbf{P}$, $\mathbf{V}$ and $\mathbf{W}$ matrices in conjunction with the $\mathbf{x}_K$ vectors. Returning to the difference equation representation of the input subsystem given by (3.10), the fast-sampled controls at $i = -1, -2, \ldots, -N$, are related to the slow-sampled controls at $i = -M, -2M, \ldots, -LM\ (= -N)$, thus:

$$\bar{\mathbf{u}}_N(-1) = \mathbf{W}_L \mathbf{u}_L(-M). \tag{3.35}$$

However, since it is necessary to obtain a representation throughout the repetitive time interval, i.e., $i \in [0, N-1]$, the $\mathbf{P}$ matrices are exploited by writing

$$\bar{\mathbf{u}}_N(-1) = \mathbf{P}_N^{(1)}(q^{-1})\bar{\mathbf{u}}_N(0) \quad \text{and} \quad \mathbf{u}_L(-M) = \mathbf{P}_L^{(1)}(q^{-1})\mathbf{u}_L(0),$$

whence, from equations (3.35) and (3.34),

$$(S_1 \text{ to } S_2) \qquad \bar{\mathbf{u}}_N(0) = \mathbf{P}_N^{(M-1)}(q^{-1})\mathbf{W}_L \mathbf{u}_L(0). \tag{3.36}$$

Exploiting the previous principles, the discretised plant/fast-rate zero-order hold combination, described originally by the set of N difference equations of (3.11), can be modelled as:

$$(S_2 \text{ to } S_3) \qquad \mathbf{A}_N(q^{-1})\mathbf{y}_N(0) = \mathbf{P}_N^{(d)}(q^{-1})\mathbf{B}_N(q^{-1})\bar{\mathbf{u}}_N(0), \tag{3.37}$$

where $\mathbf{A}_N(q^{-1}) = \mathbf{I}_N + \sum_{i=1}^{n} a_i \mathbf{P}_N^{(i)}(q^{-1})$ and $\mathbf{B}_N(q^{-1}) = \sum_{i=0}^{n_b} b_i \mathbf{P}_N^{(i)}(q^{-1})$.

The use of the $\mathbf{V}$ matrix specified in (3.31) enables the output subsystem modelled by equation (3.12) to be represented thus:

$$(S_3 \text{ to } S_4) \qquad \mathbf{y}_M(0) = \mathbf{V}_M \mathbf{y}_N(0). \tag{3.38}$$

The system model encapsulated by equations (3.36), (3.37) and (3.38) will be examined in further detail in section 3.5.

3.3 A Frequency-Domain Representation

Having formulated a polynomial system description via the use of backward-shift operators, it is instructive to construct an equivalent representation specified in terms of pulse-transforms. This is accomplished by invoking the relationship between the pulse-transforms of a signal sampled at different, albeit integer-related rates, referred to in Chapter 2 as "frequency decomposition".

Again operating in a context defined by equation (3.13), thereby implying

$$K \in \{L, M, N\},$$

it will be observed that, with K set to unity in equation (2.7) and both J and $\bar{K}$ replaced with K, the pulse-transform $X(z)$ is given by

$$X(z) = \frac{1}{K} \sum_{p=0}^{K-1} X_K \left(z_K w_K^p\right). \tag{3.39a}$$

However, $X(z)$ can be expressed alternatively as

$$X(z) = \frac{1}{K} \mathbf{w}_K' \mathbf{x}_{K_f}(z_K), \tag{3.39b}$$

in which $\mathbf{x}_{K_f}(z_K) = \left[\; X_K(z_K), \;\; X_K(z_K w_K^1), \;\; \ldots \;\; X_K(z_K w_K^{K-1}) \; \right]' \quad (\in \mathbb{C}^K)$

and $\mathbf{w}_K$ is specified in equation (3.33). A physical interpretation of the vector $\mathbf{x}_{K_f}(z_K)$ results by replacing s with $j\omega$ in $z_K (= e^{sT/K})$, $\omega \in [0, \omega_s/2)$, where

$$\omega_s = 2\pi/T \tag{3.40}$$

is the sampling rate defined with respect to the repetitive time interval. For an element $X_K(z_K w_K^p)$ of $\mathbf{x}_{K_f}(z_K)$,

$$X_K\left(z_K w_K^p\right)\Big|_{s=j\omega} = X_K\left(e^{j(\omega + p\omega_s)T/K}\right),$$

whence $\mathbf{x}_{K_f}(\cdot)$ comprises the following segments of the frequency response $X_K(e^{j\omega T/K})$, $\omega \in [0, \omega_K/2)$, in which $\omega_K = 2\pi K/T = K\omega_s$ (see (3.40)):

$$\omega \in [0, \omega_s/2), \;\; \omega \in [\omega_s, 3\omega_s/2), \;\; \ldots \;\; , \;\; \omega \in [(K-1)\omega_s, (K-1)\omega_s + \omega_s/2).$$

In addition, with a slight abuse of notation, since equation (2.3) indicates that

$$\begin{aligned} X_K\left(e^{j(\omega + p\omega_s)T/K}\right) &= \frac{K}{T} \sum_{m=-\infty}^{\infty} X\left(j\omega + jm\omega_K + jp\omega_s\right) \\ &= \frac{K}{T} \sum_{m=-\infty}^{\infty} X\left(j\omega + j(Km + p)\omega_s\right), \end{aligned}$$

then it is evident that the frequency response $X_K\left(e^{j(\omega + p\omega_s)T/K}\right)$ comprises signal components of the response $X(j\omega)$ at

$$\omega + (Km + p)\omega_s, \quad m = -\infty, \ldots, \infty.$$

In addition to the vectors $\mathbf{x}_{K_f}(\cdot)$ specified above, the polynomial modelling of multirate-sampled systems by frequency-domain techniques requires the designation of the following family of matrices:

$$\mathbf{P}_{K_f}^{(i)}(z_K^{-1}) = \text{diag}\left(z_K^{-i},\ z_K^{-i}w_K^{-i},\ \ldots,\ z_K^{-i}w_K^{-(K-1)i}\right). \tag{3.41}$$

Thus, with $GH_N^{(N)}(z_N)$ given by equation (3.9b), extending equation (3.4) to encompass the pulse-transform operators $z_N^{-i}w_N^{-i}$, $i = 0, 1, \ldots, N-1$, the frequency-domain interpretation of the discretised plant/zero-order hold, represented in the time-domain by equation (3.37), is

$$(S_2 \text{ to } S_3) \qquad \mathbf{A}_{N_f}(z_N^{-1})\mathbf{y}_{N_f}(z_N) = \mathbf{P}_{N_f}^{(d)}(z_N^{-1})\mathbf{B}_{N_f}(z_N^{-1})\bar{\mathbf{u}}_{N_f}(z_N), \tag{3.42}$$

where

$$\begin{aligned}\mathbf{A}_{N_f}(z_N^{-1}) &= \mathbf{I}_N + \sum_{i=1}^{n} a_i \mathbf{P}_{N_f}^{(i)}(z_N^{-1}) \\ &= \text{diag}\left(A(z_N^{-1}),\ A(z_N^{-1}w_N^{-1}),\ \ldots,\ A(z_N^{-1}w_N^{-(N-1)})\right),\end{aligned}$$

with $\mathbf{B}_{N_f}(z_N^{-1})$ specified accordingly.

The modelling of the input subsystem initially requires that the pulse-transfer function $H_N^{(L)}(z_N)$ given in (3.5) is defined alternatively as

$$H_N^{(L)}(z_N) = 1 + z_N^{-1} + \ldots + z_N^{-(M-1)} \triangleq H^{(L)}(z_N^{-1}). \tag{3.43}$$

Now, designating the pulse-transform $\bar{U}_N\left(z_N w_N^p\right)$, where

$$p = mL + l, \quad m \in [0, M-1], \quad l \in [0, L-1],$$

thus:

$$\bar{U}_N\left(z_N w_N^p\right) = H^{(L)}\left(z_N^{-1}w_N^{-p}\right) U_L\left(\left(z_N w_N^p\right)^M\right) = H^{(L)}\left(z_N^{-1}w_N^{-p}\right) U_L\left(z_L w_L^p\right),$$

the vectors representing the pulse-transforms of the fast- and slow-sampled controls, $\bar{\mathbf{u}}_{N_f}(z_N)$ and $\mathbf{u}_{L_f}(z_L)$, respectively, are related as follows:

$$(S_1 \text{ to } S_2) \qquad \bar{\mathbf{u}}_{N_f}(z_N) = \mathbf{H}_{N_f}^{(L)}(z_N^{-1})\mathbf{u}_{L_f}(z_L), \tag{3.44}$$

where, denoting $H^{(L)}\left(z_N^{-1}w_N^{-p}\right)$ by $H(p)$ for concision,

$$\mathbf{H}_{N_f}^{(L)}(z_N^{-1}) = \begin{bmatrix} \text{diag}\,(H(0),\ H(1),\ \ldots\ ,\ H(L-1)) \\ \text{diag}\,(H(L),\ H(L+1),\ \ldots\ ,\ H(2L-1)) \\ \vdots \qquad\qquad \vdots \qquad\qquad \vdots \\ \text{diag}\,(H((M-1)L),\ H((M-1)L+1),\ \ldots\ ,\ H(N-1)) \end{bmatrix}.$$

Nonetheless, in order to ensure compatibility with the time-domain model of equation (3.36), by defining the reciprocal polynomial $H^{(L)\star}(z_N^{-1})$ thus:

$$H^{(L)\star}(z_N^{-1}) = 1 + z_N + \ldots + z_N^{M-1},$$

and, accordingly, designating

$$\mathbf{W}_{L_f}(z_N) = \begin{bmatrix} \text{diag}\,(H^\star(0),\ H^\star(1),\ \ldots\ ,\ H^\star(L-1)) \\ \text{diag}\,(H^\star(L),\ H^\star(L+1),\ \ldots\ ,\ H^\star(2L-1)) \\ \vdots \qquad\qquad \vdots \qquad\qquad \vdots \\ \text{diag}\,(H^\star((M-1)L),\ H^\star((M-1)L+1),\ \ldots\ ,\ H^\star(N-1)) \end{bmatrix}, \tag{3.45}$$

the matrix $\mathbf{H}_{N_f}^{(L)}(z_N^{-1})$ can be specified as

$$\mathbf{H}_{N_f}^{(L)}(z_N^{-1}) = \mathbf{P}_{N_f}^{(M-1)}(z_N^{-1})\mathbf{W}_{L_f}(z_N). \tag{3.46}$$

Using a similar approach, the pulse-transform $Y_M\,(z_M w_M^m)$, $m \in [0, M-1]$, can be expressed via frequency decomposition as

$$Y_M\,(z_M w_M^m) = Y_M\left((z_N w_N^m)^L\right) = \frac{1}{L}\sum_{p=0}^{L-1} Y\left(z_N w_N^{p-l}\right),$$

and consequently the output subsystem can be described thus (cf. (3.38)):

$$\mathbf{y}_{M_f}(z_M) = \mathbf{V}_{M_f}\mathbf{y}_{N_f}(z_N), \tag{3.47}$$

with $$\mathbf{V}_{M_f} = \frac{1}{L}[\ \mathbf{I}_M\ \ \mathbf{I}_M\ \ \ldots\ \ \mathbf{I}_M\ ].$$

Finally, the relationships between the "$\mathbf{V}_f$", "$\mathbf{W}_f$" and "$\mathbf{P}_f$" matrices, corresponding to those specified in equations (3.32) and (3.34), are:

$$\mathbf{P}_{J_f}^{(i)}(z_J^{-1})\mathbf{V}_{J_f} = \mathbf{V}_{J_f}\mathbf{P}_{N_f}^{(Ki)}(z_N^{-1}) \tag{3.48}$$

and
$$\mathbf{W}_{K_f}(z_N)\mathbf{P}^{(k)}_{K_f}(z_K^{-1}) = \mathbf{P}^{(Jk)}_{N_f}(z_N^{-1})\mathbf{W}_{K_f}(z_N). \tag{3.49}$$

The transformation relating variables in the time- and frequency-domains is established by considering the pulse-transform $X_K\left(z_K w_K^p\right)$, which, during the repetitive time interval (i.e., $t \in ((k-1)T, kT/N]$), is given by

$$\begin{aligned} X_K(z_K w_K^p) &= \cdots + z_K^{-K(k-1)} \sum_{i=0}^{K-1} x((k-1)T + iT/K) z_K^{-i} w_K^{-ip} + \cdots \\ &= \cdots + z^{-k} \sum_{\kappa=0}^{K-1} x(kT - \kappa T/\kappa) z_K^{\kappa} w_K^{\kappa p} + \cdots \\ &\triangleq \left\{ x(0) + z_K w_K^p x(-J) + \cdots + z_K^{K-1} w_K^{(K-1)p} x(-(K-1)J) \right\}. \end{aligned} \tag{3.50}$$

Setting $p = 0, 1, \ldots, K-1$, in equation (3.50), the vectors $\mathbf{x}_{K_f}(z_K)$ ((3.39b)) and $\mathbf{x}_K(0)$ ((3.20)) are related thus:

$$\mathbf{x}_{K_f}(z_K) = \mathbf{T}_K(z_K)\mathbf{x}_K(0), \tag{3.51}$$

where, if $t(i,j)$ represents the $(i,j)^{th}$ element of $\mathbf{T}_K(z_K)$,

$$t(i,j) = z_K^{j-1} w_K^{(i-1)(j-1)}.$$

The inverse transformation is given by

$$\mathbf{x}_K(0) = \mathbf{T}_K^{-1}(q_K)\mathbf{x}_{K_f}(q_K), \tag{3.52}$$

in which, if $\hat{t}(i,j)$ denotes the $(i,j)^{th}$ entry in $\mathbf{T}_K^{-1}(q_K)$,

$$\hat{t}(i,j) = \frac{1}{K} q_K^{-(i-1)} w_K^{(j-1)(i-1)}.$$

The transformation matrix $\mathbf{T}$ relates the time-domain $\mathbf{P}$, $\mathbf{V}$ and $\mathbf{W}$ matrices to their frequency-domain counterparts as follows:

$$\mathbf{P}^{(i)}_{K_f}(z_K^{-1}) = \mathbf{T}_K(z_K)\mathbf{P}^{(i)}_K(z^{-1})\mathbf{T}_K^{-1}(z_K), \tag{3.53}$$

$$\mathbf{V}_{J_f} = \mathbf{T}_J(z_J)\mathbf{V}_J\mathbf{T}_N^{-1}(z_N) \tag{3.54}$$

and
$$\mathbf{W}_{K_f}(z_N) = \mathbf{T}_N(z_N)\mathbf{W}_K\mathbf{T}_K^{-1}(z_K). \tag{3.55}$$

Thus, invoking equations (3.53), (3.54) and (3.55), the following substitutions:

$$\mathbf{y}_{N_f}(z_N) = \mathbf{T}_N(z_N)\mathbf{y}_N(0) \quad \text{in (3.42) and (3.47);}$$

$$\bar{\mathbf{u}}_{N_f}(z_N) = \mathbf{T}_N(z_N)\bar{\mathbf{u}}_N(0) \quad \text{in (3.42) and (3.44);}$$

$$\mathbf{u}_{L_f}(z_L) = \mathbf{T}_L(z_L)\mathbf{u}_L(0) \quad \text{in (3.44)}$$

and

$$\mathbf{y}_{M_f}(z_M) = \mathbf{T}_M(z_M)\mathbf{y}_M(0) \quad \text{in (3.47),}$$

yields the time-domain models of equations (3.37), (3.36) and (3.38). Notice that, via equation (3.53), $\mathbf{A}_{N_f}(z_N^{-1})$ in (3.42) is related to $\mathbf{A}_N(z^{-1})$ in (3.37) thus:

$$\mathbf{A}_{N_f}(z_N^{-1}) = \mathbf{T}_N(z_N)\mathbf{A}_N(z^{-1})\mathbf{T}_N^{-1}(z_N), \tag{3.56}$$

with $\mathbf{B}_{N_f}(z_N^{-1})$ and $\mathbf{B}_N(z^{-1})$ sharing a similar relationship.

3.4 Modelling Of Stochastic Signals

This section describes how polynomial models of stochastic disturbances may be obtained. Prior to establishing the key result, it is necessary at the outset to provide certain definitions.

The following analysis concerns weakly stationary discrete-time stochastic processes $x(mT/J)$ and $y(mT/J)$, where:

(i) $E\{x(mT/J)\} = E\{y(mT/J)\} = 0$;

(ii) the cross-covariance function $r_{xy_J}(kT/J)$ is specified as

$$r_{xy_J}(kT/J) \triangleq E\{x(mT/J)y((m+k)T/J)\}; \tag{3.57}$$

(iii) the cross-spectral density $\Phi_{xy_J}(z_J)$ is given by

$$\Phi_{xy_J}(z_J) = \frac{J}{T}\sum_{k=-\infty}^{\infty} r_{xy_J}(kT/J)z_J^{-k}. \tag{3.58}$$

When y is replaced by x in equations (3.57) and (3.58), the entities $r_{xx_J}(\cdot)$ and $\Phi_{xx_J}(\cdot)$ are referred to as the autocovariance function and autospectral (or, simply, spectral) density, respectively. Notice that, henceforth, the subscripts xx may be removed for concision.

The significant result in the pulse-transform/pulse-transfer function modelling of multirate-sampled systems containing stochastic exogenous signals relates the (auto) spectral densities of the random variables $x(jT/K)$ and $x(mT/J)$, where, returning to the convention

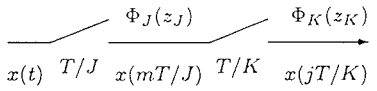

Figure 3.5. Multirate-sampling of a random variable.

utilised in Chapter 2

$$J = \bar{K}K, \quad \bar{K} > 1,$$

and was published originally by Ragazzini and Franklin (1958). It is instructive to detail the manipulations leading to this result since the "time-domain" approach employed may be applied equally to derive equation (2.7) (i.e., "frequency-decomposition"), which was acquired via the "frequency-domain" definition of the pulse-transform.

Observing that the (auto) covariance function $r(lT/K)$ of the random variable $x(jT/K)$ (see Figure 3.5) can be written as

$$r(lT/K) = \frac{1}{\bar{K}} \sum_{p=0}^{\bar{K}-1} \sum_{k=0}^{\bar{K}-1} r(lT/K + kT/J) w_{\bar{K}}^{-kp},$$

then, from equation (3.58), the spectral density $\Phi_K(z_K)$ is given by

$$\Phi_K(z_K) = \frac{K}{T} \sum_{l=-\infty}^{\infty} r(lT/K) z_K^{-l} = \frac{1}{\bar{K}^2} \frac{J}{T} \sum_{l=-\infty}^{\infty} \sum_{p=0}^{\bar{K}-1} \sum_{k=0}^{\bar{K}-1} r(lT/K + kT/J) z_J^{-l\bar{K}} z_J^{-k} w_{\bar{K}}^{-kp}.$$

Now, defining

$$\lambda = l\bar{K} + k, \quad k \in [0, \bar{K} - 1],$$

and noting that, consequently,

$$z_J^{-(l\bar{K}+k)} w_{\bar{K}}^{-kp} = z_J^{-(l\bar{K}+k)} w_{\bar{K}}^{-(l\bar{K}+k)p} = z_J^{-\lambda} w_{\bar{K}}^{-\lambda p},$$

then $\Phi_K(z_K)$ is given by:

$$\Phi_K(z_K) = \frac{1}{\bar{K}^2} \left(\frac{J}{T} \sum_{p=0}^{\bar{K}-1} \sum_{\lambda=-\infty}^{\infty} r(\lambda T/K) z_J^{-\lambda} w_{\bar{K}}^{-\lambda p} \right) = \frac{1}{\bar{K}^2} \sum_{p=0}^{\bar{K}-1} \Phi_J \left(z_J w_{\bar{K}}^{p} \right). \tag{3.59}$$

Of particular significance in the context of this thesis is the response of dynamical systems driven by discrete-time white noise. Accordingly, the signal $e(iT/N)$ is defined as a weakly stationary sequence of uncorrelated random variables with zero mean, namely,

$$r_{ee_N}(jT/N) = \begin{cases} \sigma^2 T/N, & j = 0 \\ 0, & j = \pm 1, \pm 2, \ldots, \end{cases}$$

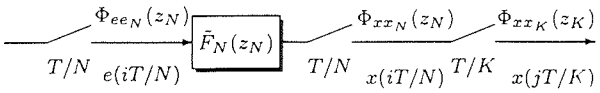

Figure 3.6. Multirate-sampled system with stochastic input.

and associated spectral density

$$\Phi_{ee_N}(z_N) = \sigma^2. \tag{3.60}$$

Additionally, the requirement that subsystem models have compatible sampling régimes implies that it is often necessary to redefine the sampling rate associated with a disturbance signal. In this respect, the forthcoming analysis describes the replacement of the fast input-/slow output-sampled subsystem possessing a stochastic input illustrated in Figure 3.6 with a single-rate, slow-sampled counterpart.

Using conventional single-rate theory, the spectral density $\Phi_{xx_N}(z_N)$ in Figure 3.6 is given by

$$\begin{aligned}\Phi_{xx_N}(z_N) &= \tilde{F}_N(z_N)\tilde{F}_N(z_N^{-1})\Phi_{ee_N}(z_N) \\ &= \tilde{F}_N(z_N)\tilde{F}_N(z_N^{-1})\sigma^2 \quad \text{(see (3.60))}.\end{aligned} \tag{3.61}$$

Now, assuming that $\tilde{F}_N(z_N)$ is specified thus:

$$\tilde{F}_N(z_N) = \frac{\tilde{C}(z_N^{-1})}{A(z_N^{-1})},$$

where $\tilde{C}$ and A are monic polynomials with degree n, with $\tilde{C}$ defined as strictly stable, and

$$K\bar{K} = N, \quad \bar{K} > 1, \tag{3.62}$$

the spectral density $\Phi_{xx_K}(z_K)$ then, from (3.61) and (3.59), is given by

$$\begin{aligned}\Phi_{xx_K}(z_K) &= \frac{1}{\bar{K}^2}\sum_{p=0}^{\bar{K}-1}\tilde{F}_N\left(z_N w_{\bar{K}}^{p}\right)\tilde{F}_N\left(z_N^{-1}w_{\bar{K}}^{-p}\right)\sigma^2 \\ &= \frac{\sigma^2}{\bar{K}^2 A_K(z_K^{-1})A_K(z_K)}\sum_{p=0}^{\bar{K}-1}\chi\left(z_N^{-1}w_{\bar{K}}^{-p}\right)\chi\left(z_N w_{\bar{K}}^{p}\right),\end{aligned} \tag{3.63}$$

in which (see (3.18)) $$A_K(z_K^{-1}) = \prod_{p=0}^{\bar{K}-1} A\left(z_N^{-1}w_{\bar{K}}^{-p}\right)$$

and $\chi(z_N^{-1}) = \tilde{C}(z_N^{-1})\bar{A}^{(K)}(z_N^{-1})$, where $\bar{A}^{(K)}(z_N^{-1}) = \prod_{j=1}^{\bar{K}-1} A\left(z_N^{-1}w_{\bar{K}}^{-j}\right)$ (see (3.17)).

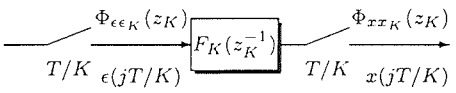

Figure 3.7. Modified disturbance subsystem model.

Expressing the polynomial $\chi(z_N^{-1})\chi(z_N)$ thus:

$$\chi(z_N^{-1})\chi(z_N) = \theta_{\bar{K}n}z_N^{\bar{K}n} + \theta_{\bar{K}n-1}z_N^{\bar{K}n-1} + \ldots + \theta_0 + \ldots + \theta_{\bar{K}n-1}z_N^{-(\bar{K}n-1)} + \theta_{\bar{K}n}z_N^{-\bar{K}n},$$

and using

$$\sum_{j=0}^{\bar{K}-1} w_{\bar{K}}^{\pm j} = 0,$$

the summation in (3.63) can be written as

$$\begin{aligned}\sum_{p=0}^{\bar{K}-1} \chi\left(z_N^{-1}w_{\bar{K}}^{-p}\right)\chi\left(z_N w_{\bar{K}}^{p}\right) &= \bar{K}\left(\theta_{\bar{K}n}z_K^{n} + \theta_{\bar{K}(n-1)}z_K^{n-1} + \ldots + \theta_0 + \ldots\right.\\ &\qquad \left. \ldots + \theta_{\bar{K}(n-1)}z_K^{-(n-1)} + \theta_{\bar{K}n}z_K^{-n}\right)\\ &\triangleq \bar{K}\rho C_K(z_K^{-1})C_K(z_K),\end{aligned}$$

in which $C_K(z_K^{-1})$, which has degree n, is defined as monic and stable. Consequently, the spectral density $\Phi_{xx_K}(\cdot)$ is given by

$$\Phi_{xx_K}(z_K) = \frac{\rho\sigma^2}{\bar{K}}\frac{C_K(z_K^{-1})C_K(z_K)}{A_K(z_K^{-1})A_K(z_K)}, \tag{3.64}$$

and the configuration of Figure 3.6 can be replaced with the subsystem illustrated in Figure 3.7, in which

$$F_K(z_K) = \frac{C_K(z_K^{-1})}{A_K(z_K^{-1})}$$

and where the spectral density of the zero-mean white noise sequence $\epsilon(jT/K)$ is

$$\Phi_{\epsilon\epsilon_K}(z_K) = \frac{\rho\sigma^2}{\bar{K}}.$$

3.5 Input-Output Models

The modelling principles established within this chapter are now exploited in the formulation of matrix fraction system representations defined with respect to the frequency- and time-domains. Thereafter, following an examination of the conditions under which the aforementioned descriptions are irreducible, the issue of causality is discussed. Finally,

the introduction of a further set of matrices, referred to as "**Q**'s", yields a systematic means of formulating both left- and right-matrix fraction models.

A frequency-domain input-output model of the system illustrated in Figure 3.3 is acquired by initially defining (see (3.17) and (3.18), respectively):

$$\bar{\mathbf{A}}_{N_f}^{(M)}\left(z_N^{-1}\right) = \operatorname{diag}\left(\bar{A}_N^{(M)}(z_N^{-1}), \bar{A}_N^{(M)}(z_N^{-1}w_N^{-1}), \ldots, \bar{A}_N^{(M)}(z_N^{-1}w_N^{-N+1})\right)$$

and $$\mathbf{A}_{M_f}\left(z_M^{-1}\right) = \operatorname{diag}\left(A_M(z_M^{-1}), A_M(z_M^{-1}w_M^{-1}), \ldots, A_M(z_M^{-1}w_M^{-M+1})\right);$$

whence, invoking (3.48) and observing that, as a consequence of (3.18),

$$\mathbf{V}_{M_f}\mathbf{A}_{N_f}^{-1}\left(z_N^{-1}\right) = \mathbf{A}_{M_f}^{-1}\left(z_M^{-1}\right)\mathbf{V}_{M_f}\bar{\mathbf{A}}_{N_f}^{(M)}\left(z_N^{-1}\right),$$

the combination of the individual subsystem models designated in equations (3.42), (3.44), (3.46) and (3.47) yields

$$\mathbf{A}_{M_f}\left(z_M^{-1}\right)\mathbf{y}_{M_f}(z_N) = \mathbf{B}_{l_f}\left(z_N^{-1}\right)\mathbf{u}_{L_f}(z_L), \tag{3.65}$$

where $$\mathbf{B}_{l_f}\left(z_N^{-1}\right) = \mathbf{V}_{M_f}\bar{\mathbf{A}}_{N_f}^{(M)}\left(z_N^{-1}\right)\mathbf{B}_{N_f}\left(z_N^{-1}\right)\mathbf{P}_{N_f}^{(d_l)}\left(z_N^{-1}\right)\mathbf{W}_{L_f},$$

in which $d_l = d+M-1$. It is instructive to ascertain the conditions whereby the left-matrix fraction $\mathbf{A}_{M_f}^{-1}\mathbf{B}_{l_f}$ is coprime by using the following lemma.

Lemma 3.5.1 (see Kučera (1991))
The left-matrix fraction $\mathbf{A}_{M_f}^{-1}\left(z_M^{-1}\right)\mathbf{B}_{l_f}\left(z_N^{-1}\right)$ will be coprime provided the matrix

$$\mathbf{\Psi}_l\left(z_N^{-1}\right) = \left[\begin{array}{cc} \mathbf{A}_{M_f}(z_N^{-L}) & \mathbf{B}_{l_f}(z_N^{-1}) \end{array}\right] \tag{3.66}$$

has full rank $\forall\ z_N^{-1}\ (\neq 0) \in \mathbb{C}$.

Employing the following notational abbreviations:

$$X\left(z_N^{-1}w_N^{-i}\right) \triangleq X_i$$

and $$z_N^{-d_l}w_N^{-d_l i}\sum_{\substack{j=0\\ j\neq k}}^{L-1} A_{jM+i}B_{kM+i}H_{kM+i}^{(L)} \triangleq \theta_{kM+i},$$

the matrix $\mathbf{\Psi}_l$ is given by

$$\mathbf{\Psi}_l = \begin{bmatrix} \sum_{j=0}^{L-1} A_{jM} & 0 & \dots & 0 & \theta_0 & \theta_{(L-1)M} & \dots & \theta_M \\ 0 & \sum_{j=0}^{L-1} A_{jM+1} & \dots & 0 & \theta_{M+1} & \theta_1 & \dots & \theta_{2M+1} \\ \vdots & \vdots & \ddots & \vdots & \vdots & \vdots & \ddots & \vdots \\ 0 & 0 & \dots & \sum_{j=0}^{L-1} A_{jM+M-1} & \theta_{N-M+1} & \theta_{N-2M-1} & \dots & \theta_{N-1} \end{bmatrix}.$$

At this juncture, the effect on $\mathbf{\Psi}_l$ of setting z_N^{-1} equal to $\mu\,(\in \mathbb{C})$ is ascertained, where μ is a zero of $A\left(z_N^{-1}\right)$ (i.e., A_0). Since $H^{(L)}\left(z_N^{-1}\right)$ (i.e., H_0) is present in the terms $\theta_{(L-1)M}$, $\theta_{(L-2)M}$, ..., θ_M, in the first row, $\mathbf{\Psi}_l$ can have full rank if and only if the minor

$$\theta_0 \sum_{i=1}^{M-1} \sum_{j=0}^{L-1} A_{jM+i} = \mu^{d_l} B(\mu)\, H^{(L)}(\mu) \prod_{i=1}^{N-1} A\left(\mu w_N^{-i}\right)$$

is not zero, whence μ must not be a zero of $H^{(L)}\left(z_N^{-1}\right)$ or $\prod_{i=1}^{N-1} A\left(z_N^{-1} w_N^{-i}\right)$.

Observing that the zeros of $H^{(L)}\left(z_N^{-1}\right)$, namely,

$$z_N = w_N^{jL}, \quad j = 1, 2, \dots, M-1,$$

correspond to s-plane zeros at

$$s = j\,(L+kN)\,\omega_s, j\,(2L+kN)\,\omega_s, \dots, j\,((M-1)\,L+kN)\,\omega_s, \quad k = \pm 1, \pm 2, \dots,$$

and that respective poles of $G(s)$ at

$$s = \sigma + j\omega \quad \text{and} \quad s = \sigma + j\omega + j\,(lN - i)\,\omega_s, \quad l = 0, \pm 1, \pm 2, \dots,$$

constitute zeros of $A\left(z_N^{-1}\right)$ and $A\left(z_N^{-1} w_N^{-i}\right)$ at

$$z_N = e^{\sigma T/N} e^{j\omega T/N},$$

then, in addition to the foregoing assumptions that $A\left(z_N^{-1}\right)$ and $B\left(z_N^{-1}\right)$ do not contain a common factor, $\mathbf{A}_{M_f}$ and $\mathbf{B}_{l_f}$ will be coprime if and only if the plant $G(s)$ does not contain poles:

(1) at $s = j\,(iL+kN)\,\omega_s$, $i = 1, 2, \ldots, M-1$, $k = \pm 1, \pm 2 \ldots$;

(2) at $s = \sigma + j\omega$ and $s = \sigma + j\bar{\omega}$, such that $\bar{\omega} - \omega = l\omega_s$, $l = \pm 1, \pm 2, \ldots$.

Designating $\mathbf{A}_{L_f}$ and $\bar{\mathbf{A}}_{N_f}^{(L)}$ in an analogous fashion to $\mathbf{A}_{M_f}$ and $\bar{\mathbf{A}}_{N_f}^{(M)}$, respectively (see (3.65)), then, since it can be shown from (3.49) that $\mathbf{A}_{N_f}^{-1}\mathbf{W}_{L_f}$ can be written as

$$\mathbf{A}_{N_f}^{-1}\left(z_N^{-1}\right)\mathbf{W}_{L_f} = \bar{\mathbf{A}}_N^{(L)}\left(z_N^{-1}\right)\mathbf{W}_{L_f}\mathbf{A}_{L_f}^{-1}\left(z_L^{-1}\right),$$

again uniting equations (3.42), (3.44), (3.46) and (3.47), the relationship between $\mathbf{y}_{M_f}$ and $\mathbf{u}_{L_f}$ may be defined in right-matrix fraction form as

$$\mathbf{y}_{M_f}(z_M) = \mathbf{B}_{r_f}\left(z_N^{-1}\right)\mathbf{A}_{L_f}^{-1}\left(z_L^{-1}\right)\mathbf{u}_{L_f}(z_L), \tag{3.67}$$

where $$\mathbf{B}_{r_f}\left(z_N^{-1}\right) = \mathbf{V}_{M_f}\bar{\mathbf{A}}_{N_f}^{(L)}\left(z_N^{-1}\right)\mathbf{B}_{N_f}\left(z_N^{-1}\right)\mathbf{P}_{N_f}^{(d_r)}\left(z_N^{-1}\right)\mathbf{W}_{L_f},$$

in which $d_r = d+L-1$. The irreducibility of the matrix fraction $\mathbf{B}_{r_f}\mathbf{A}_{L_f}^{-1}$ can be determined from the following lemma.

Lemma 3.5.2 (see Kučera (1991))
The right-matrix fraction $\mathbf{B}_{r_f}\left(z_N^{-1}\right)\mathbf{A}_{L_f}^{-1}\left(z_L^{-1}\right)$ will be coprime provided the matrix

$$\mathbf{\Psi}_r\left(z_N^{-1}\right) = \begin{bmatrix} \mathbf{A}_{L_f}(z_N^{-M}) \\ \mathbf{B}_{r_f}(z_N^{-1}) \end{bmatrix}$$

has full rank $\forall\ z_N^{-1}\,(\neq 0) \in \mathbb{C}$.

Using the notational abbreviations:

$$z_N^{-d_r} w_N^{-d_r i} \prod_{\substack{j=0 \\ j\neq k}}^{M-1} A_{jL+i} B_{kL+i} H_{kL+i} \triangleq \phi_{kM+i},$$

the matrix $\mathbf{\Psi}_r$ is arranged thus:

$$\mathbf{\Psi}_r = \begin{bmatrix} \sum_{j=0}^{M-1} A_{jL} & 0 & \cdots & 0 \\ 0 & \sum_{j=0}^{M-1} A_{jL+1} & \cdots & 0 \\ \vdots & \vdots & \ddots & \vdots \\ 0 & 0 & \cdots & \sum_{j=0}^{M-1} A_{jL+L-1} \\ \phi_0 & \phi_{(L-1)M} & \cdots & \phi_M \\ \phi_{M+1} & \phi_1 & \cdots & \phi_{2M+1} \\ \vdots & \vdots & \ddots & \vdots \\ \phi_{N-M-1} & \phi_{N-2M-1} & \cdots & \phi_{N-1} \end{bmatrix}.$$

Omitting detail of the relevant manipulations, then employing a similar argument to the left-matrix fraction case, it can be shown that the conditions on the poles of $G(s)$ such that $\mathbf{B}_{r_f}\mathbf{A}_{L_f}^{-1}$ is coprime correspond exactly to those related to $\mathbf{A}_{M_f}^{-1}\mathbf{B}_{l_f}$.

The time-domain model corresponding to equation (3.65), obtained by combining the subsystem models defined by equations (3.36), (3.37) and (3.38) and employing the following relationship emanating from (3.32), namely,

$$\mathbf{V}_M\mathbf{A}_N^{-1}(q^{-1}) = \mathbf{A}_M^{-1}(q^{-1})\mathbf{V}_M\bar{\mathbf{A}}_N^{(M)}(q^{-1}),$$

where $\bar{\mathbf{A}}_N^{(M)}(q^{-1})$ is related to $\bar{A}^{(M)}(q_N^{-1})$ in a similar manner to, $\mathbf{A}(q^{-1})$ and $A(q_N^{-1})$ respectively, (see (3.9b) and (3.37)), is given by

$$\mathbf{y}_M(0) = \mathbf{A}_M^{-1}(q^{-1})\mathbf{B}_l(q^{-1})\mathbf{u}_L(0), \tag{3.68}$$

with $$\mathbf{B}_l(q^{-1}) = \mathbf{V}_M\bar{\mathbf{A}}_N^{(M)}(q^{-1})\mathbf{B}_N(q^{-1})\mathbf{P}_N^{(d_l)}(q^{-1})\mathbf{W}_L.$$

Correspondingly, observing that from (3.34),

$$\mathbf{A}_N^{-1}(q^{-1})\mathbf{W}_L = \bar{\mathbf{A}}_N^{(L)}(q^{-1})\mathbf{W}_L\mathbf{A}_L^{-1}(q^{-1}),$$

then, again uniting equations (3.36), (3.37) and (3.38), the right-matrix fraction representation is

$$\mathbf{y}_M(0) = \mathbf{B}_r(q^{-1})\mathbf{A}_L^{-1}(q^{-1})\mathbf{u}_L(0), \tag{3.69}$$

where $$\mathbf{B}_r(q^{-1}) = \mathbf{V}_M \bar{\mathbf{A}}_N^{(L)}(q^{-1})\mathbf{B}_N(q^{-1})\mathbf{P}_N^{(d_r)}(q^{-1})\mathbf{W}_L.$$

Of course, it is possible to acquire the models of equations (3.68) and (3.69) from the corresponding frequency-domain descriptions of equations (3.65) and (3.67) by invoking the following transformations (see (3.51)):

$$\mathbf{y}_{M_f}(z_M) = \mathbf{T}_M(z_M)\mathbf{y}_M(0) \quad \text{and} \quad \mathbf{u}_{L_f}(z_L) = \mathbf{T}_L(z_L)\mathbf{u}_L(0),$$

whence $$\mathbf{A}_M = \mathbf{T}_M^{-1}\mathbf{A}_{M_f}\mathbf{T}_M, \quad \mathbf{B}_l = \mathbf{T}_M^{-1}\mathbf{B}_{l_f}\mathbf{T}_L,$$

$$\mathbf{A}_L = \mathbf{T}_L^{-1}\mathbf{A}_{L_f}\mathbf{T}_L \quad \text{and} \quad \mathbf{B}_r = \mathbf{T}_M^{-1}\mathbf{B}_{r_f}\mathbf{T}_L.$$

The $\mathbf{B}_l(q^{-1})$ and $\mathbf{B}_r(q^{-1})$ matrices can be expressed in terms of matrix-valued backward-shift operators, designated as "**Q**'s", which fulfil an analogous role to the **P**'s in the context of square matrices and are specified as follows: if $i = \mu L + l,\ l \in [0, L-1]$,

$$\mathbf{Q}_{ML}^{(i)}(q^{-1}) \triangleq q^{-\mu}\mathbf{V}_M\mathbf{P}_N^{(Ml)}(q^{-1})\mathbf{W}_L = q^{-\mu}\mathbf{Q}_0\mathbf{P}_L^{(l)}(q^{-1}) \quad \text{(see (3.34))}, \tag{3.70}$$

where $$\mathbf{Q}_0 = \mathbf{Q}_{ML}^{(0)}(q^{-1}) = \mathbf{V}_M\mathbf{W}_L.$$

Thus, for example, defining

$$\bar{A}^{(M)}(q_N^{-1})B(q_N^{-1}) \triangleq \sum_{i=0}^{Ln-1} \eta_i q_N^{-i},$$

then, supposing for simplicity of exposition that the parameter d is unity, $\mathbf{B}_l(q^{-1})$ in equation (3.68) can be written as

$$\mathbf{B}_l(q^{-1}) = \mathbf{V}_M \left(\sum_{i=0}^{Ln-1} \eta_i \mathbf{P}_N^{(i)}(q^{-1}) \right) \mathbf{P}_N^{(M)}(q^{-1})\mathbf{W}_L = \sum_{j=1}^{n} \hat{\mathbf{B}}_{l_j}\mathbf{Q}_{ML}^{(j)}(q^{-1}), \tag{3.71a}$$

where $$\hat{\mathbf{B}}_{l_j} = \operatorname{diag}\left(\beta_{(j-1)M+M-1},\ \beta_{(j-1)M},\ \beta_{(j-1)M+1},\ \cdots,\ \beta_{(j-1)M+M-2}\right),$$

in which $$\beta_{(j-1)M+i} = \sum_{m=0}^{M-1} \eta_{(j-1)M+i-m}.$$

Correspondingly, in similar circumstances, if

$$\bar{A}^{(L)}(q_N^{-1})B(q_N^{-1}) \triangleq \sum_{i=0}^{Mn-1} \chi_i q_N^{i},$$

then $\mathbf{B}_r(q^{-1})$ in equation (3.69) may be expressed as

$$\mathbf{B}_r(q^{-1}) = \sum_{j=1}^{n+1} \hat{\mathbf{B}}_{r_j}\mathbf{Q}_{ML}^{(j)}(q^{-1}), \tag{3.71b}$$

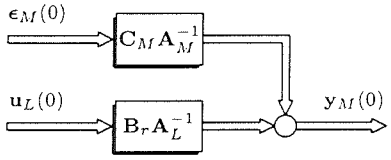

Figure 3.8. Overall lifted system model.

in which $\hat{\mathbf{B}}_{r_j}$ is defined similarly to $\hat{\mathbf{B}}_{l_j}$ and, with η_k replaced with χ_k, each β term remains as specified in equation (3.71a).

As a consequence of the considerations in the previous section regarding the disturbance signal, it is supposed that a fast-rate model specified by the polynomials $A(z_N^{-1})$ and $\tilde{C}(z_N^{-1})$ has been replaced by the following single-rate model (see (3.64)):

$$\Phi_{yy_M}(z_M) = F_M(z_M)F_M(z_M^{-1})\Phi_{\epsilon\epsilon_M}(z_M), \tag{3.72}$$

where

$$F_M(z_M) = \frac{C_M(z_M^{-1})}{A_M(z_M^{-1})},$$

in which $C_M(\cdot)$ is monic and stable and

$$\Phi_{\epsilon\epsilon_M}(z_M) = \tilde{\sigma}^2.$$

The disturbance subsystem thus can be described during the repetitive time interval by the M moving average (MA) processes

$$A_M(q_M^{-1})y(-mL) = C_M(q_M^{-1})\epsilon(-mL), \quad m \in [0, M-1],$$

which, using the modelling procedure dictated by equations (3.20), (3.21) and (3.22), may be expressed succinctly via the relationship

$$\begin{aligned}\mathbf{y}_M(0) &= \mathbf{A}_M^{-1}(q^{-1})\mathbf{C}_M(q^{-1})\epsilon_M(0) \\ &= \mathbf{C}_M(q^{-1})\mathbf{A}_M^{-1}(q^{-1})\epsilon_M(0).\end{aligned} \tag{3.73}$$

The overall lifted system model in right-matrix fraction format engendered by combining equations (3.69) and (3.73) and illustrated in Figure 3.8 then is given by

$$\mathbf{y}_M(0) = \mathbf{B}_r(q^{-1})\mathbf{A}_L^{-1}(q^{-1})\mathbf{u}_L(0) + \mathbf{C}_M(q^{-1})\mathbf{A}_M^{-1}(q^{-1})\epsilon_M(0). \tag{3.74}$$

There are two special cases of the multirate sampled-data system examined in this chapter which are worth further consideration, namely the instances whereby M/L or L/M is

an integer, as opposed to a rational number. The former situation is referred to in this thesis as a fast output-sampled (FOS) system and the relevant open-loop time-domain model, produced by replacing (L, M) with $(1, N)$ in equation (3.74) and dependent equations is

$$\begin{aligned}\mathbf{y}_N(0) &= \mathbf{A}_N^{-1}(q^{-1})\mathbf{b}_l(q^{-1})u(0) + \mathbf{A}_N^{-1}(q^{-1})\mathbf{C}_N(q^{-1})\mathbf{e}_N(0) \\ &= \mathbf{b}_r(q^{-1})\alpha^{-1}(q^{-1})u(0) + \mathbf{C}_N(q^{-1})\mathbf{A}_N^{-1}(q^{-1})\mathbf{e}_N(0), \end{aligned} \tag{3.75}$$

in which $\mathbf{C}_N(q^{-1})$ denotes the matrix arising from the polynomial $\tilde{C}(q_N^{-1})$ (see (3.24)),

where $$\mathbf{b}_l = \mathbf{B}_N\mathbf{P}_N^{(d+N-1)}\mathbf{w}_N, \quad \mathbf{b}_r = \bar{\mathbf{A}}_N^{(N)}\mathbf{B}_N\mathbf{P}_N^{(d+N-1)}\mathbf{w}_N$$

and (see (3.27)) $$\alpha(q^{-1}) \triangleq \sum_{p=0}^{N-1} A\left(q_N^{-1}w_N^{-p}\right).$$

Accordingly, a fast input-sampled (FIS) system, defined as the case in which $L = N$ and $M = 1$, is modelled thus:

$$\begin{aligned}y(0) &= \alpha^{-1}(q^{-1})\tilde{\mathbf{b}}_l'(q^{-1})\mathbf{u}_N(0) + \alpha^{-1}(q^{-1})\gamma(q^{-1})\epsilon(0) \\ &= \tilde{\mathbf{b}}_r'(q^{-1})\mathbf{A}_N^{-1}(q^{-1})\mathbf{u}_N(0) + \gamma(q^{-1})\alpha^{-1}(q^{-1})\epsilon(0), \end{aligned} \tag{3.76}$$

in which $$\tilde{\mathbf{b}}_l' = \mathbf{v}_N'\bar{\mathbf{A}}_N^{(N)}\mathbf{B}_N\mathbf{P}_N^{(d)}, \quad \tilde{\mathbf{b}}_r' = \mathbf{v}_N'\mathbf{B}_N\mathbf{P}_N^{(d)}$$

and $$\gamma(q^{-1}) \triangleq \sum_{p=0}^{N-1} \tilde{C}\left(q_N^{-1}w_N^{-p}\right).$$

3.6 Illustrative Example

This section describes the formulation of polynomial matrix models that describe a multirate-sampled system conforming to the block diagram configurations of Figures 3.1, 3.2 and 3.3. Following the establishment of individual subsystem models, both left- and right-matrix fraction time-domain descriptions are acquired, in addition to a frequency-domain interpretation. The procedure entailed in deriving an appropriate disturbance subsystem model is demonstrated subsequently. This particular example is labelled S1.

Plant Description – Example S1

The plant to be considered has the transfer function

$$G(s) = \frac{1}{s(s\tau - 1)}, \tag{3.77}$$

whereas the parameters L and M are, respectively, 2 and 3, thereby implying (see (3.1a)) that N is 6. Omitting the subscript N from the numerator and denominator polynomials, the discretised plant is given by (see (3.9b))

$$GH_N(z_6) = z_6^{-1}\frac{B(z_6^{-1})}{A(z_6^{-1})} = \frac{b_0 z_6^{-1} + b_1 z_6^{-2}}{1 + a_1 z_6^{-1} + a_2 z_6^{-2}}, \tag{3.78}$$

in which $a_1 = -(1+a)$, $a_2 = a$, $b_0 = \tau(a-1) - \bar{T}$ and $b_1 = \tau - a(\tau - \bar{T})$,

where $$a = e^{\bar{T}/\tau} \quad \text{and} \quad \bar{T} = \frac{T}{6}.$$

Notice that the notational convention is adopted henceforth of allocating numerical values only to the subscripts of arguments.

Individual Subsystem Models

Using the modelling procedure detailed in section 3.2, the difference equation representations of the input, discretised plant and output subsystems, specified by equations (3.10), (3.11) and (3.12), respectively, may be summarised thus:

$$(S_1 \text{ to } S_2) \qquad \bar{\mathbf{u}}_N(0) = \mathbf{P}_N^{(2)}(q^{-1})\mathbf{W}_L\mathbf{u}_L(0) \quad \text{(see (3.36))}, \tag{3.79}$$

where $\bar{\mathbf{u}}_N(0) = \begin{bmatrix} \bar{u}(0) & \bar{u}(-1) & \dots & \bar{u}(-5) \end{bmatrix}'$, $\mathbf{u}_L(0) = \begin{bmatrix} u(0) & u(-3) \end{bmatrix}'$

and

$$\mathbf{P}_N^{(2)}(q^{-1})\mathbf{W}_L = \begin{bmatrix} 0 & 0 & 1 & 0 & 0 & 0 \\ 0 & 0 & 0 & 1 & 0 & 0 \\ 0 & 0 & 0 & 0 & 1 & 0 \\ 0 & 0 & 0 & 0 & 0 & 1 \\ q^{-1} & 0 & 0 & 0 & 0 & 0 \\ 0 & q^{-1} & 0 & 0 & 0 & 0 \end{bmatrix} \begin{bmatrix} 1 & 0 \\ 1 & 0 \\ 1 & 0 \\ 0 & 1 \\ 0 & 1 \\ 0 & 1 \end{bmatrix} \quad \text{(see (3.21), (3.22))}$$

$$= \begin{bmatrix} 1 & 0 \\ 0 & 1 \\ 0 & 1 \\ 0 & 1 \\ q^{-1} & 0 \\ q^{-1} & 0 \end{bmatrix};$$

$$(S_2 \text{ to } S_3) \qquad \mathbf{A}_N(q^{-1})\mathbf{y}_N(0) = \mathbf{P}_N^{(1)}(q^{-1})\mathbf{B}_N(q^{-1})\bar{\mathbf{u}}_N(0) \quad \text{(see (3.37))}, \tag{3.80}$$

where $\mathbf{y}_N(0)$ is defined similarly to $\bar{\mathbf{u}}_N(0)$,

$$\begin{aligned}\mathbf{A}_N(q^{-1}) &= \mathbf{I}_6 - (1+a)\mathbf{P}_6^{(1)}(q^{-1}) + a\mathbf{P}_6^{(2)}(q^{-1}) \\ &= \begin{bmatrix} 1 & -(1+a) & a & 0 & 0 & 0 \\ 0 & 1 & -(1+a) & a & 0 & 0 \\ 0 & 0 & 1 & -(1+a) & a & 0 \\ 0 & 0 & 0 & 1 & -(1+a) & a \\ aq^{-1} & 0 & 0 & 0 & 1 & -(1+a) \\ -(1+a)q^{-1} & aq^{-1} & 0 & 0 & 0 & 1 \end{bmatrix} \quad \text{(see (3.24))}\end{aligned}$$

and $$\mathbf{P}_N^{(1)}(q^{-1})\mathbf{B}_N(q^{-1}) = b_0\mathbf{P}_6^{(1)}(q^{-1}) + b_1\mathbf{P}_6^{(2)}(q^{-1});$$

$$(S_3 \text{ to } S_4) \qquad \mathbf{y}_M(0) = \mathbf{V}_M\mathbf{y}_N(0), \tag{3.81}$$

where $$\mathbf{y}_M(0) = \begin{bmatrix} y(0) & y(-2) & y(-4) \end{bmatrix}'$$

and $$\mathbf{V}_M = \begin{bmatrix} 1 & 0 & 0 & 0 & 0 & 0 \\ 0 & 0 & 1 & 0 & 0 & 0 \\ 0 & 0 & 0 & 0 & 1 & 0 \end{bmatrix}.$$

Time-Domain Descriptions

The individual subsystem models of equations (3.79), (3.80) and (3.81) have limited practical application and, from both the perspectives of analysis and design, the respective left- and right- matrix fraction representations of equations (3.68) and (3.69) assume greater significance. In the former instance, by defining the polynomial (see (3.18))

$$\begin{aligned}A_M(q_3^{-1}) &= \prod_{p=0}^{1} A(q_6^{-1}w_6^{-3p}) \\ &= \left(1 - (1+a)q_6^{-1} + aq_6^{-2}\right)\left(1 + (1+a)q_6^{-1} + aq_6^{-2}\right) \\ &= 1 - (1+a^2)q_3^{-1} + a^2q_3^{-2}, \end{aligned} \tag{3.82}$$

the denominator matrix $\mathbf{A}_M(q^{-1})$ is given by (see (3.24))

$$\begin{aligned}\mathbf{A}_M(q^{-1}) &= \mathbf{I}_3 - (1+a^2)\mathbf{P}_3^{(1)}(q^{-1}) + a^2\mathbf{P}_3^{(2)}(q^{-1}) \\ &= \begin{bmatrix} 1 & -(1+a^2) & a^2 \\ a^2q^{-1} & 1 & -(1+a^2) \\ -(1+a^2)q^{-1} & a^2q^{-1} & 1 \end{bmatrix}. \end{aligned} \tag{3.83}$$

Now, noting that (see (3.70))

$$\mathbf{Q}_0 = \mathbf{V}_M\mathbf{W}_L = \begin{bmatrix} 1 & 0 \\ 1 & 0 \\ 0 & 1 \end{bmatrix},$$

and defining (see (3.17) for $\bar{A}^{(M)}(\cdot)$)

$$\bar{A}^{(M)}(q_6^{-1})B(q_6^{-1}) = \prod_{p=1}^{1} A(q_6^{-1}w_6^{-3p})B(q_6^{-1}) = \sum_{i=0}^{3}\eta_i q_6^{-i},$$

where $\eta_0 = b_0$, $\eta_1 = (1+a)b_0+b_1$, $\eta_2 = ab_0+(1+a)b_1$ and $\eta_3 = ab_1$,

the numerator matrix $\mathbf{B}_l(q^{-1})$ in equation (3.68) may be specified thus (see (3.71a)):

$$\begin{aligned}\mathbf{B}_l(q^{-1}) &= \text{diag}\,(\beta_2,\ \beta_0,\ \beta_1)\,\mathbf{Q}_0\mathbf{P}_2^{(1)}(q^{-1}) \\ &\quad +\text{diag}\,(\beta_5,\ \beta_3,\ \beta_4)\,\mathbf{Q}_0\mathbf{P}_2^{(2)}(q^{-1}) \\ &= \begin{bmatrix} \beta_5q^{-1} & \beta_2 \\ \beta_3q^{-1} & \beta_0 \\ \beta_1q^{-1} & \beta_4q^{-1} \end{bmatrix}, \end{aligned} \tag{3.84}$$

in which $\beta_0 = \eta_0$, $\beta_1 = \eta_0+\eta_1$, $\beta_2 = \eta_0+\eta_1+\eta_2$,

$\beta_3 = \eta_1+\eta_2+\eta_3$, $\beta_4 = \eta_2+\eta_3$ and $\beta_5 = \eta_3$.

The denominator matrix $\mathbf{A}_L(q^{-1})$ in the corresponding right-matrix fraction is dictated by $A_L(q_L^{-1})$, namely (see (3.18)),

$$A_L(q_2^{-1}) = \prod_{p=0}^{2} A(q_6^{-1}w_6^{-2p}) = 1-(1+a^3)q_2^{-1}+a^3q_2^{-2},$$

whence (see (3.24))

$$\mathbf{A}_L(q^{-1}) = \mathbf{I}_2 - (1+a^3)\mathbf{P}_2^{(1)}(q^{-1}) + a^3\mathbf{P}_2^{(2)}(q^{-1}). \tag{3.85}$$

Specifying the polynomial

$$\bar{A}^{(L)}(q_6^{-1})B(q_6^{-1}) = \prod_{p=1}^{2} A(q_6^{-1}w_6^{-2p})B(q_6^{-1}) = \sum_{i=0}^{5} \chi_i q_6^{-i},$$

where $\chi_0 = b_0, \quad \chi_1 = (1+a)b_0+b_1, \quad \chi_2 = (1+a+a^2)b_0+(a+a^2)b_1,$

$\chi_3 = (a+a^2)b_0 + (1+a+a^2)b_1, \quad \chi_4 = a^2b_0 + (a+a^2)b_1$ and $\chi_5 = a^2b_1,$

the numerator matrix $\mathbf{B}_r(q^{-1})$ can be defined thus (see (3.71b)):

$$\begin{aligned}\mathbf{B}_r(q^{-1}) = &\operatorname{diag}(\chi_0+\chi_1+\chi_2,\ \chi_0,\ \chi_0+\chi_1)\,\mathbf{Q}_0\mathbf{P}_2^{(1)}(q^{-1}) \\ &+\operatorname{diag}(\chi_3+\chi_4+\chi_5,\ \chi_1+\chi_2+\chi_3,\ \chi_2+\chi_3+\chi_4)\,\mathbf{Q}_0\mathbf{P}_2^{(2)}(q^{-1}) \\ &+\operatorname{diag}(0,\ \chi_4+\chi_5,\ \chi_5)\,\mathbf{Q}_0\mathbf{P}_2^{(3)}(q^{-1}). \qquad (3.86)\end{aligned}$$

Frequency-Domain Representation

Observing that the frequency-domain model of equation (3.65) also can be obtained by applying the transformation defined in equation (3.51) to the time-domain representation of equation (3.68), the denominator matrix is given by

$$\begin{aligned}\mathbf{A}_{M_f}(z_3^{-1}) &= \mathbf{T}_M(z_3)\mathbf{A}_M(z^{-1})\mathbf{T}_M^{-1}(z_3) \\ &= \operatorname{diag}\left(A_M(z_3^{-1}),\ A_M(z_3^{-1}w_3^{-1}),\ \ldots,\ A_M(z_3^{-1}w_3^{-2})\right), \qquad (3.87)\end{aligned}$$

where $A_M(z_3^{-1})$ is defined in equation (3.82). Designating the polynomial (see ((3.84))

$$B_l(z_6^{-1}) = \sum_{i=0}^{5} \beta_i z_6^{-i-1},$$

the numerator matrix may be written thus:

$$\begin{aligned}\mathbf{B}_{l_f}(z_6^{-1}) &= \mathbf{T}_M(z_3)\mathbf{B}_l(z^{-1})\mathbf{T}_L^{-1}(z_2) \\ &= \begin{bmatrix} B_l(z_6^{-1}) & B_l(z_6^{-1}w_6^{-3}) \\ B_l(z_6^{-1}w_6^{-4}) & B_l(z_6^{-1}w_6^{-1}) \\ B_l(z_6^{-1}w_6^{-2}) & B_l(z_6^{-1}w_6^{-5}) \end{bmatrix}. \qquad (3.88)\end{aligned}$$

Disturbance Subsystem Model

The disturbance subsystem model initially requires the definition of $\theta(\cdot)$, namely (see (3.63)):

$$\begin{aligned}\theta(z_6^{-1}) &= \bar{A}^{(M)}(z_6^{-1})\tilde{C}(z_6^{-1}) \\ &= \left(1+(1+a)z_6^{-1}+az_6^{-2}\right)\left(1+\tilde{c}_1 z_6^{-1}+\tilde{c}_2 z_6^{-2}\right) = \sum_{i=0}^{4}\theta_i z_6^{-i},\end{aligned}$$

where $\theta_0 = 1, \quad \theta_1 = 1+a+\tilde{c}_1, \quad \theta_2 = a+(1+a)\tilde{c}_1+\tilde{c}_2,$

$$\theta_3 = a\tilde{c}_1+(1+a)\tilde{c}_2 \quad \text{and} \quad \theta_4 = a\tilde{c}_2.$$

The polynomial

$$C_M(z_3^{-1}) = 1 + c_{M_1}z_3^{-1} + c_{M_2}z_3^{-2} \tag{3.89}$$

then is designated as the stable solution of (see (3.63))

$$\begin{aligned}\sum_{p=0}^{1}\theta(z_6^{-1}w_2^{-p})\theta(z_6 w_2^{p}) &= 2\left(\theta_0\theta_4 z_3^2 + \left(\sum_{i=0}^{2}\theta_i\theta_{i+2}\right)z_3 + \sum_{i=0}^{4}\theta_i^2 \right. \\ &\qquad \left. + \left(\sum_{i=0}^{2}\theta_i\theta_{i+2}\right)z_3^{-1} + \theta_0\theta_4 z_3^{-2}\right) \\ &= 2\rho C_M(z_3^{-1})C_M(z_3).\end{aligned}$$

The numerator matrix $\mathbf{C}_M(q^{-1})$ in the representation of equation (3.73) is arranged as $\mathbf{A}_M(q^{-1})$ (see (3.83)), with $-(1+a)$ and a replaced by c_{M_1} and c_{M_2}, respectively.

3.7 Conclusion

The work contained within this chapter represents the theoretical core of this thesis. The key contribution to multirate-sampled system theory concerns the embedding of the principles underpinning the decomposition procedures within a modern control framework. In the latter respect, it will be noticed that the algebraic properties related to the polynomial matrices involved facilitate the computer-aided analysis of multirate configurations. Furthermore, in contrast with single-rate system theory, the representations established in this Chapter are characterised by having alternative interpretations in the time- and frequency-domains.

Chapter Four
A General System Model

This chapter describes how the polynomial modelling techniques developed in Chapter 3 can be applied to multivariable multirate-sampled systems. Thus, whereas the lifted single-input single-output (SISO) plant and disturbance subsystem models emanate from pulse-transfer functions defined with respect to the short time interval, the corresponding multi-input multi-output (MIMO) representations are predicated upon fast-rate matrix fraction descriptions. As a consequence, it is neither practicable nor particularly beneficial to define the elements within lifted polynomial matrices in the comprehensive detail prescribed in the scalar case.

Using the artifice of fast-rate sampling switch insertion discussed in Chapter 3, section 4.1 views a multivariable system, in which each of the inputs and outputs are sampled at dissimilar intervals, as comprising distinct input, discretised plant and output subsystems. An overall lifted representation is acquired by initially combining a fast-rate lifted model of the discretised plant with a block diagonal matrix that encapsulates the dynamics of the zero-order holds. Thereafter, the required model in left-matrix fraction form results by eliminating from consideration those output signals that are not required. Adopting a corresponding approach, section 4.2 details the derivation of a compatible description of the disturbance subsystem. The issue of causality is concentrated upon in section 4.3, in which the arrangement of signals within system vectors in accordance with their related sampling instants during the repetitive time interval leads to the characterisation of lifted system matrices as being members of a particular "family". These so-called "repetitive time interval index-dependent" representations are exploited subsequently in the dynamics-assignment and predictive control methodologies described in Chapter 5. The specification of an accordant controller model in section 4.4 warrants an analysis of the absolute stability and stability robustness of the closed-loop system, an exercise that is repeated for the SISO systems examined originally in Chapter 3. The methods established in this chapter are illustrated with the aid of a detailed example in section 4.5.

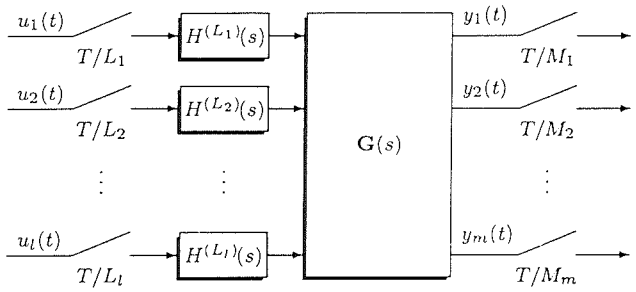

Figure 4.1. The multirate-sampled multivariable plant.

4.1 The Multivariable Plant Model

The multirate-sampled l-input/m-output plant to be considered is illustrated in Figure 4.1; the respective sampling intervals of the control and output variables are T/L_j s, $L_j \in \mathbb{Z}$, $j = 1, 2 \ldots, l$, and T/M_i s, $M_i \in \mathbb{Z}$, $i = 1, 2, \ldots, m$, and exogenous disturbance signals have been omitted for the present. Furthermore, it is assumed that

$$L_j \leq L_{j+1} \tag{4.1a}$$

and

$$M_i \leq M_{i+1}. \tag{4.1b}$$

The time-scales referred to as the short time interval and repetitive time interval (see (2.1a,b)) then are specified as

$$STI = T/\text{lcm}\,(L_1, L_2, \ldots, L_l, M_1, M_2, \ldots, M_m) = T/N \tag{4.2a}$$

and

$$RTI = T/\text{gcd}\,(L_1, L_2, \ldots, L_l, M_1, M_2, \ldots, M_m) = T, \tag{4.2b}$$

while it is also useful at this juncture to designate the parameters $\bar{L}_j$ and $\bar{M}_i$ thus:

$$\bar{L}_j = N/L_j \tag{4.3a}$$

and

$$\bar{M}_i = N/M_i. \tag{4.3b}$$

Recalling the modelling approach employed in Chapter 3 (see Figures 3.1, 3.2 and 3.3), the relationship between the pulse-transforms of signals at the i^{th} output and the j^{th} input can be expressed in terms of pulse-transfer functions designated with respect to the short time interval – and, consequently, described via equations corresponding to (3.3), (3.4) and (3.5) – by inserting fictitious fast-rate samplers at the plant input and output. Correspondingly, the system depicted in Figure 4.1 can be interpreted as the discrete-time

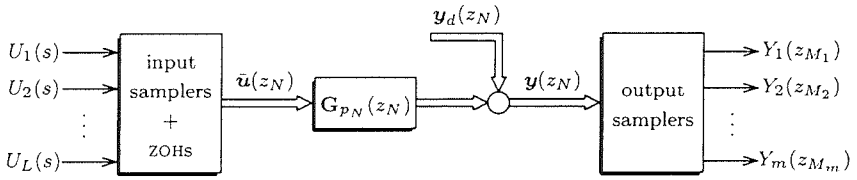

Figure 4.2. Discrete-time configuration.

configuration of Figure 4.2, in which $\boldsymbol{y}_d(z_N)$ symbolises the inclusion of m disturbance signals and the subscripts M_i related to the pulse-transforms of the outputs have been omitted for concision. The $m|l$ matrix $\mathbf{G}_{p_N}(z_N)$ represents the fast-rate pulse-transfer functions

$$Z_N\left\{G_{ij}(s)H^{(N)}(s)\right\}, \quad i=1,2,\ldots,m, \quad j=1,2,\ldots,l, \tag{4.4}$$

whereas $\boldsymbol{x}(z_N)$ $(\in \mathbb{C}^k)$, indicating $\boldsymbol{y}(z_N)$, $\boldsymbol{y}_d(z_N)$ $(\in \mathbb{C}^m)$ or $\bar{\boldsymbol{u}}(z_N)$ $(\in \mathbb{C}^l)$, denotes

$$\left[\begin{array}{cccc} X_{1_N}(z_N) & X_{2_N}(z_N) & \ldots & X_{k_N}(z_N) \end{array}\right]'. \tag{4.5}$$

It is assumed that the matrix-valued pulse-transfer function $\mathbf{G}_{p_N}(z_N)$ can be expressed as the following left-matrix fraction:

$$\mathbf{G}_{p_N}(z_N) = z_N^{-d}\boldsymbol{A}^{-1}(z_N^{-1})\boldsymbol{B}(z_N^{-1}), \quad \boldsymbol{B}(0)=\boldsymbol{B}_0(\neq \mathbf{0}), \tag{4.6}$$

where $(\boldsymbol{A},\boldsymbol{B})$ is coprime and in which it is further supposed that $\boldsymbol{A}(0)$ is upper-triangular with

$$\boldsymbol{A}_{ii}(0)=1, \quad i=1,2,\ldots,m.$$

Neglecting the disturbance signals for the time being, from comparison of equations (4.6) and (3.9b) and by analogy with (3.11) and (3.37), the subsystem defined by $\mathbf{G}_{p_N}(z_N)$ can be described by the time-domain model

$$\begin{aligned} \hat{\mathbf{A}}(q^{-1})\hat{\mathbf{y}}(0) &= \hat{\mathbf{P}}_m^{(d)}(q^{-1})\hat{\mathbf{B}}(q^{-1})\hat{\mathbf{u}}(0) \\ &= \hat{\mathbf{B}}(q^{-1})\hat{\mathbf{P}}_l^{(d)}(q^{-1})\hat{\mathbf{u}}(0), \end{aligned} \tag{4.7}$$

where:

(i) modifying the notation used in Chapter 3, with

$$\mathbf{x}_k(0) = \left[\begin{array}{cccc} x_k(0) & x_k(-1) & \ldots & x_k(-N+1) \end{array}\right]'$$

representing $\mathbf{y}_i(0)$ or $\mathbf{u}_j(0)$,

$$\hat{\mathbf{y}}(0) = \begin{bmatrix} \mathbf{y}_1'(0) & \mathbf{y}_2'(0) & \dots & \mathbf{y}_m'(0) \end{bmatrix}' \quad (\in \mathbb{R}^{mN})$$

and $$\hat{\bar{\mathbf{u}}}(0) = \begin{bmatrix} \bar{\mathbf{u}}_1'(0) & \bar{\mathbf{u}}_2'(0) & \dots & \bar{\mathbf{u}}_l'(0) \end{bmatrix}' \quad (\in \mathbb{R}^{lN});$$

(ii) the $kN|kN$ matrix $\hat{\mathbf{P}}_k^{(\lambda)}(q^{-1})$ is designated as

$$\hat{\mathbf{P}}_k^{(\lambda)}(q^{-1}) = \text{block diag}\left(\mathbf{P}_N^{(\lambda)}(q^{-1}),\ \mathbf{P}_N^{(\lambda)}(q^{-1}),\ \dots\ ,\ \mathbf{P}_N^{(\lambda)}(q^{-1})\right);$$

(iii) if $A(z_N^{-1})$ $(B(z_N^{-1}))$ represents the $(i,j)^{th}$ element of $\boldsymbol{A}(z_N^{-1})$ $(\boldsymbol{B}(z_N^{-1}))$, then $\mathbf{A}_N(q^{-1})$ $(\mathbf{B}_N(q^{-1}))$ constitutes the $(i,j)^{th}$ $N|N$ block of the $mN|mN$ matrix $\hat{\mathbf{A}}(q^{-1})$ $(mN|lN$ matrix $\hat{\mathbf{B}}(q^{-1}))$.

The relationship between the j^{th} fast- and slow-sampled controls is, from equations (3.36) (with altered notation) and (4.3a), given by

$$\bar{\mathbf{u}}_j(0) = \mathbf{H}_j(q^{-1})\mathbf{u}_j^{(Lj)}(0), \tag{4.8}$$

in which $$\mathbf{u}_j^{(Lj)}(0) = \begin{bmatrix} u_j(0) & u_j(-\bar{L}_j) & \dots & u_j(-(L_j-1)\bar{L}_j) \end{bmatrix}'$$

and $$\mathbf{H}_j(q^{-1}) = \mathbf{P}_N^{(\bar{L}_j-1)}(q^{-1})\mathbf{W}_{L_j}.$$

The l discretised zero-order holds $H_N^{(L_j)}(z_N)$, $j = 1, 2, \dots, l$, then engender the following time-domain model:

$$\hat{\bar{\mathbf{u}}}(0) = \hat{\mathbf{H}}(q^{-1})\tilde{\mathbf{u}}(0), \tag{4.9}$$

where $$\tilde{\mathbf{u}}(0) = \begin{bmatrix} \mathbf{u}_1^{(L_1)'}(0) & \mathbf{u}_2^{(L_2)'}(0) & \dots & \mathbf{u}_l^{(L_l)'}(0) \end{bmatrix}'$$

and $$\hat{\mathbf{H}}(q^{-1}) = \text{block diag}\left(\mathbf{H}_1(q^{-1}),\ \mathbf{H}_2(q^{-1}),\ \dots\ ,\ \mathbf{H}_l(q^{-1})\right).$$

Combining equations (4.7) and (4.9), the fast-sampled outputs $\hat{\mathbf{y}}(0)$ are related to the slow-sampled controls $\tilde{\mathbf{u}}(0)$ thus:

$$\hat{\mathbf{A}}(q^{-1})\hat{\mathbf{y}}(0) = \hat{\mathbf{B}}_H(q^{-1})\tilde{\mathbf{u}}(0). \tag{4.10}$$

where $$\hat{\mathbf{B}}_H(q^{-1}) = \hat{\mathbf{B}}(q^{-1})\hat{\mathbf{P}}_l^{(d)}(q^{-1})\hat{\mathbf{H}}(q^{-1}).$$

The loss of information associated with sampling the output variables at integer multiples of the short time interval is dealt with by separating each set of N fast-sampled outputs

into those signals that are measured, namely, $y_i^{(M_i)}(-k\bar{M}_i)$, $k \in [0, M_i - 1]$ (see (3.12)), and the extraneous signals, namely, $y_i^{(M_i)}(-\iota)$, $\iota \neq k\bar{M}_i$. Accordingly, introducing the permutation matrix $\mathbf{\Pi}_1$, a vector $\mathbf{y}_r(0)$ comprising re-ordered output variables is defined as

$$\mathbf{y}_r(0) = \mathbf{\Pi}_1 \hat{\mathbf{y}}(0), \quad \mathbf{y}_r(0) = \begin{bmatrix} \tilde{\mathbf{y}}'(0) & \mathbf{y}_e' \end{bmatrix}', \tag{4.11}$$

where $$\tilde{\mathbf{y}}(0) = \begin{bmatrix} \mathbf{y}_1^{(M_1)'}(0) & \mathbf{y}_2^{(M_2)'}(0) & \dots & \mathbf{y}_m^{(M_m)'}(0) \end{bmatrix}',$$

with $\mathbf{y}_i^{(M_i)}(0)$ specified analogously to $\mathbf{u}_j^{(L_j)}(0)$ (see (4.8)),

and $$\mathbf{y}_e' = \begin{bmatrix} \mathbf{y}_{1_e}' & \mathbf{y}_{2_e}' & \dots & \mathbf{y}_{m_e}' \end{bmatrix}',$$

in which $$\mathbf{y}_{i_e} = \begin{bmatrix} \dots & y_i(-\iota) & \dots \end{bmatrix}', \quad \iota \neq k\bar{M}_i, \quad k \in [0, M_i - 1].$$

The plant model that results by applying the above transformation to equation (4.10) is

$$\mathbf{A}_r(q^{-1})\mathbf{y}_r(0) = \mathbf{B}_r(q^{-1})\tilde{\mathbf{u}}(0), \tag{4.12}$$

where $$\mathbf{A}_r = \mathbf{\Pi}_1 \hat{\mathbf{A}} \mathbf{\Pi}_1' = \begin{bmatrix} \mathbf{A}_1 & \mathbf{A}_2 \\ \mathbf{A}_3 & \mathbf{A}_4 \end{bmatrix}$$

and $$\mathbf{B}_r = \mathbf{\Pi}_1 \hat{\mathbf{B}}_H = \begin{bmatrix} \mathbf{B}_1 \\ \mathbf{B}_2 \end{bmatrix}.$$

Designating the following matrix fraction, which is assumed to be coprime:

$$\mathbf{A}_{4_2}^{-1}(q^{-1})\mathbf{A}_{2_4}(q^{-1}) = \mathbf{A}_2(q^{-1})\mathbf{A}_4^{-1}(q^{-1}), \tag{4.13}$$

simple manipulation yields the lifted plant description

$$\tilde{\mathbf{A}}(q^{-1})\tilde{\mathbf{y}}(0) = \tilde{\mathbf{B}}(q^{-1})\tilde{\mathbf{u}}(0), \tag{4.14}$$

where $$\tilde{\mathbf{A}} = \mathbf{A}_{4_2}\mathbf{A}_1 - \mathbf{A}_{2_4}\mathbf{A}_3 \quad \text{and} \quad \tilde{\mathbf{B}} = \mathbf{A}_{4_2}\mathbf{B}_1 - \mathbf{A}_{2_4}\mathbf{B}_2.$$

Notice that it is assumed that $\mathbf{A}_{4_2}(q^{-1})$ specified above has a similar causal structure to that of $\mathbf{A}_1(q^{-1})$, which, for the present, can be defined as the requirement that the highest possible powers of q in corresponding elements of these matrices are identical. The topics of causality and matrix fraction conversion, including the term $\mathbf{A}_{4_2}^{-1}\mathbf{A}_{2_4}$ defined above, will be examined in greater detail subsequently.

The alternative modelling approach described in section 3.3 can be extended to the multivariable case by observing that, if the κ^{th} element in any of the "time-domain vectors" within equations (4.7), (4.9), (4.10), (4.11), (4.12) and (4.14) is

$$x_k(-j\bar{K}), \quad \bar{K} = N/K \quad \text{(see (4.3a,b))},$$

then the κ^{th}entry in the corresponding frequency-domain entity is

$$X_{k_K}(z_K w_K^j) = X_{k_K}\left(z_N^{\bar{K}} w_N^{j\bar{K}}\right).$$

Consequently, the formulation of a frequency-domain representation of the multirate-sampled multivariable plant originates by using the following equation in place of equation (4.7):

$$\begin{aligned}\hat{\mathbf{A}}_f(z_N^{-1})\hat{\mathbf{y}}_f(z_N) &= \hat{\mathbf{P}}^{(d)}_{m_f}(z_N^{-1})\hat{\mathbf{B}}_f(z_N^{-1})\hat{\mathbf{u}}_f(z_N) \\ &= \hat{\mathbf{B}}_f(z_N^{-1})\hat{\mathbf{P}}^{(d)}_{l_f}(z_N^{-1})\hat{\mathbf{u}}_f(z_N), \end{aligned} \tag{4.15}$$

where:

(i)

$$\hat{\mathbf{y}}_f(z_N) = \left[\begin{array}{cccc} \mathbf{y}_1'(z_N) & \mathbf{y}_2'(z_N) & \ldots & \mathbf{y}_m'(z_N) \end{array}\right]' \quad (\in \mathbb{C}^{mN}),$$

in which $$\mathbf{y}_i'(z_N) = \left[\begin{array}{cccc} Y_{i_N}(z_N) & Y_{i_N}(z_N w_N) & \ldots & Y_{i_N}(z_N w_N^{N-1}) \end{array}\right]',$$

with $\hat{\mathbf{u}}_f(z_N)$ defined similarly;

(ii) the $kN|kN$ matrix $\hat{\mathbf{P}}^{(\lambda)}_{k_f}(z_N^{-1})$ is designated as

$$\hat{\mathbf{P}}^{(\lambda)}_{k_f}(z_N^{-1}) = \text{block diag}\left(\mathbf{P}^{(\lambda)}_{N_f}(z_N^{-1}),\ \mathbf{P}^{(\lambda)}_{N_f}(z_N^{-1}),\ \ldots,\ \mathbf{P}^{(\lambda)}_{N_f}(z_N^{-1})\right) \quad \text{(see (3.41))};$$

(iii) if $A(z_N^{-1})$ ($B(z_N^{-1})$) represents the $(i,j)^{th}$ element of $\boldsymbol{A}(z_N^{-1})$ ($\boldsymbol{B}(z_N^{-1})$), then $\mathbf{A}_{N_f}(z_N^{-1})$ ($\mathbf{B}_{N_f}(z_N^{-1})$) (see (3.42)) constitutes the $(i,j)^{th}$ $N|N$ block of the $mN|mN$ matrix $\hat{\mathbf{A}}_f(z_N^{-1})$ ($mN|lN$ matrix $\hat{\mathbf{B}}_f(z_N^{-1})$).

Similarly, using equations (3.44) and (3.46), the input subsystem described in the time-domain via equation (4.9) can be modelled thus:

$$\hat{\mathbf{u}}_f(z_N) = \mathbf{H}_f(z_N^{-1})\tilde{\mathbf{u}}_f(z_N), \tag{4.16}$$

where $$\tilde{\mathbf{u}}_f(z_N) = \left[\begin{array}{cccc} \mathbf{u}_{1_f}^{(L_1)'}(z_N) & \mathbf{u}_{2_f}^{(L_2)'}(z_N) & \ldots & \mathbf{u}_{m_f}^{(L_m)'}(z_N) \end{array} \right]',$$

in which, omitting the subscript j from each L_j and $\bar{L}_j$ for clarity,

$$\begin{aligned} \mathbf{u}_{j_f}^{(L)}(z_N) &= \left[\begin{array}{cccc} U_{j_L}(z_L) & U_{j_L}(z_L w_L) & \ldots & U_{j_L}(z_L w_L^{L-1}) \end{array} \right]', \\ &= \left[\begin{array}{cccc} U_{j_L}(z_N^{\bar{L}}) & U_{j_L}(z_N^{\bar{L}} w_N^{\bar{L}}) & \ldots & U_{j_L}(z_N^{\bar{L}} w_N^{(L-1)\bar{L}}) \end{array} \right]' \end{aligned}$$

and $$\mathbf{H}_f(z_N^{-1}) = \text{block diag}\left(\mathbf{H}_{1_f}(z_N^{-1}),\ \mathbf{H}_{2_f}(z_N^{-1}),\ \ldots\ ,\ \mathbf{H}_{l_f}(z_N^{-1})\right),$$

where $$\mathbf{H}_{j_f}(z_N^{-1}) = \mathbf{P}_{N_f}^{(\bar{L}-1)}(z_N^{-1})\mathbf{W}_{L_f}(z_N).$$

Adopting an identical approach to that followed in the time-domain case, namely, combining equations (4.15) and (4.16), using the transformation

$$\mathbf{y}_{r_f}(z_N) = \mathbf{\Pi}_1 \hat{\mathbf{y}}_f(z_N) \quad \text{(see (4.11))}$$

to obtain $$\mathbf{A}_{r_f}(z_N^{-1})\mathbf{y}_{r_f}(z_N) = \mathbf{B}_{r_f}(z_N^{-1})\tilde{\mathbf{u}}_f(z_N) \quad \text{(cf. (4.12))}$$

and subsequently partitioning $\mathbf{A}_{r_f}$ and $\mathbf{B}_{r_f}$ as indicated in equation (4.12), the lifted frequency-domain description is

$$\tilde{\mathbf{A}}_f(z_N^{-1})\tilde{\mathbf{y}}_f(z_N) = \tilde{\mathbf{B}}_f(z_N^{-1})\tilde{\mathbf{u}}_f(z_N). \tag{4.17}$$

It will be observed that, by invoking the time- to frequency-domain transformation specified by equation (3.51), the vectors $\tilde{\mathbf{y}}_f$ and $\tilde{\mathbf{u}}_f$ in equation (4.17) can be expressed as

$$\tilde{\mathbf{y}}_f(z_N) = \mathbf{T}_{\tilde{y}}(z_N)\tilde{\mathbf{y}}(0) \tag{4.18a}$$

and $$\tilde{\mathbf{u}}_f(z_N) = \mathbf{T}_{\tilde{u}}(z_N)\tilde{\mathbf{u}}(0), \tag{4.18b}$$

where $$\mathbf{T}_{\tilde{y}}(z_N) = \text{block diag}\left(\mathbf{T}_{M_1}(z_N^{\bar{M}_1}),\ \mathbf{T}_{M_2}(z_N^{\bar{M}_2}),\ \ldots\ ,\ \mathbf{T}_{M_m}(z_N^{\bar{M}_m})\right),$$

with $\mathbf{T}_{\tilde{u}}(z_N)$ defined accordingly, whence the matrices $\tilde{\mathbf{A}}_f$ and $\tilde{\mathbf{B}}_f$ are related to $\tilde{\mathbf{A}}$ and $\tilde{\mathbf{B}}$ in equation (4.17) as follows:

$$\tilde{\mathbf{A}}_f(z_N) = \mathbf{T}_{\tilde{y}}(z_N)\tilde{\mathbf{A}}(z^{-1})\mathbf{T}_{\tilde{y}}^{-1}(z_N) \tag{4.19a}$$

and $$\tilde{\mathbf{B}}_f(z_N) = \mathbf{T}_{\tilde{y}}(z_N)\tilde{\mathbf{B}}(z^{-1})\mathbf{T}_{\tilde{u}}^{-1}(z_N). \tag{4.19b}$$

4.2 The Disturbance Subsystem Model

This section generalises the results obtained in section 3.4 to the multivariable case. In common with the plant model derived above, the disturbance subsystem is specified initially by a fast-rate pulse-transfer function matrix expressed in left-matrix fraction form.

Disregarding the plant at this stage, it is assumed that the disturbance subsystem is described thus:

$$\boldsymbol{y}(z_N) = \mathbf{G}_{d_N}(z_N)\boldsymbol{e}(z_N), \tag{4.20}$$

where $$\mathbf{G}_{d_N}(z_N) = \boldsymbol{A}^{-1}(z_N^{-1})\boldsymbol{C}(z_N^{-1}),$$

in which $\boldsymbol{C}(z_N^{-1})$ is stable, $(\boldsymbol{A}, \boldsymbol{C})$ is coprime and, again with a slight abuse of notation, $\boldsymbol{e}(z_N)$ signifies m zero-mean discrete-time white noise sources with spectral densities $\sigma_1^2, \sigma_2^2, \ldots, \sigma_m^2$. By analogy with equations (4.6) and (4.7), the lifted representation associated with (4.20) is

$$\hat{\mathbf{A}}(q^{-1})\hat{\mathbf{y}}(0) = \hat{\mathbf{C}}(q^{-1})\hat{\mathbf{e}}(0), \tag{4.21}$$

with $\hat{\mathbf{e}}(0)$ defined similarly to $\hat{\mathbf{y}}(0)$ ((4.7)) and where $\hat{\mathbf{C}}(q^{-1})$ is related to $\boldsymbol{C}(z_N^{-1})$ in an analogous fashion to $\hat{\mathbf{A}}(q^{-1})$ and $\boldsymbol{A}(z_N^{-1})$. Invoking the transformation specified in equation (4.11), the re-ordered description is

$$\mathbf{A}_r(q^{-1})\mathbf{y}_r(0) = \mathbf{C}_r(q^{-1})\hat{\mathbf{e}}(0), \tag{4.22}$$

with $$\mathbf{C}_r = \mathbf{\Pi}_1\hat{\mathbf{C}} = \begin{bmatrix} \mathbf{C}_1 \\ \mathbf{C}_2 \end{bmatrix},$$

whence it is readily shown that

$$\tilde{\mathbf{A}}(q^{-1})\tilde{\mathbf{y}}(0) = \mathbf{\Gamma}(q^{-1})\hat{\mathbf{e}}(0) = \tilde{\boldsymbol{\xi}}(0), \tag{4.23}$$

where (see (4.13)), $$\mathbf{\Gamma} = \mathbf{A}_{4_2}\mathbf{C}_1 - \mathbf{A}_{2_4}\mathbf{C}_2,$$

and in which $\tilde{\boldsymbol{\xi}}(0)$ and $\tilde{\mathbf{y}}(0)$ ((4.11)) are arranged likewise.

In order to ensure compatibility with subsequent design methodologies it is necessary to modify the above model by replacing the fast-sampled white noise sources with slower-sampled counterparts. In this respect, consider the relationship defined by the polynomial

$\Gamma_{ji_k}(q_N^{-1})$ between the signal $\xi_j(-k\bar{M}_j)$ within $\tilde{\boldsymbol{\xi}}(0)$ in equation (4.23) and the sequence $\{e_i(\upsilon T/N)\}$, namely,

$$\xi_j(-k\bar{M}_j) = \Gamma_{ji_k}(q_N^{-1})e_i(-k\bar{M}_j) = \boldsymbol{\gamma}'_{ji_k}(q^{-1})\mathbf{e}_i(0), \tag{4.24}$$

where $$\boldsymbol{\gamma}_{ji_k} = \begin{bmatrix} q^{-1}\Gamma_0 & \dots & q^{-1}\Gamma_{k\bar{M}_j-1} & \Gamma_{k\bar{M}_j} & \dots & \Gamma_{N-1} \end{bmatrix}'.$$

Addressing causality constraints by designating m_k to be the smallest integer satisfying

$$m_k\bar{M}_i = k\bar{M}_j + \mu, \quad \mu \in [0, \bar{M}_i - 1], \tag{4.25}$$

it is supposed that $\xi_j(-k\bar{M}_j)$ alternatively may be related to the white noise source $\{\epsilon_i(\mu_i T/M_i)\}$ with zero mean and spectral density defined with respect to the operator z_{M_i} of $\sigma_i^2/\bar{M}_i$ via the polynomial $\tilde{C}_{ji_k}(q_{M_i}^{-1})$ thus:

$$\xi_j(-k\bar{M}_j) = \tilde{C}_{ji_k}(q_{M_i}^{-1})\epsilon_i(-m_k\bar{M}_i) = \tilde{\mathbf{c}}'_{ji_k}(q^{-1})\boldsymbol{\epsilon}_i^{(M_i)}(0), \tag{4.26}$$

where $$\tilde{\mathbf{c}}_{ji_k} = \begin{bmatrix} q^{-1}\tilde{C}_0 & \dots & q^{-1}\tilde{C}_{m_k-1} & \tilde{C}_{m_k} & \dots & \tilde{C}_{M_i-1} \end{bmatrix}'.$$

The power spectral density $\Phi_{\xi\xi}(z)$ of the signal $\xi_j(-k\bar{M}_j)$ resulting solely from the i^{th} white noise source then is acquired by exploiting equation (3.59), whence, from equation (4.24),

$$\Phi_{\xi\xi}(z) = \frac{1}{N^2}\sum_{p=0}^{N-1}\Gamma_{ji_k}(z_N^{-1}w_N^{-p})\Gamma_{ji_k}(z_N w_N^p)\Phi_{ee_N}^{(i)}(z_N), \tag{4.27a}$$

in which $$\Phi_{ee_N}^{(i)}(z_N) = \sigma_i^2.$$

Alternatively, using equation (4.26), $\Phi_{\xi\xi}(z)$ is given by

$$\Phi_{\xi\xi}(z) = \frac{1}{\bar{M}_i^2}\sum_{p=0}^{M_i-1}\tilde{C}_{ji_k}(z_{M_i}^{-1}w_{M_i}^{-p})\tilde{C}_{ji_k}(z_{M_i}w_{M_i}^p)\Phi_{\epsilon\epsilon_{M_i}}(z_{M_i}), \tag{4.27b}$$

where $$\Phi_{\epsilon\epsilon_{M_i}}(z_{M_i}) = \frac{1}{\bar{M}_i}\sigma_i^2.$$

Now, expressing the general polynomial $X(z_K^{-1})$ thus:

$$X(z_K^{-1}) = \sum_{i=0}^{n_x} x_i z_K^{-i} = \sum_{i=0}^{K-1} z_K^{-i} X_i(z^{-1}),$$

with $$X_i(z^{-1}) = x_i + x_{2i}z^{-1} + x_{3i}z^{-2} + \dots,$$

equations (4.27a,b) can be simplified by using

$$\sum_{j=0}^{K-1} w_K^{\pm j} = 0$$

and consequently noting that

$$\sum_{p=0}^{K-1} X(z_K^{-1} w_K^{-p}) X(z_K w_K^p) = \sum_{i=0}^{K-1} z_K^{-i} w_K^{-i} X_i(z^{-1}) \sum_{i=0}^{K-1} z_K^i w_K^i X_i(z)$$
$$= K \sum_{i=0}^{K-1} X_i(z^{-1}) X_i(z). \tag{4.28}$$

Thus, using equation (4.28), equation (4.27a) can be expressed as

$$\Phi_{\xi\xi}(z) = \frac{\sigma^2}{N} \sum_{\kappa=0}^{N-1} \Gamma_\kappa(z^{-1}) \Gamma_\kappa(z) = \frac{\sigma^2}{N} \boldsymbol{\gamma}'_{ji_k}(z^{-1}) \boldsymbol{\gamma}_{ji_k}(z) \quad \text{(see (4.24))}, \tag{4.29a}$$

while, accordingly, equation (4.27a,b) becomes:

$$\Phi_{\xi\xi}(z) = \frac{\sigma^2}{M_i} \sum_{\kappa=0}^{M_i-1} \tilde{C}_\kappa(z^{-1}) \tilde{C}_\kappa(z) = \frac{\sigma^2}{M_i} \tilde{\mathbf{c}}'_{ji_k}(z^{-1}) \tilde{\mathbf{c}}_{ji_k}(z) \quad \text{(see (4.26))}. \tag{4.29b}$$

Extending the principles governing equations (4.29a,b) to address the relationships between the signals $\xi_j(-k\bar{M}_j)$, $k = 0, 1, \ldots, M_j - 1$, $j = 1, 2, \ldots, m$, and the discrete-time white noise sources $\epsilon_i(-\kappa\bar{M}_i)$, $\kappa = 0, 1, \ldots, M_i - 1$, $i = 1, 2, \ldots, m$, the vector $\tilde{\boldsymbol{\xi}}(0)$ in equation (4.23) can be substituted by

$$\tilde{\boldsymbol{\xi}}(0) = \tilde{\mathbf{C}}(q^{-1}) \tilde{\boldsymbol{\epsilon}}(0), \tag{4.30}$$

where $\tilde{\mathbf{C}}(z^{-1})$ constitutes the stable solution of

$$\tilde{\mathbf{C}}(z^{-1}) \tilde{\mathbf{C}}^\star(z^{-1}) = \boldsymbol{\Gamma}(z^{-1}) \boldsymbol{\Gamma}^\star(z^{-1}).$$

Therefore, from equations (4.23) and (4.30), the lifted disturbance subsystem model is

$$\tilde{\mathbf{A}}(q^{-1}) \tilde{\mathbf{y}}(0) = \tilde{\mathbf{C}}(q^{-1}) \tilde{\boldsymbol{\epsilon}}(0). \tag{4.31}$$

4.3 The Repetitive Time Interval Index-Dependent Model

This section describes an alternative lifted description in which the arrangement of signals within vectors is dictated by their associated sample instants during the repetitive time

interval. The resultant "repetitive time interval index-dependent" matrices present a means of addressing causality issues and constitute a useful analytical tool.

Initially, using the symbol ι in place of i (see (3.7)), the relevant sampling instants are listed retrogressively as follows:

$$\iota = 0, \mu_1, \ldots, \mu_\theta, \ldots, \mu_\Theta,$$

and

$$\iota = 0, \lambda_1, \ldots, \lambda_\phi, \ldots, \lambda_\Phi,$$

in which (see (4.1a,b)),

$$\mu_1 = \bar{M}_m, \quad \mu_\Theta = (M_m - 1)\bar{M}_m, \quad \lambda_1 = \bar{L}_l \quad \text{and} \quad \lambda_\Phi = (L_l - 1)\bar{L}_l,$$

while it is supposed that permutation matrices $\mathbf{\Pi}_2$ and $\mathbf{\Pi}_3$ organise the entries within the corresponding vectors accordingly. The vectors $\bar{\mathbf{y}}(0)$ (and $\bar{\boldsymbol{\epsilon}}(0)$) and $\bar{\mathbf{u}}(0)$ consequently are defined as:

$$\bar{\mathbf{y}}(0) = \mathbf{\Pi}_2\tilde{\mathbf{y}}(0) = \begin{bmatrix} \mathbf{y}_0'(0) & y_m(-\mu_1) & \ldots & y_i(-\mu_\theta) & \ldots & y_m(-\mu_\Theta) \end{bmatrix}', \tag{4.32}$$

where

$$\mathbf{y}_0(0) = \begin{bmatrix} y_1(0) & y_2(0) & \ldots & y_m(0) \end{bmatrix}',$$

with $\bar{\boldsymbol{\epsilon}}(0)$ designated likewise, and

$$\bar{\mathbf{u}}(0) = \mathbf{\Pi}_3\tilde{\mathbf{u}}(0) = \begin{bmatrix} \mathbf{u}_0'(0) & u_l(-\lambda_1) & \ldots & u_j(-\lambda_\phi) & \ldots & u_l(-\lambda_\Phi) \end{bmatrix}', \tag{4.33}$$

where

$$\mathbf{u}_0(0) = \begin{bmatrix} u_1(0) & u_2(0) & \ldots & u_l(0) \end{bmatrix}'.$$

Applying the above transformations to the model obtained by uniting equations (4.14) and (4.31) and disregarding the signals $y_m(-\mu_1)$ and $u_l(-\lambda_1)$, the overall system description is

$$\bar{\mathbf{y}}(0) = \mathbf{A}^{-1}(q^{-1})\mathbf{B}(q^{-1})\bar{\mathbf{u}}(0) + \mathbf{A}^{-1}(q^{-1})\mathbf{C}(q^{-1})\bar{\boldsymbol{\epsilon}}(0), \tag{4.34}$$

where $\mathbf{A}(q^{-1}) = \mathbf{\Pi}_2\tilde{\mathbf{A}}(q^{-1})\mathbf{\Pi}_2' =$

$$\begin{bmatrix} \mathbf{A}_{00}(q^{-1}) & \ldots & \mathbf{a}_{0\theta}(q^{-1}) & \ldots & \mathbf{a}_{0\Theta}(q^{-1}) \\ \vdots & \ddots & \vdots & \ddots & \vdots \\ q^{-1}\mathbf{a}_{\theta 0}'(q^{-1}) & \ldots & a_{\theta\theta}(q^{-1}) & \ldots & a_{\theta\Theta}(q^{-1}) \\ \vdots & \ddots & \vdots & \ddots & \vdots \\ q^{-1}\mathbf{a}_{\Theta 0}'(q^{-1}) & \ldots & q^{-1}a_{\Theta\theta}(q^{-1}) & \ldots & a_{\Theta\Theta}(q^{-1}) \end{bmatrix},$$

with $\mathbf{A}(0)$ upper-triangular, in which

$$\mathbf{A}_{00_{11}}(0) = \ldots = \mathbf{A}_{00_{mm}}(0) = \ldots = a_{\theta\theta}(0) = \ldots = a_{\Theta\Theta}(0) = 1,$$

and $$\mathbf{B}(q^{-1}) = \mathbf{\Pi}_2\tilde{\mathbf{B}}(q^{-1})\mathbf{\Pi}_3' = \begin{bmatrix} q^{-1}\mathbf{B}_{00}(q^{-1}) & \ldots & \mathbf{b}_{0\phi}(q^{-1}) & \ldots & \mathbf{b}_{0\Phi}(q^{-1}) \\ \vdots & \ddots & \vdots & \ddots & \vdots \\ q^{-1}\mathbf{b}'_{\theta 0}(q^{-1}) & \ldots & b_{\theta\phi}(q^{-1}) & \ldots & b_{\theta\Phi}(q^{-1}) \\ \vdots & \ddots & \vdots & \ddots & \vdots \\ q^{-1}\mathbf{b}'_{\Theta 0}(q^{-1}) & \ldots & b_{\Theta\phi}(q^{-1}) & \ldots & b_{\Theta\Phi}(q^{-1}) \end{bmatrix},$$

in which, with $b_{\theta\phi}(q^{-1})$ denoting the element within $\mathbf{B}(q^{-1})$ relating $y_i(-\mu_\theta)$ to $u_j(-\lambda_\phi)$,

$$b_{\theta\phi}(0) = \begin{cases} b_{\theta\phi_0}, & \mu_\theta \leq \lambda_\phi - d \\ 0, & \mu_\theta > \lambda_\phi - d. \end{cases}$$

With the provisos that the leading coefficients of its diagonal elements in general will not be unity and that $\mathbf{C}(0)$ is block upper-triangular, $\mathbf{C}(q^{-1})$ otherwise is organised similarly to $\mathbf{A}(q^{-1})$.

It is assumed that the open-loop system model of equation (4.34) can be expressed in right-matrix fraction form as

$$\bar{\mathbf{y}}(0) = \mathbf{B}_a(q^{-1})\mathbf{A}_b^{-1}\bar{\mathbf{u}}(0) + \mathbf{C}_a(q^{-1})\mathbf{A}_c^{-1}(q^{-1})\bar{\boldsymbol{\epsilon}}(0), \tag{4.35}$$

in which $(\mathbf{B}_a, \mathbf{A}_b)$ and $(\mathbf{C}_a, \mathbf{A}_c)$ are coprime. Given the arrangement of $\mathbf{A}$, $\mathbf{B}$ and $\mathbf{C}$ above, it is beneficial to confer a corresponding structure on each of the matrices in equation (4.35), in addition to those defined subsequently, by specifying that if $\mathbf{X}(q^{-1})$ denotes the denominator of a matrix fraction then $\mathbf{X}(0)$ is block upper-triangular. Consequently, while their corresponding elements constitute polynomials with different degrees and coefficients, it is possible to view certain matrices as being members of a set which have the same dimensions and causally relate "repetitive time interval index-dependent" system vectors identically. In this respect, the notation "$\mathbf{Y} \sim \mathbf{X}$" is introduced at this juncture to indicate that "$\mathbf{Y}$ possesses a similar causal structure to $\mathbf{X}$". Thus, for instance (see (4.34)), $\mathbf{A} \sim \mathbf{C}$.

Accordingly, designating

$$\mathbf{X}(q^{-1}) = \begin{bmatrix} \mathbf{X}_{00}(q^{-1}) & \cdots & \mathbf{x}_{0\phi}(q^{-1}) & \cdots & \mathbf{x}_{0\Phi}(q^{-1}) \\ \vdots & \ddots & \vdots & \ddots & \vdots \\ q^{-1}\mathbf{x}'_{\phi 0}(q^{-1}) & \cdots & x_{\phi\phi}(q^{-1}) & \cdots & x_{\phi\Phi}(q^{-1}) \\ \vdots & \ddots & \vdots & \ddots & \vdots \\ q^{-1}\mathbf{x}'_{\Phi 0}(q^{-1}) & \cdots & q^{-1}x_{\Phi\phi}(q^{-1}) & \cdots & x_{\Phi\Phi}(q^{-1}) \end{bmatrix}, \tag{4.36}$$

it is supposed that $\mathbf{A}_b \sim \mathbf{X}$, where $\mathbf{A}_b(0)$ is strictly upper-triangular with each diagonal element equal to unity. Moreover, observing that the respective pre- and post-multiplication of $\mathbf{B}$ by $\mathbf{A}$ and $\mathbf{X}$ preserves the causal structure of $\mathbf{B}$, it is apparent from equations (4.34) and (4.35) that $\mathbf{B}_a \sim \mathbf{B}$. Similar considerations regarding the structures of $\mathbf{AC}_a$ and $\mathbf{CA}_c$ reveal that, with $\mathbf{A}_c(0)$ and $\mathbf{A}(0)$ arranged likewise, $\mathbf{A}_c \sim \mathbf{C}$ and $\mathbf{C}_a \sim \mathbf{C}$.

Returning to equation (4.13), the term $\mathbf{A}_{4_2}^{-1}\mathbf{A}_{2_4}$ may be acquired by invoking the use of matrix fractions with the structures described above and consequently specifying

$$\check{\mathbf{A}}_{4_2}^{-1}(q^{-1})\check{\mathbf{A}}_{2_4}(q^{-1}) = \mathbf{A}_2(q^{-1})\mathbf{A}_4^{-1}(q^{-1}), \tag{4.37}$$

in which $\check{\mathbf{A}}_{4_2}(0)$ is upper-triangular with all its elements along the principal diagonal equal to unity. Compatibility with the model of equation (4.14) then requires that $\mathbf{A}_{4_2}(q^{-1})$ and $\mathbf{A}_{2_4}(q^{-1})$ are defined thus:

$$\mathbf{A}_{4_2}(q^{-1}) = \mathbf{\Pi}'_2\check{\mathbf{A}}_{4_2}(q^{-1})\mathbf{\Pi}_2 \tag{4.38a}$$

and

$$\mathbf{A}_{2_4}(q^{-1}) = \mathbf{\Pi}'_2\check{\mathbf{A}}_{2_4}(q^{-1}). \tag{4.38b}$$

4.4 The Closed-Loop System Description

The designation in this section of controller models that are accordant with the foregoing "lifted" representations of the plant and disturbance subsystem warrants the formulation of the corresponding closed-loop system description. Thereafter, the absolute stability and stability robustness of both single-input single-output (SISO) and multi-input multi-output (MIMO) multirate-sampled feedback configurations are addressed.

It is supposed initially that the computational delay between the receipt of a measurement and the application of a control can be neglected. The control law therefore is

realised by an algorithm which is specified thus:

$$\bar{\mathbf{u}}(0) = -\mathbf{R}^{-1}(q^{-1})\mathbf{S}(q^{-1})\bar{\mathbf{y}}(0), \tag{4.39a}$$

where $\mathbf{R} \sim \mathbf{X}$ and, with $s_{\phi\theta}(q^{-1})$ defined as the polynomial relating $u_j(-\lambda_\phi)$ to $y_i(-\mu_\theta)$, where the structure imposed on the "numerator" matrix by causality constraints is

$$\mathbf{S}(q^{-1}) = \begin{bmatrix} \mathbf{S}_{00}(q^{-1}) & \dots & \mathbf{s}_{0\theta}(q^{-1}) & \dots & \mathbf{s}_{0\Theta}(q^{-1}) \\ \vdots & \ddots & \vdots & \ddots & \vdots \\ q^{-1}\mathbf{s}'_{\phi 0}(q^{-1}) & \dots & s_{\phi\theta}(q^{-1}) & \dots & s_{\phi\Theta}(q^{-1}) \\ \vdots & \ddots & \vdots & \ddots & \vdots \\ q^{-1}\mathbf{s}'_{\Phi 0}(q^{-1}) & \dots & s_{\Phi\theta}(q^{-1}) & \dots & s_{\Phi\Theta}(q^{-1}) \end{bmatrix},$$

in which

$$s_{\phi\theta}(0) = \begin{cases} s_{\phi\theta_0}, & \lambda_\phi \leq \mu_\theta \\ 0, & \lambda_\phi > \mu_\theta. \end{cases}$$

An alternative model, in right-matrix fraction form, is

$$\bar{\mathbf{u}}(0) = -\mathbf{S}_r(q^{-1})\mathbf{R}_s^{-1}(q^{-1})\bar{\mathbf{y}}(0), \tag{4.39b}$$

in which $\mathbf{R}_s \sim \mathbf{C}$ and $\mathbf{S}_r \sim \mathbf{S}$. Notice that, if necessary, it is relatively straightforward to accommodate computational lags within the numerator terms $\mathbf{S}$ and $\mathbf{S}_r$ above, while, if the compensator constituted a dynamical system specified by a matrix-valued transfer function, the pairs $(\mathbf{R}, \mathbf{S})$ and $(\mathbf{S}_r, \mathbf{R}_s)$ would be obtained via the procedure followed to engender $(\mathbf{A}, \mathbf{B})$ ((4.34)) or $(\mathbf{B}_a, \mathbf{A}_b)$ ((4.35)).

Prior to defining the corresponding SISO models, it is useful to address causality issues by designating the parameter m_l. Thus, the control $u(-lM)$, $l \in [0, L-1]$, is dependent upon the measurements $y(-m_l L)$, $y(-(m_l+1)L)$, ... , in which, using the Euclidean division property, m_l ($\in [0, M]$) is obtained from

$$lM = m_l L - \lambda, \quad \lambda \in [0, L-1], \tag{4.40}$$

where, if $M > L$, then each of the indices m_l will be distinct. On the other hand, if $L > M$, there will exist at least two identical indices m_j and m_{j+1}, implying that the most recent output signal employed by both the controls $u(-jM)$ and $u(-(j+1)M)$ will be $y(-m_l L)$. Notice that, if $m_j = M$, then the most recent output signal used by $u(-jM)$ will be $y(-N)$.

By analogy with the matrix $\mathbf{Q}_{ML}^{(0)}$ ((3.70)), which was utilised to model $M|L$ matrices, the corresponding entity in the $L|M$ case, $\mathbf{Q}_{LM}(q^{-1})$, is specified as follows: if $\theta(i,j)$ denotes the $(i,j)^{th}$ element of $\mathbf{Q}_{LM}(q^{-1})$, then, from equation (4.40),

$$\begin{aligned} \theta(l+1, m_l+1) &= 1, \quad m_l \in [0, M-1]; \\ \theta(l+1, 1) &= q^{-1}, \quad m_l = M; \\ \theta(i,j) &= 0, \quad \text{otherwise.} \end{aligned} \tag{4.41}$$

Accordingly, the scalar multirate-sampled digital controller may be described thus:

$$\mathbf{u}_L(0) = -\mathbf{R}^{-1}(q^{-1})\mathbf{S}(q^{-1})\mathbf{y}_M(0), \tag{4.42a}$$

where $$\mathbf{R}(q^{-1}) = \sum_{i=0}^{n_r} \hat{\mathbf{R}}_i \mathbf{P}_L^{(i)}(q^{-1}), \quad \hat{\mathbf{R}}_i = \text{diag}\left(r_{i_0}, r_{i_1}, \ldots, r_{i_{L-1}}\right)$$

and $$\mathbf{S}(q^{-1}) = \sum_{i=0}^{n_s} \hat{\mathbf{S}}_i \mathbf{Q}_{LM}(q^{-1})\mathbf{P}_M^{(i)}(q^{-1}), \quad \hat{\mathbf{S}}_i = \text{diag}\left(s_{i_0}, s_{i_1}, \ldots, s_{i_{L-1}}\right).$$

In the alternative, right-matrix fraction model, namely,

$$\mathbf{u}_L(0) = -\mathbf{S}_r(q^{-1})\mathbf{R}_s^{-1}(q^{-1})\mathbf{y}_M(0), \tag{4.42b}$$

the numerator matrix $\mathbf{S}_r(q^{-1})$ is defined similarly to $\mathbf{S}(q^{-1})$ in (4.42a), whereas

$$\mathbf{R}_s(q^{-1}) = \sum_{i=0}^{n_{rs}} \hat{\mathbf{R}}_{s_i} \mathbf{P}_M^{(i)}(q^{-1}),$$

in which $\hat{\mathbf{R}}_{s_i}$ denotes a diagonal $M|M$ matrix. Notice that other matrices arranged similarly to $\mathbf{R}$ and $\mathbf{R}_s$ will be specified in Chapter 5.

In the special case of a fast output-sampled (FOS) system (i.e., $L = 1$, $M = N$), the term $\mathbf{Q}_{LM}(q^{-1})$ becomes

$$\mathbf{v}_N' \quad \left(= \begin{bmatrix} 1 & 0 & \ldots & 0 \end{bmatrix} \quad \text{(see (3.31))}\right),$$

and the control law in left-matrix fraction form therefore is given by

$$u(0) = -\rho^{-1}(q^{-1})\mathbf{s}'(q^{-1})\mathbf{y}_N(0), \tag{4.43}$$

in which $$\rho(q^{-1}) = \sum_{i=0}^{n_\rho} \rho_i q^{-i},$$

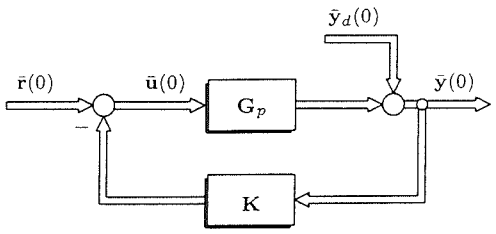

Figure 4.3. Closed-loop multirate-sampled MIMO system.

and

$$\begin{aligned}\mathbf{s}'(q^{-1}) &= \sum_{i=0}^{n_s} s_i \mathbf{v}_N' \mathbf{P}_N^{(i)}(q^{-1}) \\ &= \begin{bmatrix} s_0 + s_N q^{-1} + \dots & s_1 + s_{N+1} q^{-1} + \dots & \dots & s_{N-1} + s_{2N-1} q^{-1} + \dots \end{bmatrix}.\end{aligned}$$

In the complementary scenario (i.e., $L = N$, $M = 1$), referred to in Chapter 3 as a fast input-sampled (FIS) system, the $\mathbf{Q}_{LM}(q^{-1})$ matrix becomes

$$\mathbf{P}_N^{(N-1)}(q^{-1})\mathbf{w}_N \quad \left(= \begin{bmatrix} 1 & q^{-1} & \dots & q^{-1} \end{bmatrix}' \quad \text{(see (3.21) and (3.33))} \right),$$

whence the corresponding controller is

$$\mathbf{u}_N(0) = -\mathbf{R}^{-1}(q^{-1})\mathbf{s}(q^{-1})\mathbf{y}(0), \tag{4.44}$$

where, with L replaced by N, $\mathbf{R}(q^{-1})$ is as defined in (4.42a), and

$$\begin{aligned}\mathbf{s}(q^{-1}) &= \sum_{i=0}^{n_s} \hat{\mathbf{S}}_i \mathbf{P}_N^{(N-1)}(q^{-1})\mathbf{w}_N \\ &= \begin{bmatrix} s_{0_0} + s_{1_0} q^{-1} + \dots & s_{0_1} q^{-1} + s_{1_1} q^{-2} + \dots & \dots & s_{0_{N-1}} q^{-1} + s_{1_{N-1}} q^{-2} + \dots \end{bmatrix}'.\end{aligned}$$

A block diagram model of the multirate-sampled MIMO feedback system is depicted in Figure 4.3, in which, omitting the arguments for concision and generality,

$$\mathbf{G}_p = \mathbf{A}^{-1}\mathbf{B} = \mathbf{B}_a \mathbf{A}_b^{-1} \qquad \text{(see (4.34) and (4.35))}$$

and

$$\mathbf{K} = \mathbf{R}^{-1}\mathbf{S} = \mathbf{S}_r \mathbf{R}_s^{-1}. \qquad \text{(see (4.42a,b)),}$$

and where $\bar{\mathbf{y}}_d$ and $\bar{\mathbf{r}}$ denote "lifted" disturbance and reference signals with similar dimensions to, respectively, $\bar{\mathbf{y}}$ and $\bar{\mathbf{u}}$. The signals $\bar{\mathbf{y}}$ and $\bar{\mathbf{u}}$ are related to $\bar{\mathbf{y}}_d$ and $\bar{\mathbf{r}}$ via the sensitivity functions S_1 and S_2 as follows:

$$\bar{\mathbf{y}} = S_1 \bar{\mathbf{y}}_d, \quad S_1 = (\mathbf{I} + \mathbf{G}_p \mathbf{K})^{-1} \tag{4.45a}$$

and $$\bar{\mathbf{u}} = \boldsymbol{S}_2\bar{\mathbf{r}}, \quad \boldsymbol{S}_2 = (\mathbf{I} + \mathbf{K}\mathbf{G}_p)^{-1}. \tag{4.45b}$$

Now, observing that $\boldsymbol{S}_1$ and $\boldsymbol{S}_2$ may be defined in terms of polynomial matrices thus:

$$\boldsymbol{S}_1 = \mathbf{R}_s\left(\mathbf{A}\mathbf{R}_s + \mathbf{B}\mathbf{S}_r\right)^{-1}\mathbf{A}$$

and $$\boldsymbol{S}_2 = \mathbf{A}_b\left(\mathbf{R}\mathbf{A}_b + \mathbf{S}\mathbf{B}_a\right)^{-1}\mathbf{R},$$

the closed-loop "denominator" matrix is given by, alternatively,

$$\mathbf{A}_{cl_1}(q^{-1}) = \mathbf{A}(q^{-1})\mathbf{R}_s(q^{-1}) + \mathbf{B}(q^{-1})\mathbf{S}_r(q^{-1}) \tag{4.46a}$$

and $$\mathbf{A}_{cl_2}(q^{-1}) = \mathbf{R}(q^{-1})\mathbf{A}_b(q^{-1}) + \mathbf{S}(q^{-1})\mathbf{B}_a(q^{-1}). \tag{4.46b}$$

Defining the closed-loop characteristic polynomial (CLCP) thus:

$$\alpha_{cl}(z^{-1}) = \det\left(\mathbf{A}_{cl_1}(z^{-1})\right) = \det\left(\mathbf{A}_{cl_2}(z^{-1})\right), \tag{4.47}$$

the closed-loop system will be asymptotically stable if and only if $\alpha_{cl}(z^{-1})$ is stable.

Substituting $(\mathbf{A}, \mathbf{B})$ and $(\mathbf{B}_a, \mathbf{A}_b)$ in (4.46a,b) with $(\mathbf{A}_M, \mathbf{B}_l)$ ((3.68)) and $(\mathbf{B}_r, \mathbf{A}_L)$ ((3.69)) and with $(\mathbf{S}_r, \mathbf{R}_s)$ and $(\mathbf{R}, \mathbf{S})$ as specified in equation (4.42a,b), the above result applies equally to the SISO multirate-sampled feedback system. In the scalar FOS scenario, the CLCP is given by (see (3.75) and (4.43))

$$\alpha_{cl}(z^{-1}) = \rho(z^{-1})\alpha(z^{-1}) + \mathbf{s}'(z^{-1})\mathbf{b}_r(z^{-1}), \tag{4.48}$$

whereas (see (4.44)), defining $\rho_s(z^{-1}) = \det\left(\mathbf{R}(z^{-1})\right)$

and $$\mathbf{s}_r(z^{-1}) = \operatorname{adj}\left(\mathbf{R}(z^{-1})\right)\mathbf{s}(z^{-1}),$$

the CLCP in the corresponding FIS configuration, obtained from equations (3.76) and (4.44), is

$$\alpha_{cl}(z^{-1}) = \rho_s(z^{-1})\alpha(z^{-1}) + \tilde{\mathbf{b}}_l'(z^{-1})\mathbf{s}_r(z^{-1}). \tag{4.49}$$

In both the FOS and FIS cases it is possible to gauge relative stability by determining the return ratio $Q(z)$, namely, the pulse-transfer function of the system elements enclosed by the sampler operating at T s. Thus, observing that the FOS control law corresponds to the following "implicit" pulse-transfer function (cf. (2.16) and (2.17))

$$U(z) = -Z\left\{K_N(z_N)Y_N(z_N)\right\}, \quad K_N(z_N) = \frac{S(z_N^{-1})}{\rho(z^{-1})} \quad \text{(see (4.43))},$$

the return ratio in this scenario is given by

$$\begin{aligned} Q(z) &= Z\left\{K_N(z_N)GH_N^{(N)}(z_N)H_N^{(1)}(z_N)\right\} \quad \text{(see (3.4) and (3.5))} \\ &= \frac{\mathbf{s}'(z^{-1})\mathbf{b}_r(z^{-1})}{\rho(z^{-1})\alpha(z^{-1})}. \end{aligned} \tag{4.50}$$

The gain and phase margins can then be ascertained in the usual manner by plotting the frequency response

$$Q(e^{j\omega T}), \quad \omega \in [0, \pi/T).$$

Evidently, a similar approach may be used to evaluate the stability margins in the FIS system.

The assessment of relative stability via conventional frequency responses in general multirate-sampled SISO feedback systems is not possible since the return ratio cannot be expressed as a pulse-transfer function. However, invoking results customarily associated with continuous-time multivariable control theory, Thompson (1986) has described how in this instance the gain and phase margins may be defined as the least conservative of those engendered by the characteristic gain loci of an open-loop model obtained via the switch decomposition technique. This approach corresponds to plotting $\upsilon_{L_j}(e^{j\omega T})$, $i = 1, 2, \ldots, L$, or $\upsilon_{M_j}(e^{j\omega T})$, $j = 1, 2, \ldots, M$, where the $\upsilon_{L_j}(z)$'s denote the eigenvalues of

$$\mathbf{Q}_L(z) = \mathbf{R}^{-1}(z^{-1})\mathbf{S}(z^{-1})\mathbf{B}_r(z^{-1})\mathbf{A}_L^{-1}(z^{-1}) \tag{4.51a}$$

and the $\upsilon_{M_j}(z)$'s constitute the eigenvalues of

$$\mathbf{Q}_M(z) = \mathbf{A}_M^{-1}(z^{-1})\mathbf{B}_l(z^{-1})\mathbf{S}_r(z^{-1})\mathbf{R}_s^{-1}(z^{-1}). \tag{4.51b}$$

Although the use of either $\mathbf{Q}_M(z)$ or $\mathbf{Q}_L(z)$ will yield the same result, it is more appropriate from a practical perspective to employ $\mathbf{Q}_L$ ($\mathbf{Q}_M$) when $M > L$ ($L > M$).

The problem of gauging the stability robustness of multirate-sampled multivariable systems remains largely unresolved. However, in light of Thompson's technique, one possible approach could involve determining

$$\sigma_p = \max_{\omega \in [0, \pi/T)} |\sigma_i(e^{j\omega T})|, \quad i = 1, 2, \ldots . \sum_{j=1}^{k} K_j. \tag{4.52}$$

where $\sigma_i(z)$ denotes an eigenvalue of either $\boldsymbol{S}_1(z)$ or $\boldsymbol{S}_2(z)$ (see equations (4.45a,b)), with

$$K = M(L) \quad \text{and} \quad k = m(l)$$

in the case of $\boldsymbol{S}_1$ ($\boldsymbol{S}_2$).

4.5 Illustrative Example

The procedure entailed in establishing lifted representations of two multirate-sampled multivariable configurations is demonstrated in this section. The first example, denoted M1, is an unstable single-input two-output system, whereas the second concerns a two-input two-output system labelled M2. In common with the scalar system examined in Chapter 3, the parameter N is restricted to a low value in each instance to ensure expositional clarity.

Example M1

In this example, the vector-valued plant is described by

$$\mathbf{g}(s) = \begin{bmatrix} \dfrac{1}{s+1} \\ \dfrac{1}{s-1} \end{bmatrix}, \tag{4.53}$$

and it is supposed that the signals $y_1(t)$, $y_2(t)$ and $u(t)$ are sampled at intervals of, respectively, T/M_1, T/M_2 and T/L_1 s, where

$$M_1 = 1, \quad M_2 = 3 \quad \text{and} \quad L_1 = 2.$$

Verifying from equation (4.2a) that N is 6, the pulse-transfer function model of the discretised plant is

$$\mathbf{g}_{p_N}(z_N) = z_6^{-1} \begin{bmatrix} \dfrac{b_1}{1 - a_1 z_6^{-1}} \\ \dfrac{b_2}{1 - a_2 z_6^{-1}} \end{bmatrix}, \tag{4.54a}$$

where $$b_1 = 1 - a_1, \quad b_2 = a_2 - 1,$$

in which $$a_1 = a = e^{-T/6} \quad \text{and} \quad a_2 = 1/a \triangleq \bar{a}.$$

Evidently, equation (4.54a) can be written as the following left-matrix fraction (see (4.6)):

$$\mathbf{g}_{p_N}(z_N) = z_6^{-1}\boldsymbol{A}(z_6^{-1})\boldsymbol{b}(z_6^{-1}), \tag{4.54b}$$

where $\boldsymbol{A}(z_N^{-1}) = \begin{bmatrix} 1 - az_6^{-1} & 0 \\ 0 & 1 - \bar{a}z_6^{-1} \end{bmatrix}$ and $\boldsymbol{b}(z_N^{-1}) = \begin{bmatrix} b_1 \\ b_2 \end{bmatrix}$.

Applying the techniques described in section 4.1, the fast-sampled outputs $\hat{\mathbf{y}}(0)$ are related to the slow-sampled control $\tilde{\mathbf{u}}(0)$ thus (see (4.10)):

$$\hat{\mathbf{A}}(q^{-1})\hat{\mathbf{y}}(0) = \hat{\mathbf{B}}_H(q^{-1})\tilde{\mathbf{u}}(0), \tag{4.55}$$

in which $\hat{\mathbf{y}}(0) = \begin{bmatrix} y_1(0) & y_1(-1) & \dots & y_1(-5) & y_2(0) & y_2(-1) & \dots & y_2(-5) \end{bmatrix}'$,

$$\tilde{\mathbf{u}}(0) = \begin{bmatrix} u(0) & u(-3) \end{bmatrix}',$$

$$\hat{\mathbf{A}}(q^{-1}) = \text{block diag}\left(\mathbf{I}_6 - a\mathbf{P}_6^{(1)}(q^{-1}), \mathbf{I}_6 - \bar{a}\mathbf{P}_6^{(1)}(q^{-1})\right)$$

and, with $\hat{\mathbf{B}}(q^{-1}) = \begin{bmatrix} b_1\mathbf{I}_6 \\ b_2\mathbf{I}_6 \end{bmatrix}$, $\hat{\mathbf{P}}_l^{(d)}(q^{-1})\left(= \hat{\mathbf{P}}_1^{(1)}(q^{-1})\right) = \mathbf{P}_6^{(1)}(q^{-1})$

and (see (4.8) and (4.9))

$$\hat{\mathbf{H}}(q^{-1}) = \mathbf{H}_1(q^{-1}) = \mathbf{P}_6^{(2)}(q^{-1})\mathbf{W}_2,$$

where $\hat{\mathbf{B}}_H(q^{-1}) = \hat{\mathbf{B}}(q^{-1})\hat{\mathbf{P}}_l^{(d)}(q^{-1})\hat{\mathbf{H}}(q^{-1}) = \begin{bmatrix} 0 & b_1\mathbf{w}_3 \\ q^{-1}b_1\mathbf{w}_3 & 0 \\ 0 & b_2\mathbf{w}_3 \\ q^{-1}b_2\mathbf{w}_3 & 0 \end{bmatrix}$.

The designation of the permutation matrix $\boldsymbol{\Pi}_1$ in accordance with the following vectors (see (4.11)):

$$\tilde{\mathbf{y}}(0) = \begin{bmatrix} y_1(0) & y_2(0) & y_2(-2) & y_2(-4) \end{bmatrix}'$$

and $\mathbf{y}_e = \begin{bmatrix} y_1(-1) & y_2(-1) & y_1(-2) & y_1(-3) & y_2(-3) & y_1(-4) & y_1(-5) & y_2(-5) \end{bmatrix}'$,

leads to the plant model

$$\mathbf{A}_r(q^{-1})\tilde{\mathbf{y}}(0) = \mathbf{B}_r(q^{-1})\tilde{\mathbf{u}}(0), \tag{4.56}$$

in which $\mathbf{A}_1(q^{-1}) = \mathbf{I}_4$, and the non-zero entities in $\mathbf{A}_2(q^{-1})$, $\mathbf{A}_3(q^{-1})$ and $\mathbf{A}_4(q^{-1})$ are:

$$\mathbf{A}_2(1,1) = -a, \quad \mathbf{A}_2(2,2) = \mathbf{A}_2(3,5) = \mathbf{A}_2(4,8) = -\bar{a};$$

$$\mathbf{A}_3(2,3) = \mathbf{A}_3(5,4) = -\bar{a}, \quad \mathbf{A}_3(7,1) = -aq^{-1}, \quad \mathbf{A}_3(8,2) = -\bar{a}q^{-1};$$

$$\mathbf{A}_4(1,1) = \mathbf{A}_4(2,2) = \ldots = \mathbf{A}_4(8,8) = 1,$$

$$\mathbf{A}_4(1,3) = \mathbf{A}_4(3,4) = \mathbf{A}_4(4,6) = \mathbf{A}_4(6,7) = -a,$$

and where $$\mathbf{B}_r(q^{-1}) = \begin{bmatrix} \mathbf{B}_1(q^{-1}) \\ \mathbf{B}_2(q^{-1}) \end{bmatrix},$$

with $$\mathbf{B}_1(q^{-1}) = \begin{bmatrix} 0 & b_1 \\ 0 & b_2 \\ 0 & b_2 \\ b_2q^{-1} & 0 \end{bmatrix} \quad \text{and} \quad \mathbf{B}_2(q^{-1}) = \begin{bmatrix} 0 & b_1 \\ 0 & b_2 \\ 0 & b_1 \\ b_1q^{-1} & 0 \\ b_2q^{-1} & 0 \\ b_1q^{-1} & 0 \\ b_1q^{-1} & 0 \\ b_2q^{-1} & 0 \end{bmatrix}.$$

Using the left-matrix fraction $\mathbf{A}_{4_2}^{-1}\mathbf{A}_{2_4}$ (see (4.13)), where

$$\mathbf{A}_{4_2}(q^{-1}) = \mathbf{I}_4 \quad \text{and} \quad \mathbf{A}_{2_4}(q^{-1}) = -\begin{bmatrix} a & 0 & a^2 & a^3 & 0 & a^4 & a^5 & 0 \\ 0 & \bar{a} & 0 & 0 & 0 & 0 & 0 & 0 \\ 0 & 0 & 0 & 0 & \bar{a} & 0 & 0 & 0 \\ 0 & 0 & 0 & 0 & 0 & 0 & 0 & \bar{a} \end{bmatrix},$$

the lifted plant description in left-matrix fraction form is given by (see (4.14))

$$\tilde{\mathbf{A}}(q^{-1})\tilde{\mathbf{y}}(0) = \tilde{\mathbf{B}}(q^{-1})\tilde{\mathbf{u}}(0), \tag{4.57}$$

where $$\tilde{\mathbf{A}}(q^{-1}) = \mathbf{I}_4 - \mathbf{A}_{2_4}(q^{-1})\mathbf{A}_3(q^{-1}) = \begin{bmatrix} 1 - a^6q^{-1} & 0 & 0 & 0 \\ 0 & 1 & -\bar{a}^2 & 0 \\ 0 & 0 & 1 & -\bar{a}^2 \\ 0 & -\bar{a}^2q^{-1} & 0 & 1 \end{bmatrix}$$

and $$\tilde{\mathbf{B}}(q^{-1}) = \mathbf{B}_1(q^{-1}) - \mathbf{A}_{2_4}(q^{-1})\mathbf{B}_2(q^{-1}) = \begin{bmatrix} (a^3 + a^4 + a^5)b_1q^{-1} & (1 + a + a^2)b_1 \\ 0 & (1 + \bar{a})b_2 \\ \bar{a}b_2q^{-1} & b_2 \\ (1 + \bar{a})b_2q^{-1} & 0 \end{bmatrix}.$$

Expressed as a right-matrix fraction, the plant model is (see (4.36)):

$$\bar{\mathbf{y}}(0) = \mathbf{B}_a(q^{-1})\mathbf{A}_b^{-1}(q^{-1})\bar{\mathbf{u}}(0), \tag{4.58}$$

in which $$\mathbf{A}_b(q^{-1}) = \begin{bmatrix} 1+q^{-1} & -(a^3+\bar{a}^3) \\ -(a^3+\bar{a}^3)q^{-1} & 1+q^{-1} \end{bmatrix}$$

and $$\mathbf{B}_a(q^{-1}) = \begin{bmatrix} -(1+a+a^2)\bar{a}^3 b_1 q^{-1} & (1+a+a^2)b_1 \\ -(1+a+a^2)ab_2 q^{-1} & (1+\bar{a}+\bar{a}^2)b_2 \\ (1+\bar{a}-a^4)\bar{a}b_2 q^{-1} & b_2-(1+a)ab_2 q^{-1} \\ (1+\bar{a})b_2 q^{-1} - ab_2 q^{-2} & (1-a^4-a^5)\bar{a}^2 b_2 q^{-1} \end{bmatrix}.$$

It will be observed that $\mathbf{A}_b(0)$ is upper-triangular and that the structures of $\mathbf{B}_a(0)$ above and $\mathbf{B}(0)$ in equation (4.57) are identical. Notice that, since the elements within the respective vector pairs $\tilde{\mathbf{y}}(0)$ and $\bar{\mathbf{y}}(0)$, and $\tilde{\mathbf{u}}(0)$ and $\bar{\mathbf{u}}(0)$, are arranged identically, the matrices $\tilde{\mathbf{A}}$ and $\tilde{\mathbf{B}}$ in equation (4.57) equate to $\mathbf{A}$ and $\mathbf{B}$ in the repetitive time interval index-dependent model ((4.34)).

It is supposed that the disturbance subsystem model is specified by the matrix

$$C(z_N^{-1}) = \begin{bmatrix} 1+c_1 z_6^{-1} & 0 \\ 0 & 1+c_2 z_6^{-1} \end{bmatrix}. \tag{4.59}$$

Following the procedure summarised by equations (4.21) and (4.22), the vector $\tilde{\boldsymbol{\xi}}(0)$ in equation (4.23) is

$$\tilde{\boldsymbol{\xi}}(0) = \boldsymbol{\Gamma}(q^{-1})\hat{\mathbf{e}}(0), \quad \boldsymbol{\Gamma}(q^{-1}) = \begin{bmatrix} \boldsymbol{\gamma}_1'(q^{-1}) & \mathbf{0}' \\ \mathbf{0} & \boldsymbol{\Gamma}_2(q^{-1}) \end{bmatrix}, \tag{4.60}$$

in which

$$\boldsymbol{\gamma}_1(q^{-1}) = \begin{bmatrix} 1+a^5 c_1 q^{-1} & a+c_1 & (a+c_1)a & (a+c_1)a^2 & (a+c_1)a^3 & (a+c_1)a^4 \end{bmatrix}'$$

and $$\boldsymbol{\Gamma}_2(q^{-1}) = \begin{bmatrix} 1 & \bar{a}+c_2 & \bar{a}c_2 & 0 & 0 & 0 \\ 0 & 0 & 1 & \bar{a}+c_2 & \bar{a}c_2 & 0 \\ \bar{a}c_2 q^{-1} & 0 & 0 & 0 & 1 & \bar{a}+c_2 \end{bmatrix}.$$

The lifted disturbance subsystem model then is given by equation (4.31), with $\tilde{\mathbf{C}}(q^{-1})$ designated as

$$\tilde{\mathbf{C}}(q^{-1}) = \begin{bmatrix} \tilde{c}_{1_0} + \tilde{c}_{1_1}q^{-1} & 0 & 0 & 0 \\ 0 & \tilde{c}_{2_0} & \tilde{c}_{2_1} & 0 \\ 0 & 0 & \tilde{c}_{2_0} & \tilde{c}_{2_1} \\ 0 & \tilde{c}_{2_1}q^{-1} & 0 & \tilde{c}_{2_0} \end{bmatrix},$$

where the parameters $\tilde{c}_{1_0}$, $\tilde{c}_{1_1}$, $\tilde{c}_{2_0}$ and $\tilde{c}_{2_1}$, which represent the stable solution of the spectral factorisation defined in equation (4.30), are determined from the following equations:

$$\begin{aligned} \tilde{c}_{1_0}\tilde{c}_{1_1} &= a^5 c_1 \\ \tilde{c}_{1_0}^2 + \tilde{c}_{1_1}^2 &= 1 + a^{10}c_1^2 + (a + c_1)^2(1 + a^2 + a^4 + a^6 + a^8) \\ \tilde{c}_{2_0}\tilde{c}_{2_1} &= \bar{a}c_2 \\ \tilde{c}_{2_0}^2 + \tilde{c}_{2_1}^2 &= 1 + \bar{a}^2 c_2^2 + (\bar{a} - c_2)^2. \end{aligned}$$

However, it is convenient to define $\tilde{\mathbf{C}}(q^{-1})$ alternatively as

$$\tilde{\mathbf{C}}(q^{-1}) = \begin{bmatrix} 1 + \tilde{c}_1 q^{-1} & 0 & 0 & 0 \\ 0 & 1 & \tilde{c}_2 & 0 \\ 0 & 0 & 1 & \tilde{c}_2 \\ 0 & \tilde{c}_2 q^{-1} & 0 & 1 \end{bmatrix}, \tag{4.61}$$

with $$\tilde{c}_1 = \frac{\tilde{c}_{1_1}}{\tilde{c}_{1_0}} \quad \text{and} \quad \tilde{c}_2 = \frac{\tilde{c}_{2_1}}{\tilde{c}_{2_0}},$$

and where the variances of the white noise sources $\{\epsilon_1(\cdot)\}$ and $\{\epsilon_2(\cdot)\}$ have been scaled accordingly. As mentioned above, the equivalence of the vectors $\tilde{\mathbf{y}}(0)$ and $\bar{\mathbf{y}}(0)$, and thus $\tilde{\boldsymbol{\epsilon}}(0)$ and $\bar{\boldsymbol{\epsilon}}(0)$, implies that the matrix $\mathbf{C}(q^{-1})$ in equation (4.34) is identical to $\tilde{\mathbf{C}}(q^{-1})$ above. Furthermore, it is relatively straightforward to establish that the matrices $\mathbf{A}_c(q^{-1})$ and $\mathbf{C}_a(q^{-1})$ defining the lifted disturbance model in right-matrix fraction form are identical to, $\mathbf{A}(q^{-1})$ and $\mathbf{C}(q^{-1})$ respectively.

Example M2

This example concerns the coupled-tanks system depicted in Figure 4.4, where

$$\frac{A_2}{A_1} = \mu \ (< 1),$$

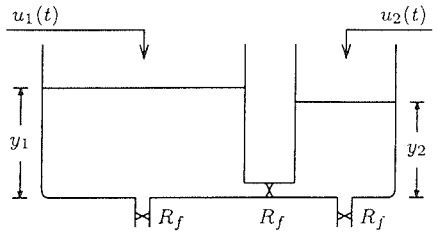

Figure 4.4. Coupled-tanks system.

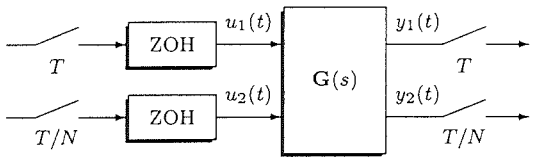

Figure 4.5. Sampling scheme for coupled-tanks system.

in which A_1 and A_2 denote the cross-sectional areas of tanks 1 and 2 and where the fluid resistance R_f associated with the three valves are identical. The controls $u_1(t)$ and $u_2(t)$ represent the input flow rates in m^3/s, while the outputs $y_1(t)$ and $y_2(t)$ denote the water levels in each tank. Linearised with respect to a specific operating point, the plant is described thus:

$$\mathbf{y}(s) = \mathbf{G}(s)\mathbf{u}(s), \tag{4.62}$$

with
$$\mathbf{G}(s) = \frac{1}{s^2 + (2+2\mu)\,s + 3\mu} \begin{bmatrix} s+2\mu & \mu \\ \mu & \mu\,(s+2) \end{bmatrix}.$$

In accordance with the desired rise times of the signals $y_1(t)$ and $y_2(t)$ in response to respective step changes in reference inputs $r_1(t)$ and $r_2(t)$ in a closed-loop system to be designed subsequently, the sampling scheme illustrated in Figure 4.5 is envisaged. From equations (4.1a,b) and (4.2a.b), it can be established that

$$L_1 = M_1 = 1 \quad \text{and} \quad L_2 = M_2 = N.$$

The matrix fraction representation of the discretised plant in equation (4.6) then may be specified generically by

$$\boldsymbol{A}(z_N^{-1}) = \begin{bmatrix} 1 - a_1 z_N^{-1} & -a_2 \\ -a_3 z_N^{-1} & 1 - a_4 z_N^{-1} \end{bmatrix} \quad \text{and} \quad \boldsymbol{B}(z_N^{-1}) = \begin{bmatrix} b_1 & -b_2 \\ b_3 & b_4 \end{bmatrix}, \quad \text{with} \quad d = 1.$$

Two particular scenarios shall be considered, namely:

(i) $T = 0.15\,\mathrm{s}$, $N = \mu = 3$, whence

$$a_1 = 0.9012, \quad a_2 = 0.0552, \quad a_3 = 0.1232, \quad a_4 = 0.7438,$$

and $\quad b_1 = 0.0475, \quad b_2 = 0.0039, \quad b_3 = 0.0033 \quad \text{and} \quad b_4 = 0.1297;$

(ii) $T = 0.15\,\mathrm{s}$, $N = \mu = 8$, whence

$$a_1 = 0.0214, \quad a_2 = 0.9617, \quad a_3 = 0.1271, \quad a_4 = 0.7420,$$

and $\quad b_1 = 0.0184, \quad b_2 = 0.0015, \quad b_3 = 0.0013 \quad \text{and} \quad b_4 = 0.1297.$

The step responses of both the continuous time and the sampled-data systems for scenario (i) are presented in Figures 4.6 and 4.7, respectively. Notice that the model defined above will be modified subsequently to produce a control law that incorporates integral action in an illustration of multirate-sampled feedback system design in the next chapter.

4.6 Conclusion

This chapter has generalised the principles established for scalar systems in Chapter 3 to the multivariable case. Bearing in mind that the approaches utilised are conceptually identical, the reliance of the lifted multi-input multi-output models on an original non-unique matrix fraction description of the fast-rate discretised plant implies that they cannot be specified in comparable detail to the corresponding single-input single-output models. As reflected by the comments pertaining to the structures of the leading coefficient matrices of each polynomial matrix, it will be observed that the notion of causality is pivotal in defining the multirate-sampled plant and controller representations. In this respect, the so-called repetitive time interval index-dependent models, which naturally have counterparts specified with respect to the frequency-domain, are exploited in the design techniques formulated in the next chapter.

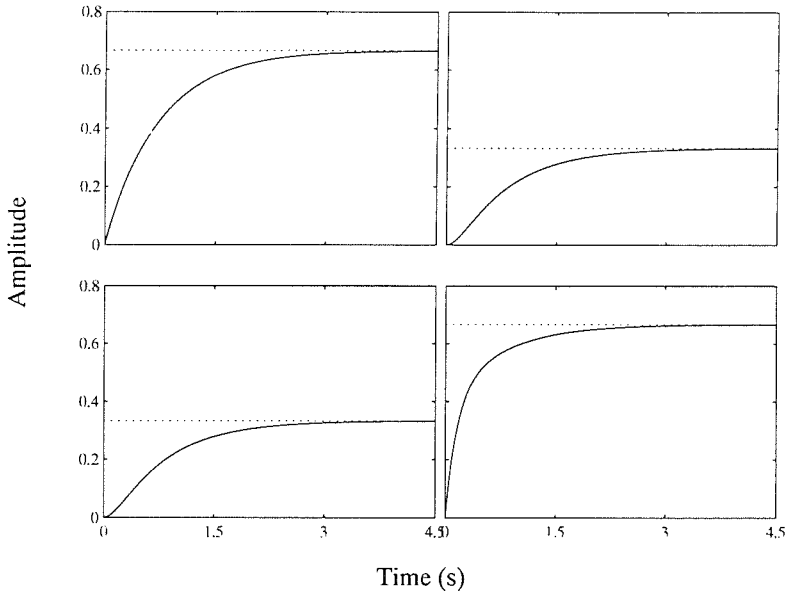

Figure 4.6. Step response of continuous time system.

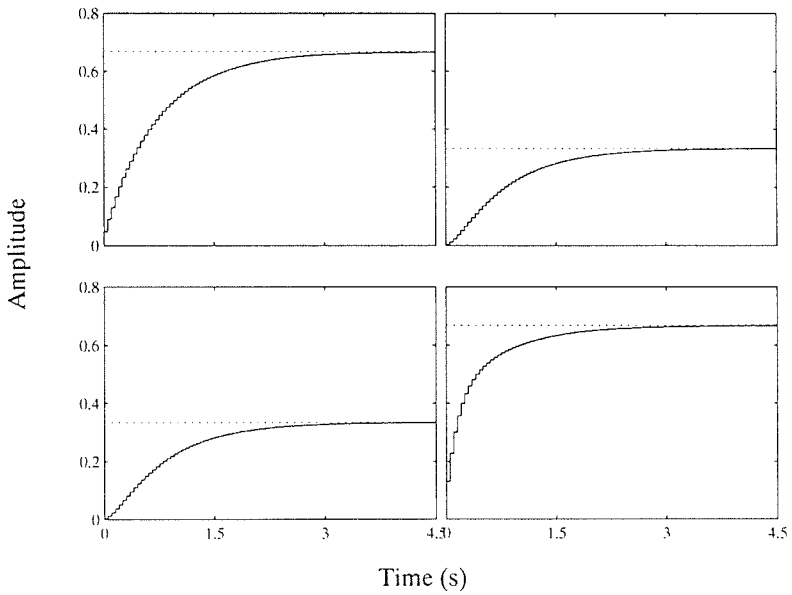

Figure 4.7. Step response of sampled data system.

Chapter Five

Multirate-Sampled Feedback System Design

The incorporation of the foregoing polynomial methods within the framework of established control design methodologies is addressed in this chapter. Specifically, dealing principally with the multi-input multi-output (MIMO) case, it is demonstrated that the lifted system models acquired previously are conducive to the synthesis of control laws via the minimisation of quadratic performance criteria. Subsequently, means of enhancing the flexibility of these design approaches are examined.

The chapter commences in section 5.1 with a summary of multirate LQG control design by Kučera's polynomial equations approach. Following a proof of the main result, related considerations, such as the determination of the "minimum degree solution" and a dynamics-assignment interpretation of the optimal controller, are discussed. A numerical example then is used in section 5.2 to illustrate the technique. In section 5.3 attention is focused upon the modifications necessary to the Generalised Predictive Control strategy to warrant its use in a multirate-sampling context, whilst a related numerical example in section 5.4 demonstrates the use of the approach. Section 5.5 subsequently describes how both the optimal and predictive control methodologies can introduce integral action within the controller and incorporate dynamic weighting in the cost function. The feasibility of solving the LQG "tracking" and "feedforward" problems is also discussed, following which section 5.6 contains related numerical examples.

5.1 Optimal Control

The synthesis of feedback systems excited by stochastic disturbances via the minimisation of a performance index that penalises the output and control signal variances represents a cornerstone of modern control. Known alternatively as optimal or Linear Quadratic Gaussian (LQG) control, the derivation technique customarily associated with the state-space approach involves combining the solutions to two separate problems, specified by Riccati equations in each instance. This axiom, referred to as the *certainty equivalence princi-*

ple or, simply, the *separation theorem*, implies that the optimal controller is engendered by unifying the state estimator (namely, the celebrated Kalman filter), which provides the best estimate of the system states from the observed outputs, and a linear feedback control law (namely, the "Linear Quadratic Regulator" (LQR)), obtained by minimising a quadratic performance index weighting the deviation from equilibrium of the output and control signals in response to some initial perturbation. Optimal control has proven to be effective in addressing some multivariable problems, although drawbacks pertaining to a perceived lack of stability and performance robustness provided the motivation for the development of synthesis methods, known generically as the H_∞ approach, that use information more commonly encountered in classical feedback system design via frequency responses.

The polynomial equations approach to synthesising LQG controllers, attributed to Kučera (1979) and Youla *et al.* (1976a,b), is the result of attempts to correct technical deficiencies in contributions, such as Newton *et al.* (1957), made two decades earlier. Although its significance originally lay primarily in presenting a theoretical alternative to the state-space approach, this methodology is now a practical proposition with the advent of POLYNOMIAL TOOLBOX. Expositionally, the procedure adopted concerns an initial summary of the key result as applied to the lifted representations derived in Chapter 4, followed by the proof. Topics such as the non-uniqueness of the matrix fractions used and the interpretation of the optimal control solution as a special case of dynamics-assignment are addressed subsequently. Additionally, certain enhancements to the method described are dealt with in section 5.5. The computational issues associated with the proposed approach are detailed in Appendix C, which additionally addresses a further design example.

The Multirate-Sampled LQG Control Law

Open-Loop System Model

It is assumed that the open-loop system is described thus:

$$\bar{\mathbf{y}}(0) = \mathbf{B}_a(q^{-1})\mathbf{A}_b^{-1}\bar{\mathbf{u}}(0) + \mathbf{C}_a(q^{-1})\mathbf{A}_c^{-1}(q^{-1})\bar{\boldsymbol{\epsilon}}(0). \qquad ((4.35))$$

where $\bar{\mathbf{y}}(0)$ (and $\bar{\boldsymbol{\epsilon}}(0)$) and $\bar{\mathbf{u}}(0)$ are defined in, respectively, equations (4.32) and (4.33).

Cost Function

The performance index to be minimised is

$$J = E\left\{\bar{\mathbf{y}}'(0)\bar{\mathbf{y}}(0) + \bar{\mathbf{u}}'(0)\boldsymbol{\Xi}\bar{\mathbf{u}}(0)\right\}, \tag{5.1}$$

where $\boldsymbol{\Xi} = \text{block diag}\left(\boldsymbol{\Xi}_1, \boldsymbol{\Xi}_2, \ldots, \boldsymbol{\Xi}_l\right)$, in which $\boldsymbol{\Xi}_i = \xi_i \mathbf{I}_{L_i}$.

Optimal Control Solution

With the proviso that each of the matrix fractions designated subsequently is coprime, defining:

(i) the right-matrix fraction,

$$\mathbf{B}_c\mathbf{C}_b^{-1} = \mathbf{C}^{-1}\mathbf{B}; \tag{5.2}$$

(ii) $\mathbf{D}(q^{-1})$ to be the stable solution of

$$\mathbf{D}^\star\mathbf{D} = \mathbf{A}_b^\star\boldsymbol{\Xi}\mathbf{A}_b + \mathbf{B}_a^\star\mathbf{B}_a, \tag{5.3}$$

then the matrices determining the control law

$$\mathbf{R}_o(q^{-1})\bar{\mathbf{u}}(0) = -\mathbf{S}_o(q^{-1})\bar{\mathbf{y}}(0) \tag{5.4}$$

that minimises the cost function of equation (5.1) for the system model of equation (4.35) are obtained from the left-matrix fraction

$$\mathbf{C}_o^{-1}\begin{bmatrix}\mathbf{R}_o & \mathbf{S}_o\end{bmatrix} = \begin{bmatrix}\mathbf{R}_{md} & \mathbf{S}_{md}\end{bmatrix}\begin{bmatrix}\mathbf{C}_b & \mathbf{0}\\ \mathbf{0} & \mathbf{C}_a\end{bmatrix}^{-1}, \tag{5.5}$$

where $(\mathbf{R}_{md}, \mathbf{S}_{md})$, in addition to $\boldsymbol{\Lambda}_{md}^\star$, denote the solution $(\mathbf{R}, \mathbf{S})$ of minimum degree with respect to $\boldsymbol{\Lambda}^\star$ of the coupled diophantine equations

$$\mathbf{A}_b^\star\boldsymbol{\Xi}\mathbf{C}_b + \boldsymbol{\Lambda}^\star\mathbf{B}_c = \mathbf{D}^\star\mathbf{R} \tag{5.6}$$

$$\mathbf{B}_a^\star\mathbf{C}_a - \boldsymbol{\Lambda}^\star\mathbf{A}_c = \mathbf{D}^\star\mathbf{S}. \tag{5.7}$$

Proof

The proof presented below is based upon the variational approach proposed by Sternad and Ahlén (1993). The above result also may be established using the "completing-the-squares" method of Kučera (1979).

In seeking to establish the compensator which minimises the cost function of equation (5.1), the effect of controller parameter variations on feedback system performance is interpreted as being analogous to an appropriate feedforward contribution from the m white noise sources represented by $\bar{\epsilon}(0)$. Thus, the regulator is specified as

$$\bar{\mathbf{u}}(0) = -\mathbf{K}_o(q^{-1})\bar{\mathbf{y}}(0) + \mathbf{F}(q^{-1})\bar{\epsilon}(0), \tag{5.8}$$

with $\mathbf{K}_o$ and $\mathbf{F}$ defined as causal and rational, in which $\mathbf{K}_o$ is assumed to be nominally optimal and where the resultant closed-loop system is required to be stable.

Combining equations (5.8) and (4.35), both the output and control signals are separated into the optimal entities $\bar{\mathbf{y}}_o(0)$ and $\bar{\mathbf{u}}_o(0)$ and perturbations $\bar{\mathbf{y}}_p(0)$ and $\bar{\mathbf{u}}_p(0)$ resulting from the variational term, namely:

$$\bar{\mathbf{y}}(0) = \bar{\mathbf{y}}_o(0) + \bar{\mathbf{y}}_p(0) \quad \text{and} \quad \bar{\mathbf{u}}(0) = \bar{\mathbf{u}}_o(0) + \bar{\mathbf{u}}_p(0), \tag{5.9}$$

where $\bar{\mathbf{y}}_o = \mathbf{T}_0\bar{\epsilon}$, $\bar{\mathbf{y}}_p = \mathbf{B}_a\mathbf{T}_1\mathbf{F}\bar{\epsilon}$, $\bar{\mathbf{u}}_o = -\mathbf{K}_0\mathbf{T}_0\bar{\epsilon}$ and $\bar{\mathbf{u}}_p = \mathbf{A}_b\mathbf{T}_1\mathbf{F}\bar{\epsilon}$,

in which $\mathbf{T}_0 = \left(\mathbf{I} + \mathbf{B}_a\mathbf{A}_b^{-1}\mathbf{K}_o\right)^{-1}\mathbf{C}_a\mathbf{A}_c^{-1}$ and $\mathbf{T}_1 = \left(\mathbf{A}_b + \mathbf{K}_o\mathbf{B}_a\right)^{-1}$.

It will be observed from $\mathbf{T}_0$ and $\mathbf{T}_1$ in equation (5.9) that, since the feedback loop is unaffected, the control variation preserves stability. The performance index now may be written as

$$J = J_0 + 2J_1 + J_2, \tag{5.10}$$

where $J_0 = E\left\{\bar{\mathbf{y}}_o'\bar{\mathbf{y}}_o + \bar{\mathbf{u}}_o'\Xi\bar{\mathbf{u}}_o\right\}$, $J_1 = E\left\{\bar{\mathbf{y}}_o'\bar{\mathbf{y}}_p + \bar{\mathbf{u}}_o'\Xi\bar{\mathbf{u}}_p\right\}$

and $J_2 = E\left\{\bar{\mathbf{y}}_p'\bar{\mathbf{y}}_p + \bar{\mathbf{u}}_p'\Xi\bar{\mathbf{u}}_p\right\}$.

The LQG control solution is obtained by determining $\mathbf{K}_o$ such that, regardless of $\mathbf{F}$, $J_1 = 0$ in equation (5.10). In this case no alternative controller could minimise J further, since, from equation (5.10), J_0 and J_2 (≥ 0) are, respectively, entirely independent of,

and dictated solely by, the variational term. Accordingly, invoking Parseval's formula and using $\mathrm{tr}\,(\mathbf{XY}) = \mathrm{tr}\,(\mathbf{YX})$, the cross term is given by

$$\begin{aligned} J_1 &= E\left\{\mathrm{tr}\left((\mathbf{T}_0\bar{\epsilon})\,(\mathbf{B}_a\mathbf{T}_1\mathbf{F}\bar{\epsilon})'\right) - \mathrm{tr}\left(\left(\Xi^{1/2}\mathbf{K}_o\mathbf{T}_0\bar{\epsilon}\right)\left(\Xi^{1/2}\mathbf{A}_b\mathbf{T}_1\mathbf{F}\bar{\epsilon}\right)'\right)\right\} \\ &= \frac{1}{2\pi j}\oint_{|z|=1}\mathrm{tr}\left(\mathbf{T}_0\Sigma\mathbf{F}^\star\mathbf{T}_1^\star\mathbf{B}_a^\star - \Xi^{1/2}\mathbf{K}_o\mathbf{T}_0\Sigma\mathbf{F}^\star\mathbf{T}_1^\star\mathbf{A}_b^\star\Xi^{1/2}\right)\frac{dz}{z} \\ &= \frac{1}{2\pi j}\oint_{|z|=1}\mathrm{tr}\left(\Sigma\mathbf{F}^\star\mathbf{T}_1^\star\left(\mathbf{B}_a^\star - \mathbf{A}_b^\star\Xi\mathbf{K}_o\right)\mathbf{T}_0\right)\frac{dz}{z}, \end{aligned} \tag{5.11}$$

in which $E\{\bar{\epsilon}(0)\bar{\epsilon}'(0)\} = \Sigma$. Notice, that, since $\mathbf{F}$ and $\mathbf{T}_1$ (and $\mathbf{T}_0$) have been assumed stable, the matrices $\mathbf{F}^\star$ and $\mathbf{T}_1^\star$ in equation (5.11) contain poles in $|z| > 1$. Hence, to obtain $J_1 = 0$, it is required that

$$\left(\mathbf{B}_a^\star - \mathbf{A}_b^\star\Xi\mathbf{K}_o\right)\mathbf{T}_0 = \mathbf{\Lambda}^\star \tag{5.12}$$

where, $\mathbf{\Lambda}^\star$ is a polynomial matrix whose invariant zeros lie strictly outside $|z| = 1$.

The diophantine equations (5.6) and (5.7) are obtained by:

(i) post-multiplying equation (5.12) by $\mathbf{T}_0^{-1}$;

(ii) expressing $\mathbf{K}_o$ as the right-matrix fraction

$$\mathbf{K}_o = \check{\mathbf{S}}\check{\mathbf{R}}^{-1}, \tag{5.13}$$

where $\qquad \check{\mathbf{R}} = \mathbf{C}_a\mathbf{R}_s \quad \text{and} \quad \check{\mathbf{S}} = \mathbf{C}_b\mathbf{S}_r;$

(iii) using the right-matrix fraction defined in equation (5.2), whence equation (5.12) can be written as

$$\mathbf{Q}_1(z, z^{-1})\mathbf{R}_s(z^{-1}) = \mathbf{Q}_2(z, z^{-1})\mathbf{S}_r(z^{-1}), \tag{5.14}$$

where $\qquad \mathbf{Q}_1 = \mathbf{B}_a^\star\mathbf{C}_a - \mathbf{\Lambda}^\star\mathbf{A}_c \quad \text{and} \quad \mathbf{Q}_2 = \mathbf{A}_b^\star\Xi\mathbf{C}_b + \mathbf{\Lambda}^\star\mathbf{B}_c.$

Introducing the coprime left-matrix fraction

$$\mathbf{R}^{-1}\mathbf{S} = \mathbf{Q}_2^{-1}\mathbf{Q}_1, \tag{5.15}$$

it is evident that $\qquad \mathbf{Q}_2 = \mathbf{XR} \quad \text{and} \quad \mathbf{Q}_1 = \mathbf{XS}.$

or, equivalently, from equation (5.14),

$$\mathbf{A}_b^{\star}\boldsymbol{\Xi}\mathbf{C}_b + \boldsymbol{\Lambda}^{\star}\mathbf{B}_c = \mathbf{X}\mathbf{R} \tag{5.16}$$

$$\mathbf{B}_a^{\star}\mathbf{C}_a - \boldsymbol{\Lambda}^{\star}\mathbf{A}_c = \mathbf{X}\mathbf{S}. \tag{5.17}$$

The problem then reduces to determining the matrix $\mathbf{X}$. Post-multiplying equations (5.16) and (5.17) by, respectively, $\mathbf{C}_b^{-1}\mathbf{A}_b$ and $\mathbf{C}_a^{-1}\mathbf{B}_a$, adding the resultant equations, utilising equation (5.3) and subsequently dividing by $\mathbf{D}^{\star}\mathbf{D}$, the ensuing identity is

$$\mathbf{I} = \mathbf{D}^{-1}\left(\mathbf{D}^{\star}\right)^{-1}\mathbf{X}\left(\mathbf{R}\mathbf{C}_b^{-1}\mathbf{A}_b + \mathbf{S}\mathbf{C}_a^{-1}\mathbf{B}_a\right). \tag{5.18}$$

It can be established now that

$$\mathbf{X} = \mathbf{D}^{\star},$$

thereby implying that equations (5.16) and (5.17) are equivalent to equations (5.6) and (5.7) respectively, since equation (5.18) then becomes the well-known Bezout identity defining the coprimeness of the pair $(\mathbf{B}_a, \mathbf{A}_b)$, namely,

$$\mathbf{M}\mathbf{A}_b + \mathbf{N}\mathbf{B}_a = \mathbf{I}, \tag{5.19}$$

in which $\mathbf{M} = \mathbf{D}^{-1}\mathbf{R}\mathbf{C}_b^{-1}$ and $\mathbf{N} = \mathbf{D}^{-1}\mathbf{S}\mathbf{C}_a^{-1}$.

Notice that $\mathbf{M}$ and $\mathbf{N}$ are stable, rational matrices free of unstable hidden modes, since $\mathbf{C}_a$, $\mathbf{C}_b$ and $\mathbf{D}$ are stable. Specifying $(\mathbf{R}_{md}, \mathbf{S}_{md}, \boldsymbol{\Lambda}_{md}^{\star})$ to be the minimum-degree solution of equations (5.6) and (5.7), the optimal controller is given by

$$\mathbf{K}_0 = \left(\mathbf{R}_{md}\mathbf{C}_b^{-1}\right)^{-1}\mathbf{S}_{md}\mathbf{C}_a^{-1},$$

or, alternatively, removing the factor related to the disturbance subsystem model by invoking the left-matrix fraction defined in equation (5.5),

$$\mathbf{K}_o = \mathbf{R}_o^{-1}\mathbf{S}_o = \mathbf{S}_{r_o}\mathbf{R}_{s_o}^{-1} \quad \text{(see (5.13))}. \tag{5.20}$$

□

Remarks

1. Non-uniqueness of Matrix Fractions

The LQG compensator $(\mathbf{R}_o, \mathbf{S}_o)$ remains unaffected if $(\mathbf{B}_a, \mathbf{A}_b)$, $(\mathbf{C}_a, \mathbf{A}_c)$ and $(\mathbf{B}_c, \mathbf{C}_b)$ are replaced by $(\mathbf{B}_a\mathbf{U}_1, \mathbf{A}_b\mathbf{U}_1)$, $(\mathbf{C}_a\mathbf{U}_2, \mathbf{A}_c\mathbf{U}_2)$ and $(\mathbf{B}_c\mathbf{U}_3, \mathbf{C}_b\mathbf{U}_3)$, respectively, where

$\mathbf{U}_i(q, q^{-1})$, $i = 1, 2, 3$, denote unimodular matrices. The matrices used above to derive the optimal control law therefore are neither unique nor require to be arranged as specified in equations (4.35) or (4.36). Nonetheless, it is clearly advantageous from an expositional perspective to deal with polynomial matrices in standard representative forms emanating from the repetitive time interval index-dependent models designated in Chapter 4.

2. Minimum Degree Solution ($\mathbf{R}_{md}$, $\mathbf{S}_{md}$, $\mathbf{\Lambda}^{\star}_{md}$)

In contrast with the single-rate case, the "solution $(\mathbf{R}, \mathbf{S})$ of minimum degree with respect to $\mathbf{\Lambda}^{\star}$" is not necessarily determined by a triple $(\mathbf{R}, \mathbf{S}, \mathbf{\Lambda}^{\star})$ in which the highest power of q in each column of $\mathbf{\Lambda}^{\star}$ is minimised and therefore requires clarification in this context. Since it is shown subsequently that $\mathbf{\Lambda}$ is structured likewise to $\mathbf{B}$, namely, using the notation introduced in Chapter 4, $\mathbf{\Lambda} \sim \mathbf{B}$, and that each row (column) of $\mathbf{\Lambda}$ ($\mathbf{\Lambda}^{\star}$) consequently represents sets of polynomials in $q_{L_j}^{-1}$ (q_{L_j}), $j = 1, 2, \ldots, l$, then $\mathbf{\Lambda}^{\star}_{md}$ signifies the matrix $\mathbf{\Lambda}^{\star}$ whose elements correspond to the solution with minimal degrees of q_{L_j}, $j = 1, 2, \ldots, l$, in each column. Expressing the k^{th} column of $\mathbf{\Lambda}^{\star}$, namely, $\boldsymbol{\lambda}^{\star}_k(q)$, thus:

$$\boldsymbol{\lambda}^{\star}_k(q) = \boldsymbol{\lambda}^{k}_0 + \boldsymbol{\lambda}^{(k)}_1 q + \ldots + \boldsymbol{\lambda}^{(k)}_{n_k} q^{n_k}, \tag{5.21}$$

and defining the parameter v_k as denoting the total number of non-zero entities in $\boldsymbol{\lambda}^{(k)}_i$, $i = 0, 1, \ldots, n_k$, then $\mathbf{\Lambda}^{\star}_{md}$ is given by the solution in which each v_k is minimal.

3. Polynomial Matrix Structures

The structure of the matrix $\mathbf{D}$ specified by the spectral factorisation problem of equation (5.3) may be ascertained by recalling that $\mathbf{A}_b \sim \mathbf{X}$ (see (4.36)) and $\mathbf{B}_a \sim \mathbf{B}$ (see (4.35)). Since $\mathbf{X}(0)$ is block upper-triangular and the zero entries with $\mathbf{B}(0)$ form a block lower-triangular sub-matrix, the $(i, j)^{th}$ elements of both $\mathbf{A}^{\star}_b \mathbf{\Xi} \mathbf{A}_b$ and $\mathbf{B}^{\star}_a \mathbf{B}_a$ can be expressed thus:

$$\chi_{ij}(q, q^{-1}) = \begin{cases} \displaystyle\sum_{k=-n_\chi+1}^{n_\chi} \chi_{ijk} q^k, & i < j \\ \chi_{ii0} + \displaystyle\sum_{k=1}^{n_\chi} \chi_{iik}(q^k + q^{-k}), & i = j \\ \displaystyle\sum_{k=-n_\chi}^{n_\chi+1} \chi_{ijk} q^{-k}, & i > j. \end{cases} \tag{5.22}$$

Thus, since $\mathbf{D}^\star\mathbf{D}$ and $\mathbf{X}^\star\mathbf{X}$ possess similar structures, $\mathbf{D} \sim \mathbf{X}$. Inspection of equation (5.6), in which $\mathbf{A}_b^\star\Xi\mathbf{C}_b$ evidently is arranged similarly to $\mathbf{X}^\star\mathbf{X}$, then reveals that $\mathbf{\Lambda} \sim \mathbf{B}$ and, additionally, confirms that $\mathbf{R} \sim \mathbf{X}$ (see (4.39a)). Furthermore, it is supposed that $\mathbf{B}_c \sim \mathbf{B}$ and $\mathbf{C}_b \sim \mathbf{X}$ in equation (5.2), while $\mathbf{C}_o \sim \mathbf{X}$ in equation (5.5).

4. Dynamics-Assignment Interpretation

The optimal controller can be derived instead via a single diophantine equation emanating from equations (5.6) and (5.7). First, following the procedure adopted in deriving equation (5.18), namely, post-multiplying equations (5.6) and (5.7) by $\mathbf{C}_b^{-1}\mathbf{A}_b$ and $\mathbf{C}_a^{-1}\mathbf{B}_a$, respectively, and summing the resultant equations, then removing the common factor $\mathbf{D}^\star$ by invoking equation (5.3), it is established that

$$\mathbf{R}\mathbf{C}_b^{-1}\mathbf{A}_b + \mathbf{S}\mathbf{C}_a^{-1}\mathbf{B}_a = \mathbf{D}. \tag{5.23}$$

Now defining the right-matrix fraction

$$\begin{bmatrix} \mathbf{A}_1 \\ \mathbf{B}_1 \end{bmatrix} \mathbf{C}_1^{-1} = \begin{bmatrix} \mathbf{C}_b & \mathbf{0} \\ \mathbf{0} & \mathbf{C}_a \end{bmatrix}^{-1} \begin{bmatrix} \mathbf{A}_b \\ \mathbf{B}_a \end{bmatrix}, \tag{5.24}$$

in which $\mathbf{A}_1 \sim \mathbf{X}$, $\mathbf{B}_1 \sim \mathbf{B}$ and $\mathbf{C}_1 \sim \mathbf{X}$, then post-multiplication of equation (5.23) by $\mathbf{C}_1$ engenders the polynomial matrix equation

$$\mathbf{R}\mathbf{A}_1 + \mathbf{S}\mathbf{B}_1 = \mathbf{D}\mathbf{C}_1, \tag{5.25}$$

which can be used as an alternative to equations (5.6) and (5.7). Moreover, it will be observed that, when applied to equation (5.23), the matrix fraction defined in equation (5.5) implies that the LQG controller $(\mathbf{R}_o,\mathbf{S}_o)$ satisfies the diophantine equation

$$\mathbf{R}_o\mathbf{A}_b + \mathbf{S}_o\mathbf{B}_a = \mathbf{C}_o\mathbf{D}. \tag{5.26}$$

Equation (5.26) reveals a fundamental property of optimal control, namely, that the poles of the closed-loop system constitute the union of those resulting from the spectral factorisation problem and those corresponding to the invariant zeros of the disturbance subsystem numerator matrix, determined by the characteristic polynomials of $\mathbf{D}(q^{-1})$ and $\mathbf{C}_o(q^{-1})$ respectively.

5. The SISO Case

In contrast with the terms $\mathbf{B}_r\mathbf{A}_L^{-1}$ ((3.69)) and $\mathbf{C}_M\mathbf{A}_M^{-1}$ ((3.73)) that define the respective lifted plant and disturbance subsystem models in the general SISO case, the denominator matrices within the remaining matrix fractions required in the optimal control solution and its dynamics-assignment interpretation (see equations (5.2), (5.5) and (5.24)) in general possess structures which do not conform to that of $\mathbf{F}_K(q^{-1})$ in equation (3.24). Denoted by $\mathbf{X}(q^{-1})$, it is assumed that $\mathbf{C}_b$, $\mathbf{C}_o$, $\mathbf{C}_1$ and $\mathbf{A}_1$ instead are organised thus (cf. (4.42a,b)):

$$\mathbf{X}(q^{-1}) = \sum_{i=0}^{n_x} \hat{\mathbf{X}}_i \mathbf{P}_L^{(i)}(q^{-1}), \tag{5.27}$$

with $\hat{\mathbf{X}}_i = \text{diag}\left(x_{i_0}, x_{i_1}, \ldots, x_{i_{L-1}}\right)$ and where $\hat{\mathbf{X}}_o = \mathbf{I}_L$ in the case of $\mathbf{A}_1$, whereas, denoted by $\mathbf{Y}(q^{-1})$, whilst $\mathbf{B}_c$, $\mathbf{\Lambda}$ and $\mathbf{B}_1$ can be specified as a summation of "$\mathbf{Q}$" matrices, namely,

$$\mathbf{Y}(q^{-1}) = \sum_{j=1}^{n_y} \hat{\mathbf{Y}}_i \mathbf{Q}_{ML}^{(j)}(q^{-1}), \tag{5.28}$$

in which $$\hat{\mathbf{Y}}_i = \text{diag}\left(y_{i_0}, y_{i_1}, \ldots, y_{i_{M-1}}\right),$$

the term y_{i_m}, unlike those designating $\hat{\mathbf{B}}_{l_j}$ in equation (3.71a), cannot be associated with a particular polynomial. Notice that $\mathbf{R}_o$ and $\mathbf{S}_o$ are arranged likewise to $\mathbf{R}$ and $\mathbf{S}$, respectively, in equation (4.42a).

The structure of the matrix $\mathbf{D}$ in the scalar scenario, defined as the stable solution of the spectral factorisation problem ((5.3)), may be ascertained by introducing the following results concerning the adjoints of the "$\mathbf{Q}$" and "$\mathbf{P}$" matrices:

(i)

$$\left(\hat{\mathbf{Y}}_j \mathbf{Q}_{ML}^{(j)}\right)^\star \left(\hat{\mathbf{Y}}_j \mathbf{Q}_{ML}^{(i)}\right) = \begin{cases} \hat{\mathbf{Y}}_{ij}\left(\mathbf{P}_L^{(j-i)}\right)^\star, & j > i \\ \hat{\mathbf{Y}}_{ii}, & j = i \\ \mathbf{P}_L^{(i-j)}\hat{\mathbf{Y}}_{ij}, & j < i \end{cases}; \tag{5.29}$$

(ii) specifying $i = \mu L + l$, $l \in [0.\, L-1]$,

$$\left(\mathbf{P}_L^{(i)}\right)^\star = \begin{cases} q^{\mu+1}\mathbf{P}_L^{(L-l)}, & l \in [1, L-1] \\ q^\mu, & l = 0 \end{cases}. \tag{5.30}$$

Accordingly, from the definitions of $\mathbf{A}_L$ (cf. $\mathbf{F}_K(q^{-1})$ in (3.24)) and $\mathbf{B}_r$ ((3.71b)), then, using equations (5.29) and (5.30), in the general SISO case equation (5.3) becomes

$$\begin{aligned}\mathbf{D}^*\mathbf{D} &= \left(\mathbf{I}_L + \sum_{i=1}^{n} a_{L_i}\mathbf{P}_L^{(i)}\right)^* \left(\mathbf{I}_L + \sum_{i=1}^{n} a_{L_i}\mathbf{P}_L^{(i)}\right) + \xi_1 \left(\sum_{j=1}^{n+1} \hat{\mathbf{B}}_{r_j}\mathbf{Q}_{ML}^{(j)}\right)^* \left(\sum_{j=1}^{n+1} \hat{\mathbf{B}}_{r_j}\mathbf{Q}_{ML}^{(j)}\right) \\ &= \hat{\mathbf{\Delta}}_0 + \sum_{i=1}^{n} \hat{\mathbf{\Delta}}_i \left(\mathbf{P}_L^{(i)}\right)^* + \sum_{i=1}^{n} \mathbf{P}_L^{(i)}\hat{\mathbf{\Delta}}_i,\end{aligned}$$

where $\hat{\mathbf{\Delta}}_i = \text{diag}\left(\delta_{i_0}, \delta_{i_1}, \ldots, \delta_{i_{L-1}}\right)$. Observing that, if $i = \mu L + l$, $l \in [0, L-1]$,

$$\mathbf{P}_L^{(i)}\hat{\mathbf{X}} = \hat{\mathbf{X}}_R^{(i)}\mathbf{P}_L^{(i)}, \tag{5.31}$$

in which the rearranged diagonal matrix $\hat{\mathbf{X}}_R^{(i)}$ is given by

$$\hat{\mathbf{X}}_R^{(i)} = \mathbf{P}_L^{(l)}(1)\hat{\mathbf{X}}\mathbf{P}_L^{(L-l)}(1), \quad l \in [1, L-1],$$

with $\hat{\mathbf{X}}_R^{(i)} = \hat{\mathbf{X}}$, $l = 0$, then the matrix $\mathbf{D}$ may be expressed as

$$\mathbf{D} = \sum_{i=0}^{n} \mathbf{P}_L^{(i)}\hat{\mathbf{D}}_i = \sum_{i=0}^{n} \hat{\mathbf{D}}_{i_R}^{(i)}\mathbf{P}_L^{(i)}, \tag{5.32}$$

with $\hat{\mathbf{D}}_i = \text{diag}\left(d_{i_0}, d_{i_1}, \ldots, d_{i_{L-1}}\right)$ and $\hat{\mathbf{D}}_{i_R}^{(i)}$ similarly defined, where the $\hat{\mathbf{D}}_i$ terms can be acquired by solving the $(n+1)L$ equations in $(n+1)L$ variables specified by

$$\sum_{i=0}^{n-j} \hat{\mathbf{D}}_i \hat{\mathbf{D}}_{(i+j)_R}^{(j)} = \hat{\mathbf{\Delta}}_{j_R}^{(j)}, \quad j = 0, 1, \ldots, n. \tag{5.33}$$

Consequently, $\mathbf{D}$ conforms to the structure of $\mathbf{R}$ in equation (4.42a).

A summary of the matrices and polynomials that define the optimal control solution for the general SISO case and the scenarios hitherto referred to as fast output-sampled (FOS) and fast input-sampled (FIS) is provided in Table 5.1.

5.2 Illustrative Example – Optimal Control

This section outlines the derivation of an LQG compensator for the system labelled M1, which was examined originally in Chapter 4. Initially addressing the general solution, attention focuses upon establishing the structures of each of the polynomial matrices involved and, consequently, the nature of the difference equations that specify the optimal control law. The dynamics-assignment approach then is utilised to acquire the LQG control solution and related stability margins in a numerical example.

Table 5.1. Optimal control solution – SISO case.

MIMO	SISO	FOS	FIS
$\mathbf{A}_b$	$\mathbf{A}_L$	α	$\mathbf{A}_N$
$\mathbf{B}_a$	$\mathbf{B}_r$	b_r	$\tilde{\mathrm{b}}'_r$
$\mathbf{A}_c$	$\mathbf{A}_M$	$\mathbf{A}_N$	α
$\mathbf{C}_a$	$\mathbf{C}_M$	$\mathbf{C}_N$	γ
$\mathbf{C}_b$	$\mathbf{C}_b$	γ	γ
$\mathbf{B}_c$	$\mathbf{B}_c$	$\bar{\mathbf{C}}_N^{(N)}\mathrm{b}_l$	$\tilde{\mathrm{b}}'_l$
$\mathbf{D}$	$\mathbf{D}$	d	$\mathbf{D}$
$\mathbf{\Lambda}$	$\mathbf{\Lambda}$	λ	$\tilde{\lambda}'$
$\mathbf{R}$	$\mathbf{R}$	ρ	$\mathbf{R}$
$\mathbf{R}_o$	$\mathbf{R}_o$	ρ	$\mathbf{R}$
$\mathbf{S}$	$\mathbf{S}$	s'	$\tilde{\mathrm{s}}$
$\mathbf{S}_o$	$\mathbf{S}_o$	$\mathrm{s}'\bar{\mathbf{C}}_N^{(N)}$	$\tilde{\mathrm{s}}$
$\mathbf{C}_o$	$\mathbf{C}_o$	γ	γ
$\mathbf{A}_1$	$\mathbf{A}_1$	α	$\mathbf{A}_N$
$\mathbf{B}_1$	$\mathbf{B}_1$	$\bar{\mathbf{C}}_N^{(N)}\mathrm{b}_r$	$\tilde{\mathrm{b}}'_r$
$\mathbf{C}_1$	$\mathbf{C}_1$	γ	γ

Table 5.2. Polynomial matrix structures.

Matrix	Equation	Structure
$\mathbf{C}_b$	(5.2)	$\tilde{\mathbf{X}}$
$\mathbf{B}_c$	(5.2)	$\tilde{\mathbf{Y}}$
$\mathbf{D}$	(5.3)	$\tilde{\mathbf{X}}$
$\mathbf{R}_{md}$	(5.6)	$\tilde{\mathbf{X}}$
$\mathbf{\Lambda}_{md}$	(5.6), (5.7)	$\tilde{\mathbf{Y}}$
$\mathbf{R}_o$	(5.5)	$\tilde{\mathbf{X}}$
$\mathbf{C}_o$	(5.5)	$\tilde{\mathbf{X}}$

LQG Controller Derivation

It is useful at this juncture to specify the following matrices:

$$\tilde{\mathbf{X}}(q^{-1}) = \begin{bmatrix} \tilde{x}_{11_0} + \tilde{x}_{11_1}q^{-1} & \tilde{x}_{12_0} \\ \tilde{x}_{21_1}q^{-1} & \tilde{x}_{22_0} + \tilde{x}_{22_1}q^{-1} \end{bmatrix} \tag{5.34}$$

and

$$\tilde{\mathbf{Y}}(q^{-1}) = \begin{bmatrix} \tilde{y}_{11_1}q^{-1} & \tilde{y}_{12_0} \\ \tilde{y}_{21_1}q^{-1} & \tilde{y}_{22_0} \\ \tilde{y}_{31_1}q^{-1} & \tilde{y}_{32_0} + \tilde{y}_{32_1}q^{-1} \\ \tilde{y}_{41_1}q^{-1} + \tilde{y}_{41_2}q^{-2} & \tilde{y}_{42_1}q^{-1} \end{bmatrix}. \tag{5.35}$$

Thus, bearing in mind that $\mathbf{A}$, $\mathbf{B}$, $\mathbf{C}$, $\mathbf{C}_a$, $\mathbf{A}_c$, $\mathbf{A}_b$ and $\mathbf{B}_a$ have been defined in Chapter 4 (see equations (4.56), (4.57) and (4.60)), the controller numerator matrices are given by

$$\mathbf{S}_{md} = \begin{bmatrix} s_{11_0} & s_{12_0} & 0 & 0 \\ s_{21_1}q^{-1} & 0 & 0 & s_{24_0} \end{bmatrix} \tag{5.36}$$

and

$$\mathbf{S}_o = \begin{bmatrix} \bar{s}_{11_0} & \bar{s}_{12_0} & \bar{s}_{13_0} & \bar{s}_{14_0} \\ \bar{s}_{21_1}q^{-1} & \bar{s}_{22_1}q^{-1} & \bar{s}_{23_1}q^{-1} & \bar{s}_{24_0} \end{bmatrix}, \tag{5.37}$$

whilst the structures of the remaining matrices concerned are summarised in Table 5.2.

Consequently, from Table 5.2 and equations (5.34) and (5.37), the optimal control law of equation (5.5) may be interpreted as being specified by the two difference equations:

$$\bar{r}_{11_0}u(0) + \bar{r}_{12_0}u(-3) + \bar{r}_{11_1}u(-6) = -\left(\bar{s}_{11_0}y_1(0) + \bar{s}_{12_0}y_2(0) + \bar{s}_{13_0}y_2(-2) + \bar{s}_{14_0}y_2(-4)\right) \quad (5.38a)$$

$$\bar{r}_{22_0}u(-3) + \bar{r}_{21_1}u(-6) + \bar{r}_{22_1}u(-9) = -\left(\bar{s}_{21_1}y_1(-6) + \bar{s}_{24_0}y_2(-4) + \bar{s}_{22_0}y_2(-6) + \bar{s}_{23_1}y_2(-8)\right) \quad (5.38b)$$

Numerical Example

In this example it is supposed that:

(i) the repetitive time interval is

$$T = 6\log_e 1.04 = 0.2353 \text{ s},$$

whence (see equation (4.54a)),

$$a_1 = a = 0.9615, \quad b_1 = 0.0385, \quad a_2 = \bar{a} = 1.04 \quad \text{and} \quad b_2 = 0.04;$$

(ii) the disturbance model is specified by (see equation (4.59))

$$c_1 = -0.75 \quad \text{and} \quad c_2 = -0.8;$$

(iii) the control weighting parameter is (see equation (5.1))

$$\xi_1 = 0.115.$$

Solving equation (5.3) for the above value of ξ_1, it is found that

$$\mathbf{D}(q^{-1}) = \begin{bmatrix} 0.4489 + 0.2492q^{-1} & -0.6770 \\ -0.6865q^{-1} & 0.4648 + 0.2409q^{-1} \end{bmatrix}.$$

The closed-loop poles related to the plant – determined by the zeros of $z^2\det\left(\mathbf{D}(z^{-1})\right)$ – then are given by

$$z = 0.3643 \quad \text{and} \quad z = 0.7899,$$

while those associated with the disturbance subsystem – dictated by the characteristic polynomial of $\mathbf{C}_o(z^{-1})$ (or, equivalently, $\mathbf{C}$, $\mathbf{C}_a$, $\mathbf{C}_b$ or $\mathbf{C}_1$) – are located at

$$z = 0.4838 \quad \text{and} \quad z = 0.3831.$$

The dynamics-assignment approach to determining the LQG controller is dependent upon the following matrices, obtained from the matrix fraction conversion defined in equation (5.25):

$$\mathbf{A}_1(q^{-1}) = \begin{bmatrix} 1 + 0.1963q^{-1} & -1.5452 \\ -4.7548q^{-1} & 1 + 5.0951q^{-1} \end{bmatrix},$$

$$\mathbf{B}_1(q^{-1}) = \begin{bmatrix} -0.1050q^{-1} & 0.1110 \\ -0.0046q^{-1} - 0.0215q^{-2} & 0.1539 - 0.0822q^{-1} \\ 0.1157q^{-1} - 0.0918q^{-2} & 0.0400 - 0.0310q^{-1} \\ 0.0816q^{-1} - 0.0802q^{-2} & 0.0846q^{-1} - 0.0473q^{-2} \end{bmatrix}$$

and $$\mathbf{C}_1(q^{-1}) = \begin{bmatrix} 1 - 0.4068q^{-1} & 0.0251 \\ 0.1790q^{-1} & 1 - 0.4556q^{-1} \end{bmatrix}.$$

The minimal degree solution of the single diophantine equation ((5.25)), defined with respect to $\mathbf{R}$, is

$$\mathbf{R}_{md} = \begin{bmatrix} 0.4489 - 0.4485q^{-1} & -0.0642 \\ 1.5529q^{-1} & 0.4648 - 0.0154q^{-1} \end{bmatrix}$$

and $$\mathbf{S}_{md} = \begin{bmatrix} -0.0308 & 0.6202 & 0 & 0 \\ 0.0268q^{-1} & 0 & 0 & 0.6592 \end{bmatrix}.$$

The final stage of the derivation procedure concerns the right- to left-matrix fraction conversion of equation (5.5), which yields

$$\mathbf{R}_o = \begin{bmatrix} 0.4489 - 0.0931q^{-1} & 0.1634 \\ 0.2387q^{-1} & 0.4648 - 0.0743q^{-1} \end{bmatrix}$$

$$\mathbf{S}_o = \begin{bmatrix} -0.0308 & 0.6202 & 0.4505 & 0.3676 \\ 0.0238q^{-1} & 0.5381q^{-1} & 0.3908q^{-1} & 0.6592 \end{bmatrix}$$

and $$\mathbf{C}_o = \begin{bmatrix} 1 - 0.4304q^{-1} & 0.0613 \\ 0.0957q^{-1} & 1 - 0.4306q^{-1} \end{bmatrix}.$$

Utilising the technique proposed by Thompson (1986), in which the return ratio is defined as the path enclosed by the sampler at the controller output, the phase margin is

$$PM = 48.4214^\circ.$$

whereas the upper and lower gain margins are given by

$$GM_u = +16.4479\text{dB} \quad \text{and} \quad GM_l = -8.3904\text{dB}.$$

5.3 Predictive Control

The application of predictive control strategies was traditionally associated with self-tuning regulators, whereby an identification algorithm provides estimates of the system parameters required to calculate the control law at each sample instant. Nevertheless, it is important to emphasise that the ever-increasing sophistication of the predictive control approach engendered by three decades of research implies that nowadays this methodology is increasingly being viewed as an alternative to LQG controller design in the non-adaptive context considered in this section. Additionally, in contrast with other control design methods, predictive control affords the possibility of addressing system nonlinearities by incorporating them as constraints when formulating the design problem. In this case, the predictive control law is acquired by solving a constrained optimisation problem. The specific approach described in this section concerns control algorithms customarily encountered in an adaptive framework – referred to nowadays as *model-based predictive control* (MBPC) – as opposed to the techniques known as "Model Predictive Heuristic Control" (Richalet *et al.* (1978)) and "Dynamic Matrix Control" (Cutler and Ramaker (1979), Prett and Gillette (1979)) commonly employed in the process and petrochemical industries.

Developments in MBPC emanate from Åström and Wittenmark's self-tuning regulator (Åström and Wittenmark (1973)). In this paper, a "minimum-variance" control algorithm was introduced – namely, based upon information available at the k^{th} sample instant, a controller which minimised the variance of the output signal at the $(k+d)^{th}$ sample instant, where d denotes the plant dead time. The inherent drawback in minimum-variance control in failing to guarantee the closed-loop stability of configurations containing nonminimum-phase plants provided the motivation for the Generalised Minimum Variance (GMV) self-tuning controller (Clarke and Gawthrop (1975)), in which the control and predicted output signals were weighted dynamically within the performance index. Other notable contributions in MBPC are Peterka's predictive controller (Peterka (1984)), Ydstie's extended-horizon design (Ydstie (1984)) and the EPSAC algorithm (De Keyser

and Van Cauwenberghe (1982)).

The theoretical work contained in this section is founded upon the Generalised Predictive Control (GPC) algorithm by Clarke *et al.* (1987a,b). While penalising the variances of future controls, the GPC strategy attempts to drive the predicted outputs "close" to a known reference signal throughout a "prediction horizon" from the $(k_1 + d)^{th}$ to the $(k_2 + d)^{th}$ sample instants, thereby resulting in a suggested sequence of future controls. However, only the control at the k_1^{th} sample instant is actually implemented and, in an adaptive framework, the control law is re-calculated given new information available at the $(k_1+1)^{th}$ sample instant. Since the formulation of the problem is such that, if used, the set of future controls would be applied in open-loop, this *receding horizon* approach belongs to the class known as "Open-Loop-Feedback Optimal Control" (Bertsekas (1976)). This section details the derivation of predictive controllers for the lifted plant model in left matrix fraction form in Chapter 4, exploiting the underlying principles in extending the basic GPC technique to the multirate-sampled case described by Truman and Govan (2000a). In common with the procedure used to describe the LQG approach, modifications to the basic technique, such as the introduction of integral action by adopting an incremental system model – the customary formulation of the GPC design problem – are addressed in section 5.5. Notice that, while the underlying principles remain unaffected, the derivation technique differs somewhat from that employed by Clarke *et al.* (1987a,b).

Problem Outline

The forthcoming analysis deals with the "regulator" problem and concerns the derivation with respect to a horizon p repetitive time intervals in advance of a predictive control law at the sample instants denoted by $\iota = \lambda_\nu$, where (see section 4.3)

$$\lambda_\nu \in \{0, \lambda_1, \ldots, \lambda_\phi, \ldots, \lambda_\Phi\}\,.$$

Initially, it is assumed that the output (and, therefore, the white noise) and control sampling instants are synchronised as follows:

$$\ldots < \mu_\kappa < \lambda_\nu \leq \mu_{\kappa+1} \ldots < \lambda_{\nu+1} \ldots, \tag{5.39a}$$

whereas it is supposed additionally that

$$d \leq \lambda_\nu - \mu_\kappa. \tag{5.39b}$$

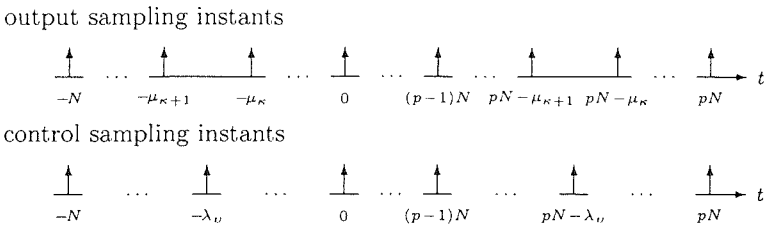

Figure 5.1. Timing diagram.

where d denotes the dead time of the discretisied plant model (see (4.6)). As discussed in the sequel, the proposed approach is not unduly restrictive and can be modified readily to account for alternative situations.

Suppressing the subscripts i and j related to each control and output for concision, the problem being considered may be summarised as that of obtaining the sequence $\{u_{o_\nu}(-\lambda_\nu),\ u_{o_\nu}(-\lambda_{\nu-1}),\ \ldots,\ u_{o_\nu}(pN-\lambda_{\nu+1})\}$ minimising a quadratic performance index that penalises the outputs $y(-\mu_\kappa),\ y(-\mu_{\kappa-1}),\ \ldots,\ y(pN-\mu_{\kappa+1})$, in addition to the aforementioned controls. Thus, as depicted in the timing diagram of Figure 5.1, the prediction horizon is defined as $t \equiv pN-\mu_{\kappa+1}$. In common with the use of the GPC algorithm in an adaptive context, the "optimal" predictive control at $t \equiv -\lambda_\nu$ then is specified to be $u_{o_\nu}(-\lambda_\nu)$, while the overall multirate-sampled predictive control law constitutes the amalgamation of the individual controls $u_{o_0}(0),\ u_{o_1}(-\lambda_1),\ \ldots,\ u_{o_\Phi}(-\lambda_\Phi)$. The primary focus of attention therefore involves the formulation of an appropriate model – the so-called "p repetitive time intervals-ahead" representation – that encapsulates the problem defined above.

p Repetitive Time Intervals-Ahead Representation

The predictive model is predicated upon the repetitive time interval index-dependent description established in Chapter 4, namely,

$$\bar{\mathbf{y}}(0) = \mathbf{A}^{-1}(q^{-1})\mathbf{B}(q^{-1})\bar{\mathbf{u}}(0)+\mathbf{A}^{-1}(q^{-1})\mathbf{C}(q^{-1})\bar{\epsilon}(0). \qquad ((4.34))$$

Defining the following vectors,

$$\bar{\mathbf{y}}(N-\mu_{\kappa+1}) = \left[\ y(N-\mu_{\kappa+1}) \quad \ldots \quad \mathbf{y}'(0) \quad \ldots \quad y(-\mu_\kappa)\ \right]' \qquad (5.40a)$$

with $\bar{\epsilon}(N-\mu_{\kappa+1})$ specified accordingly, and

$$\bar{\mathbf{u}}(N-\lambda_{\nu+1}) = \left[\ u(N-\lambda_{\nu+1}) \quad \ldots \quad \mathbf{u}'(0) \quad \ldots \quad u(-\lambda_\nu)\ \right]', \qquad (5.40b)$$

it is assumed that $\bar{\mathbf{y}}(0)$ (and $\bar{\boldsymbol{\epsilon}}(0)$) and $\bar{\mathbf{u}}(0)$ are related to the above vectors thus:

$$\bar{\mathbf{y}}(0) = \mathbf{P}_y^{(N-\mu_{\kappa+1})}(q^{-1})\bar{\mathbf{y}}(N-\mu_{\kappa+1}) \tag{5.41a}$$

and

$$\bar{\mathbf{u}}(0) = \mathbf{P}_u^{(N-\lambda_{\nu+1})}(q^{-1})\bar{\mathbf{u}}(N-\lambda_{\nu+1}). \tag{5.41b}$$

Notice that $\mathbf{P}_y^{(\cdot)}$ and $\mathbf{P}_u^{(\cdot)}$ are simply generalisations of the $\mathbf{P}_K^{(\cdot)}$ matrices introduced in Chapter 3 (see (3.21)) and, in fact, become $\mathbf{P}_M^{(\cdot)}$ and $\mathbf{P}_L^{(\cdot)}$, respectively, in the scalar case. Consequently, using

$$\left(\mathbf{P}_x^{(k)}(q^{-1})\right)^{-1} = q\mathbf{P}_x^{(N-k)}(q^{-1}),$$

then, from equation (4.34), the vector $\bar{\mathbf{y}}(N-\mu_{\kappa+1})$ is given by

$$\mathbf{A}_\nu(q^{-1})\bar{\mathbf{y}}(N-\mu_{\kappa+1}) = \mathbf{B}_\nu(q^{-1})\bar{\mathbf{u}}(N-\lambda_{\nu+1}) + \mathbf{C}_\nu(q^{-1})\bar{\boldsymbol{\epsilon}}(N-\mu_{\kappa+1}), \tag{5.42}$$

where

$$\mathbf{A}_\nu(q^{-1}) = \mathbf{P}_y^{(N-\mu_{\kappa+1})}(q^{-1})\mathbf{A}(q^{-1})\left(q\mathbf{P}_y^{\mu_{\kappa+1}}(q^{-1})\right)$$

with $\mathbf{C}_\nu(q^{-1})$ designated likewise, and

$$\mathbf{B}_\nu(q^{-1}) = \mathbf{P}_y^{(N-\mu_{\kappa+1})}(q^{-1})\mathbf{B}(q^{-1})\left(q\mathbf{P}_u^{(\lambda_{\nu+1})}(q^{-1})\right).$$

Observing that all "$\mathbf{C}$" matrices and "$\boldsymbol{\epsilon}$" vectors are defined analogously to "$\mathbf{A}$" matrices and "$\mathbf{y}$" vectors, respectively, the p repetitive time intervals-ahead model additionally requires that $\mathbf{A}_\nu(q^{-1})$ and $\mathbf{B}_\nu(q^{-1})$ are expressed thus:

$$\mathbf{A}_\nu(q^{-1}) = \sum_{i=0}^{n} \mathbf{A}_\nu^{(i)} q^{-i} \tag{5.43a}$$

and

$$\mathbf{B}_\nu(q^{-1}) = \sum_{i=0}^{n_b} \mathbf{B}_\nu^{(i)} q^{-i}, \tag{5.43b}$$

and that the vectors $\check{\mathbf{y}}_\nu$ and $\check{\mathbf{u}}_\nu$ are designated as

$$\check{\mathbf{y}}_\nu = \left[\begin{array}{cccc} \bar{\mathbf{y}}'(pN-\mu_{\kappa+1}) & \bar{\mathbf{y}}'((p-1)N-\mu_{\kappa+1}) & \ldots & \bar{\mathbf{y}}'(N-\mu_{\kappa+1}) \end{array}\right]' \tag{5.44a}$$

and

$$\check{\mathbf{u}}_\nu = \left[\begin{array}{cccc} \bar{\mathbf{u}}'(pN-\lambda_{\nu+1}) & \bar{\mathbf{u}}'((p-1)N-\lambda_{\nu+1}) & \ldots & \bar{\mathbf{u}}'(N-\lambda_{\nu+1}) \end{array}\right]'. \tag{5.44b}$$

Invoking the above definitions, when extended to encompass p repetitive time intervals, the model of equation (5.42) becomes

$$\begin{aligned}\check{\mathbf{A}}_\nu\check{\mathbf{y}}_\nu + \check{\mathbf{A}}_\nu^\dagger(q^{-1})\bar{\mathbf{y}}(-\mu_{\kappa+1}) = \check{\mathbf{B}}_\nu\check{\mathbf{u}}_\nu + \check{\mathbf{B}}_\nu^\dagger(q^{-1})\bar{\mathbf{u}}(-\lambda_{\nu+1}) \\ +\check{\mathbf{C}}_\nu\check{\boldsymbol{\epsilon}}_\nu + \check{\mathbf{C}}_\nu^\dagger(q^{-1})\bar{\boldsymbol{\epsilon}}(-\mu_{\kappa+1}),\end{aligned} \tag{5.45}$$

in which

$$\check{\mathbf{A}}_\nu = \begin{bmatrix} \mathbf{A}_\nu^{(0)} & \mathbf{A}_\nu^{(1)} & \dots & \mathbf{A}_\nu^{(p-1)} \\ \mathbf{0} & \mathbf{A}_\nu^{(0)} & \dots & \mathbf{A}_\nu^{(p-2)} \\ \vdots & \vdots & \ddots & \vdots \\ \mathbf{0} & \mathbf{0} & \dots & \mathbf{A}_\nu^{(0)} \end{bmatrix}, \quad \mathbf{A}_\nu^\dagger(q^{-1}) = \begin{bmatrix} \sum_{i=p}^{n} \mathbf{A}_\nu^{(i)} q^{-(i-p)} \\ \sum_{i=p-1}^{n} \mathbf{A}_\nu^{(i)} q^{-(i-p+1)} \\ \vdots \\ \sum_{i=1}^{n} \mathbf{A}_\nu^{(i)} q^{-(i-1)} \end{bmatrix},$$

$$\check{\mathbf{B}}_\nu = \begin{bmatrix} \mathbf{B}_\nu^{(0)} & \mathbf{B}_\nu^{(1)} & \dots & \mathbf{B}_\nu^{(p-1)} \\ \mathbf{0} & \mathbf{B}_\nu^{(0)} & \dots & \mathbf{B}_\nu^{(p-2)} \\ \vdots & \vdots & \ddots & \vdots \\ \mathbf{0} & \mathbf{0} & \dots & \mathbf{B}_\nu^{(0)} \end{bmatrix} \quad \text{and} \quad \mathbf{B}_\nu^\dagger(q^{-1}) = \begin{bmatrix} \sum_{i=p}^{n_b} \mathbf{B}_\nu^{(i)} q^{-(i-p)} \\ \sum_{i=p-1}^{n_b} \mathbf{B}_\nu^{(i)} q^{-(i-p+1)} \\ \vdots \\ \sum_{i=1}^{n_b} \mathbf{B}_\nu^{(i)} q^{-(i-1)} \end{bmatrix}.$$

Cost Function

Again omitting the subscripts i and j from equation (5.45), the p repetitive time intervals-ahead representation is

$$\check{\mathbf{y}}_\nu = \mathbf{\Gamma}_\nu \mathbf{u}_\nu + \mathbf{f}_\nu(q^{-1}) + \check{\mathbf{A}}_\nu^{-1} \check{\mathbf{C}}_\nu \boldsymbol{\epsilon}_\nu, \tag{5.46}$$

in which $$\mathbf{\Gamma}_\nu = \check{\mathbf{A}}_\nu^{-1} \check{\mathbf{B}}_\nu$$

and $$\mathbf{f}_\nu(q^{-1}) = \check{\mathbf{A}}_\nu^{-1} \left(-\mathbf{A}_\nu^\dagger(q^{-1}) \bar{\mathbf{y}}(-\mu_{\kappa+1}) + \mathbf{B}_\nu^\dagger(q^{-1}) \bar{\mathbf{u}}(-\lambda_{\nu+1}) + \mathbf{C}_\nu^\dagger(q^{-1}) \bar{\boldsymbol{\epsilon}}(-\mu_{\kappa+1}) \right).$$

The cost function related to the sample instants at $t = -\lambda_\nu$ then is designated as

$$J_\nu = E\left\{ \check{\mathbf{y}}_\nu' \check{\mathbf{y}}_\nu + \check{\mathbf{u}}_\nu \mathbf{\Lambda}_\nu \check{\mathbf{u}}_\nu \right\}, \tag{5.47}$$

where $\mathbf{\Lambda}_\nu$ is a diagonal weighting matrix and in which the expectation operator is conditioned upon the data known at $t = -\lambda_\nu$.

Optimal Predictive Control Solution

Neglecting the term $\check{\mathbf{A}}_\nu^{-1} \check{\mathbf{C}}_\nu \boldsymbol{\epsilon}_\nu$ in equation (5.46), which represents data in advance of the instant $t \equiv -\lambda_\nu$, the performance index of equation (5.47) is minimised by setting

$\partial J_\nu/\partial \check{\mathbf{u}}_\nu = 0$, whence the optimal sequence of controls throughout the prediction horizon is

$$\check{\mathbf{u}}_{o_\nu} = -\left(\mathbf{\Lambda}_\nu + \mathbf{\Gamma}'_\nu \mathbf{\Gamma}_\nu\right)^{-1} \mathbf{\Gamma}'_\nu \mathbf{f}_\nu(q^{-1}). \tag{5.48}$$

The "optimal" predictive control law at $t \equiv -\lambda_\nu$ for the j^{th} control then represents the last row of equation (5.48), namely,

$$R_\nu(q_N^{-1})u_j(-\lambda_\nu) = -\mathbf{s}'_{y_\nu}(q^{-1})\mathbf{y}(-\mu_{\kappa+1}) + \mathbf{s}'_{\epsilon_\nu}(q^{-1})\boldsymbol{\epsilon}(-\mu_{\kappa+1}). \tag{5.49}$$

Repeating the procedure described above for each control $u_j(-\lambda_\nu)$, $j = 1, 2, \ldots, l$, for each relevant sampling instant $\lambda_\nu \in \{0, \lambda_1, \ldots, \lambda_\Phi\}$, the overall predictive control law is given by

$$\mathbf{R}(q^{-1})\bar{\mathbf{u}}(0) = -\mathbf{S}_y(q^{-1})\bar{\mathbf{y}}(0) + \mathbf{S}_\epsilon(q^{-1})\bar{\boldsymbol{\epsilon}}(0). \tag{5.50}$$

Predictive Controller

Due to its dependency upon the white noise signal $\bar{\boldsymbol{\epsilon}}(0)$, the predictive compensator cannot be implemented directly. Correspondingly, specifying the following left-matrix fraction:

$$\mathbf{C}_{s_\epsilon}^{-1}(q^{-1})\mathbf{S}_{c_\epsilon}(q^{-1}) = \mathbf{S}_\epsilon(q^{-1})\mathbf{C}^{-1}(q^{-1}), \tag{5.51}$$

in which $\mathbf{C}_{s_\epsilon}(0)$ is required to be block upper-triangular, then the combination of the control law of equation (5.50) with the "repetitive time interval index-dependent" plant description of equation (4.34) yields the controller

$$\bar{\mathbf{u}}(0) = -\mathbf{R}_o^{-1}(q^{-1})\mathbf{S}_o(q^{-1})\bar{\mathbf{y}}(0), \tag{5.52}$$

where $\mathbf{R}_o = \mathbf{C}_{s_\epsilon}\mathbf{R} + \mathbf{S}_{c_\epsilon}\mathbf{B}$, and $\mathbf{S}_o = \mathbf{C}_{s_\epsilon}\mathbf{S}_y - \mathbf{S}_{c_\epsilon}\mathbf{A}$.

Remarks

1. Generalisation of Approach

Expression (5.39a) represents the case in which a control at $t \equiv -\lambda_\nu$ directly precedes and immediately follows, measurements at $t \equiv -\mu_\kappa$ and $t \equiv -\mu_{\kappa+1}$ respectively. As indicated by the following interlacing of sampling instants:

$$\ldots \mu_\kappa < \lambda_{\nu-\zeta+1} < \lambda_{\nu-\zeta+2} < \ldots < \lambda_\nu \leq \mu_{\kappa+1} \ldots < \lambda_{\nu+1} \ldots, \tag{5.53}$$

when two or more controls are applied in succession, the methodology described in this section remains unaltered until equation (5.49), at which juncture the "optimal" predictive control laws at the sample instants $t \equiv \lambda_{\nu-\zeta+1}$, $t \equiv -\lambda_{\nu-\zeta+2}, \ldots, t \equiv -\lambda_\nu$, are specified to constitute the last ζ rows of equation (5.48).

Now consider the situation in which, instead of expressions (5.39b), the time-delay d is given by

$$d = \upsilon N + \tilde{d}, \quad \tilde{d} \in [0, N-1]. \tag{5.54}$$

In this event, the matrices $\mathbf{B}_\nu^{(0)}, \mathbf{B}_\nu^{(1)}, \ldots, \mathbf{B}_\nu^{(\nu-1)}$, in equation (5.45) vanish and the elements in $\mathbf{B}_\nu^{(\upsilon)}$ relating an output $y_i(\upsilon N - \mu_\theta)$ to $u_j(-\lambda_\nu)$ are zero for

$$\mu_\theta + \tilde{d} > \lambda_\nu. \tag{5.55}$$

Thus, although penalised within the cost function of equation (5.47), since the outputs at the sampling instants $t \equiv \upsilon N - \mu_\theta, t \equiv \upsilon N - \mu_{\theta+1}, \ldots, t \equiv -\mu_\kappa$, are unaffected by the controls $u_j(-\lambda_\nu)$, they are irrelevant with regard to computing the predictive controller. In such circumstances, it may be necessary to increase the parameter p by υ or $\upsilon + 1$ to compensate.

2. The SISO Case

The matrices $\mathbf{A}_\nu$, $\mathbf{B}_\nu$ and $\mathbf{C}_\nu$ determining the p repetitive time intervals-ahead representation are obtained from equations (3.68) and (3.73) and by observing that the subscript ν corresponds to the index l ($\in [0, L-1]$) in equation (4.40). Replacing l by j to avoid confusion with the matrix $\mathbf{B}_l$ in equation (3.68), equation (5.42) becomes

$$\mathbf{A}_j(q^{-1})\mathbf{y}_M((M-m_j)L) = \mathbf{B}_j(q^{-1})\mathbf{u}_L((L-j-1)M) + \mathbf{C}_j(q^{-1})\boldsymbol{\epsilon}_M((M-m_j)L), \tag{5.56}$$

where $$\mathbf{A}_j(q^{-1}) = \mathbf{P}_M^{(M-m_j)}(q^{-1})\mathbf{A}_M(q^{-1})\left(q\mathbf{P}_M^{(m_j)}(q^{-1})\right),$$

with $\mathbf{C}_j(q^{-1})$ defined similarly, and

$$\mathbf{B}_j(q^{-1}) = \mathbf{P}_M^{(M-m_j)}(q^{-1})\mathbf{B}_l(q^{-1})\left(q\mathbf{P}_L^{(j+1)}(q^{-1})\right).$$

Bearing in mind the comments pertaining to equation (4.40) and the above discussion regarding the application of several controls in succession, in the event when $L > M$ and, therefore,

$$m_{j-\xi+1} = m_{j-\xi+2} = \ldots = m_j, \tag{5.57}$$

it suffices to specify equation (5.56) for j and m_j alone. Moreover, when $m_j = M$, it is convenient to combine this particular model with that acquired for $m_j = 0$ by adding LM $(= N)$ to each matrix superscript and vector argument. As a result, equation (5.56) need only be evaluated for $j = 0, 1, \ldots, J-1$, where

$$J = \min(L, M). \tag{5.58}$$

In the FOS scenario, the model corresponding to equation (5.42) results by observing that $d \geq 1$ and consequently defining $\mathbf{b}_l$ in equation (3.75) as

$$\mathbf{b}_l(q^{-1}) = q^{-1}\mathbf{b}_{l_1}(q^{-1}), \quad \mathbf{b}_{l_1} = \mathbf{B}_N\mathbf{P}_N^{(d-1)}\mathbf{w}_N,$$

whence
$$\mathbf{A}_N(q^{-1})\mathbf{y}_N(N) = \mathbf{b}_{l_1}(q^{-1})u(0) + \mathbf{C}_N(q^{-1})\mathbf{e}_N(N). \tag{5.59}$$

Accordingly, specifying

$$\tilde{\mathbf{b}}'_l(q^{-1}) = \tilde{\mathbf{b}}'_{l_1}(q^{-1})\mathbf{P}_N^{(1)}(q^{-1}), \quad \tilde{\mathbf{b}}'_{l_1} = \mathbf{v}'_N\bar{\mathbf{A}}_N^{(N)}\mathbf{B}_N\mathbf{P}_N^{(d-1)},$$

in equation (3.76), the corresponding FIS representation is

$$\alpha(q^{-1})y(N) = \tilde{\mathbf{b}}'_{l_1}(q^{-1})\mathbf{u}_N(N-1) + \gamma(q^{-1})\epsilon(N). \tag{5.60}$$

5.4 Illustrative Example – Predictive Control

The derivation of a predictive controller for the system denoted as M1 is considered in this section. Whilst the primary objective is to demonstrate the principles established in section 5.3, it is instructive to compare the structure of the predictive control law with its LQG counterpart, acquired in section 5.2.

Predictive Controller Derivation

The initial stage in the derivation procedure concerns the designation of the sampling instants $-\mu_\kappa$, $-\lambda_\nu$, $-\mu_{\kappa+1}$ and $-\lambda_{\nu+1}$ for each control applied during the repetitive time interval. Bearing in mind that the system vectors are

$$\bar{\mathbf{y}}(0) = \begin{bmatrix} y_1(0) & y_2(0) & y_2(-2) & y_2(-4) \end{bmatrix}' \quad \text{and} \quad \bar{\mathbf{u}}(0) = \begin{bmatrix} u(0) & u(-3) \end{bmatrix}',$$

then, addressing the control $u(0)$, the sampling instants are interlaced thus (see (5.39a)):

$$\ldots \mu_\kappa < \lambda_\nu = \mu_{\kappa+1} < \mu_{\kappa+2} < \lambda_{\nu+1} \ldots, \tag{5.61}$$

where $\mu_\kappa = -2, \quad \lambda_\nu = \mu_{\kappa+1} = 0 \ (\mu_{\kappa+2} = 2) \quad \text{and} \quad \lambda_{\nu+1} = 3.$

The vectors $\bar{\mathbf{y}}(N-\mu_{\kappa+1})$ and $\bar{\mathbf{u}}(N-\lambda_{\nu+1})$ then are specified respectively as (see (5.40a,b))

$$\bar{\mathbf{y}}(N-\mu_{\kappa+1}) = \bar{\mathbf{y}}(6) = \begin{bmatrix} y_1(6) & y_2(6) & y_2(4) & y_2(2) \end{bmatrix}' \tag{5.62a}$$

and

$$\bar{\mathbf{u}}(N-\lambda_{\nu+1}) = \bar{\mathbf{u}}(3) = \begin{bmatrix} u(3) & u(0) \end{bmatrix}', \tag{5.62b}$$

which are related to $\bar{\mathbf{y}}(0)$ and $\bar{\mathbf{u}}(0)$ via the permutation matrices (see (5.41a,b))

$$\mathbf{P}_y^{(N-\mu_{\kappa+1})}(q^{-1}) = q^{-1}\mathbf{I}_4 \quad \text{and} \quad \mathbf{P}_u^{(N-\lambda_{\nu+1})}(q^{-1}) = \begin{bmatrix} 0 & 1 \\ q^{-1} & 0 \end{bmatrix} \left(= \mathbf{P}_2^{(1)}(q^{-1})\right).$$

Using the subscript $\nu = 0$, the $\mathbf{A}_0(q^{-1})$ and $\mathbf{B}_0(q^{-1})$ matrices specified in equations (5.43a,b) are given (via equation (5.42)) by

$$\mathbf{A}_0(q^{-1}) = \mathbf{A}_0^{(0)} + \mathbf{A}_0^{(1)} q^{-1}, \tag{5.63}$$

where $$\mathbf{A}_0^{(0)} = \begin{bmatrix} 1 & 0 & 0 & 0 \\ 0 & 1 & -\bar{a}^2 & 0 \\ 0 & 0 & 1 & -\bar{a}^2 \\ 0 & 0 & 0 & 1 \end{bmatrix} \quad \text{and} \quad \mathbf{A}_0^{(1)} = \begin{bmatrix} -a^6 & 0 & 0 & 0 \\ 0 & 0 & 0 & 0 \\ 0 & 0 & 0 & 0 \\ 0 & -\bar{a}^2 & 0 & 0 \end{bmatrix},$$

and

$$\mathbf{B}_0(q^{-1}) = \mathbf{B}_0^{(0)} = \begin{bmatrix} (1+a+a^2)b_1 & (a^3+a^4+a^5)b_1 \\ (1+\bar{a})b_2 & 0 \\ b_2 & \bar{a}b_2 \\ 0 & (1+\bar{a})b_2 \end{bmatrix}. \tag{5.64}$$

Notice that, with a^6 and $\bar{a}^2$ replaced with $-\tilde{c}_1$ and $-\tilde{c}_2$, respectively, $\mathbf{C}_0(q^{-1})$ is defined similarly to $\mathbf{A}_0(q^{-1})$. Selecting the parameter p as 3, the vectors $\check{\mathbf{y}}_0$ and $\check{\mathbf{u}}_0$ are (see (5.44a,b))

$$\check{\mathbf{y}}_0 = \begin{bmatrix} \bar{\mathbf{y}}'(18) & \bar{\mathbf{y}}'(12) & \bar{\mathbf{y}}'(6) \end{bmatrix}' \quad \text{and} \quad \check{\mathbf{u}}_0 = \begin{bmatrix} \bar{\mathbf{u}}'(15) & \bar{\mathbf{u}}'(9) & \bar{\mathbf{u}}'(3) \end{bmatrix}',$$

whereas the matrices in equation (5.45) are:

$$\check{\mathbf{A}}_0 = \begin{bmatrix} \mathbf{A}_0^{(0)} & \mathbf{A}_0^{(1)} & \mathbf{0} \\ \mathbf{0} & \mathbf{A}_0^{(0)} & \mathbf{A}_0^{(1)} \\ \mathbf{0} & \mathbf{0} & \mathbf{A}_0^{(0)} \end{bmatrix}, \quad \mathbf{A}_0^\dagger = \begin{bmatrix} \mathbf{0} \\ \mathbf{0} \\ \mathbf{A}_0^{(1)} \end{bmatrix},$$

with $\check{\mathbf{C}}_0$ and $\mathbf{C}_0^\dagger$ arranged accordingly, and

$$\check{\mathbf{B}}_0 = \begin{bmatrix} \mathbf{B}_0^{(0)} & \mathbf{0} & \mathbf{0} \\ \mathbf{0} & \mathbf{B}_0^{(0)} & \mathbf{0} \\ \mathbf{0} & \mathbf{0} & \mathbf{B}_0^{(0)} \end{bmatrix} \quad \text{and} \quad \mathbf{B}_0^\dagger = \begin{bmatrix} \mathbf{0} \\ \mathbf{0} \\ \mathbf{0} \end{bmatrix}.$$

Repeating the above procedure for the control $u(-3)$, the resultant sampling instants are ordered thus:

$$\ldots \mu_\kappa < \lambda_\nu < \mu_{\kappa+1} < \lambda_{\nu+1} = \mu_{\kappa+2} \ldots, \tag{5.65}$$

where $\mu_\kappa = 2, \quad \lambda_\nu = 3, \quad \mu_{\kappa+1} = 4 \quad \text{and} \quad \lambda_{\nu+1}\,(= \mu_{\kappa+2}) = 6.$

The permutation matrices relating

$$\bar{\mathbf{y}}(N - \mu_{\kappa+1}) = \bar{\mathbf{y}}(2) = \begin{bmatrix} y_2(2) & y_1(0) & y_2(0) & y_2(-2) \end{bmatrix}' \tag{5.66a}$$

and

$$\bar{\mathbf{u}}(N - \lambda_{\nu+1}) = \bar{\mathbf{u}}(0) = \begin{bmatrix} u(0) & u(-3) \end{bmatrix}' \tag{5.66b}$$

to, respectively, $\bar{\mathbf{y}}(0)$ and $\bar{\mathbf{u}}(0)$, are

$$\mathbf{P}_y^{(N-\mu_{\kappa+1})}(q^{-1}) = \begin{bmatrix} 0 & 1 & 0 & 0 \\ 0 & 0 & 1 & 0 \\ 0 & 0 & 0 & 1 \\ q^{-1} & 0 & 0 & 0 \end{bmatrix} \left(= \mathbf{P}_4^{(1)}(q^{-1})\right) \quad \text{and} \quad \mathbf{P}_u^{(N-\lambda_{\nu+1})}(q^{-1}) = \mathbf{I}_2,$$

whence, with the subscript $\nu = 1$, the matrices in equations (5.43a,b) are:

$$\mathbf{A}_1(q^{-1}) = \mathbf{A}_1^{(0)} + \mathbf{A}_1^{(1)} q^{-1}, \tag{5.67}$$

in which $\mathbf{A}_1^{(0)} = \begin{bmatrix} 1 & 0 & -\bar{a}^2 & 0 \\ 0 & 1 & 0 & 0 \\ 0 & 0 & 1 & -\bar{a}^2 \\ 0 & 0 & 0 & 1 \end{bmatrix}$ and $\mathbf{A}_1^{(1)} = \begin{bmatrix} 0 & 0 & 0 & 0 \\ 0 & -a^6 & 0 & 0 \\ 0 & 0 & 0 & 0 \\ -\bar{a}^2 & 0 & 0 & 0 \end{bmatrix}$,

with $\mathbf{C}_1(q^{-1})$ specified likewise, and

$$\mathbf{B}_1(q^{-1}) = \mathbf{B}_1^{(0)} + \mathbf{B}_1^{(1)} q^{-1}. \tag{5.68}$$

where $\mathbf{B}_1^{(0)} = \begin{bmatrix} (1+\bar{a})b_2 & 0 \\ 0 & (1+a+a^2)b_1 \\ 0 & (1+\bar{a})b_2 \\ 0 & b_2 \end{bmatrix}$ and $\mathbf{B}_1^{(1)} = \begin{bmatrix} 0 & 0 \\ (a^3+a^4+a^5)b_1 & 0 \\ 0 & 0 \\ \bar{a}b_2 & 0 \end{bmatrix}$.

The vectors $\check{\mathbf{y}}_1$ and $\check{\mathbf{u}}_1$ are (see (5.44a,b))

$$\check{\mathbf{y}}_1 = \begin{bmatrix} \bar{\mathbf{y}}'(14) & \bar{\mathbf{y}}'(8) & \bar{\mathbf{y}}'(2) \end{bmatrix}' \quad \text{and} \quad \check{\mathbf{u}}_1 = \begin{bmatrix} \bar{\mathbf{u}}'(12) & \bar{\mathbf{u}}'(6) & \bar{\mathbf{u}}'(0) \end{bmatrix}',$$

whereas the matrices $\check{\mathbf{A}}_1$ and $\mathbf{A}_1^\dagger$ (and $\check{\mathbf{C}}_1$ and $\mathbf{C}_1^\dagger$) are arranged in accordance with, respectively, $\check{\mathbf{A}}_0$ and $\mathbf{A}_0^\dagger$. In this instance, the matrices $\check{\mathbf{B}}_1$ and $\mathbf{B}_1^\dagger$ also are organised similarly to, respectively, $\check{\mathbf{A}}_0$ and $\mathbf{A}_0^\dagger$.

Numerical Example

Using identical values as in section 5.2, namely,

$$a_1 = a = 0.9615, \quad b_1 = 0.0385, \quad a_2 = \bar{a} = 1.04 \quad \text{and} \quad b_2 = 0.04,$$

the last rows of equation (5.48), obtained by minimising J_ν, $\nu = 0, 1$, for weighting matrices

$$\mathbf{\Lambda}_0 = 0.0375\mathbf{I}_6 \quad \text{and} \quad \mathbf{\Lambda}_1 = 0.375\mathbf{I}_6,$$

with respect to the 3 repetitive time intervals-ahead representation of equation (5.46), yields the following control laws (see (5.49)):

$$R_0(q_6^{-1})u(0) = -\mathbf{s}'_{y_0}(q^{-1})\bar{\mathbf{y}}(0) + \mathbf{s}'_{\epsilon_0}(q^{-1})\bar{\boldsymbol{\epsilon}}(0), \tag{5.69a}$$

with

$$R_0(q_6^{-1}) = 1,$$

$$\mathbf{s}_{y_0}(q^{-1}) = \begin{bmatrix} -0.1020 & 5.3888 & 0 & 0 \end{bmatrix}'$$

and

$$\mathbf{s}_{\epsilon_0}(q^{-1}) = \begin{bmatrix} -0.0624 & 3.6185 & 0 & 0 \end{bmatrix}',$$

and

$$R_1(q_6^{-1})u(-3) = -\mathbf{s}'_{y_1}(q^{-1})\bar{\mathbf{y}}(-4) + \mathbf{s}'_{\epsilon_1}(q^{-1})\bar{\boldsymbol{\epsilon}}(-4), \tag{5.69b}$$

with

$$R_1(q_6^{-1}) = 1 + 0.1212q_6^{-3},$$

$$\mathbf{s}_{y_1}(q^{-1}) = \begin{bmatrix} 2.4359 & 0.2203 & 0 & 0 \end{bmatrix}'$$

and

$$\mathbf{s}_{\epsilon_1}(q^{-1}) = \begin{bmatrix} 1.6357 & 0.1349 & 0 & 0 \end{bmatrix}'.$$

Eliminating the terms dependent upon the white noise sources via the combination of equations (5.69a,b) with the open-loop model and evaluation of the left-matrix fraction in equation (5.51), the predictive controller is specified by (see (5.52))

$$\mathbf{R}_o = \begin{bmatrix} 1 - 0.1272q^{-1} & 0.4339 \\ 0.3271q^{-1} & 1 - 0.2927q^{-1} \end{bmatrix}$$

and $$\mathbf{S}_o = \begin{bmatrix} -0.0396 & 1.7703 & 1.2857 & 0.9662 \\ 0.0826q^{-1} & 0.7093q^{-1} & 0.5152q^{-1} & 0.8002 \end{bmatrix}.$$

Scaling the entries within the corresponding polynomial matrices in the LQG regulator derived in section 5.2 such that the diagonal entries in $\mathbf{R}_o(0)$ are 1, whence

$$\mathbf{R}_{o_{LQG}}(q^{-1}) = \begin{bmatrix} 1 - 0.2074q^{-1} & 0.3640 \\ 0.5136q^{-1} & 1 - 0.1599q^{-1} \end{bmatrix}'$$

and $$\mathbf{S}_{o_{LQG}}(q^{-1}) = \begin{bmatrix} -0.0686 & 1.3160 & 1.0036 & 0.8189 \\ 0.0512q^{-1} & 1.1577q^{-1} & 0.8408q^{-1} & 1.4182 \end{bmatrix}',$$

it will be observed that the predictive controller bears a marked resemblance, both in terms of its structure and numerical values. The latter aspect is confirmed by noting that the phase margin is

$$PM = 48.4389^\circ \ \text{(cf. } 48.4214^\circ),$$

and that the gain margins are

$$GM_u = +15.0200\text{dB} \ \text{(cf. } +16.4479\text{dB)} \quad \text{and} \quad GM_l = -8.1083\text{dB} \ \text{(cf. } -8.3904\text{dB)}.$$

While the choice of the parameters determining $\mathbf{\Lambda}_0$ and $\mathbf{\Lambda}_1$ in the above example engender satisfactory results, in general it is by no means clear how appropriate weighting matrices $\mathbf{\Lambda}_\nu$ should be selected. Accordingly, this topic constitutes a possible future research area.

5.5 Enhancement of Design Methods

The optimal and predictive control design approaches described earlier in this chapter may prove to be somewhat restrictive in certain practical applications without modification. Of particular significance in this respect is the desirability of introducing integral action within the multirate-sampled controller to ensure the asymptotic tracking of step changes in reference signals and the possible incorporation of dynamic weighting within performance indices as a means of producing satisfactory stability robustness. Whilst addressing both these issues, this section additionally outlines the possible extension of the foregoing design methods to encompass the "tracking" and "feedforward" problems.

Integral Action

The incorporation of integral action within the controller is facilitated by assuming that the disturbance signal is drifting, thereby necessitating the use of an ARIMAX (Auto-Regressive Integrated-Moving Average-eXtended) system representation. Given that this artifice is rarely justifiable from a physical perspective, the term "optimal controller" may constitute a misnomer and LQG control theory then represents a design aid rather than a genuine synthesis technique in this context. The following analysis details the procedure involved in the MIMO case, whilst the general SISO, FOS and FIS cases are dealt with in the sequel.

In the MIMO scenario, it is supposed that the fast-rate discretised system model is described by the ARIMAX representation

$$\boldsymbol{y}(z_N) = z_N^{-d}\boldsymbol{A}^{-1}(z_N^{-1})\boldsymbol{B}(z_N^{-1})\bar{\boldsymbol{u}}(z_N) + \boldsymbol{D}^{-1}(z_N^{-1})\boldsymbol{A}^{-1}(z_N^{-1})\tilde{\boldsymbol{C}}(z_N^{-1})\boldsymbol{e}(z_N), \tag{5.70}$$

where $$\boldsymbol{D}(z_N^{-1}) = \left(1 - z_N^{-1}\right)\mathbf{I}_M.$$

Disregarding the disturbance subsystem for the present, pre-multiplication of equation (5.70) by $\boldsymbol{D}(z_N^{-1})$ and utilisation of the procedure summarised by equations (4.7), (4.8), (4.9) and (4.10) yields the model:

$$\begin{aligned}\hat{\mathbf{A}}_\Delta(q^{-1})\hat{\mathbf{y}}(0) &= \hat{\boldsymbol{\Delta}}_m(q^{-1})\hat{\mathbf{B}}(q^{-1})\hat{\mathbf{P}}_l^{(d)}(q^{-1})\hat{\mathbf{H}}(q^{-1})\tilde{\mathbf{u}}(0)\\ &= \hat{\mathbf{B}}(q^{-1})\hat{\mathbf{P}}_l^{(d)}\hat{\boldsymbol{\Delta}}_l(q^{-1})\hat{\mathbf{H}}(q^{-1})\tilde{\mathbf{u}}(0),\end{aligned} \tag{5.71}$$

where the $kN|kN$ matrix $\hat{\boldsymbol{\Delta}}_k(q^{-1})$ is designated generically as

$$\hat{\boldsymbol{\Delta}}_k(q^{-1}) = \text{block diag}\left(\boldsymbol{\Delta}_N(q^{-1}), \boldsymbol{\Delta}_N(q^{-1}), \ \ldots\ , \ \boldsymbol{\Delta}_N(q^{-1})\right),$$

with $$\boldsymbol{\Delta}_K(q^{-1}) = \mathbf{I}_K - \mathbf{P}_K^{(1)}(q^{-1}),$$

and $$\hat{\mathbf{A}}_\Delta(q^{-1}) = \hat{\boldsymbol{\Delta}}_m(q^{-1})\hat{\mathbf{A}}(q^{-1}).$$

Before proceeding further, it is necessary to introduce the following result related to the $\mathbf{W}_K$ matrices (see (3.33)):

$$\boldsymbol{\Delta}_N(q^{-1})\mathbf{W}_K = \mathbf{W}_K^\dagger\boldsymbol{\Delta}_K(q^{-1}), \tag{5.72}$$

where, with $K\bar{K} = N$,

$$\mathbf{W}_K^\dagger = \text{block diag}\left(\mathbf{w}_{\bar{K}}^\dagger, \mathbf{w}_{\bar{K}}^\dagger, \ \ldots\ , \ \mathbf{w}_{\bar{K}}^\dagger\right).$$

in which $$\mathbf{w}_{\bar{K}}^{\dagger} = \begin{bmatrix} 0 & \dots & 0 & 1 \end{bmatrix}' \quad (\in \mathbb{R}^{\bar{K}}).$$

Consequently, it can be established from equations (4.8) and (4.9) that

$$\hat{\mathbf{\Delta}}_l(q^{-1})\hat{\mathbf{H}}(q^{-1}) = \hat{\mathbf{H}}_\Delta(q^{-1})\hat{\mathbf{\Delta}}_H(q^{-1}), \tag{5.73}$$

where $$\hat{\mathbf{H}}_\Delta = \text{block diag}\left(\mathbf{P}_N^{(\bar{L}_1-1)}\mathbf{W}_{L_1}^{\dagger}, \mathbf{P}_N^{(\bar{L}_2-1)}\mathbf{W}_{L_2}^{\dagger}, \dots, \mathbf{P}_N^{(\bar{L}_l-1)}\mathbf{W}_{L_l}^{\dagger}\right)$$

and $$\hat{\mathbf{\Delta}}_H = \text{block diag}\left(\mathbf{\Delta}_{L_1}, \mathbf{\Delta}_{L_2}, \dots, \mathbf{\Delta}_{L_l}\right)$$

Specifying the derivative of each control thus:

$$\begin{aligned} u_{\Delta_j}(-l_j\bar{L}_j) &= \left(1 - q_{L_j}^{-1}\right) u_j(-l_j\bar{L}_j) \\ &= u_j(-l_j\bar{L}_j) - u_j(-(l_j+1)\bar{L}_j), \quad l_j = 0, 1, \dots, L_j - 1, \quad j = 1, 2, \dots, l, \end{aligned}$$

then, exploiting the theory developed in Chapter 3, the vector $\tilde{\mathbf{u}}_\Delta(0)$ comprising the control derivatives specified throughout the repetitive time interval is, using the definitions of $\hat{\mathbf{\Delta}}_H$ and $\mathbf{\Delta}_K$ in equations (5.73) and (5.71), respectively, given by

$$\tilde{\mathbf{u}}_\Delta(0) = \hat{\mathbf{\Delta}}_H(q^{-1})\tilde{\mathbf{u}}(0). \tag{5.74}$$

Invoking equations (5.73) and (5.74) and re-instating the disturbance signal, the lifted representation relating the fast-sampled outputs to the slow-sampled controls and fast-sampled white-noise sources is

$$\hat{\mathbf{A}}_\Delta(q^{-1})\hat{\mathbf{y}}(0) = \hat{\mathbf{B}}_{H_\Delta}(q^{-1})\tilde{\mathbf{u}}_\Delta(0) + \hat{\mathbf{C}}(q^{-1})\hat{\mathbf{e}}(0), \tag{5.75}$$

where $$\hat{\mathbf{B}}_{H_\Delta} = \hat{\mathbf{B}}\hat{\mathbf{P}}_l^{(d)}\hat{\mathbf{H}}_\Delta.$$

The overall lifted representation then is given by

$$\tilde{\mathbf{A}}_\Delta(q^{-1})\tilde{\mathbf{y}}(0) = \tilde{\mathbf{B}}_\Delta(q^{-1})\tilde{\mathbf{u}}_\Delta(0) + \tilde{\mathbf{C}}_\Delta(q^{-1})\tilde{\boldsymbol{\epsilon}}(0), \tag{5.76}$$

where $(\tilde{\mathbf{A}}_\Delta, \tilde{\mathbf{B}}_\Delta)$ are obtained from $(\hat{\mathbf{A}}_\Delta, \hat{\mathbf{B}}_{H_\Delta})$ by following the method summarised by equations (4.11), (4.12) and (4.13), whereas $\tilde{\mathbf{C}}_\Delta\tilde{\boldsymbol{\epsilon}}$ is acquired from $\hat{\mathbf{A}}_\Delta$ and $\hat{\mathbf{C}}\hat{\mathbf{e}}$ via the technique detailed in section 4.3.

Bearing in mind that the matrix $\mathbf{C}_{M_\Delta}$ and polynomial γ_Δ arise from equation (3.63) in which the following substitutions are made:

(SISO) $$A_K(z_K^{-1}) \longleftarrow \left(1 - z_M^{-1}\right) A_M(z_M^{-1})$$

Table 5.3. Lifted ARIMAX models: scalar case.

	$\tilde{\mathbf{A}}_\Delta$	$\tilde{\mathbf{B}}_\Delta$	$\tilde{\mathbf{C}}_\Delta$
SISO	$\boldsymbol{\Delta}_M \mathbf{A}_M$	$\mathbf{V}_M \bar{\boldsymbol{\Delta}}_N^{(M)} \bar{\mathbf{A}}_N^{(M)} \mathbf{B}_N \mathbf{P}_N^{(M+d-1)} \mathbf{W}_L^\dagger$	$\mathbf{C}_{M_\Delta}$
FOS	$\boldsymbol{\Delta}_N \mathbf{A}_N$	$\mathbf{B}_N \mathbf{P}_N^{(N+d-1)} \mathbf{w}_N^\dagger$	$\mathbf{C}_N$
FIS	$\left(1 - z^{-1}\right) \alpha$	$\mathbf{v}'_N \bar{\boldsymbol{\Delta}}_N^{(N)} \bar{\mathbf{A}}_N^{(N)} \mathbf{B}_N \mathbf{P}_N^{(d)}$	γ_Δ

$$\bar{A}^{(K)}(z_N^{-1}) \longleftarrow \left(1 + z_N^{-1} + \ldots + z_N^{-L+1}\right) \bar{A}^{(M)}(z_N^{-1}) \quad \text{(see (3.17))};$$

(FIS)
$$A_K(z_K^{-1}) \longleftarrow \left(1 - z^{-1}\right) \alpha(z^{-1})$$

$$\bar{A}^{(K)}(z_N^{-1}) \longleftarrow \left(1 + z_N^{-1} + \ldots + z_N^{-N+1}\right) \bar{A}^{(N)}(z_N^{-1}) \quad \text{(see (3.17))},$$

the terms $\tilde{\mathbf{A}}_\Delta$, $\tilde{\mathbf{B}}_\Delta$ and $\tilde{\mathbf{C}}_\Delta$ in the general SISO, FOS and FIS cases are given in Table 5.3.

Dynamic Weighting

In order to improve stability robustness or as a means of meeting performance criteria, is often necessary to incorporate dynamic weighting within the cost function. It is proposed to demonstrate how this may be accomplished in multirate-sampled configurations by focusing solely upon the MIMO LQG problem, in which the performance index, given originally by equation (5.1), now is defined thus:

$$J = E\left\{\boldsymbol{\eta}'(0)\boldsymbol{\eta}(0)\right\}, \quad \boldsymbol{\eta}(0) = \begin{bmatrix} \boldsymbol{\Omega}(q^{-1})\bar{\mathbf{y}}(0) \\ \boldsymbol{\Upsilon}(q^{-1})\bar{\mathbf{u}}(0) \end{bmatrix}. \tag{5.77}$$

With the matrix $\mathbf{D}$ specified to be the stable solution of (cf. (5.3))

$$\mathbf{D}^\star\mathbf{D} = \mathbf{A}_b^\star \boldsymbol{\Upsilon}^\star \boldsymbol{\Upsilon} \mathbf{A}_b + \mathbf{B}_a^\star \boldsymbol{\Omega}^\star \boldsymbol{\Omega} \mathbf{B}_a, \tag{5.78}$$

the optimal controller is, as beforehand, acquired from equation (5.5), where ($\mathbf{R}_{md}$, $\mathbf{S}_{md}$, $\boldsymbol{\Lambda}_{md}^\star$) represents the minimum degree solution of the diophantine equations

$$\mathbf{A}_b^\star \boldsymbol{\Upsilon}^\star \boldsymbol{\Upsilon} \mathbf{C}_b + \boldsymbol{\Lambda}^\star \mathbf{B}_c = \mathbf{D}^\star \mathbf{R} \tag{5.79}$$

$$\mathbf{B}_a^\star \boldsymbol{\Omega}^\star \boldsymbol{\Omega} \mathbf{C}_a - \boldsymbol{\Lambda}^\star \mathbf{A}_c = \mathbf{D}^\star \mathbf{S}. \tag{5.80}$$

The matrices $\boldsymbol{\Omega}$ and $\boldsymbol{\Upsilon}$ may de derived from corresponding entities defined with respect to the short time interval. For example, by analogy with the procedure used to engender

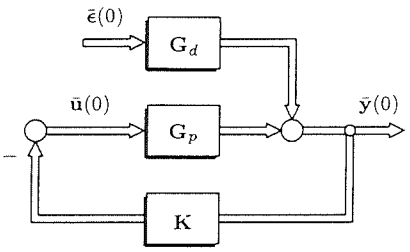

Figure 5.2. The regulator problem.

$\mathbf{A}(q^{-1})$ ((4.34)) from $\boldsymbol{A}(z_N^{-1})$ ((4.6)) (see (4.7) ($\hat{\mathbf{A}}$), (4.12) ($\mathbf{A}_r$) and (4.14) ($\tilde{\mathbf{A}}$)), the specification of an appropriate $\boldsymbol{W}(z_N^{-1})$ will result in the weighting matrix $\boldsymbol{\Omega}(q^{-1})$. The use of a similar approach will yield $\boldsymbol{\Upsilon}(q^{-1})$ from some $\boldsymbol{V}(z_N^{-1})$, although in this instance each of the complementary operations is governed by the arrangement of signals within the vectors $\hat{\mathbf{u}}(0)$ ((4.7)), $\tilde{\mathbf{u}}(0)$ ((4.9)) and $\bar{\mathbf{u}}(0)$ ((4.34)).

Alternative Control Problems

Thus far, this thesis has been concerned solely with the regulator problem encapsulated by the block diagram model of Figure 5.2. Nonetheless, there are many instances in which more sophisticated methods are required to model and control system satisfactorily. Consequently, focusing on the MIMO LQG approach throughout and eschewing detailed solutions, the following analysis outlines alternative control problems which may be addressed using the methods developed hitherto.

It can be readily shown that the regulator problem subsumes instances in which a feedback system is driven by two or more exogenous disturbances. In this respect, consider the discretised plant/disturbance subsystem model

$$\boldsymbol{y}(z_N) = \mathbf{G}_{p_N}(z_N)\bar{\boldsymbol{u}}(z_N) + \mathbf{G}_{\nu_N}(z_N)\boldsymbol{\nu}(z_N), \quad \boldsymbol{y}, \boldsymbol{\nu} \in \mathbb{C}^m, \quad \bar{\boldsymbol{u}} \in \mathbb{C}^l, \tag{5.81}$$

in which $\mathbf{G}_{p_N}(z_N) = z_N^{-d}\boldsymbol{A}_p^{-1}(z_N^{-1})\boldsymbol{B}_p(z_N^{-1})$ and $\mathbf{G}_{\nu_N}(z_N) = \boldsymbol{A}_\nu^{-1}(z_N^{-1})\boldsymbol{E}_\nu(z_N^{-1})$.

It is supposed additionally that the input to the digital controller is the system error signal $\boldsymbol{e}(z_N)$, defined thus:

$$\boldsymbol{e}(z_N) = \boldsymbol{r}(z_N) - \boldsymbol{y}(z_N) - \boldsymbol{\mu}(z_N), \quad \boldsymbol{e}, \boldsymbol{r}, \boldsymbol{\mu} \in \mathbb{C}^m, \tag{5.82}$$

where $\boldsymbol{r}(z_N) = \mathbf{G}_{\zeta_N}(z_N)\boldsymbol{\zeta}(z_N), \quad \boldsymbol{\zeta} \in \mathbb{C}^m, \quad$ with $\quad \mathbf{G}_{\zeta_N}(z_N) = \boldsymbol{A}_\zeta^{-1}(z_N^{-1})\boldsymbol{F}_\zeta(z_N^{-1})$.

and in which $\boldsymbol{\mu}(z_N)$ and $\boldsymbol{r}(z_N)$ represent, respectively, measurement noise and the reference signal. Notice that, with a slight abuse of notation, $\boldsymbol{\nu}(z_N)$, $\boldsymbol{\mu}(z_N)$ and $\boldsymbol{\zeta}(z_N)$ denote m weakly stationary discrete-time white signals with zero mean. Defining

$$\begin{aligned}\left[\begin{array}{ccc} \mathbf{G}_{p_N}(z_N) & \mathbf{G}_{\nu_N}(z_N) & \mathbf{G}_{\zeta_N}(z_N) \end{array}\right] &= \left[\begin{array}{ccc} z_N^{-d}\boldsymbol{A}_p^{-1}\boldsymbol{B}_p & \boldsymbol{A}_\nu^{-1}\boldsymbol{E}_\nu & \boldsymbol{A}_\zeta^{-1}\boldsymbol{F}_\zeta \end{array}\right] \\ &= \boldsymbol{A}^{-1}\left[\begin{array}{ccc} z_N^{-d}\boldsymbol{B} & \boldsymbol{E} & \boldsymbol{F} \end{array}\right], \end{aligned} \tag{5.83}$$

where it is supposed that each of the subsystems $\mathbf{G}_{p_N}$, $\mathbf{G}_{\nu_N}$ and $\mathbf{G}_{\zeta_N}$ is free of unstable hidden models, the matrix $\tilde{\boldsymbol{C}}(z_N^{-1})$ is deemed to represent the stable solution of

$$\tilde{\boldsymbol{C}}^\star\tilde{\boldsymbol{C}} = \boldsymbol{A}^\star\boldsymbol{\Sigma}_\mu\boldsymbol{A} + \boldsymbol{E}\boldsymbol{\Sigma}_\nu\boldsymbol{E}^\star + \boldsymbol{F}\boldsymbol{\Sigma}_\zeta\boldsymbol{F}^\star, \tag{5.84}$$

in which the diagonal $m|m$ matrices $\boldsymbol{\Sigma}_\mu$, $\boldsymbol{\Sigma}_\nu$ and $\boldsymbol{\Sigma}_\zeta$ represent the power spectral densities of the white noise sources.

Using the techniques detailed in section 4.1 and 4.2 to acquire, respectively, the plant model $\mathbf{G}_p$ and the lifted MA process $\mathbf{C}(q^{-1})\bar{\mathbf{e}}(0)$, the system defined above can be modelled thus:

$$\bar{\mathbf{e}}(0) = -\mathbf{G}_p(q^{-1})\bar{\mathbf{u}}(0) + \mathbf{G}_d(q^{-1})\bar{\boldsymbol{\epsilon}}(0), \tag{5.85}$$

in which $\mathbf{G}_p(q^{-1}) = \mathbf{A}^{-1}(q^{-1})\mathbf{B}(q^{-1})$ and $\mathbf{G}_d(q^{-1}) = \mathbf{A}^{-1}(q^{-1})\mathbf{C}(q^{-1})$.

The comparison of equation (5.85) with equation (4.35) indicates that minimisation of the performance index (cf. (5.77))

$$J = E\left\{\boldsymbol{\eta}'(0)\boldsymbol{\eta}(0)\right\}, \quad \boldsymbol{\eta}(0) = \left[\begin{array}{c} \boldsymbol{\Omega}(q^{-1})\bar{\mathbf{e}}(0) \\ \boldsymbol{\Upsilon}(q^{-1})\bar{\mathbf{u}}(0) \end{array}\right], \tag{5.86}$$

will engender the optimal controller specified by the diophantine equations (5.79) and (5.80) and the matrix fraction conversion of equation (5.5). The equivalent closed-loop configuration therefore may be depicted as the block diagram model of Figure 5.3, in which it will be observed that the controller $\mathbf{K}(q^{-1})$ appears in the forward path.

The "tracking" problem – namely, the requirement that the output $\bar{\mathbf{y}}$ follows a stochastic reference $\bar{\mathbf{r}}$ as closely as possible in the presence of other random disturbances – is addressed more commonly by the "two degrees-of-freedom" controller structure schematically represented for the multirate MIMO case in Figure 5.4. Šebek (1983) demonstrated

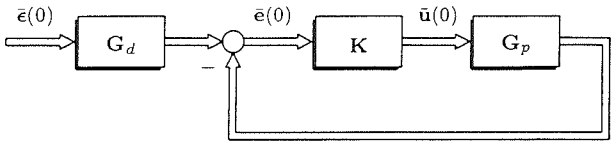

Figure 5.3. Equivalent closed-loop configuration.

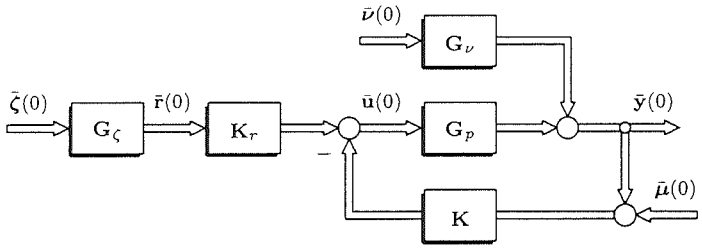

Figure 5.4. The tracking problem.

that the polynomial solution of the minimisation of

$$J = E\left\{\eta'(0)\eta(0)\right\}, \quad \eta(0) = \begin{bmatrix} \Omega(q^{-1})\left(\bar{r}(0) - \bar{y}(0)\right) \\ \Upsilon(q^{-1})\bar{u}(0) \end{bmatrix} \tag{5.87}$$

for the plant and disturbance signals defined above produced the control law

$$\bar{u}(0) = -\mathbf{K}(q^{-1})\left(\bar{y}(0) + \bar{\mu}(0)\right) + \mathbf{K}_r(q^{-1})\bar{r}(0), \tag{5.88}$$

where $\mathbf{K}(q^{-1})$ represents the "regulator solution" obtained previously and, specified via a further diophantine equation, in which $\mathbf{K}_r(q^{-1})$ denotes the "reference controller".

The second major extension to the regulator problem was the derivation by Hunt and Šebek (1989) of a solution to the "feedforward" problem, in which a separate feedforward compensator effected the rejection of a measurable disturbance. Depicted schematically in Figure 5.5, the vectors $\bar{\mathbf{m}}$ and $\bar{\mathbf{n}}$ denote the measurable and unmeasurable disturbances generated by applying the white noise source $\bar{\omega}$ to the blocks labelled $\mathbf{G}_m$ and $\mathbf{G}_n$, whereas $\mathbf{K}_f$ denotes the feedforward controller. The LQG control law minimising the performance index of equation (5.77) then assumes the structure

$$\bar{u}(0) = -\mathbf{K}(q^{-1})\left(\bar{y}(0) + \bar{\mu}(0)\right) + \mathbf{K}_f(q^{-1})\bar{\mathbf{m}}(0). \tag{5.89}$$

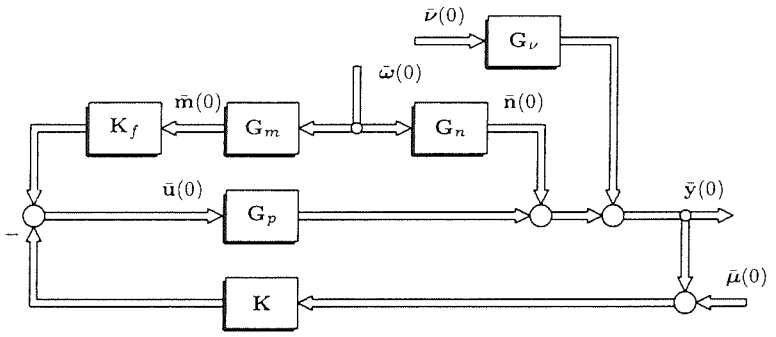

Figure 5.5. The feedforward problem.

Modified Predictive Control Solution

The approach utilised in section 5.3 to synthesise multirate-sampled predictive control laws for the regulator problem can accommodate the modifications described in this section. The following analysis accordingly describes the procedure entailed in deriving a "two degrees-of-freedom" predictive controller that incorporates integral action.

The initial system model is acquired by invoking the permutation matrices $\mathbf{\Pi}_2$ and $\mathbf{\Pi}_3$ specified in equation (4.32), whence equation (5.76) may be written as

$$\mathbf{A}_\Delta(q^{-1})\bar{\mathbf{y}}(0) = \mathbf{B}_\Delta(q^{-1})\bar{\mathbf{u}}_\Delta(0) + \mathbf{C}_\Delta(q^{-1})\bar{\epsilon}(0). \tag{5.90}$$

Introducing the signals

$$\psi_i(-\iota) = \omega_i(q_N^{-1})\left(y_i(-\iota) - r_i(-\iota)\right), \quad i = 1, 2, \ldots, m,$$

in which it is assumed that each reference signal $r_i(-\iota)$ is known throughout the relevant predictive interval $t \in [-\mu_\kappa, pN - \mu_{\kappa+1}]$, then, using the methods detailed earlier in this section, the vector $\bar{\psi}$ can be defined thus:

$$\bar{\psi}(0) = \mathbf{\Omega}(q^{-1})\left(\bar{\mathbf{y}}(0) - \bar{\mathbf{r}}(0)\right). \tag{5.91}$$

The designation of the left-matrix fraction

$$\mathbf{A}_{\Delta\Omega}^{-1}(q^{-1})\mathbf{\Omega}_a(q^{-1}) = \mathbf{\Omega}(q^{-1})\mathbf{A}_\Delta^{-1}(q^{-1}) \tag{5.92}$$

consequently warrants the definition, from equations (5.90) and (5.91), of the following

model:

$$\mathbf{A}_{\Delta_\Omega}(q^{-1})\bar{\psi}(0) = \mathbf{\Omega}_a(q^{-1})\mathbf{B}_\Delta(q^{-1})\bar{\mathbf{u}}(0) + \mathbf{\Omega}_a(q^{-1})\mathbf{C}_\Delta(q^{-1})\bar{\epsilon}(0) - \mathbf{A}_{\Delta_\Omega}(q^{-1})\mathbf{\Omega}(q^{-1})\bar{\mathbf{r}}(0). \tag{5.93}$$

For concision, using the symbols $\mathbf{A}$, $\mathbf{B}$, $\mathbf{C}$ and $\mathbf{D}$ to signify entities related to $\mathbf{A}_{\Delta_\Omega}$, $\mathbf{\Omega}_a\mathbf{B}_\Delta$, $\mathbf{\Omega}_a\mathbf{C}_\Delta$ and $\mathbf{A}_{\Delta_\Omega}\mathbf{\Omega}$, respectively, the resultant p repetitive time intervals-ahead representation (cf. (5.46)) is

$$\check{\psi}_\nu = \mathbf{\Gamma}_\nu \check{\mathbf{u}}_{\Delta_\nu} + \mathbf{f}_{1_\nu}(q^{-1}) - \mathbf{f}_{2_\nu}(q^{-1}) + \check{\mathbf{A}}_\nu^{-1}\check{\mathbf{C}}_\nu \boldsymbol{\epsilon}_\nu, \tag{5.94}$$

where

$$\mathbf{f}_{1_\nu}(q^{-1}) = \check{\mathbf{A}}_\nu^{-1}\left(-\mathbf{A}_\nu^\dagger(q^{-1})\mathbf{\Omega}(q^{-1})\bar{\mathbf{y}}(-\mu_{\kappa+1}) + \mathbf{B}_\nu^\dagger(q^{-1})\bar{\mathbf{u}}_\Delta(-\lambda_{\nu+1}) + \mathbf{C}_\nu^\dagger(q^{-1})\bar{\epsilon}(-\mu_{\kappa+1})\right)$$

and $$\mathbf{f}_{2_\nu}(q^{-1}) = \check{\mathbf{A}}_\nu^{-1}\left(\check{\mathbf{D}}_\nu\check{\mathbf{r}}_\nu + \left(\mathbf{D}_\nu^\dagger(q^{-1}) - \mathbf{A}_\nu^\dagger(q^{-1})\mathbf{\Omega}(q^{-1})\right)\mathbf{r}_\nu(-\mu_{\kappa+1})\right).$$

Minimisation of the cost function of equation (5.46), in which $\check{\mathbf{y}}_\nu$ is replaced with $\check{\psi}_\nu$, consequently yields the optimal control sequence (see (5.48)) with respect to $t = -\lambda_\nu$ and ultimately, via equations (5.51) and (5.52), the overall predictive controller. Notice that, if it is assumed that each reference signal $r_i(\cdot)$ constitutes a unit step applied at $t \equiv -N$, it can be established readily that the vector $\mathbf{f}_{2_\nu}(q^{-1})$ in equation (5.96) may be described thus:

$$\mathbf{f}_{2_\nu}(q^{-1}) = q^{-1}\sum_{i=1}^{m}\boldsymbol{\xi}_{\nu_i}(q^{-1})r_i(0). \tag{5.95}$$

As a consequence, it is relatively straightforward to compute the optimal predictive control law

$$\mathbf{R}(q^{-1})\bar{\mathbf{u}}_\Delta(0) = -\mathbf{S}_y(q^{-1})\bar{\mathbf{y}}(0) + \mathbf{S}_\epsilon(q^{-1})\bar{\epsilon}(0) + q^{-1}\mathbf{S}_r(q^{-1})\bar{\mathbf{r}}(0). \tag{5.96}$$

Replacing $\mathbf{A}$, $\mathbf{B}$ and $\mathbf{C}$ in equations (5.51) and (5.52) with $\mathbf{A}_\Delta$, $\mathbf{B}_\Delta$ and $\mathbf{C}_\Delta$, respectively, the "two degrees-of-freedom" predictive controller is described by (cf. (5.88))

$$\bar{\mathbf{u}}_\Delta(0) = -\mathbf{R}_{\Delta_o}^{-1}(q^{-1})\mathbf{S}_o(q^{-1})\bar{\mathbf{y}}(0) + q^{-1}\mathbf{R}_{\Delta_o}^{-1}(q^{-1})\mathbf{S}_{r_o}(q^{-1})\bar{\mathbf{r}}(0), \tag{5.97}$$

where $$\mathbf{S}_{r_o}(q^{-1}) = \mathbf{C}_{s_\epsilon}(q^{-1})\mathbf{S}_r(q^{-1}).$$

5.6 Illustrative Examples – Enhancement of Design Methods

This section demonstrates how the aforementioned modifications to the optimal and predictive synthesis techniques impart flexibility to the control design process and identifies the effect certain multirate sampling schedules have on feedback system performance. Initially, LQG controllers are derived for system S1, where the primary design consideration concerns the generation of acceptable stability margins. Corresponding FOS and FIS LQG feedback systems are obtained and a comparison is made of the respective transient responses. In the second example, formulation of incremental models of the coupled-tanks system M2 warrants the design of multivariable LQG compensators possessing integrator terms.

Example S1

Numerical Values

It is assumed that the plant model is specified by the following parameters:

$$\tau = 3 \quad \text{(see (3.77))} \quad \text{and} \quad T = 0.5321\,\text{s},$$

whence (see (3.78)), $$a = 1.03,$$

while the disturbance subsystem (see (3.63)) is designated by the polynomial

$$\tilde{C}(z_6^{-1}) = 1 - 1.5z_6^{-1} + 0.75z_6^{-1}.$$

The overall multirate-sampled system then, from equations (3.83), (3.84) and (3.89), respectively, is defined by the matrices

$$\mathbf{A}_M(q^{-1}) = \begin{bmatrix} 1 & -2.0609 & 1.0609 \\ 1.0609q^{-1} & 1 & -2.0609 \\ -2.0609q^{-1} & 1.0609q^{-1} & 1 \end{bmatrix},$$

$$\mathbf{B}_l(q^{-1}) = \begin{bmatrix} 0.0014q^{-1} & 0.0094 \\ 0.0095q^{-1} & 0.0013 \\ 0.0053q^{-1} & 0.0055q^{-1} \end{bmatrix}$$

and $$\mathbf{C}_M(q^{-1}) = \begin{bmatrix} 1 & -0.9009 & 0.4466 \\ 0.4466q^{-1} & 1 & -0.9009 \\ -0.9009q^{-1} & 0.4466q^{-1} & 1 \end{bmatrix}.$$

LQG Controller Design

In the first design attempt, minimisation of the cost function of equation (5.1) for the SISO case (see Table 5.1) in which

$$\Xi = \mathbf{I}_2$$

yields the optimal controller $K_o(q^{-1})$, specified by the matrices (see (5.4))

$$\mathbf{R}_o(q^{-1}) = \begin{bmatrix} 1.1881 + 0.3538q^{-1} & -0.1729 \\ -0.1793q^{-1} & 1.1881 + 0.2233q^{-1} \end{bmatrix}$$

and $$\mathbf{S}_o(q^{-1}) = \begin{bmatrix} 14.2188 & -0.7406 & -12.1841 \\ -6.8955q^{-1} & -7.1062q^{-1} & 14.9745 \end{bmatrix}.$$

The remaining matrices entailed in the derivation of the LQG control solution, namely, $\mathbf{B}_a(q^{-1})$ and $\mathbf{A}_b(q^{-1})$ (i.e., $\mathbf{B}_r(q^{-1})$ and $\mathbf{A}_r(q^{-1})$ - see Table 5.1), $\mathbf{B}_c(q^{-1})$ and $\mathbf{C}_b(q^{-1})$ ((5.2)), $\mathbf{D}(q^{-1})$ ((5.3)), $\mathbf{C}_o(q^{-1})$ ((5.5)) and $\mathbf{R}_{md}(q^{-1})$, $\mathbf{S}_{md}(q^{-1})$ and $\mathbf{\Lambda}_{md}(q^{-1})$ ((5.6) and (5.7)) are listed in Appendix A.

The above controller produces "plant poles" (namely, the zeros of $z^2\det\left(\mathbf{D}(z^{-1})\right)$) at

$$z = 0.7548 \pm j0.1716,$$

corresponding to a damping factor ζ of 0.7533 and a natural frequency of resonance ω_n of 0.6389 rad/s. The poles related to the disturbance model (given by the zeros of $z^2\det\left(\mathbf{C}_x(z^{-1})\right)$, where $\mathbf{C}_x$ represents $\mathbf{C}$, $\mathbf{C}_a$ (i.e., $\mathbf{C}_M$), $\mathbf{C}_b$ or $\mathbf{C}_o$) are located at

$$z = -0.2380 \pm j0.1802,$$

with associated values of ζ and ω_n of 0.4363 and 5.2083 rad/s, respectively. It will be observed that the dominant closed-loop poles, specified with respect to the repetitive time interval of T s, conform to conventional sampling rate selection criteria and are located at positions in the z-plane which normally would be deemed acceptable in single-rate digital feedback systems with a sampling interval of T s. Bode plots of the characteristic gain

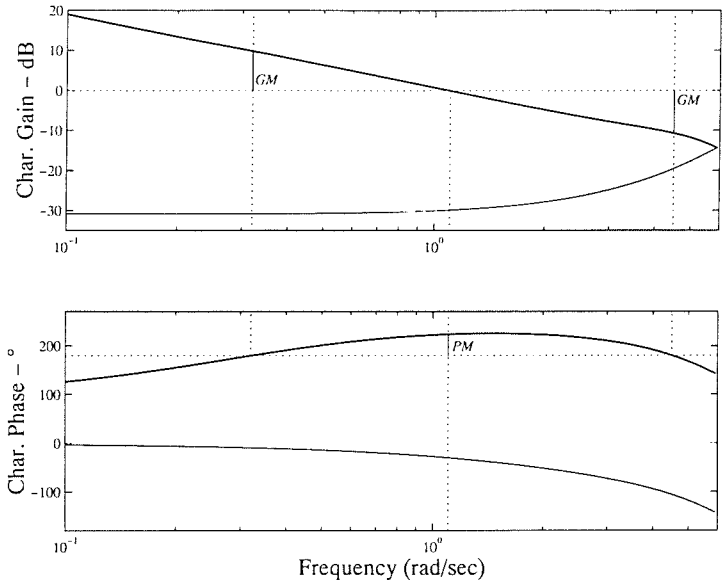

Figure 5.6. Bode plot of characteristic gain loci - system S1.

loci related to the return ratio $\mathbf{Q}_L(z)$ (See (4.51a)) provided in Figure 5.6 reveal that the margins of stability are

$$PM = 43.4273°,$$

$$GM_u = +10.7914\text{dB} \quad \text{and} \quad GM_l = -9.7223\text{dB}.$$

Striving to enhance relative stability, a second control design engendered by minimising J in equation (5.77), where

$$\mathbf{\Omega}(q^{-1}) = \mathbf{I}_3 - 0.95\mathbf{P}_3^{(1)}(q^{-1}) \quad \text{and} \quad \mathbf{\Psi}(q^{-1}) = 0.0125\mathbf{I}_2,$$

produces the LQG compensator specified by

$$\mathbf{R}_o(q^{-1}) = \begin{bmatrix} 0.1320 + 0.0396q^{-1} & -0.0212 \\ -0.0211q^{-1} & 0.1320 + 0.0247q^{-1} \end{bmatrix}$$

and

$$\mathbf{S}_o(q^{-1}) = \begin{bmatrix} 1.4797 & -0.1132 & -1.3021 \\ -0.7437q^{-1} & -0.7477q^{-1} & 1.5404 \end{bmatrix}.$$

Observing that the "disturbance subsystem poles" are invariant, the closed-loop "plant poles" are

$$z = 0.7043 \quad \text{and} \quad z = 0.8627.$$

with related values of ω_n of 0.6588 and 0.2776 rad/s, respectively. The stability margins in this instance are

$$PM = 49.7071^\circ,$$

$$GM_u = +11.3339\text{dB} \quad \text{and} \quad GM_l = -9.6271\text{dB}.$$

FOS and FIS LQG Designs

It is instructive to examine comparable control designs for FOS and FIS sampling schedules in which $N = 6$. In the former instance, minimisation of J in equation (5.1) with

$$\Xi = 4.$$

produces the control solution $(\rho(q^{-1}), \mathrm{s}'_o(q^{-1}))$, where

$$\rho(q^{-1}) = 2.8223 + 2.6392q^{-1} + 0.6111q^{-2}$$

and

$$\mathrm{s}_o(q^{-1}) = \begin{bmatrix} 27.3859 + 11.5534q^{-1} \\ 14.3053 + 6.0351q^{-1} \\ 0.9186 + 0.3875q^{-1} \\ -9.3512 - 3.9450q^{-1} \\ -14.7157 - 6.2082q^{-1} \\ -15.0601 - 6.3535q^{-1} \end{bmatrix}.$$

In the complementary FIS scenario, the term Ξ in equation (5.1) is given by

$$\Xi = 0.1\mathbf{I}_6,$$

and the resultant optimal controller $(\mathbf{R}(q^{-1}), \tilde{\mathrm{s}}(q^{-1}))$ is specified by

$$\mathbf{R}(q^{-1}) = \begin{bmatrix} 0.3353 & -0.4360 & 0.0448 & 0 & 0 & 0 \\ 0 & 0.3353 & -0.2800 & 0.3072 & 0 & 0 \\ 0 & 0 & 0.3353 & -0.6414 & 0.3072 & 0 \\ 0 & 0 & 0 & 0.3353 & -0.6414 & 0.3072 \\ 0.3072q^{-1} & 0 & 0 & 0 & 0.3353 & -0.6414 \\ -0.6414q^{-1} & 0.1486q^{-1} & 0 & 0 & 0 & 0.3353 \end{bmatrix}$$

Table 5.4. FOS and FIS feedback system designs.

	FOS	FIS
plant poles	$0.7550 \pm j0.1721$	$0.7490 \pm j0.1756$
disturbance subsystem poles	$-0.4219, -0.4219$	$-0.0741 \pm j0.2805$
PM	41.3363°	38.1075°
GM_u	12.2126dB	10.0154dB
GM_l	−9.4037dB	−9.1155dB

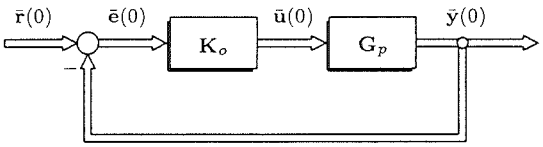

Figure 5.7. Insertion of LQG controller in forward path.

and
$$\tilde{\mathbf{s}}(q^{-1}) = \begin{bmatrix} 3.5053 - 3.0051q^{-1} \\ 4.4730q^{-1} - 3.9726q^{-2} \\ 4.2731q^{-1} - 3.7692q^{-2} \\ 4.0761q^{-1} - 3.5706q^{-2} \\ 3.8821q^{-1} - 3.3768q^{-2} \\ 3.6917q^{-1} - 3.1882q^{-2} \end{bmatrix}.$$

The "plant poles", the "disturbance subsystem poles" – namely, the zeros of $z^2 \det\left(\tilde{\mathbf{C}}(z_6^{-1})\right)$ (FOS) and $z^2\nu(z^{-1})$ (FIS) – and the respectively stability margins for the two configurations are listed in Table 5.4.

Bearing in mind that the above designs are only "optimal" with regard to a specific disturbance, it is useful to examine the transient response of the FOS and FIS feedback systems to deterministic inputs. Consequently, as illustrated in Figure 5.7, in each case the optimal controller is inserted in the forward path and unit step reference signals are applied.

The resultant responses of both the output and control signals for the FOS and FIS configurations are depicted in Figure 5.8 and 5.9, respectively. Although there is little

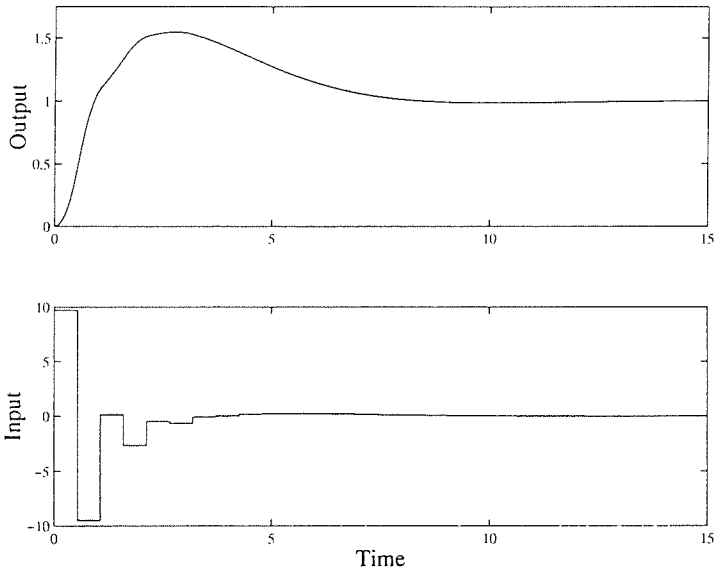

Figure 5.8. Transient response in FOS control system.

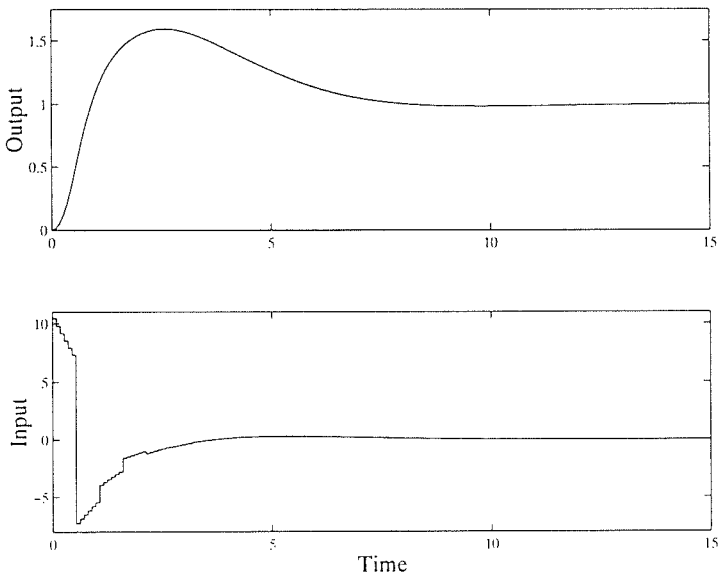

Figure 5.9. Transient response in FIS control system.

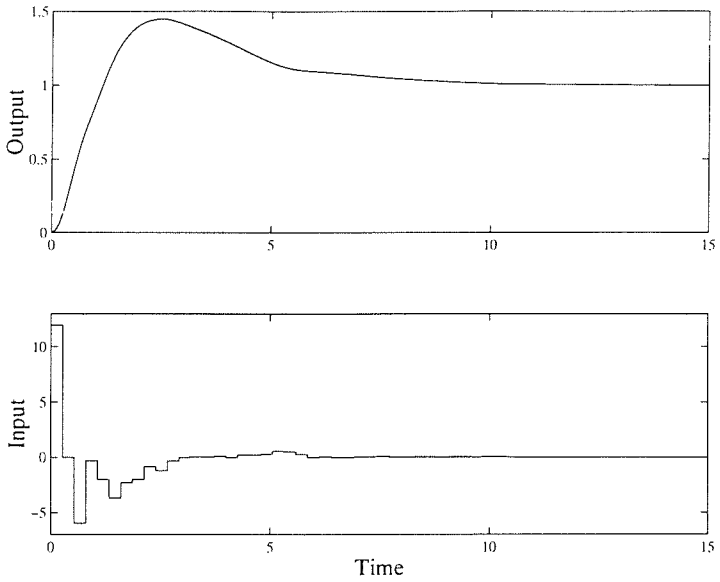

Figure 5.10. Transient response in general multirate control system.

discernible difference between the two sampling strategies in terms of the behaviour of the output signal, it is evident that control activity in the two cases differs markedly. In fact, it has been established by Truman and Govan (2000b,c), that the FOS scheme behaves similarly to conventional single-rate controllers implemented with sampling intervals of either T/N s or T s in terms of the transient behaviour of both the control and output signals.

For comparative purposes, the transient response of the general SISO system is shown in Figure 5.10. Notice that the overshoot exhibited in each of the output signals in Figure 5.8, 5.9 and 5.10 is caused by the phase lead introduced by the controller necessary to ensure closed-loop stability. This problem can be circumvented by implementing a "two degree-of-freedom" control law via the approach outlined in section 5.5.

Discussion

The nature of the control signal in the FIS scheme can be explained qualitatively by considering the first-order controller defined thus:

$$U_N(z_N) = K_N(z_N)E(z) \quad \text{(cf. (2.8) or (2.17))},$$

where

$$K_N(z_N) = \frac{s}{1 - rz_N^{-1}}, \quad r > 0.$$

The relationship between the incremental controls $u_\Delta(-\iota)$ – namely, $u(-\iota) - u(-\iota-1)$ (see (5.74)) – and the error signal $e(-\iota)$ during the repetitive time interval can be expressed thus:

$$\begin{aligned} u_\Delta(0) &= r u_\Delta(-1) + s\,(e(0) - e(-N))\,; \\ u_\Delta(\iota) &= r u_\Delta(-\iota - 1), \quad \iota \in [1, N-1]. \end{aligned} \tag{5.98}$$

Consideration of the magnitude of the control increments, namely, $|u_\Delta(-\iota)|$, $\iota \in [0, N-1]$, in equation (5.98) indicates that the control signal may exhibit a noticeable change at each "slow-rate" sampling instant kT s, following which, provided $r < 1$, it will tend to decay exponentially.

The FOS LQG control law is specified by the "implicit" pulse-transform/pulse-transfer function relationship

$$U(z) = Z\left\{K_N(z_N)E_N(z_N)\right\} \quad \text{(cf. (2.10) or (2.18) and (2.19))},$$

where, by comparison of the relevant entries in Table 5.1 and equations (4.43) and (4.50),

$$K_N(z_N) = \frac{S(z_N^{-1})\bar{\tilde{C}}^{(N)}(z_N^{-1})}{\rho(z^{-1})}. \tag{5.99}$$

The inherent anti-aliasing nature of the FOS optimal compensator may be demonstrated by considering the i^{th} factor of the polynomial $\bar{\tilde{C}}^{(N)}(z_N^{-1})$, namely, $\bar{\tilde{C}}_i^{(N)}(z_N^{-1})$, which, if $\tilde{C}_i(z_N^{-1}) = 1 - cz_N^{-1}$, is given by ((3.17))

$$\bar{\tilde{C}}_i^{(N)}(z_N^{-1}) = 1 + cz_N^{-1} + \ldots + c^{N-1}z_N^{-N+1}.$$

Thus, if c is real and close to unity, then $\bar{\tilde{C}}_i^{(N)}(z_N^{-1})$ will resemble the so-called "comb filter" characteristic of the discretised zero-order hold $H_N(z_N)$ (see (3.45)), namely,

$$H_N^{(N)}(z_N) = H^{(N)}(z_N^{-1}) = 1 + z_N^{-1} + \ldots + z_N^{-N+1}.$$

Consequently, if one or more zeros of $z_N^{n_c}\tilde{C}(z_N^{-1})$ lie in proximity to $(1,0)$ and N is sufficiently large (e.g., $N \geq 8$), $\bar{\tilde{C}}(z_N^{-1})$ will act as a low-pass FIR (finite impulse response) filter, significantly attenuating frequency components of the output signal $Y(e^{j\omega T/N})$ outside $\omega \in [0, \omega_s/2)$. As discussed by Truman and Govan (2000b,c), this low-pass characteristic suppresses high-frequency noise signals, albeit at the expense of introducing a certain degree of phase lag. Finally, it has been established by Truman and Govan (2000a) and Truman and Govan (2001) that the FOS predictive compensator shares this property.

Example M2

This example concerns the design of feedback systems for the coupled-tanks model M2. The design objectives simply require that there should be zero steady-state error to step changes in the reference signals and that the closed-loop poles should have natural frequencies of resonance in accordance with the sampling schedule deployed. The strategy adopted aims to yield relatively low-order controllers by presupposing that it is justifiable in this instance to simplify the disturbance subsystem model such that all "**C**'s" are, in fact, identity matrices, thereby resulting in the use of "ARIX" representations throughout. Initially, a lifted ARIX model is acquired, following which predictive and LQG compensators are derived when the sampling ratio N is 3. The LQG design then is repeated for a scenario in which N is increased to 8.

Lifted ARIX Model

The lifted time-domain representation of the discretised plant $\mathbf{G}_{p_N}(z_N)$ is given by equation (4.10), whence,

$$\hat{\mathbf{A}}(q^{-1})\hat{\mathbf{y}}(0) = \hat{\mathbf{B}}_H(q^{-1})\tilde{\mathbf{u}}(0), \tag{5.100}$$

where $$\hat{\mathbf{y}}(0) = \begin{bmatrix} \mathbf{y}_1'(0) & \mathbf{y}_2'(0) \end{bmatrix}',$$

$$\tilde{\mathbf{u}}(0) = \begin{bmatrix} u_1(0) & \mathbf{u}_2'(0) \end{bmatrix}' \left(= \begin{bmatrix} u_1(0) & u_2(0) & u_2(-1) & u_2(-2) \end{bmatrix}' \right),$$

$$\hat{\mathbf{A}}(q^{-1}) = \begin{bmatrix} \mathbf{I}_3 - a_1\mathbf{P}_3^{(1)} & -a_2\mathbf{I}_3 \\ -a_3\mathbf{P}_3^{(1)} & \mathbf{I}_3 - a_4\mathbf{P}_3^{(1)} \end{bmatrix} \quad \text{and} \quad \hat{\mathbf{B}}_H(q^{-1}) = \begin{bmatrix} b_1\mathbf{w}_3q^{-1} & -b_2\mathbf{P}_3^{(1)} \\ b_3\mathbf{w}_3q^{-1} & b_4\mathbf{P}_3^{(1)} \end{bmatrix}.$$

The pre-multiplication of $\hat{\mathbf{A}}(q^{-1})$ and $\hat{\mathbf{B}}_H(q^{-1})$ by $\hat{\mathbf{\Delta}}_2(q^{-1})$ ((5.71)) produces

$$\hat{\mathbf{A}}_\Delta(q^{-1})\hat{\mathbf{y}}(0) = \hat{\mathbf{B}}_{H_\Delta}(q^{-1})\tilde{\mathbf{u}}_\Delta(0), \tag{5.101}$$

where $$\hat{\mathbf{A}}_\Delta(q^{-1}) = \begin{bmatrix} \mathbf{I}_3 - (1+a_1)\mathbf{P}_3^{(1)} + a_3\mathbf{P}_3^{(2)} & -a_2\left(\mathbf{I}_3 - \mathbf{P}_3^{(1)}\right) \\ a_3\left(\mathbf{P}_3^{(1)} - \mathbf{P}_3^{(2)}\right) & \mathbf{I}_3 - (1+a_4)\mathbf{P}_3^{(1)} + a_4\mathbf{P}_3^{(2)} \end{bmatrix}$$

and $$\hat{\mathbf{B}}_{H_\Delta}(q^{-1}) = \begin{bmatrix} b_1\mathbf{w}_3^\dagger q^{-1} & -b_2\mathbf{P}_3^{(1)} \\ b_3\mathbf{w}_3^\dagger q^{-1} & b_4\mathbf{P}_3^{(1)} \end{bmatrix}.$$

The overall lifted ARIX model is obtained via the following procedure.

(i) The vector $\mathbf{y}_r(0)$ and permutation matrix $\mathbf{\Pi}_1$ are defined thus:

$$\mathbf{y}_r(0) = \mathbf{\Pi}_1 \hat{\mathbf{y}}(0), \quad \mathbf{y}_r(0) = \begin{bmatrix} \tilde{\mathbf{y}}'(0) & \mathbf{y}_e' \end{bmatrix}', \tag{(4.11)}$$

where

$$\tilde{\mathbf{y}}(0) = \begin{bmatrix} y_1(0) & y_2(0) & y_2(-1) & y_2(-2) \end{bmatrix}' \quad \text{and} \quad \mathbf{y}_e = \begin{bmatrix} y_1(-1) & y_1(-2) \end{bmatrix}';$$

(ii) the matrices $\mathbf{A}_{r_\Delta}$ and $\mathbf{B}_{r_\Delta}$ then are given by (see (4.12)):

$$\mathbf{A}_{r_\Delta} = \mathbf{\Pi}_1 \hat{\mathbf{A}}_\Delta \mathbf{\Pi}_1' = \begin{bmatrix} \mathbf{A}_1 & \mathbf{A}_2 \\ \mathbf{A}_3 & \mathbf{A}_4 \end{bmatrix} \quad \text{and} \quad \mathbf{B}_{r_\Delta} = \mathbf{\Pi}_1 \hat{\mathbf{B}}_{H_\Delta} = \begin{bmatrix} \mathbf{B}_1 \\ \mathbf{B}_2 \end{bmatrix},$$

where

$$\mathbf{A}_1 = \begin{bmatrix} 1 & -a_2 & a_2 & 0 \\ 0 & 1 & -(1+a_4) & a_4 \\ a_3 q^{-1} & a_4 q^{-1} & 1 & -(1+a_4) \\ -a_3 q^{-1} & -(1+a_4) q^{-1} & a_4 q^{-1} & 1 \end{bmatrix},$$

$$\mathbf{A}_2 = \begin{bmatrix} -(1+a_1) & a_1 \\ -a_3 & a_3 \\ 0 & -a_3 \\ a_3 q^{-1} & 0 \end{bmatrix},$$

$$\mathbf{A}_3 = \begin{bmatrix} a_1 q^{-1} & 0 & -a_2 & a_2 \\ -(1+a_1) q^{-1} & a_2 q^{-1} & 0 & -a_2 \end{bmatrix}, \quad \mathbf{A}_4 = \begin{bmatrix} 1 & -(1+a_1) \\ a_1 q^{-1} & 1 \end{bmatrix},$$

$$\mathbf{B}_1 = \begin{bmatrix} b_1 q^{-1} & 0 & -b_2 & 0 \\ b_3 q^{-1} & 0 & b_4 & 0 \\ b_3 q^{-1} & 0 & 0 & b_4 \\ b_3 q^{-1} & b_4 q^{-1} & 0 & 0 \end{bmatrix} \quad \text{and} \quad \mathbf{B}_2 = \begin{bmatrix} b_1 q^{-1} & 0 & 0 & -b_2 \\ b_1 q^{-1} & -b_2 q^{-1} & 0 & 0 \end{bmatrix};$$

(iii) inserting the values for the parameters a_i and b_i, $i = 1, 2, 3, 4$ given in section 4.5 and acquiring the left-matrix fraction $\mathbf{A}_{42}^{-1}\mathbf{A}_{24}$ (see (4.13)), the relevant model is given by (cf. (5.76))

$$\tilde{\mathbf{A}}_\Delta(q^{-1})\tilde{\mathbf{y}}(0) = \tilde{\mathbf{B}}_\Delta(q^{-1})\tilde{\mathbf{u}}_\Delta(0), \tag{5.102}$$

$$\text{where} \qquad \tilde{\mathbf{A}}_\Delta = \begin{bmatrix} 1-0.7320q^{-1} & -0.0552 & -0.0497 & -0.0448 \\ -0.1000q^{-1} & 1 & -0.7506 & -0.0061 \\ -0.1110q^{-1} & 0 & 1 & -0.7506 \\ -0.1232q^{-1} & -0.7438q^{-1} & 0 & 1 \end{bmatrix}$$

$$\text{and} \qquad \tilde{\mathbf{B}}_\Delta = \begin{bmatrix} 0.1288q^{-1} & -0.0031q^{-1} & -0.0039 & -0.0035 \\ 0.0144q^{-1} & -0.00043q^{-1} & 0.1297 & -0.00048 \\ 0.0091q^{-1} & -0.00048q^{-1} & 0 & 0.1297 \\ 0.0033q^{-1} & 0.1297q^{-1} & 0 & 0 \end{bmatrix};$$

(iv) observing that $\bar{\mathbf{y}}(0)$ and $\bar{\mathbf{u}}(0)$ are identical to, respectively, $\tilde{\mathbf{y}}(0)$ and $\tilde{\mathbf{u}}(0)$, then the relevant model is given by

$$\mathbf{A}_\Delta(q^{-1})\bar{\mathbf{y}}(0) = \mathbf{B}_\Delta(q^{-1})\bar{\mathbf{u}}(o) + \bar{\epsilon}(0), \tag{5.103}$$

where $$\mathbf{A}_\Delta = \tilde{\mathbf{A}}_\Delta \quad \text{and} \quad \mathbf{B}_\Delta = \tilde{\mathbf{B}}_\Delta.$$

The representation of equation (5.103) now is used to derive predictive and LQG compensators for the regulator problem considered in section 5.1 and 5.3. It is envisaged that acceptable transient responses will result by placing these controllers in the forward path of the feedback loop (see Figure 5.7) and it is therefore considered unnecessary to acquire the "two degrees-of-freedom" control laws described in section 5.5.

Predictive Control Design

The parameters μ_κ, $\mu_{\kappa+1}$, λ_ν and $\lambda_{\nu+1}$ required to designate the predictive controller are defined for each of the relevant control sampling instants $t \equiv 0$, $t \equiv -1$ and $t \equiv -2$ by expressing (5.39a) in each instance as follows:

$$\ldots\ \mu_\kappa < \lambda_\nu = \mu_{\kappa+1} < \lambda_{\nu+1} = \mu_{\kappa+2} \ldots .$$

The relevant values are given in Table 5.5.

Choosing p to be 4, the matrices $\check{\mathbf{A}}_\nu$, $\check{\mathbf{A}}_\nu^\dagger$, $\check{\mathbf{B}}_\nu$ and $\check{\mathbf{B}}_\nu^\dagger$, $\nu = 0, 1, 2$, specifying the model

Table 5.5. Parameters determining predictive controller.

instant	$\dot{\mu}_\kappa$	λ_ν	$\mu_{\kappa+1}$	$\lambda_{\nu+1}$
0	-1	0	0	1
-1	0	1	1	2
-2	1	2	2	3

of equation (5.45) are organised thus:

$$\breve{\mathbf{A}}_\nu = \begin{bmatrix} \mathbf{A}_\nu^{(0)} & \mathbf{A}_\nu^{(1)} & \mathbf{A}_\nu^{(2)} & \mathbf{0} \\ \mathbf{0} & \mathbf{A}_\nu^{(0)} & \mathbf{A}_\nu^{(1)} & \mathbf{A}_\nu^{(2)} \\ \mathbf{0} & \mathbf{0} & \mathbf{A}_\nu^{(0)} & \mathbf{A}_\nu^{(1)} \\ \mathbf{0} & \mathbf{0} & \mathbf{0} & \mathbf{A}_\nu^{(0)} \end{bmatrix}, \quad \breve{\mathbf{A}}_\nu^\dagger = \begin{bmatrix} \mathbf{0} \\ \mathbf{0} \\ \mathbf{A}_\nu^{(2)} \\ \mathbf{A}_\nu^{(1)} + \mathbf{A}_\nu^{(2)} q^{-1} \end{bmatrix},$$

$$\breve{\mathbf{B}}_\nu = \begin{bmatrix} \mathbf{B}_\nu^{(0)} & \mathbf{B}_\nu^{(1)} & \mathbf{0} & \mathbf{0} \\ \mathbf{0} & \mathbf{B}_\nu^{(0)} & \mathbf{B}_\nu^{(1)} & \mathbf{0} \\ \mathbf{0} & \mathbf{0} & \mathbf{B}_\nu^{(0)} & \mathbf{B}_\nu^{(1)} \\ \mathbf{0} & \mathbf{0} & \mathbf{0} & \mathbf{B}_\nu^{(0)} \end{bmatrix} \quad \text{and} \quad \breve{\mathbf{B}}_\nu^\dagger = \begin{bmatrix} \mathbf{0} \\ \mathbf{0} \\ \mathbf{0} \\ \mathbf{B}_\nu^{(1)} \end{bmatrix}.$$

Notice that, since

$$\breve{\mathbf{C}}_\nu = \mathbf{I}_{12} \quad \text{and} \quad \breve{\mathbf{C}}_\nu^\dagger = \mathbf{0}, \quad \nu = 0, 1, 2,$$

then, from equations (5.46) and (5.47), the predictive control law is not influenced by the disturbance subsystem.

Minimising the cost function of equation (5.46), in which the vector $\breve{\mathbf{u}}_\nu$ comprises the control derivatives $u_{i_\Delta}(\cdot)$ and the weighting matrices are

$$\mathbf{\Lambda}_0 = \text{diag}\,(0.005,\ 0.75,\ 0.75,\ 0.75)\,,$$

and

$$\mathbf{\Lambda}_1 = \mathbf{\Lambda}_2 = \text{diag}\,(0.1,\ 10,\ 10,\ 10)\,,$$

and following the procedure encapsulated by equations (5.48), (5.49), (5.50) and (5.51), the predictive controller is given by

$$\bar{\mathbf{u}}_\Delta(0) = -\mathbf{R}_{\Delta_o}^{-1}(q^{-1})\mathbf{S}_o(q^{-1})\bar{\mathbf{y}}(0). \tag{5.104}$$

where

$$\mathbf{R}_{\Delta_o}(q^{-1}) = \begin{bmatrix} 1+0.2083q^{-1} & 0.0345q^{-1} & 0.0195-0.0108q^{-1} & 0.0270-0.0051q^{-1} \\ 0.0359q^{-1} & 1+0.2071q^{-1} & 0.1509-0.0021q^{-1} & 0.1826-0.0010q^{-1} \\ 0.0067q^{-1} & -0.4533q^{-1} & 1 & 0.0056 \\ 0.0152q^{-1} & 0.1069q^{-1} & -0.2683q^{-1} & 1+0.000075q^{-1} \end{bmatrix}$$

and $$\mathbf{S}_o(q^{-1}) = \begin{bmatrix} 1.8644-1.1915q^{-1} & 0.3596 & -0.3757 & -0.0730 \\ 0.2728-0.2335q^{-1} & 1.7548 & -1.2176 & -0.0143 \\ 0.0641q^{-1} & 2.5898q^{-1} & 3.5539 & -6.1407 \\ -4.2243q^{-1} & 1.5296q^{-1} & -0.0174q^{-1} & 2.9416 \end{bmatrix}.$$

LQG Control Design

The LQG design results by minimising

$$J = E\left\{\bar{\mathbf{y}}'(0)\bar{\mathbf{y}}(0) + \bar{\mathbf{u}}'_{\Delta}(0)\boldsymbol{\Xi}\bar{\mathbf{u}}_{\Delta}(0)\right\}, \tag{5.105}$$

where $$\boldsymbol{\Xi} = \mathbf{I}_4,$$

for the plant specified in equation (5.103). The matrices $\mathbf{B}_a$, $\mathbf{A}_b$, ((4.35)), $\mathbf{D}$ ((5.3)), and $\mathbf{R}_{\Delta_{md}}$ and $\mathbf{S}_{md}$ ((5.6) and (5.7)) determining the optimal control solution are provided in Appendix B. Scaled as in Example S1, the matrices defining the LQG controller are:

$$\mathbf{R}_{\Delta_o}(q^{-1}) = \begin{bmatrix} 1 & 0.0523 & -0.0320 & -0.0069 \\ 0 & 1 & -0.0050 & -0.0011 \\ 0.0430q^{-1} & -0.0125q^{-1} & 1-0.0048q^{-1} & -0.0247-0.0010q^{-1} \\ 0.0518q^{-1} & -0.0151q^{-1} & -0.0058q^{-1} & 1-0.0013q^{-1} \end{bmatrix}$$

and $$\mathbf{S}_o(q^{-1}) = \begin{bmatrix} 2.4607-1.6174q^{-1} & 0.6550 & -0.7748 & 0 \\ 0.2753-0.2519q^{-1} & 2.5502 & -1.7057 & 0 \\ 0.2828q^{-1}-0.2423q^{-2} & 0 & 2.7168 & -1.8748 \\ 0.3476q^{-1}-0.2919q^{-2} & -1.8095q^{-1} & 0 & 2.6485 \end{bmatrix}.$$

Comparison of Designs

A comparison between the predictive and LQG designs can be made from the data provided in Table 5.6. Given the similarities between the values of the coefficients of polynomials

Table 5.6. Comparison between predictive and LQG designs.

	predictive	LQG
ω_n	1.8333, 7.9067	2.6025, 7.6838
ζ	0.6817, 0.8588	0.8252, 0.8252
k_1	7.1452	6.5772
k_2	4.0801	6.1332
k	3.5900	5.7805

within respective elements of the matrices $\mathbf{R}_{\Delta_o}$ and $\mathbf{S}_o$ governing the two control solutions, the corresponding proximity of the dominant closed-loop poles is not surprising. A measure of stability robustness is provided in each instance by the parameters k_1, k_2 and k which denote, respectively, the permissible increases in the gains of loop 1 and 2 individually and both loops simultaneously that guarantee closed-loop stability.

LQG Design: $N = 8$

In this scenario, the performance index to be minimised is

$$J = E\left\{\bar{\mathbf{y}}'(o)\bar{\mathbf{y}}(o) + \bar{\mathbf{u}}'_{\Delta}(0)\boldsymbol{\Xi}\bar{\mathbf{u}}_{\Delta}(0)\right\}, \tag{5.106}$$

where $$\boldsymbol{\Xi} = \mathbf{I}_9.$$

The closed-loop "poles" resulting from this design are positioned at locations in the z-plane corresponding to

$$\omega_{n_1} = 2.5843 \text{ rad/s} \quad \text{and} \quad \zeta_1 = 0.8160;$$

$$\omega_{n_2} = 20.6400 \text{ rad/s} \quad \text{and} \quad \zeta_2 = 0.8159.$$

thereby justifying the sampling strategy. The feedback system remains asymptotically stable for the following values of k_1, k_2 and k:

$$k_1 \in (0, 6.8572], \quad k_2 \in (0, 5.3922], \quad \text{and} \quad k \in (0, 5.3820].$$

The resultant controller $(\mathbf{R}_{\Delta_o}, \mathbf{S}_o)$ may be separated into two components:

(i) a time-invariant control, namely,

$$u_{\Delta_1}(0) + \sum_{i=0}^{7} r_{12_i} q_8^{-i} u_{\Delta_2}(0) = -\left(s_{11_0} + s_{11_1} q^{-1}\right) y_1(0) - \left(s_{12_0} + s_{12_1} q_8^{-1}\right) y_2(0), \qquad (5.107a)$$

where $r_{12_0} = 0.0227$, $r_{12_1} = -0.2639$, $r_{12_2} = -0.1673$, $r_{12_3} = -0.1008$,

$r_{12_4} = -0.0563$, $r_{12_5} = -0.0278$, $r_{12_6} = -0.0109$, $r_{12_7} = -0.0024$,

$s_{11_0} = 2.3761$, $s_{11_1} = -1.5309$,

$s_{12_0} = 2.2092$ and $s_{12_1} = -2.4255$;

(ii) a cyclically time-varying control, namely,

$$\left(1 + \sum_{i=1}^{7} r_{22_i}^{(0)} q_8^{-i}\right) u_{\Delta_2}(0) = -\left(s_{21_0}^{(0)} + s_{21_1}^{(0)} q^{-1}\right) y_1(0) - \left(s_{22_0}^{(0)} + {}_{22_1}^{(0)}\, q_8^{-1}\right) y_2(0);$$

$$\left(1 + \sum_{i=1}^{7} r_{22_i}^{(\iota)} q_8^{-i}\right) u_{\Delta_2}(0) + r_{21_0}^{(\iota)} u_{\Delta_1}(-8) = -\left(s_{21_0}^{(\iota)} + s_{21_1}^{(\iota)} q^{-1}\right) y_1(-8) - \left(s_{22_0}^{(\iota)} + {}_{22_1}^{(\iota)}\, q_8^{-1}\right) y_2(-\iota), \qquad (5.107b)$$

$\iota = 1, 2, \ldots, 7.$

Plots representing the variation in the values of the parameters r_{21_0}, s_{21_0}, s_{21_1}, s_{22_0} and s_{22_1} during the repetitive time interval are displayed in Figure 5.11, where the periodic nature of the control law of equation (5.107b) is evident. In this example, the magnitudes of the parameters $r_{22_i}^{(\iota)}$, $i = 0, 1, \ldots, 7$, $\iota = 0, 1, \ldots, 7$, are, in general, rather small (i.e., < 0.1), as evinced by

$r_{22_1}^{(4)} = -0.0803$, $r_{22_2}^{(4)} = -0.0567$, $r_{22_3}^{(4)} = -0.0394$, $r_{22_4}^{(4)} = -0.0267$,

$r_{22_5}^{(4)} = -0.0175$, $r_{22_5}^{(4)} = -0.0111$, and $r_{22_7}^{(4)} = -0.0067$.

The above observations suggest that it may be desirable from a practical perspective to consider the substitution of the periodic, fast-sampled contribution to the control law with a time-invariant counterpart. Furthermore, the feasibility of reducing the order of the controller denominator matrix also may constitute a topic for future research.

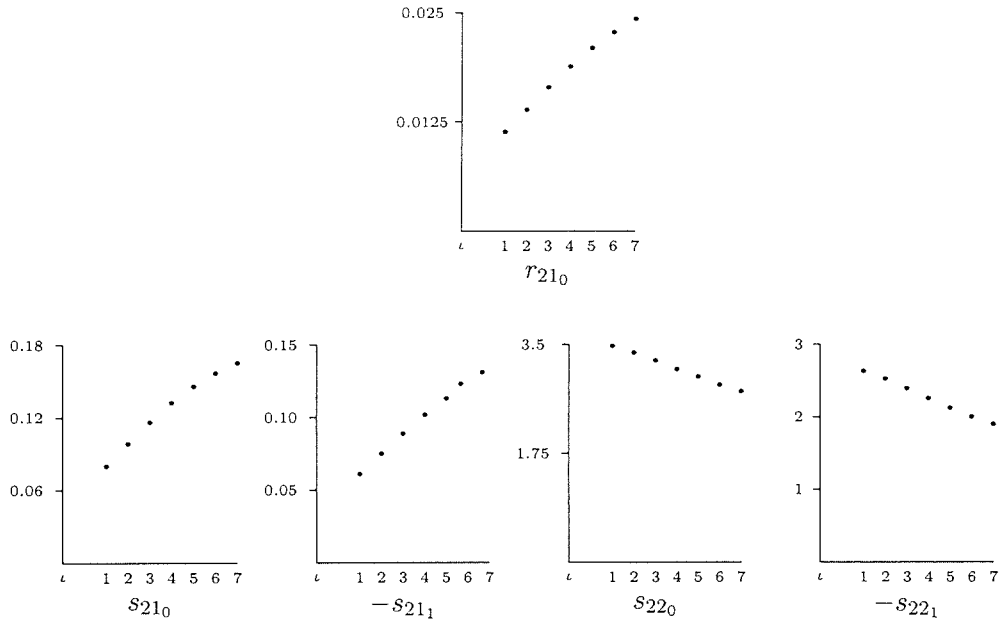

Figure 5.11. Variations in parameter values.

5.7 Conclusion

This chapter has confirmed that the polynomial representations obtained in Chapters 3 and 4 can be used to design multirate-sampled feedback systems via existing methodologies. It is apparent that the "repetitive time interval index-dependent" matrices defining lifted system models are compatible with the polynomial approach to LQG control design provided "minimum degree solutions" are specified appropriately. Similar comments apply to the use of the GPC strategy, although it is emphasised that the derivation technique detailed in this chapter is at variance with the approach employed in the literature. The possible use of multirate sampling as a means of improving feedback system performance remains largely unresolved, notwithstanding the demonstration of the intrinsic low-pass filtering nature of fast output-sampled optimal and predictive compensators.

Chapter Six
Conclusion

This thesis has established the principles and methods entailed in the modelling and analysis of multirate sampled-data systems utilising a transfer function-based framework, commonly referred to as the polynomial equations approach. Moreover, it has been demonstrated that the proposed methodology, which affords dual time- and frequency-domain interpretations, facilitates the synthesis of multirate-sampled feedback systems via the minimisation of quadratic performance criteria, thereby proffering an alternative to the state-space control design techniques customarily employed in this context.

The principal theoretical developments and contributions contained within the thesis may be summarised thus:

Chapter 2

The theoretical foundations described in Chapter 2 governing the proposed modelling approach constitute the frequency and switch decomposition procedures that were introduced in the 1950's. The use of an illustrative example clearly highlighted the problems associated with multirate-sampled systems analysis using either decomposition. However, bearing in mind the intuitive appeal that transfer function models hold for many control practitioners, it was apparent that there existed scope for incorporating the principles underpinning the decomposition techniques within a modern control context, thereby exploiting available computer-aided control system analysis/design packages.

Chapter 3

The assimilation of the decomposition procedures within the polynomial equations approach was detailed in Chapter 3, where pulse-transform/transfer function analysis and the insertion of fictitious fast-rate sampling switches and a zero-order hold were used to separate a SISO multirate-sampled configuration into "discretised plant", input and output subsystems. The definition of certain backward-shift operators then warranted the inter-

pretation of the plant model as specifying sets of difference equations at particular sampling instants throughout one cycle of the sequence of sampling operations. Subsequently, a systematic means of arranging the relevant cyclically time-varying difference equation model in matrix-vector format was established, with care taken to emphasise the algebraic properties linking polynomials emanating from pulse-transfer functions with their corresponding polynomial matrix representations. The introduction of two non-square block diagonal permutation matrices facilitated the extension of the basic modelling approach to encompass the switching operations related to the zero-order hold of the input subsystem and the sampling rate conversion imposed by the output subsystem.

Observing that the above approach is closely related to the time-domain-orientated switch decomposition technique, attention then focused upon the derivation of corresponding frequency-domain models of each of the three subsystems, in addition to the transformation matrices linking vector-valued variables in each domain. The modelling of stochastic disturbances via the proposed methodology was addressed by invoking the frequency decomposition of the spectral densities of a random variable sampled at different rates, while compatibility of the related sampling rate with that of the output subsystem was specified via an ensuing spectral factorisation. The remainder of Chapter 3 was devoted to the amalgamation of the individual subsystem descriptions into left- and right-matrix fraction representations, designated alternatively with respect to the time- and frequency-domains. Thereafter, polynomial models were derived for each of the "special cases" of fast input- and fast output-sampled systems. The chapter concluded with a simple numerical example that illustrated the foregoing techniques.

Chapter 4

The formulation of polynomial descriptions of multirate-sampled multivariable configurations was dealt with in Chapter 4. Utilising a conceptually-identical strategy to that employed in the SISO case, the chief distinguishing feature of the MIMO scenario involved the necessity to predicate all ensuing topological operations on a left-matrix fraction model of the discretised plant pulse-transfer function matrix. Consequently, the strong algebraic relationships obtained between polynomials and their related polynomial matrices in Chapter 3 have no counterparts in the general l-input/m-output case. Nevertheless,

the procedure entailed in acquiring a left-matrix fraction description of the multivariable system was straightforward, albeit requiring a matrix fraction conversion, whereas the derivation of the compatible stochastic disturbance subsystem description necessitated a matrix-valued spectral factorisation.

The key issue of causality was addressed by designating a so-called "index-dependent" time-domain model in which the elements within system vectors were arranged in accordance with their chronological order with regard to the sampling sequence. It was therefore possible to ascribe specific structures to each of the polynomial matrices determining the overall system representation and to extend this principle to its right-matrix fraction alternative. Hitherto neglected, similar considerations were applied to obtain corresponding models of both multivariable and scalar multirate-sample digital controllers. Following an examination of the criteria available for gauging the stability robustness of multirate-sampled configurations, an illustrative example summarised the principles established in this chapter.

Chapter 5

Since the foregoing theoretical developments assist only the analysis of multirate-sampled systems, the objective of Chapter 5 was to investigate the incorporation of the polynomial modelling methodology within established control system design procedures. Accordingly, arguably the two most popular synthesis techniques – LQG and predictive control – were considered to be suitable vehicles in this respect. With the proviso that the structures of the relevant matrices are designated via the criteria described in Chapter 4, it was found that the polynomial modelling methodology was entirely compatible with the LQG design approach, in which the optimal solution is specified via coupled diophantine equations. The method adhered to in the generalised predictive control approach involved the derivation of individual control laws at each of the control signal sampling instants within the overall sampling sequence and subsequently combining these. Once again, provided causality issues were addressed by utilising "index-dependent" matrix structures, no significant theoretical problems emerged. Subsequently, means of introducing integral action and engendered "two degrees-of-freedom" controller structures were outlined. The general principles concerned in each instance were demonstrated with the aid of numerical

examples.

While it can be stated that there are no theoretical pitfalls related to the design methodologies discussed in this chapter, certain practical problems remain. Specifically, in common with the single-rate case, a systematic means of choosing appropriate dynamic weighting polynomials/polynomial matrices within the cost functions specifying the multirate LQG control problem remains elusive. A further difficulty relates to the selection of the control weighting parameters within the performance index of the predictive methodology, where an evaluation of their suitability can only be ascertained following the computation of the overall multirate-sampled control law and an evaluation of the resultant closed-loop pole locations.

The issue of whether multirate sampling can enhance feedback system performance was not a major consideration in this thesis. Nonetheless, the use of polynomial models has revealed that the flexibility borne by the additional controller numerator parameters in "fast output-sampled" feedback systems designed via either the optimal or predictive control approaches manifested itself in a low-pass FIR filter structure. Leaving overall performance relatively unaffected, the complementary "fast input-sampled" mechanism was shown to engender idiosyncratic control action. In conclusion, however, it appears likely that the imposition of alternative multirate sampling schedules can improve certain aspects of control performance only at the expense of others. Furthermore, "rules-of-thumb" governing sampling interval choice in single-rate systems accordingly apply to the period of the sampling sequence in the multirate case.

The work contained in this thesis highlights several areas for possible further research. For example, it is of interest to note that, although the optimal and predictive multirate controllers are periodic with respect to the sampling cycle, thereby raising the prospect of implementational difficulties, their parameters do not vary significantly in certain circumstances. This phenomenon suggests the feasibility of synthesising time-invariant compensators that emulate their cyclical counterparts. Since polynomial descriptions are conducive to system identification via parametric models, there exists the possibility of designing self-tuning control systems that, as discussed in the Introduction, incorporate fast output-sampling to simulate full state-feedback. Such adaptive systems then may pos-

sess greater flexibility in terms of control design than conventionally sampled self-tuners. Other topics worthy of further consideration include the facility of addressing nonlinear elements within the predictive control problem formulation, thus yielding an overall control law via the combination of the solutions of a set of constrained optimisation problems, and improved techniques for assessing the stability robustness of multirate-sampled multi-input multi-output configurations.

Appendix A

Example S1

$$\mathbf{B}_a(q^{-1}) = \begin{bmatrix} 0.0125q^{-1} & 0.0122 \\ 0.0177q^{-1} & 0.0013 + 0.0056q^{-1} \\ 0.0053q^{-1} + 0.0014q^{-2} & 0.0179q^{-1} \end{bmatrix}$$

$$\mathbf{A}_b(q^{-1}) = \begin{bmatrix} 1 + 1.0927q^{-1} & -2.0927 \\ -2.0927q^{-1} & 1 + 1.0927q^{-1} \end{bmatrix}$$

$$\mathbf{B}_c(q^{-1}) = \begin{bmatrix} 0.0082q^{-1} & 0.0106 \\ 0.0138q^{-1} & 0.0013 + 0.0036q^{-1} \\ 0.0053q^{-1} + 0.00092q^{-2} & 0.0126q^{-1} \end{bmatrix}$$

$$\mathbf{C}_b(q^{-1}) = \begin{bmatrix} 1 + 0.2989q^{-1} & -0.3505 \\ -0.3454q^{-1} & 1 + 0.2981q^{-1} \end{bmatrix}$$

$$\mathbf{D}(q^{-1}) = \begin{bmatrix} 1.1881 + 0.9197q^{-1} & -2.0776 \\ -2.0776q^{-1} & 1.1881 + 0.9197q^{-1} \end{bmatrix}$$

$$\mathbf{C}_o(q^{-1}) = \begin{bmatrix} 1 + 0.4016q^{-1} & -0.3450 \\ -0.4276q^{-1} & 1 + 0.2219q^{-1} \end{bmatrix}$$

$$\mathbf{R}_{md}(q^{-1}) = \begin{bmatrix} 1.1881 + 0.2633q^{-1} & -0.1794 \\ -0.0816q^{-1} & 1.1881 + 0.3000q^{-1} \end{bmatrix}$$

$$\mathbf{S}_{md}(q^{-1}) = \begin{bmatrix} 14.2188 & -13.5504 & 0 \\ -14.3062q^{-1} & 0 & 14.9745 \end{bmatrix}$$

$$\mathbf{\Lambda}_{md}(q^{-1}) = \begin{bmatrix} -13.0630q^{-1} & 14.3587 \\ -14.4535q^{-1} & 16.0224 + 0.0056q^{-1} \\ 15.1778q^{-1} + 0.0014q^{-2} & -13.7478q^{-1} \end{bmatrix}$$

Appendix B

Example M2

$$\mathbf{B}_a = \begin{bmatrix} 0.0638q^{-1} & -2.5112q^{-1} & 0.0033 & 0.0029 \\ -2.6029q^{-1} & 102.3858q^{-1} & 0.1297 & -0.1174 \\ 0.0043q^{-1} & 0 & 0 & 0.1297 \\ 0.0033q^{-1} & 0 & 0 & 0 \end{bmatrix}$$

$$\mathbf{A}_b = \begin{bmatrix} 1 & -39.4343 & -0.0370 & 0 \\ 14.8610q^{-1} & 1 - 584.55q^{-1} & -0.7460 & 0.6703 \\ -20.1977q^{-1} & 793.5q^{-1} & 1 - 0.0009q^{-1} & -1.6518 \\ -0.0563q^{-1} & 2.7801q^{-1} & -0.0029q^{-1} & 1 \end{bmatrix}$$

$$\mathbf{D} = \begin{bmatrix} 1.1815 - 0.8464q^{-1} & 0.0618 & -0.0917 & 0.0343 \\ -13.8351q^{-1} & 1.1833 - 0.5665q^{-1} & -2.7511 & 2.1468 \\ 37.2136q^{-1} & 2.1463q^{-1} & 1.1840 - 0.5662q^{-1} & -2.7515 \\ -26.2555q^{-1} & -2.7519q^{-1} & 2.1459q^{-1} & 1.1845 - 0.5659q^{-1} \end{bmatrix}$$

$$\mathbf{R}_{\Delta_{md}} = \begin{bmatrix} 1.1815 & 0.0618 & -0.0378 & -0.0082 \\ 0 & 1.1833 & -0.0059 & -0.0013 \\ 0.0509q^{-1} & -0.0148q^{-1} & 1.1840 - 0.0057q^{-1} & -0.0292 - 0.0012q^{-1} \\ 0.0614q^{-1} & -0.0178q^{-1} & -0.0068q^{-1} & 1.1845 - 0.0015q^{-1} \end{bmatrix}$$

$$\mathbf{S}_{md} = \begin{bmatrix} 2.9073 - 1.9110q^{-1} & 0.7738 & -0.9154 & 0 \\ 0.3258 - 0.2980q^{-1} & 3.0176 & -2.0183 & 0 \\ 0.3348q^{-1} - 0.2869q^{-2} & 0 & 3.2166 & -2.2198 \\ 0.4118q^{-1} - 0.3458q^{-2} & -2.1434q^{-1} & 0 & 3.1372 \end{bmatrix}$$

Appendix C
Computational Aspects

This section addresses the computational issues associated with using polynomial methods to model, analyse and design multirate-sampled control systems. In particular, an examination of the software that implements each of the key algorithms identifies the benefits and drawbacks of the polynomial approach.

The section commences by investigating the key algorithms required by the methodology, namely, matrix fraction conversion, spectral factorisation and diophantine equation solving. In addition to outlining the computational techniques concerned, simple modifications that enable software intended for single-rate applications to encompass multirate problems are described. Prior to discussing how the theory developed in previous chapters may be incorporated within the package POLYNOMIAL TOOLBOX, the capabilities and limitations of the software are discussed. To conclude this section, a design example is utilised to illuminate the computational procedures and implementation issues.

C.1 Mathematical Algorithms

The theory related to the modelling and synthesis of multirate-sampled control systems via the polynomial approach has been demonstrated in the previous chapters to be relatively straightforward and potentially computationally attractive. In particular, the theory mainly requires elementary operations involving polynomial matrices, which are described within Gantmakher (1959) or Kučera (1979). Nonetheless, there are a small number of specialised computational techniques namely: polynomial matrix fraction conversions, spectral factorisation and linear matrix diophantine equation-solvers.

Polynomial Matrix Fraction Descriptions

The concept of polynomial matrix fraction descriptions in the context of linear multivariable control literature was initially devised by Rosenbrock (1970), Wolovich (1974) and Kučera (1979) and concerns the definition of a rational transfer function matrix $\mathbf{G}$ as ei-

ther $\mathbf{A}_l^{-1}\mathbf{B}_l$ or $\mathbf{B}_r\mathbf{A}_r^{-1}$, where $\mathbf{A}_l$, $\mathbf{B}_l$, $\mathbf{B}_r$ and $\mathbf{A}_r$ are polynomial matrices. It is important to reiterate that the above polynomial matrix fractions are neither unique nor may possess the "causal structures" specified in previous chapters, as may be demonstrated by writing

$$\mathbf{G} = \mathbf{A}_l^{-1}\mathbf{B}_l = (\mathbf{U}_1\mathbf{A}_l)^{-1}(\mathbf{U}_1\mathbf{B}_l) \tag{C.1a}$$

and

$$\mathbf{G} = \mathbf{B}_r\mathbf{A}_r^{-1} = \mathbf{B}_r\mathbf{U}_2(\mathbf{A}_r\mathbf{U}_2)^{-1}, \tag{C.1b}$$

where $\mathbf{U}_1$ and $\mathbf{U}_2$ are unimodular matrices.

It is advantageous to utilise existing algorithms for the derivation and translation of coprime polynomial matrix fraction representations, for instance, the general numerical methods of Kučera (1979), Patel (1981), Datta and Gangopadhyay (1992), Strijbos (1996) and Mahmood *et al.* (1998). The calculations required to establish the matrix fraction from the rational transfer function matrix $\mathbf{G}(z^{-1})$ can be achieved by identifying the least common denominator $d(z^{-1})$, whence the resultant right matrix fraction description $\mathbf{N}(d\mathbf{I})^{-1}$ is translated to a coprime left matrix fraction. The dual situation can be achieved by a similar technique. Similarly, the translation between left- and right-coprime matrix fractions can be reduced to the general linear polynomial matrix equation,

$$\begin{bmatrix} \mathbf{B}_l & -\mathbf{A}_l \end{bmatrix} \begin{bmatrix} \mathbf{A}_r \\ \mathbf{B}_r \end{bmatrix} = \mathbf{0}, \tag{C.2}$$

of which an elegant solution can be obtained via the computation of the right null space of $[\mathbf{B}_l \ -\mathbf{A}_l]$. Basilio and Kouvaritakis (1997) provide a simple algorithm based on the Sylvester resultant matrices. The same technique can be employed for the dual situation.

The matrices $\mathbf{U}_1$ and $\mathbf{U}_2$ ((C.1a,b)) can be used to engender the upper-triangular structures which the control design techniques require for $\mathbf{A}_l(0)$ and $\mathbf{A}_r(0)$. Writing

$$\mathbf{A}_l(q^{-1}) = \mathbf{A}_{l_0} + \sum_{i=1}^{n} \mathbf{A}_{l_i} q^{-i}, \tag{C.3}$$

then the pre-multiplication of an arbitrary $\mathbf{A}_l(q^{-1})$ by an appropriate lower-triangular matrix $\mathbf{U}_1$ will produce an upper-triangular $\mathbf{U}_1\mathbf{A}_{l_0}$ (and, thus, $\mathbf{U}_1\mathbf{A}_l(0)$) and, consequently, the "causal" structures required of $\mathbf{A}_l$ and $\mathbf{B}_l$. A lower-triangular matrix $\mathbf{U}_2$ similarly can be used to yield a "causal" pair $(\mathbf{B}_r, \mathbf{A}_r)$.

Spectral Factorisation of Polynomial Matrices

Polynomial spectral factorisation was initially devised by Wiener (1949) to obtain the frequency-domain solution of stochastic filtering problems and, subsequently, the technique has played a significant role in control theory. In the context of this thesis it has been demonstrated that the task of establishing stable spectral factors is fundamental for the modelling of multirate stochastic signals and determining the diophantine equations related to optimal control synthesis.

The spectral factorisation of polynomial matrices has been the focus of considerable research (Kučera, 1979, Ježek and Kučera, 1985, Šebek, 1993, Kwakernaak and Šebek, 1994) in which solutions are generally obtained from one of a series of established algorithms, which include: diagonalisation, successive symmetric factor extraction, interpolation and a solution based on an algebraic Riccati equation. Within the context of discrete-time systems, the algorithm by Ježek and Kučera (1985) can be employed directly without modification to establish the Schur spectral factor of a para-Hermitian polynomial matrix by performing a Newton-Raphson iterative scheme based on a Sylvester matrix algorithm. Alternatively, Kučera (1979) provides an efficient algorithm which produces a Hurwitz polynomial matrix based on iterative Cholesky factorisation technique derived from geometric convergence. Additional remarks relating to spectral factorisation can be found in Tuel (1968), Åström and Wittenmark (1997) and Kwakernaak (2000).

Linear Diophantine Equations

Linear polynomial diophantine equations are a special type of abstract algebraic problem which often arises naturally in control theory, the importance of which was initially recognised by Volgin (1962) and further emphasised by Kučera (1979, 1993). This research has demonstrated that the optimal synthesis techniques explored in Chapter 5 are dependent upon the solution of linear equations based on polynomial matrices.

The diophantine equation has alternative descriptions, although in this text the problem is predicated on the unilateral linear matrix equation in the general form

$$\mathbf{X}\mathbf{A} + \mathbf{Y}\mathbf{B} = \mathbf{C}, \tag{C.4}$$

where, with $\mathbf{A}$, $\mathbf{C}$ and $\mathbf{X}$ square, the polynomial matrices $\mathbf{A}$, $\mathbf{B}$ and $\mathbf{C}$ are given while

$\mathbf{X}$ and $\mathbf{Y}$ are unknown. A diophantine equation of this type possesses an infinite number of solutions whenever it is solvable, and the problem will have a solution if, and only if, the greatest common right divisor of the matrices $\mathbf{A}$ and $\mathbf{B}$ is a right divisor of $\mathbf{C}$. This statement follows directly from the Euclidean division principle, thus implying that with the matrices $\mathbf{A}$ and $\mathbf{B}$ defined as coprime, the diophantine equation is solvable. The general solution to the diophantine equation can be given in the form

$$\mathbf{X} = \mathbf{X}_0 - \mathbf{T}\tilde{\mathbf{B}} \quad \text{and} \quad \mathbf{Y} = \mathbf{Y}_0 + \mathbf{T}\tilde{\mathbf{A}}, \tag{C.5}$$

where $\mathbf{X}_0$ and $\mathbf{Y}_0$ are any particular solution, with $\mathbf{T}$ an arbitrary polynomial matrix and $\tilde{\mathbf{A}}$ and $\tilde{\mathbf{B}}$ defined as the coprime polynomial matrices such that $\mathbf{B}\mathbf{A}^{-1} = \tilde{\mathbf{A}}^{-1}\tilde{\mathbf{B}}$. Determination of the general solution of equation (C.4) can be obtained by utilising the extended Euclidean algorithm and has been well documented; see, for example, Blankinship (1963), Kučera (1979), Šebek and Kučera (1981), and Sain (1975).

In addition, the problem of the set of coupled diophantine equations, defined by (5.6) and (5.7), can be simplified to a single bilateral diophantine equation by rearranging the two coupled equations into the form

$$\mathbf{D}^* \begin{bmatrix} \mathbf{R} & \mathbf{S} \end{bmatrix} + \mathbf{\Lambda}^* \begin{bmatrix} -\mathbf{B}_c & \mathbf{A}_c \end{bmatrix} = \begin{bmatrix} \mathbf{A}_b^* \mathbf{\Xi} \mathbf{C}_b & \mathbf{B}_a^* \mathbf{C}_a \end{bmatrix} \tag{C.6}$$

where the unknowns $\mathbf{R}$, $\mathbf{S}$ and $\mathbf{\Gamma}^*$ can be ascertained via the procedure outlined by Kučera (1979).

In the context of "polynomial" multirate control theory, it has been established that the solution to the linear diophantine equation conforms with the concept of causality; in other words, the matrices $\mathbf{S}$ and $\mathbf{R}$ in (4.39a) must exhibit a specific causal structure. Therefore, since conventional algorithms are incapable of identifying a causal solution, a slight modification to the problem is required. Based upon the elementary arithmetic operations required to solve unilateral linear diophantine equations, a solution can be derived by separating the problem into smaller, more flexible calculations which deal with a single row of $\mathbf{X}$, $\mathbf{Y}$ and $\mathbf{C}$ at a time, i.e., $\mathbf{x}_i'$, $\mathbf{y}_i'$ and $\mathbf{c}_i'$. In addition, the inclusion of two masking matrices $\mathbf{X}_x \in \mathbb{R}^{l \times l}$ and $\mathbf{X}_y \in \mathbb{R}^{m \times m}$ permits the introduction of causality into the diophantine equation, allowing the structure of both $\mathbf{X}$ and $\mathbf{Y}$ to be defined as causal. The masking matrices are simply diagonal matrices whose elements are either simply 1

or the backward-shift operator z^{-1}, depending on the required structure. Therefore, the diophantine equation (C.4) may alternatively be expressed as

$$\mathbf{x}_i'\mathbf{X}_{x_i}\mathbf{A} + \mathbf{y}_i'\mathbf{X}_{y_i}\mathbf{B} = \mathbf{c}_i' \quad i = 1, 2, \ldots, l,$$

with the i^{th} row of the overall causal solution defined as the combination of $\mathbf{x}_i'$ and $\mathbf{X}_{x_i}$ or $\mathbf{y}_i'$ and $\mathbf{X}_{y_i}$. Additionally, the masking matrices may also be exploited to ensure that the optimal control law exhibits the desired form and structure as defined in Chapter 4.

C.2 Implementation

In practical applications it is impossible to perform numerical calculations without the assistance of a software package, except for the simplest of problems. However, with the creation of POLYNOMIAL TOOLBOX, implementation of the related theory is now a practical proposition, enabling researchers, design engineers and mathematicians to appreciate the opportunities that the polynomial approach supports in the field of control.

MATLAB is a high performance object-oriented interactive computer-aided control system analysis and synthesis software package for scientific and engineering numerical calculations and data visualisation, the functionality of which can be extended within the context of this research by POLYNOMIAL TOOLBOX. The capabilities of the software include classical and optimal design tools for techniques such as pole-placement and dead-beat, optimal and robust control.

Mathematical Algorithms

With the discrete-time backward shift operator defined previously, polynomial matrix algorithms based on basic arithmetic calculations can be implemented by the comprehensive set of elementary and arithmetic operations within POLYNOMIAL TOOLBOX, which are documented in Kwakernaak and Šebek (1999). In addition, the principal algorithms fundamental to the theory are also included within the software, for example, *'spf'*, *'xaybc'* and *'lmf2rmf'*.

Based on the algorithm by Ježek and Kučera (1985), the routine *'spf'*, translated by Henrion, Kwakernaak and Pejchova, solves the polynomial spectral factorisation of symmetric polynomial matrices. While the methodology is computationally attractive and

directly applicable to the multirate scenario, the fundamental difficulty arises due to poor numerical conditioning, a problem that can be overcome for matrices of relatively small dimensions by specifying an additional reduced tolerance argument.

The algorithm by Strijbos (1996) forms the commands *'rat2lmf'* (*'rat2rmf'*) for performing the conversion of rational transfer function matrix models into a left- (right-) polynomial matrix fraction format. In addition, the routine *'lmf2rmf'* by Henrion, Kwakernaak and Pejchova, performs the translation of a left-matrix fraction to a coprime right-matrix fraction via the null space. Similarly, the routine *'rmf2lmf'* translates a (not necessarily coprime) right-matrix fraction to a coprime left-matrix fraction. The conceptual problem with the solutions that these commands produce lies in the fact that the matrices are not "causal" and/or block upper-triangular, as the theory requires, but in most cases this can be overcome by simple manipulation.

The polynomial matrix equation solver command *'xaybc'*, formulated by Henrion, establishes a particular solution of the polynomial matrix unilateral diophantine equation, derived through the Sylvester matrix method and an iterative scheme. In addition, the command *'axybc'*, establishes the solution to the bilateral diophantine equation. The causality constraints addressed earlier can be incorporated into the script to establish a causal solution.

Technical Complications

Since POLYNOMIAL TOOLBOX is based on the complex MATLAB command line interface, it can be rather abstract, although opportunities exist to amend the metaphor. Specifically, through the built-in application development platform, alternative interfaces can be developed to enable a more visual and user-friendly interactive approach for solving specific problems.

A number of difficulties arise within the software package when it is used within a multirate context. For example, the framework in which the software is set does not permit both the discrete-time forward- and backward-shift operators to be defined within a single global variable string. Thus, equations such as (5.3) and the coupled diophantine equations (5.6) and (5.7) become conceptually demanding. However, problems of this

nature can still be solved but do become hazardous, and have to be handled with extreme care and caution.

The theory established has identified the significance of the distinctive concept of causality within multirate-sampled systems and, in particular, controller derivation. In contrast, however, this factor is irrelevant within single-rate system theory and therefore the diophantine equation solver algorithms in POLYNOMIAL TOOLBOX do not incorporate causality constraints. The inability of the algorithms to devise a solution in a causal form limits the problems for which solutions can be derived, although incorporating the simple modifications described in section C.1 alleviates the situation considerably. In a few situations, especially when the degree of the system is large and the size of M is low, the structure of the matrices cannot be defined precisely by the use of masking matrices. In these instances, calculations could easily be undertaken by hand.

Furthermore, the inability of the software to deal with more than one backward-shift operator simultaneously can be problematic within the frequency-domain. This problem can be overcome by defining all expressions with respect to z_N^{-1}, but this approach consequently leads to high-order matrices. In addition, since numerical calculations in this instance are based upon polynomials possessing complex coefficients, it is advised that to avoid troublesome situations the time-domain interpretation is adopted.

Computational Limitations

Theoretically, there are no limitations to the capabilities of the software, with associated literature by Kwakernaak and Šebek (1999) promoting reliable and effective numerical algorithms. However, following an extensive exploratory evaluation of versions 1.6 and 2.0, a number of bugs and fundamental complications were identified, such as problems related to the computational load and numerical conditioning of particular algorithms.

Practical limitations dominate computational considerations, especially in extreme circumstances. For instance, the imprecision of the spectral factorisation algorithm, in addition to the poor numerical conditioning of polynomials and subsequent matrices, is an influencing factor in the derivation of the solution of the linear diophantine equation. The aforementioned lack of precision, an effect that appears to be a function of the dimension,

order and numerical conditioning of matrices involved, is evident in some of the basic commands such as determination of the adjoint, multiplication of matrices or, particularly, the conversion between descriptions. Nevertheless, the problem can be alleviated to some extent by reducing the relative global tolerance. Additionally, the main problem within calculations occurs when the fast-rate sampling interval becomes excessively small, in which case the discretised numerator polynomial coefficients have very small values, and this factor subsequently begins to conflict with the global tolerance of the built-in algorithms. Consequently, since the number of short time intervals within a problem can potentially become large, thereby resulting in substantial matrix dimensions for even the simplest of systems, the range of problems that can be dealt with at present is restricted somewhat.

However, with the new release of POLYNOMIAL TOOLBOX, (2.5), several algorithms have been improved to reflect recent research achievements. In particular, the linear polynomial matrix equation solvers are believed to perform faster and more accurately, especially for larger matrices. It is therefore anticipated that the problems associated with the integration of the theory into an adaptive context could now be researched.

C.3 Design Example: The Inverted Pendulum

This section describes the computational procedures associated with implementing the theory developed in previous chapters. Specifically, utilising POLYNOMIAL TOOLBOX to create a polynomial matrix environment based on the backward-shift operator, the design of a multirate-sampled control system for an inverted pendulum is detailed. The case study is repeated subsequently for a scenario in which there is a relatively low degree of synchronisation between the relevant sampling instants.

The initial input of data is that used in MATLAB, with the exception of the definition of polynomials and polynomial matrices, which utilises the macro *pol* to define an environment that is compatible with POLYNOMIAL TOOLBOX. A number of simple functions based upon the computational instructions outlined previously can be created within MATLAB, thereby facilitating data input and, in particular, the formulation of matrices with large dimensions. Specifically, exploiting the capabilities of POLYNOMIAL TOOLBOX to create a

polynomial matrix environment based on the backward shift operator, basic functions can be produced related to the determination of the dependent matrices.

Pmatrix(lambda,K,domain) – The command is based on the definition of the special structured set of matrices defined in section 4.1, where the input arguments *lambda* and K represents the superscript and the number of fast samples, respectively. In a more general solution the input argument is a row vector relating to the individual superscripts $\lambda_1, \lambda_2, \ldots, \lambda_k$, which enables a more flexible macro.

The additional optional input parameter *domain* defines the domain in which the algorithm is set. With the parameter set to *time*, the algorithm proceeds according to the definition in the time-domain, whereas the option *frequency* selects the frequency-domain. The default setting is the time-domain and is the same for all subsequent commands.

toeplitz(plyX,K,domain) – The command computes the set of cyclical difference equations in matrix form over K sampling intervals with respect to the polynomial matrix *plyX* in accordance with section 4.1.

Vmatrix(J,N,type,domain) – The function returns the matrix $\mathbf{V}$ which is a more general solution to the definition of (3.32). This macro extends the concept to the multivariable case where the input arguments J and N represent a row vector containing the sampling rates and the number of fast rate samples, respectively. In addition, the third argument *'type'* represents whether the selection of the samples represents the measured of phantom sample instants, either *'1'* or *'2'* respectively. This represents a convenient way in which to distinguish between samples.

Wmatrix(K,N,domain) – The routine is similar to the macro above, in that it determines the general multivariable matrix $\mathbf{W}$ in accordance with the general definition of (3.34). The input arguments K and N represent a row vector containing the sampling rates and the number of fast rate samples, respectively.

permutation(N,J,i) – This macro is based on the set of transposition permutation

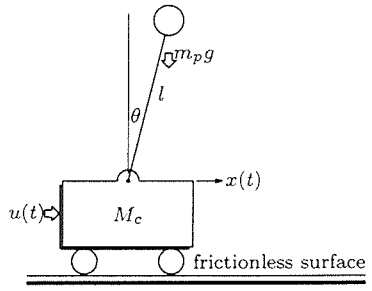

Figure C.1. Inverted pendulum.

matrices which relate vector arrangements. In particular the matrix $\mathbf{\Pi}_1$ ((4.11)) is defined by *permutation(N,M,1)*, whereas the matrices $\mathbf{\Pi}_2$ ((4.32)) and $\mathbf{\Pi}_3$ ((4.33)) are defined by *permutation(N,M,2)* and *permutation(N,L,3)*, respectively, where the input arguments N, J and i are the number of fast rate samples, the row vector the relevant sampling rates and the matrix subscript, respectively.

Notice that the MATLAB output, unless required, will be omitted for concision.

Problem Definition

The problem to be considered is depicted in Figure C.1, where an inverted pendulum is mounted on a motor-driven cart. It is desired to maintain the pendulum in a vertical position and return the cart to its reference position in the presence of exogenous disturbances via the application to the cart of the force u.

Assuming that the angle of rotation θ is small, a linearised model of the system may be described thus:

$$(M_c + m_p)\,\ddot{x} + m_p l\ddot{\theta} = u \tag{C.7a}$$

$$\left(I + m_p l^2\right)\ddot{\theta} + m_p l\ddot{x} = m_p g l\theta, \tag{C.7b}$$

where I is the moment of inertia of the pendulum rod about its centre of gravity and M_c and m_p are the masses of the cart and pendulum, respectively. However, since it is assumed that the pendulum mass is concentrated at the top of the rod and that the rod is mass less, the moment of inertia of the pendulum about its centre of gravity is zero. In addition, to simplify calculations further, it is supposed that M is significantly larger

than m, whence $(M+m) \approx M$. Therefore, from equations (C.7a,b), the plant can be described by the following transfer function model:

$$\mathbf{g}(s) = \frac{1}{M_c l}\begin{bmatrix} l/s^2 \\ -1/\left(s^2 g/l\right) \end{bmatrix}, \tag{C.8}$$

where in this example the mass of the cart M_c is 0.5 kg and the length of the pendulum is 0.5 m. In the first sampling schedule to be considered, the output signals $x(t)$ and $\theta(t)$ and the input signals $u(t)$ are sampled at intervals of T/M_1, T/M_2 and T/L_1 s, respectively, where T is 0.15 s, and

$$L_1 = 1, \quad M_1 = 2 \quad \text{and} \quad M_2 = 3.$$

Verifying from equations (4.2a,b) that N is 6, the pulse-transform model of the discretised plant is

$$\mathbf{g}_{p_N}(z_N) = z_6^{-1}\begin{bmatrix} \dfrac{b_1\left(1+z_6^{-1}\right)}{\left(1-z_6^{-1}\right)^2} \\ \dfrac{-b_2\left(1+z_6^{-1}\right)}{1-a_1 z_6^{-1}+z_6^{-2}} \end{bmatrix}, \tag{C.9a}$$

where $\quad b_1 = (T/N)^2/2M_c, \quad b_2 = -\left(1-\cosh\left(T/N\sqrt{-g/l}\right)\right)/M_c g$

and $\quad a_1 = 2\cosh\left(T/N\sqrt{g/l}\right).$

Evidently, equation (C.9a) can be written as the following left-matrix fraction (see (4.6)):

$$\mathbf{g}_{p_N}(z_N) = z_6^{-1}\boldsymbol{A}(z_6^{-1})\boldsymbol{b}(z_6^{-1}), \tag{C.9b}$$

where $\boldsymbol{A}(z_N^{-1}) = \begin{bmatrix} \left(1-z_6^{-1}\right)^2 & 0 \\ 0 & 1-a_1 z_6^{-1}+z_6^{-2} \end{bmatrix}$ and $\boldsymbol{b}(z_N^{-1}) = \begin{bmatrix} b_1+b_1 z_6^{-1} \\ -b_2-b_2 z_6^{-1} \end{bmatrix}$.

The problem of deriving the above left-matrix fraction is computed by the POLYNOMIAL TOOLBOX conversion command *rat2lmf*, where, if the matrices $\boldsymbol{A}$ and $\boldsymbol{b}$ are named (*AplyX*) and (*BplyX*), respectively, then the script is:

```
[BplyX,AplyX] = rat2lmf(num,den);
BplyX = inv(diag(diag(AplyX{0})))*BplyX;
AplyX = inv(diag(diag(AplyX{0})))*AplyX;
```

Notice that the last two lines of the script have been introduced to ensure that the condition $\boldsymbol{A}_{ii}(0) = 1$, $i = 1, 2, \ldots, m$, is satisfied.

The Polynomial Matrix-Vector Lifted System Representation

The polynomial lifted system representation, specified by equations (4.34) and (4.35), can be established through the implementation of the techniques described in section 4.1. Neglecting the noise model temporarily, the fast-sampled outputs $\hat{\mathbf{y}}(0)$ are related to the slow-sampled control $\tilde{\mathbf{u}}(0)$ thus (see (4.10)):

$$\hat{\mathbf{A}}(q^{-1})\hat{\mathbf{y}}(0) = \hat{\mathbf{B}}_H(q^{-1})\tilde{\mathbf{u}}(0),$$

where $\hat{\mathbf{y}}(0) = \begin{bmatrix} y_1(0) & y_1(-1) & \dots & y_1(-5) & y_2(0) & y_2(-1) & \dots & y_2(-5) \end{bmatrix}'$

and $$\tilde{u}(0) = u(0);$$

$$\hat{\mathbf{A}}(q^{-1}) = \text{block diag}\left(\mathbf{I}_6 - 2\mathbf{P}_6^{(1)}(q^{-1}) + \mathbf{P}_6^{(2)}(q^{-1}), \mathbf{I}_6 - a_1\mathbf{P}_6^{(1)}(q^{-1}) + \mathbf{P}_6^{(2)}(q^{-1})\right),$$

and, with $$\hat{\mathbf{B}}(q^{-1}) = \begin{bmatrix} b_1\mathbf{I}_6 + b_1\mathbf{P}_6^{(1)}(q^{-1}) \\ -b_2\mathbf{I}_6 - b_2\mathbf{P}_6^{(1)}(q^{-1}) \end{bmatrix}, \quad \hat{\mathbf{P}}_l^{(d)}(q^{-1}) = \mathbf{P}_6^{(1)}(q^{-1})$$

and $$\hat{\mathbf{H}}(q^{-1}) = \mathbf{P}_6^{(5)}(q^{-1})\mathbf{W}_1 = \begin{bmatrix} 1 \\ q^{-1}\mathbf{w}_5 \end{bmatrix},$$

where $$\hat{\mathbf{B}}_H(q^{-1}) = \hat{\mathbf{B}}(q^{-1})\hat{\mathbf{P}}_l^{(d)}(q^{-1})\hat{\mathbf{H}}(q^{-1}) = \begin{bmatrix} 2b_1\mathbf{w}_5q^{-1} \\ b_1q^{-1} + b_1q^{-2} \\ -2b_2\mathbf{w}_5q^{-1} \\ -b_2q^{-1} - b_2q^{-2} \end{bmatrix}.$$

Construction of the matrices $\hat{\mathbf{A}}$ (*Ahat*) and $\hat{\mathbf{B}}_H$ (*Bhat*) can be effected for any sampling ratio N by the following script, which is based on the commands *toeplitz*, *Wmatrix* and *Pmatrix* outlined previously:

```
Ahat = toeplitz(AplyX,N);
Hhat = Pmatrix(Lbar-1,N)*Wmatrix(L,N);
Bhat = toeplitz(BplyX,N)*Pmatrix(d*ones(1,m),N)*Hhat;
```

The designation of the permutation matrix $\mathbf{\Pi}_1$ in accordance with the following vectors:

$$\tilde{\mathbf{y}}(0) = \begin{bmatrix} y_1(0) & y_2(0) & y_2(-2) & y_1(-3) & y_2(-4) \end{bmatrix}'$$

and $$\mathbf{y}_e = \begin{bmatrix} y_1(-1) & y_2(-1) & y_1(-2) & y_2(-3) & y_1(-4) & y_1(-5) & y_2(-5) \end{bmatrix}'.$$

leads to the plant model

$$\mathbf{A}_r(q^{-1})\tilde{\mathbf{y}}(0) = \mathbf{B}_r(q^{-1})\tilde{\mathbf{u}}(0),$$

where $\mathbf{A}_r = \mathbf{\Pi}_1\hat{\mathbf{A}}\mathbf{\Pi}_1' = \begin{bmatrix} \mathbf{A}_1 & \mathbf{A}_2 \\ \mathbf{A}_3 & \mathbf{A}_4 \end{bmatrix}$ and $\mathbf{B}_r = \mathbf{\Pi}_1\hat{\mathbf{B}} = \begin{bmatrix} \mathbf{B}_1 \\ \mathbf{B}_2 \end{bmatrix}$

The rearrangement of the matrices may be performed by the *permutation* command; for example, *permutation(N,M,1)*Atilde*permutation(N,M,1).'*. However, since it is the individual submatrices $\mathbf{A}_1$ (*A1*), $\mathbf{A}_2$ (*A2*), $\mathbf{A}_3$ (*A3*) and $\mathbf{A}_4$ (*A4*) that are required, it is more convenient to utilise the *Vmatrix* command. Thus, for instance, the matrix $\mathbf{A}_1$ can be established by the command *Vmatrix(M,N,1)*Ahat*Vmatrix(M,N,1).* , while $\mathbf{A}_2$ can be established correspondingly by *Vmatrix(M,N,1)*Ahat*Vmatrix(M,N,2).'*.

Using the matrix fraction $\mathbf{A}_{4_2}^{-1}\mathbf{A}_{2_4}$ (see (4.13)), the lifted plant description in left-matrix fraction form is given by (see (4.14))

$$\tilde{\mathbf{A}}(q^{-1})\tilde{\mathbf{y}}(0) = \tilde{\mathbf{B}}(q^{-1})\tilde{\mathbf{u}}(0),$$

where $\tilde{\mathbf{A}}(q^{-1}) = \mathbf{A}_{4_2}\mathbf{A}_1 - \mathbf{A}_{2_4}\mathbf{A}_3 = \begin{bmatrix} 1+q^{-1} & 0 & 0 & -2 & 0 \\ 0 & 1 & 2-a_1^2 & 0 & 1 \\ 0 & -(1-a_1^2)q^{-1} & 1-q^{-1} & 0 & 1-a_1^2 \\ -2q^{-1} & 0 & 0 & 1+q^{-1} & 0 \\ 0 & (2-a_1^2)q^{-1} & q^{-1} & 0 & 1 \end{bmatrix}$

and $\tilde{\mathbf{B}}(q^{-1}) = \mathbf{A}_{4_2}\mathbf{B}_1 - \mathbf{A}_{2_4}\mathbf{B}_2 = \begin{bmatrix} 18b_1q^{-1} \\ -2b_2\left(2+a_1\right)q^{-1} \\ -b_2q^{-1}\left(2+a_1\right)\left(1-q^{-1}\right) \\ 9b_1q^{-1}\left(1+q^{-1}\right) \\ -b_2\left(2+a_1\right)q^{-1}\left(1+q^{-1}\right) \end{bmatrix}$.

In the POLYNOMIAL TOOLBOX environment, the manipulation above can be carried out by utilising the right- to left-matrix fraction conversion command *rmf2lmf* to obtain the terms $\mathbf{A}_{2_4}$ (*A24*) and $\mathbf{A}_{4_2}$ (*A42*):

```
[A24,A42] = rmf2lmf(Vmatrix(M,N,1)*Ahat*Vmatrix(M,N,2).',...
    Vmatrix(M,N,2)*Ahat*Vmatrix(M,N,2).');
```

and, consequently, the lifted left-matrix fraction system description is obtained by the following code:

```
Atilde = A42*Vmatrix(M,N,1)*Ahat*Vmatrix(M,N,1).'-...
    A24*Vmatrix(M,N,2)*Ahat*Vmatrix(M,N,1).';
Btilde = A42*Vmatrix(M,N,1)*Bhat-A24*Vmatrix(M,N,2)*Bhat;
```

Expressed as a right-matrix fraction, the plant model is

$$\bar{\mathbf{y}}(0) = \mathbf{B}_a(q^{-1})\mathbf{A}_b^{-1}(q^{-1})\bar{\mathbf{u}}(0),$$

where inserting the values for the parameters a_1, b_1 and b_2, the relevant matrices are given by

in which $\mathbf{A}_b(q^{-1}) = 1 - 4.4579q^{-1} + 6.9159q^{-2} + 4.4579q^{-3} + q^{-4}$

and $\mathbf{B}_a(q^{-1}) = \begin{bmatrix} 0.0225q^{-1} - 0.0328q^{-2} - 0.0328q^{-3} + 0.0225q^{-4} \\ -0.0467q^{-1} + 0.0467q^{-2} + 0.0467q^{-3} - 0.0467q^{-4} \\ -0.0203q^{-1} - 0.0274q^{-2} + 0.1107q^{-3} - 0.0580q^{-4} - 0.0050q^{-5} \\ 0.0056q^{-1} + 0.0199q^{-2} - 0.0717q^{-3} + 0.0199q^{-4} + 0.0056q^{-5} \\ -0.0050q^{-1} - 0.0580q^{-2} + 0.1107q^{-3} - 0.0274q^{-4} - 0.0203q^{-5} \end{bmatrix}.$

The equivalent right-matrix fraction description above can be derived directly by the left- to right-matrix fraction conversion command *lmf2rmf*:

```
[Ba,Ab] = lmf2rmf(Bbar,Abar);
```

In this example, it is supposed that the disturbance subsystem model is specified by the matrix

$$\tilde{C}(z_N^{-1}) = \begin{bmatrix} 1 + c_1 z_6^{-1} & 0 \\ 0 & 1 + c_2 z_6^{-1} \end{bmatrix}.$$

The procedure summarised in section 4.2 by equations (4.21) and (4.22) can be used to derive the lifted disturbance subsystem model. The designation of the stable solution $\tilde{\mathbf{C}}$ (*Ctilde*) can be established through the use of the spectral factorisation command *spf* provided within POLYNOMIAL TOOLBOX, after the Toepltiz matrix $\hat{\mathbf{C}}$ has been restructured to establish the matrix $\boldsymbol{\Gamma}$ (*Gamma*). The relevant commands are:

```
Chat = toeplitz(CplyX,N):
Gamma = A42*Vmatrix(M,N,1)*Chat-A24*Vmatrix(M,N,2)*Chat;
Ctilde = spf(Gamma*Gamma,1e-10):
Ctilde = inv(diag(diag(Ctilde{0})))*Ctilde:
```

It will be observed that the modelling script detailed above has been written in a general form to enable the code to be extended to any configuration and not limited to the sampling rates initially selected. In this example, it was found that values c_1 and c_2 of -0.4313 and -0.2661 respectively, engenders a $\tilde{\mathbf{C}}$ matrix with related zeros very close to the origin. Consequently, all "C" matrices are henceforth modelled as identity matrices.

LQG Controller Derivation

The representation established above can be used in conjunction with the dynamics-assignment approach to derive the LQG compensator solution for the regulator problem considered in section 5.1. From the theory detailed in Chapter 5, it is known that the controller numerator matrix can be defined by

$$\mathbf{S}_{md} = \begin{bmatrix} s_{11_0} & s_{12_0} & s_{13_0} & s_{14_0} & 0 \end{bmatrix}.$$

Inspection of this transposed vector identifies that the concept of causality is not an issue, and it is therefore possible to employ conventional algorithms to establish the optimal control solution $\mathbf{R}_{md}$ (R) and $\mathbf{S}_{md}$ (S) via the diophantine equation defined in equation ((5.25)). The dynamics-assignment approach to determining the LQG controller is dependent upon the matrices obtained from the conversions of matrix fraction descriptions defined in equations (5.2) and (5.24), which can be undertaken by using the macros *lmf2rmf* and *rmf2lmf* as demonstrated above.

The control weighting parameters can be used to move the closed-loop-poles to desirable location within the unit disc; by trial-and-error, a value of 1 was selected for this example. Solving equation (5.3) to determine the stable solution d (D) via the spectral factorisation solver

$$D = spf(zi*Ab'*Xi*Ab+Ba'*Ba,1e\text{-}10);$$

yields $\quad d(q^{-1}) = 2.2080 - 6.1286q^{-1} + 6.2625q^{-2} - 2.7802q^{-3} + 0.4529q^{-4}.$

It will be observed that since the degree of the matrices $\mathbf{A}_b$ and $\mathbf{B}_a$ are not equal, an additional z^{-1} term has been included within the script, thus ensuring that the matrix is para-Hermitian and that the correct terms are related. The closed-loop poles related to

the plant – determined by the zeros of $z^4 d(z^{-1})$ – are located at $z = 0.5124 \pm j0.0305$ and $z = 0.8754 \pm j0.1101$.

The minimal degree solution of the single diophantine equation ((5.25)) is dependent upon the relevant matrices possessing specific structures. For this reason, in order to use conventional algorithms, a masking matrix $\mathbf{X}_y$ (Xy) must be introduced into the diophantine equations as explained in section C.1. Based upon the structure of the $\mathbf{S}_{md}$ matrix above, the masking matrix takes the form

$$\boldsymbol{X}_y = \text{diag}\,(1,\ 1,\ 1,\ 1,\ 0)$$

Consequently, the minimal degree solution of the single diophantine equation ((5.25)), defined with respect to $\mathbf{R}$, can be derived from the matrix polynomial equation solver command *xaybc* by:

*[R,S] = xaybc(A1,diag(Xy)B1,D*C1,'miny');*

which yields

$$R_{md} = 2.2080 + 0.3869q^{-1} \quad \text{and} \quad \mathbf{S}_{md} = \begin{bmatrix} -17.1100 & 16.4029 & -119.1203 & 95.4416 & 0 \end{bmatrix}$$

The final stage of the derivation of the optimal matrices $\mathbf{R}_o(q^{-1})$ and $\mathbf{S}_o(q^{-1})$ concerns the right- to left-matrix fraction conversion of equation (5.5); this procedure is not required in this example owing to the structure of the $\mathbf{C}$ matrices specified above.

Analysis

The performance of the feedback system can be assessed by the response and the margins of stability of the system, which are given by

$$PM = 23.3752^\circ,$$

$$GM_u = +15.9317\text{dB} \quad \text{and} \quad GM_l = -6.9511\text{dB}.$$

A simulation of the closed-loop system realised by SIMULINK produces the responses of both the outputs and the control signal depicted in Figures C.2 and C.3.

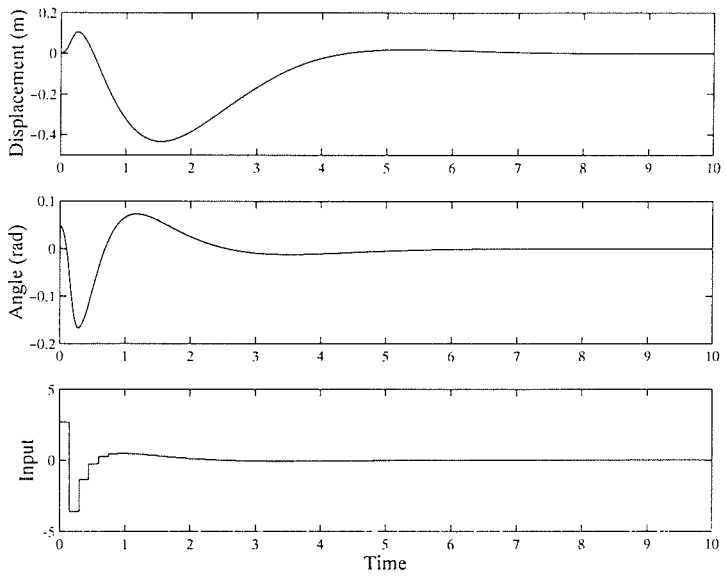

Figure C.2. Transient response from an initial pendulum angle.

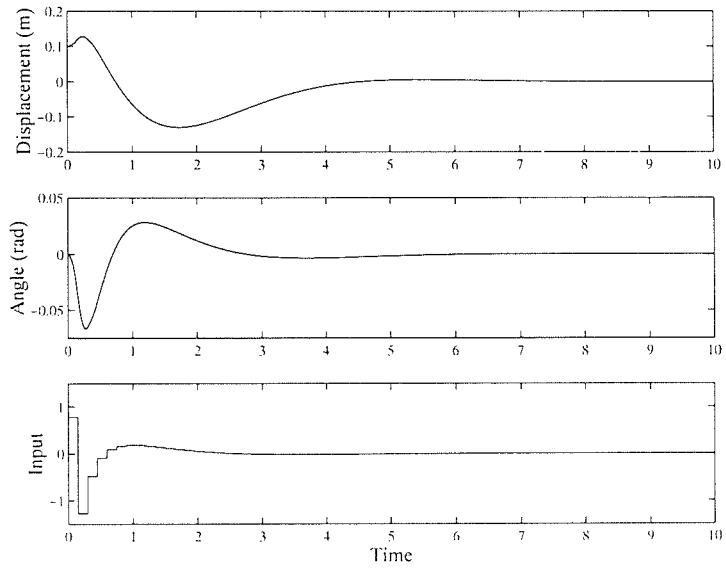

Figure C.3. Transient response from an initial displacement of the cart.

The values of L_1, M_1 and M_2 above were chosen primarily for expositional clarity. In a rather more representative example, it is supposed now that

$$L_1 = 4, \quad M_1 = 2 \quad \text{and} \quad M_2 = 5,$$

whence $N = 20$ (See (4.1a,b)).

With the exception of the diophantine equation (5.25) solver, the code defined above can be used to derive the optimal controller. In this particular situation, the acquisition of $(\mathbf{R}_o, \mathbf{S}_o)$ is dependent upon the use of the masking matrices described in section C.1. Noting that the last two lines engender the causal structures required, the relevant code is given by

```
for i = 1:sum(L)
    eval(['[r' num2str(i) ',s' num2str(i) '] = xaybc(diag(Xx(i,:))*A1,'...
        'diag(Xy(i,:))*B1,D(i,:)*C1,"miny");'])
    eval(['R(i,1:sum(L)) = r' num2str(i) '*diag(Xx(i,:));'])
    eval(['S(i,1:sum(M)) = s' num2str(i) '*diag(Xy(i,:));'])
end
```

In this case the causal structures of the matrices $\mathbf{S}_{md}$ and $\mathbf{R}_{md}$ are defined by

$$\mathbf{S}_{md} = \begin{bmatrix} s_{11_0} & s_{12_0} & s_{13_0} & 0 & s_{15_0} & 0 & 0 \\ s_{21_1}q^{-1} & 0 & 0 & s_{24_0} & s_{25_0} & s_{26_0} & 0 \\ s_{31_1}q^{-1} & 0 & 0 & 0 & s_{35_0} & s_{36_0} & s_{37_0} \\ s_{41_1}q^{-1} & s_{42_1}q^{-1} & 0 & 0 & s_{45_1}q^{-1} & 0 & s_{47_0} \end{bmatrix}$$

and

$$\mathbf{R}_{md} = \begin{bmatrix} d_{11_0} & d_{12_0} & d_{13_0} & d_{14_0} \\ d_{21_1}q^{-1} & d_{22_0} & d_{23_0} & d_{24_0} \\ d_{31_1}q^{-1} & d_{32_1}q^{-1} & d_{33_0} & d_{34_0} \\ d_{41_1}q^{-1} & d_{42_1}q^{-1} & d_{43_1}q^{-1} & d_{44_0} \end{bmatrix};$$

therefore, the masking matrices are defined by

$$\mathbf{X}_{x_i} = \operatorname{diag}\left(\mathbf{X}_x(i,:)\right), \quad \mathbf{X}_x = \begin{bmatrix} 1 & 1 & 1 & 1 \\ q^{-1} & 1 & 1 & 1 \\ q^{-1} & q^{-1} & 1 & 1 \\ q^{-1} & q^{-1} & q^{-1} & 1 \end{bmatrix}$$

$$\mathbf{X}_{y_i} = \mathrm{diag}\left(\mathbf{X}_y(i,:)\right), \quad \mathbf{X}_y = \begin{bmatrix} 1 & 1 & 1 & 0 & 1 & 1 & 0 \\ q^{-1} & 0 & 0 & 1 & 1 & 1 & 0 \\ q^{-1} & 0 & 0 & 0 & 1 & 1 & 1 \\ q^{-1} & q^{-1} & 0 & 0 & q^{-1} & 0 & 1 \end{bmatrix}.$$

Consequently, the optimal control law is defined by:

$$\mathbf{S}_o = \begin{bmatrix} -9.2692 & -89.0946 & 77.9952 & 0 & 8.9156 & 0 & 0 \\ 9.0924q^{-1} & 0 & 0 & -98.4414 & -9.4460 & 86.1802 & 0 \\ 8.9156q^{-1} & 0 & 0 & 0 & -9.2692 & -95.2219 & 83.3609 \\ -9.4460q^{-1} & 80.6335q^{-1} & 0 & 0 & 9.0924q^{-1} & 0 & -92.1074 \end{bmatrix}$$

and

$$\mathbf{R}_o = \begin{bmatrix} 0.8576 & 0.1030 & -0.0125 & 0 \\ -0.0128q^{-1} & 0.8576 & 0.2880 & 0.00044 \\ -0.0032q^{-1} & 0 & 0.8576 & 0.2489 \\ 0.1663q^{-1} & -0.0384q^{-1} & -0.0128q^{-1} & 0.8576 \end{bmatrix}.$$

C.4 Conclusion

This section has addressed computational issues associated with the formulation of polynomial descriptions and control laws for multirate-sampled systems. In particular, with the assistance of the computer-aided control system analysis and design package POLYNOMIAL TOOLBOX to simplify numerical computations and algebraic procedures, an illustrative design example has served to reflect the inherent possibilities of polynomial theory as applied to multirate systems. Although in some cases the specialised computational techniques are not directly applicable to the multirate scenario, the simple methods presented in section C.1 can be utilised effectively to overcome such problems.

BIBLIOGRAPHY

Åström, K. J. and Wittenmark, B. (1973). On self-tuning regulators, *Automatica* **9**: 185–199.

Åström, K. J. and Wittenmark, B. (1997). *Computer Controlled Systems: Theory & Design*, third edn, Prentice Hall, Englewood Cliffs, NJ.

Al-Rahmani, H. M. and Franklin, G. F. (1990). A new optimal multirate control of linear periodic and time - invariant systems, *IEEE Transactions on Automatic Control* **35**(4): 406–415.

Al-Rahmani, H. M. and Franklin, G. F. (1992). Multirate control: A new approach, *Automatica* **28**(1): 35–44.

Albertos, P., Salt, J. and Tornero, J. (1996). Dual-rate adaptive control, *Automatica* **32**(7): 1027–1030.

Amit, N. (1980). *Optimal control of multirate digital control systems*, Ph.D. dissertation, Department of Aeronautics and Astronautics, Stanford University, Stanford.

Araki, M. (1993). Recent developments in digital control theory, *Proceedings of the 12th Triennial World Congress of the International Federation of Automatic Control*, Vol. 9, Sydney, pp. 251–259.

Araki, M. and Hagiwara, T. (1986). Pole assignment by multirate sampled-data output feedback, *International Journal of Control* **44**(6): 1661–1673.

Araki, M. and Yamamoto, K. (1986). Multivariable multirate sampled-data systems: State-space descriptions, transfer characteristics and nyquist criterion, *IEEE Transactions on Automatic Control* **31**(2): 145–154.

Araki, M., Fukumitsu, K. and Hagiwara, T. (1999). Simultaneous stabilization and pole assignment by two level controllers consisting of a gain feedback and a multirate input controller, *Journal of Dynamic Systems, Measurement & Control* **121**(2): 302–305.

Araki, M., Hagiwara, T. and Soma, H. (1992). Application of multilevel multirate sampled-data controllers to simultaneous pole assignment problem, *Proceedings IEEE Conference on Decision & Control*, Tucson, pp. 1762–1767.

Arvanitis, K., Kalogeropoulos, G. and Santas, E. (1999). Adaptive pole positioning in MIMO linear systems by periodic multirate-input controllers, *Journal of Mathematical Analysis & Applications* **237**(2): 463–504.

Arvanitis, K., Paraskevopoules, P. and Vernardos, A. (2000). Multirate adaptive temperature control of greenhouse, *Computers and Electronics in Agriculture* **26**: 303–320.

Bamieh, B., Pearson, J., Francis, B. and Tannenbaum (1991). A lifting technique for linear periodic systems with applications to sampled-data control, *Systems and Control Letters* **17**: 79–88.

Basilio, J. and Kouvaritakis, B. (1997). An algorithm for coprime matrix fraction description using Sylvester matrices, *Linear Algebra and its Applications* **266**: 107–125.

Berg, M. C., Amit, N. and Powell, J. D. (1988). Multirate digital control system design, *IEEE Transactions on Automatic Control* **33**(12): 1139–1150.

Berger, C. and Peduto, D. (1997). Robust digital control using multirate input sampling, *International Journal of Control* **67**(5): 813–824.

Bertsekas, D. (1976). *Dynamic Programming and Stochastic Control*, Academic Press, New York, USA.

Bittanti, S. and Colaneri, P. (1998). *Wiley Encyclopaedia of Electrical and Electronic Engineering (Ed. J.G. Webster)*, Vol. 16, Wiley, New York, chapter Periodic control, pp. 59–74.

Bittanti, S., Colaneri, P. and De Nicolao, G. (1988). Two techniques for the solution of the discrete-time periodic riccati equation, *Linear Algebra in Signals, Systems and Control* pp. 315–331.

Bittanti, S., Colaneri, P. and De Nicolao, G. (1990). An algebraic ricatti equation for the discrete-time periodic prediction problem, *Systems & Control Letters* **14**(1): 71–78.

Blankinship, W. A. (1963). A new version of the Euclidean algorithm, *American Mathematics monthly* **70**: 742–745.

Boykin, W. H. and Frazier, B. D. (1975a). Analysis of multi-loop multirate sampled-data systems, *American Institute of Aeronautics and Astronautics Journal* **13**(4): 453–456.

Boykin, W. H. and Frazier, B. D. (1975b). Multirate sampled-data systems via vector operators, *IEEE Transactions on Automatic Control* **20**(4): 548–551.

Carini, P., Micheli, R. and Scattolini, R. (1990). Multirate self-tuning predictive control with application to a binary distillation column, *International Journal of System Science* **21**(1): 51–64.

Chammas, A. B. and Leondes, C. T. (1979). Pole assignment by piecewise constant output feedback, *International Journal of Control* **29**(1): 31–38.

Chen, T. and Qiu, L. (1994). H_∞ design of general multirate sampled-data control systems, *Automatica* **30**(7): 1139–1152.

Clarke, D. and Gawthrop, P. (1975). Self-tuning controller, *Proceedings of the Institute of Electrical and Electronic Engineering* **122**: 929–934.

Clarke, D., Mohtadi, C. and Tuffs, P. (1987a). Generalized predictive control – Pt. 1: The basic algorithm, *Automatica* **23**(2): 137–148.

Clarke, D., Mohtadi, C. and Tuffs, P. (1987b). Generalized predictive control – Pt. 2: Extensions and interpretations, *Automatica* **23**(2): 149–160.

Coffey, T. and Williams, I. (1966). Stability analysis of multiloop, multirate sampled systems, *American Institute of Aeronautics and Astronautics Journal* **4**(12): 2178–2190.

Colaneri, P. and De Nicolao, G. (1995). Multirate LQG control of continuous-time stochastic systems, *Automatica* **31**(4): 591–596.

Colaneri, P., Scattolini, R. and Schiavoni, N. (1992). LQG optimal control of multirate sampled-data systems, *IEEE Transactions on Automatic Control* **37**(5): 675–682.

Cutler, C. and Ramaker, B. (1979). Constrained multivariable control of a hydrocracker reactor, *Proc. Am. Control Conference*, pp. 1014–1020.

Datta, K. and Gangopadhyay, S. (1992). Coprime matrix fraction description via orthogonal structure theorem, *IEEE Transactions on Automatic Control* **37**: 1517–1520.

De Keyser, R. and Van Cauwenberghe, A. (1982). Typical application possibilities for self-tuning predictive control, *Proceedings IFAC Symp. on Identification & System Parameter Estimation*, Vol. 2, pp. 1552–1557.

Er, M. J. and Anderson, B. D. (1991). Practical issues in multirate output controllers, *International Journal of Control* **53**(5): 1005–1020.

Er, M. J. and Anderson, B. D. (1992). Performance study of multirate output controllers under noise disturbances, *International Journal of Control* **56**(3): 531–545.

Er, M. J., Anderson, B. D. and Yan, W.-Y. (1994). Gain margin improvements using generalized sampled-data hold function based multirate output compensators, *Automatica* **30**(3): 461–470.

Gantmakher, F. (1959). *The Theory of Matrices*, Vol. 1 and 2, Chelsea Publishing, New York.

Garcia, C., Prett, D. and Morari, M. (1991). Model predictive control: theory and practice - a survey, *Automatica* **25**: 335–348.

Glasson, D. P. (1983). Development and applications of multirate digital control, *IEEE Control Systems Magazine* **3**(4): 2–8.

Godbout, L. F., Jordan, D. and Striefler, M. E. (1994). Pole placement algorithms for multirate-sampled linear systems, *Automatica* **30**(4): 723–727.

Guilandoust, M., Morris, A. and Tham, M. (1987). Adaptive inferential control, *Proceedings of the Institution of Electrical Engineers, part D* **134**: 171–179.

Hagiwara, T. and Araki, M. (1988). Design of a stable state feedback controller based on the multirate sampling of the plant output, *IEEE Transactions on Automatic Control* **33**(9): 812–819.

Hagiwara, T., Fujimura, T. and Araki, M. (1990). Generalized multirate-output controllers, *International Journal of Control* **52**(3): 597–612.

Horowitz, I. (1963). *Synthesis of Feedback Systems*. Academic Press. New York.

Hunt, K. and Šebek, M. (1989). Optimal multivariable regulation with disturbance measurement feedforward, *International Journal of Control* **49**: 373–378.

Ježek, J. (1982). New algorithm for minimal solution of linear polynomial equations, *Kybernetika* **18**(6): 505–516.

Ježek, J. and Kučera, V. (1985). Efficient algorithm for matrix spectral factorisation, *Automatica* **21**(6): 663–669.

Jury, E. I. (1961). Sampling schemes in sampled-data control systems, *IRE Transactions on Automatic Control* pp. 86–88.

Jury, E. I. (1967). A note on multirate sampled-data systems, *IEEE Transactions on Automatic Control* **12**: 319–320.

Kabamba, P. (1987). Control of linear systems using generalised sampled-data hold functions, *IEEE Transactions on Automatic Control* **32**: 772–783.

Kaczorek, T. (1985). Pole-placement for linear discrete-time systems by periodic output feedbacks, *Systems and Control Letters* (6): 267–269.

Kalman, R. and Bertram, J. (1959). A unified approach to the theory of sampling systems, *Journal of the Franklin Institute* **267**: 405–436.

Kando, H. and Iwazumi, T. (1986). Multirate digital control design of an optimal regulator via singular perturbation theory, *International Journal of Control* **44**(6): 1555–1578.

Kranc, G. (1957). Input-output analysis of multirate feedback systems, *IRE Transactions on Automatic Control* **3**: 21–28.

Kučera, V. (1979). *Discrete Linear Control - The polynomial equation approach*, Wiley, Chichester, UK.

Kučera, V. (1991). *Analysis and Design of Discrete Linear Control Systems*, Prentice Hall, Hemel Hempstead, UK.

Kučera, V. (1993). Diophantine equations in control - a survey, *Automatica* **29**(6): 1361–1375.

Kučera, V. and Šebek, M. (1984). A polynomial solution to regulation and tracking, Pt. 1, *Kybernetika* **20**: 177–188.

Kwakernaak, H. (2000). A descriptor algorithm for the spectral factorisation of polynomial matrices, *IFAC Symposium on Robust Control Design*, Prague, Czech Republic.

Kwakernaak, H. and Šebek, M. (1994). Polynomial j-spectral factorization, *IEEE Transactions on Automatic Control* **39**(2): 315–328.

Kwakernaak, H. and Šebek, M. (1999). *Polynomial Toolbox 2.0 Manual*, The Polyx.

Lee, J., Gelormino, M. S. and Morari, M. (1992). Model predictive control of multi-rate sampled data systems: a state-space approach, *International Journal of Control* **55**(1): 153–191.

Lee, J.-W. and Oh, J.-H. (2000). Comparison of performance and computational efficiency in multirate LQG control, *International Journal of Systems Science* **31**(5): 669–676.

Lennartson, B. (1988). Periodic solutions of riccati equations applied to multirate sampling, *International Journal of Control* **48**(3): 1025–1042.

Ling, K. and Lim, K. (1996). A state-space GPC with extensions to multirate control, *Automatica* **32**(7): 1067–1071.

Liu, G. and Patton, R. (1998). *Multirate sampled-data system control via eigenstructure assignment*, Eigenstructure assignment for control system design, Wiley, Chichester, chapter 8.

Longhi, S. (1994). Structural properties of multirate sampled-data systems, *IEEE Transactions on Automatic Control* **39**(3): 692–696.

Lu, W., Fisher, D. G. and Shah, S. L. (1990). Multirate constrained adaptive control, *International Journal of Control* **51**(6): 1439–1456.

MacFarlane, A. G. and Postlethwaite, I. (1977). The generalised nyquist stability criterion and multivariable root loci, *International Journal of Control* **25**: 81–127.

Mahmood, S., Pugh, A., Karampetakis, N. and Hayton, G. (1998). Structural properties of column (row) reduced MFDs, *International Journal of Control* **69**(1): 111–130.

Meyer, D. G. (1990a). A new class of shift-varying operators, their shift-invariant equivalents and multirate digital systems, *IEEE Transactions on Automatic Control* **35**(4): 429–433.

Meyer, D. G. (1990b). A parameterisation of stabilizing controllers for multirate sampled-data systems, *IEEE Transactions on Automatic Control* **35**(2): 233–236.

Meyer, D. G. (1992). Cost translation and a lifting approach to the multirate LQG problem, *IEEE Transactions on Automatic Control* **37**(9): 1411–1415.

Meyer, D. G. and Burrus, C. (1975). A unified analysis of multirate and periodically time-varying digital filters, *IEEE Transactions on Circuit and Systems* **22**: 165–168.

Moore, K. L., Bhattacharyya, S. and Dahleh, M. (1993). Capabilities and limitations of multirate control schemes, *Automatica* **29**(4): 941–951.

Newton, G., Gould, L. and Kaiser, J. (1957). *Analytical Design of Linear Feedback Controls*, Wiley, New York.

Patel, R. (1981). Computation of matrix fraction descriptions of linear time-invariant systems, *IEEE Transactions on Automatic Control* **26**: 148–161.

Peterka, V. (1972). On steady state minimum variance control strategy, *Kybernetika* **8**: 219–232.

Peterka, V. (1984). Predictor-based self-tuning control, *Automatica* **20**: 39–50.

Prett, D. and Gillette, R. (1979). Optimisation and constrained multivariable control of a catalytic cracking unit, *AIChE National Mtg*, Houston, Texas.

Qiu, L. and Chen, T. (1994). H_2-optimal design of multirate sampled-data systems, *IEEE Transactions on Automatic Control* **39**(12): 2506–2511.

Ragazzini, J. and Franklin, G. F. (1958). *Sampled Data Control Systems*, McGraw Hill, New York.

Ravi, R., Khargonekar, P., Minto, K. and Nett, C. (1990). Controller parameterisation for fast-rate time-varying multirate plants, *IEEE Transactions on Automatic Control* **35**(11): 1259–1262.

Richalet, J., Rault, A., Testud, J. and Papon, J. (1978). Model predictive heuristic control, *Automatica* **14**: 413–428.

Rosenbrock, H. (1970). *State space and multivariable theory*, Wiley-Interscience, New York.

Sågfors, M. F., Toivorien, H. and Lennartson, B. (2000). State-space solution to the periodic multirate H_∞ control of multirate: A lifting approach, *IEEE Transactions on Automatic Control* **45**(12): 2345–2350.

Sain, M. (1975). A free-modular algorithm for minimal design of linear multivariable systems, *Proceedings of the 6^{th} IFAC Congress*, Boston.

Scattolini, R. (1988). Self-tuning control of systems with infrequent and delay output sampling, *Proceedings of the Institution of Electrical Engineers, part D* **35**: 213–221.

Scattolini, R. and Schiavoni, N. (1995). A multirate model-based predictive controller, *IEEE Transactions on Automatic Control* **40**(6): 1093–1097.

Schauer, T. and Hunt, K. (2000). Linear modelling and controller design for the single limb movement of paraplegics using FES, *Proceedings of the 4th IFAC Symposium on Modelling and Control in Biomedical Systems*, Greifswald, Germany.

Šebek, M. (1981). Optimal tracking via polynomial matrix equations, *International Journal of Systems Science* **12**: 357–369.

Šebek, M. (1983). Direct polynomial approach to discrete-time stochastic tracking. *Problems of Control and Information Theory* **12**: 293–302.

Šebek, M. (1993). *Polynomial methods in optimal control and filtering*, IEE Control Engineering Series, Peter Peregrinus, London, chapter 10: J-Spectral factorisation algorithms.

Šebek, M. and Kučera, V. (1981). Matrix equations arising in regulator problems, *Kybernetika* **17**: 128–139.

Šebek, M. and Kučera, V. (1982). Polynomial approach to quadratic tracking in discrete linear systems, *IEEE Transactions on Automatic Control* **27**: 1248–1250.

Šebek, M., Kwakernaak, H., Henrion, D. and Pejchová, S. (1998). Recent progress in polynomial methods and polynomial toolbox for MATLAB version 2.0, *Proceedings of the Conference on Decision and Control, IEEE*, Tampa, Florida, pp. 3661–3668.

Shu, H. and Chen, T. (1995). State-space approach to discrete-time H_2-optimal control with a causality constraint, *Systems & Control Letters* **26**(1): 69–77.

Sklansky, J. and Ragazzini, J. (1955). Analysis of errors in sampled-data feedback systems, *AIEE Transactions* **74**: 65–71.

Söderström, T. (1980). *Methods and applications in adaptive control*, Berlin, Springer-Verlag.

Sternad, M. and Ahlén, A. (1993). A novel derivation methodology for polynomial - LQ controller design, *IEEE Transactions on Automatic Control* **38**(1): 116–121.

Strijbos, R. (1996). Calculation of right matrix fraction descriptions: an algorithm, *Proceedings of the 4th IEEE Mediterranean Symposium on New Directions in Control and Automation*, Maleme, Krete, Greece, pp. 478–482.

Thompson, P. (1986). Gain and phase margins of multirate sampled-data feedback systems, *International Journal of Control* **44**(3): 833–846.

Truman, A. W. and Govan, M. (2000a). Multirate-sampled digital feedback system design via a predictive control approach, *IEE Proceedings – Control Theory & Applications* **147**(3): 293–302.

Truman, A. W. and Govan, M. (2000b). Polynomial LQG design of subrate digital feedback systems via frequency decomposition, *Optimal Control Applications & Methods* **21**: 211–232.

Truman, A. W. and Govan, M. (2000c). Polynomial LQG synthesis of subrate digital feedback systems, *IEE Proceedings – Control Theory & Applications* **147**(3): 247–256.

Truman, A. W. and Govan, M. (2001). Predictive control of fast output-sampled digital feedback systems via a polynomial approach, *Proceedings of the Institution of Mechanical Engineers, part I* **215**: 211–233.

Tuel, W. J. (1968). Computer algorithm for spectral factorisation of rational matrices, *IBM Journal Research Development* **12**: 163–170.

Viassolo, D. E. and Rotea, M. A. (1998). Practical design of multirate output controllers, *Proceedings of the 37th IEEE Conference on Decision & Control*, Tampa, USA, pp. 337–342.

Volgin, L. (1962). *The elements of the theory of controllers*, Soviet Radio, Moscow.

Voulgaris, P. G. and Bamieh, B. (1993). Optimal H_∞ and H_2 control of hybrid multirate systems, *Systems & Control Letters* **20**(4): 249–261.

Voulgaris, P. G., Dahleh, M. A. and Valavani, L. S. (1994). H_∞ and H_2 optimal controllers for periodic and multirate systems, *Automatica* **30**(2): 251–263.

Werner, H. (1998). Multimodel robust control by fast output sampling - an LMI approach, *Automatica* **34**(12): 1625–1630.

Werner, H. (1999). Tracking and disturbance rejection for an uncertain system using fast output sampling, *European Journal of Control* **5**(1): 129–137.

Wiener, N. (1949). *Extrapolation, Interpolation and Smoothing of Stationery Time Series*, Wiley, New York.

Wolovich, W. (1974). *Linear Multivariable Systems*, Springer, New York.

Ydstie, B. (1984). Extended horizon adaptive control, 9^{th} *World Congress of the IFAC*, Budapest, Hungary.

Yen, N.-Z. and Wu, Y.-C. (1993). On a general optimal algorithm for multirate output feedback controllers for linear stochastic periodic systems, *IEEE Transactions on Automatic Control* **38**(6): 939–943.

Youla, D. C., Bongiorno, J. J. and Jabr, H. A. (1976a). Modern Wiener-Hopf design of optimal controllers – Pt. 1: the single-input-output case, *IEEE Transactions on Automatic Control* **21**(1): 3–13.

Youla, D. C., Jabr, H. A. and Bongiorno, J. J. (1976b). Modern Wiener-Hopf design of optimal controllers – Pt. 2: the multivariable case, *IEEE Transactions on Automatic Control* **21**(3): 319–338.

Zhang, Q. and Tomizuka, M. (1988). Multirate sampling adaptive control and its application to thermal systems, *International Journal of Control* **47**: 135–144.